

All-order prescription for facet regions in massless wide-angle scattering

Yao Ma

*Institute for Theoretical Physics, ETH Zürich,
8093 Zürich, Switzerland*

E-mail: yaomay@phys.ethz.ch

ABSTRACT: We take a step toward answering a long-standing question in the asymptotic expansion of Feynman integrals: how to systematically determine the regions in the Expansion-by-Regions technique for multiscale processes? Focusing on generic massless wide-angle scattering, we provide an all-order momentum-space prescription for facet regions, which generally dominate—and in most cases exhaust—the contributions in a given asymptotic expansion. This extends the Euclidean-space picture, where regions correspond to specific subgraphs, to the complexities of Minkowski space. Our results are derived from a novel analytical approach combining graph theory and convex geometry; as a key byproduct, we uncover for the first time the algebraic structure underlying momentum modes (collinear, soft, and their hierarchies).

Contents

1	Introduction	1
2	Basic concepts and notation	5
2.1	Kinematic setup	5
2.2	Momentum modes	6
2.3	Parametric representation, polytope, and spanning (2-)trees	8
3	Algebraic and graphical structure of modes	11
3.1	The \wedge and \vee operations	11
3.2	Mode subgraphs	18
4	The fundamental pattern	21
5	Further requirements of the mode subgraphs	24
5.1	The connectivity requirements	25
5.2	The infrared-compatibility requirement	30
5.2.1	Basic idea: delivery of infrared scalings	30
5.2.2	Formal constructions and statement	32
5.3	Implications from the infrared-compatibility requirement	35
5.4	Summary and matching to known expansions	37
6	Proof of the subgraph requirements	39
6.1	Proof of the First Connectivity Theorem	40
6.2	Structures of leading terms	46
6.2.1	$\mathcal{U}^{(R)}$ terms	47
6.2.2	Classification of $\mathcal{F}^{(R)}$ terms	48
6.2.3	$\mathcal{F}_I^{(R)}$ terms	49
6.2.4	$\mathcal{F}_{II}^{(R)}$ terms	50
6.2.5	Summary	64
6.2.6	Proof of the Second Connectivity Theorem	65
6.3	The infrared-compatibility requirement	65
6.3.1	Proof of sufficiency	66
6.3.2	Proof of necessity	73
7	Verification with more multiloop examples	81
7.1	A three-loop example: two-to-two scattering	82
7.2	A six-loop example: one-to-three decay plus a soft emission	90
7.3	Extension to massive cases: revisiting a recent work on $gg \rightarrow HH$	98

8 Conclusions and outlook	102
A Some details in section 6	105
A.1 Comparing the kinematic factors in proving (6.5)	105
A.2 Solving for weights in figures 28b and 28c	106
A.3 Derivation of eqs. (6.73) and (6.74)	108

1 Introduction

Evaluating multiscale Feynman integrals remains one of the central challenges in precision calculations for high-energy physics, particularly at particle colliders. These integrals often arise in processes involving widely separated energy scales, where exact analytical evaluation is often intractable, necessitating approximate methods, such as asymptotic expansions, which capture the dominant contributions across different kinematic regimes.

Among various techniques for deriving asymptotic expansions for Feynman integrals, the *Expansion by Regions* (EbR, also referred to as the “Method of Regions”) [1] has become a standard tool for obtaining such expansions in a wide variety of kinematic limits. The basic idea of EbR is to decompose the integration domain into distinct “regions”, each characterized by a specific homogeneous scaling of the integration variables (momenta or parameters). In each region, the integrand is expanded accordingly in powers of the small expansion parameters, and the resulting contributions are integrated over the full space after an appropriate analytic continuation. Although a rigorous mathematical proof of this method is still lacking, its reliability is well established by numerous examples. A crucial step in applying EbR is the identification of all relevant regions contributing to the asymptotic expansion.

For asymptotic expansions in Euclidean space, such as large-mass or large-momentum expansions, the structure of these regions is well understood from a graph-theoretical perspective. Specifically, each relevant region corresponds to a particular assignment of large loop momenta within an “asymptotically irreducible subgraph” [2–5]. Moreover, a mathematical proof has been established that summing the expanded contributions over all such subgraphs exactly reproduces the original Feynman integral. In this sense, EbR is equivalent to “expansion by subgraphs”.

In Minkowski space, however, the richer infrared structure renders the identification of regions considerably more nontrivial. For a long time, this task was performed on a case-by-case basis, often guided by heuristic arguments derived from explicit calculations and physical intuition. Only in recent years has a more systematic geometric approach emerged, which associates a multiscale N -propagator Feynman graph \mathcal{G} with an $(N+1)$ -dimensional polytope $\Delta(\mathcal{G})$ in Lee-Pomeransky parameter space and identifies regions with certain codimension-1 faces—called “lower facets”—of this polytope [6–9]. The entries of the vector normal to each lower facet encode the scaling exponents of the corresponding region. Building on this, several

computer programs, such as Asy2 [7], ASPIRE [8], and pySecDec [10], have been developed to automate region identification.

Nevertheless, our understanding of region structures remains incomplete. A key limitation is that certain contributing regions can lie in the interior (rather than on the boundary) of the polytope and are therefore invisible to the geometric method above. We refer to these as *hidden regions* [11–13], in contrast to the *facet regions* that reside on the boundaries. Identifying hidden regions is technically demanding, and no fully systematic approach exists so far. Although refs. [7, 8] showed that some hidden regions can be unveiled through suitable variable changes, this technique relies on the linear cancellation structure in the \mathcal{F} polynomial, and is not generally applicable. For instance, in massless two-to-two scattering, hidden regions first appear at three loops and involve quadratic cancellations in \mathcal{F} , requiring more intricate treatments [11]. Thus, the state-of-the-art approach to hidden regions is still far from systematic, and is mostly limited to the onset loop order where hidden regions arise.

For massless wide-angle scattering processes, hidden regions are generally rare [11]. In most cases, facet regions alone exhaust the contributions in the expansion, and the geometric approach to regions is fully reliable. Even so, a complete understanding of facet regions has been lacking. First, the geometric approach yields regions in terms of scalings of the Lee-Pomeransky parameters, leaving the physical interpretation in momentum space obscure, which often requires nontrivial translation. Second, as the polytope dimension increases with the number of propagators, existing computational tools provide regions only to a finite order, preventing direct access to a formal, all-order prescription of the full region structure.

The second limitation identified above is particularly subtle, because the region structure depends sensitively on both the external kinematics and the graph topology. For example, consider the massless form factor in figure 1 in the following infrared limit: the external momentum q_1 is off shell ($q^2 \sim 1$), while p_1 and p_2 are on shell ($p_1^2, p_2^2 \ll 1$) and point along distinct lightcones. Near this kinematic point, different asymptotic expansions yield distinct region structures, as listed below.¹

- $p_1^2/q_1^2 \sim p_2^2/q_1^2 \sim \lambda$. There are four regions (where $Q \sim \mathcal{O}(1)$ is the hard scale):

$$\begin{aligned} \text{hard region } (H) : \quad & k^\mu \sim Q(1, 1, 1); \\ \text{collinear-1 region } (C_1) : \quad & k^\mu \sim Q(1, \lambda, \sqrt{\lambda}); \\ \text{collinear-2 region } (C_2) : \quad & k^\mu \sim Q(\lambda, 1, \sqrt{\lambda}); \\ \text{soft region } (S) : \quad & k^\mu \sim Q(\lambda, \lambda, \lambda). \end{aligned}$$

¹In this paper, the virtuality of the soft mode is $\mathcal{O}(\lambda^2)$ while that of the collinear is $\mathcal{O}(\lambda)$, consistent with the terminology in ref. [14–17]. In some other literature, this soft mode is referred to as the “infrared mode” [18] or the “ultrasoft mode” [19–23].

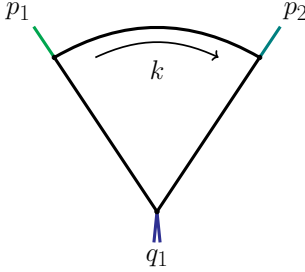


Figure 1. The one-loop form factor with all the edges massless. Even for expanding this relatively simple graph near the same infrared limit ($p_1^2, p_2^2 \ll 1$ and $q_1^2 \sim 1$), the region structure depends strongly on the precise form of the expansion.

- $p_1^2/q_1^2 \sim \lambda$ and $p_2^2/q_1^2 \sim \lambda^2$. There are four regions:

$$\begin{aligned}
 \text{hard region } (H) : & \quad k^\mu \sim Q(1, 1, 1); \\
 \text{collinear-1 region } (C_1) : & \quad k^\mu \sim Q(1, \lambda, \sqrt{\lambda}); \\
 (\text{collinear-2})^2 \text{ region } (C_2^2) : & \quad k^\mu \sim Q(\lambda^2, 1, \lambda); \\
 \text{soft} \cdot \text{collinear-2 region } (SC_2) : & \quad k^\mu \sim Q(\lambda^2, \lambda, \lambda^{3/2}).
 \end{aligned}$$

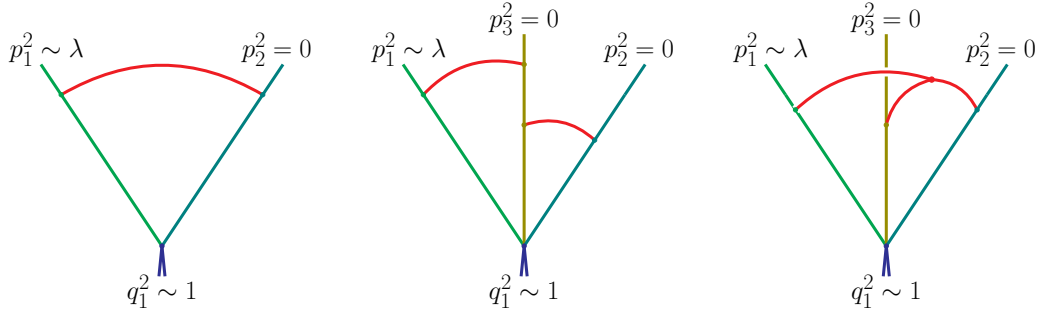
- $p_1^2/q_1^2 \sim \lambda$ and $p_2^2/q_1^2 = 0$. There are two regions:

$$\begin{aligned}
 \text{hard region } (H) : & \quad k^\mu \sim Q(1, 1, 1); \\
 \text{collinear-1 region } (C_1) : & \quad k^\mu \sim Q(1, \lambda, \sqrt{\lambda}).
 \end{aligned}$$

These examples illustrate that even for this relatively simple graph, the region structure depends highly on the external kinematics: changing the hierarchical relations among the virtualities can alter the scalings of individual regions, introduce hierarchical modes (e.g., C_2^2 or SC_2), or cause certain regions to disappear. In particular, we note that in the third kinematics above ($p_1^2/q_1^2 \sim \lambda$ and $p_2^2/q_1^2 = 0$), the C_2 and S regions are both absent, because their corresponding expanded integrals are *scaleless* and thus vanishing.

Even for fixed external kinematics, whether a given loop-momentum configuration contributes as a region depends crucially on the graph topology. As we have just explained, the configuration in figure 2a is scaleless, where the **red** curve represents the soft propagator while the **green** and **teal** lines represent the collinear-1 and collinear-2 propagators, respectively. Similarly, the configuration in figure 2b, which can be seen as a two-loop generalization, is also scaleless. Note that in these examples, we have set $q_1^2 \sim 1$, $p_1^2 \sim \lambda$, and p_2, p_3 strictly on shell ($p_2^2 = p_3^2 = 0$). However, under the same kinematics, if we change the topology of the two-loop graph into figure 2c, the obtained configuration is scaleful, and must therefore be included as a region.

The primary goal of this paper is to resolve these subtleties by extending the expansion-by-subgraphs paradigm in Euclidean space to generic massless wide-angle scattering with



(a) A scaleless configuration. (b) A scaleless configuration. (c) A scaleful region.

Figure 2. Three examples where the loop momenta are all soft. The expanded integrals corresponding to (a) and (b) are scaleless, and should not be taken into account in EbR. In contrast, (c) leads to a scaleful integral and should be considered as one region.

non-exceptional momenta in Minkowski space. To this end, we unify the various asymptotic expansions illustrated above (and others arising in massless wide-angle scattering) under a single framework called the *virtuality expansion* (defined in section 2.1). Within this framework, we systematically analyze the region structure for arbitrary loop orders, numbers of external legs, and orders in the expansion parameter. Specifically, we address two central questions: (1) *Given a virtuality expansion, what are the allowed momentum modes (collinear, soft, and their hierarchies)?* (2) *What requirements must subgraphs associated with these modes satisfy, in order to yield scaleful contributions?* Answering these questions enables us to derive the complete set of facet regions directly from a Feynman graph and its external kinematics, providing an all-order prescription in momentum space while circumventing the limitation of computer codes.

Our approach combines convex geometry with graph theory. On the one hand, for each region the leading terms in the expansion all correspond to points on a “lower facet” of the polytope $\Delta(\mathcal{G})$. On the other hand, these leading terms can be characterized by the minimum spanning (2-)trees of \mathcal{G} . Consequently, the problem of identifying regions can be reformulated as follows: *we seek all scalings of the Lee-Pomeransky parameters x_1, \dots, x_N , such that the parameter-space points, which are corresponding to the minimum spanning (2-)trees of \mathcal{G} , span a lower facet of $\Delta(\mathcal{G})$.*

This approach was introduced in the author’s previous work [24], where it was applied to two special cases of the virtuality expansion: the “on-shell expansion” and the “soft expansion”. There, all-order prescriptions for the region structure were derived, with the on-shell case proven rigorously and the soft case resting on a conjecture about the allowed momentum modes. The general prescription presented here will unify and extend those results to arbitrary virtuality hierarchies, while simultaneously validating the earlier conjecture for the soft expansion.

As a key byproduct of this analysis, we uncover, for the first time, the algebraic structure

underlying the infinitely many momentum modes that arise in generic virtuality expansions. These modes admit a natural partial order by their softness; defining join and meet operations on this partially ordered set (poset) endows it with the structure of a lattice. We explore further algebraic properties of this lattice, which are essential for deriving region structures.

This paper is organized as follows. In section 2, we introduce the basic concepts and notation that form the foundation of our analysis. In section 3, we study the structure of momentum modes from both algebraic and graphic perspectives. We then derive the general prescription for facet regions: section 4 establishes a fundamental pattern under natural assumptions, while section 5 presents the subgraph requirements, which constitute the main results of this paper. Notably, these requirements constrain not only the connections among subgraphs, but also the mode structure: given an expansion, one can determine which modes can appear in arbitrary graphs; in particular, the phenomenon of “cascading modes” is always absent. The proofs of these requirements, which constitute the most technical part of the paper, are provided in section 6. In section 7, we verify our prescription against computer-generated regions for two multiloop graphs, and point out the potential of this work to extend beyond massless Feynman integrals by connecting it with a recent study on quark mass corrections to $gg \rightarrow HH$ [25]. We conclude in section 8 with a summary and an outlook for future research. Additional technical details are collected in appendix A.

2 Basic concepts and notation

In this section, we lay the foundation for our region analysis by introducing basic concepts and notation. In section 2.1, we define the virtuality expansion, which encompasses a wide range of expansions for massless wide-angle kinematics. In section 2.2, we formulate the momentum modes that typically appear in the virtuality expansion, define their virtuality degrees, and introduce a partial order on them. In section 2.3, we demonstrate, within the Lee–Pomeransky representation of Feynman integrals, how the leading terms of the expansion, certain boundaries of a constructed polytope, and the minimum spanning (2-)trees of \mathcal{G} are interrelated.

2.1 Kinematic setup

For the massless wide-angle kinematics in this paper, we consider general external kinematics where the external momenta can be classified into three sets. The first set consists of momenta p_1, \dots, p_K , each p_i collinear to a specific lightlike vector β_i^μ , with the component $p_i \cdot \bar{\beta}_i^2$ at the hard scale $Q \sim \mathcal{O}(1)$. The second set includes hard external momenta q_1, \dots, q_L whose components are all at the hard scale. The third set includes soft on-shell momenta l_k^μ , whose components are all small (possibly vanishing at different rates).

²Let $\beta_i^\mu \equiv \frac{1}{\sqrt{2}}(1, \hat{\mathbf{v}}_i)$, where $\hat{\mathbf{v}}_i$ is a unit three-vector. Then $\bar{\beta}_i^\mu \equiv \frac{1}{\sqrt{2}}(1, -\hat{\mathbf{v}}_i)$ is the null vector opposite to β_i^μ , satisfying $\beta_i \cdot \bar{\beta}_i = 1$.

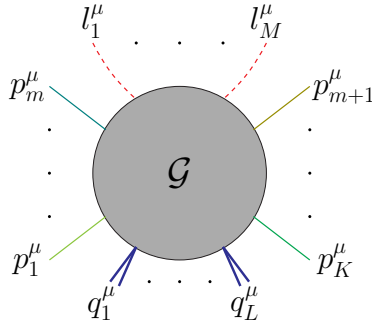


Figure 3. General wide-angle scattering graph \mathcal{G} , with external momenta $\{p_i^\mu\}_{i=1,\dots,K}$, $\{q_j^\mu\}_{j=1,\dots,L}$ and $\{l_k\}_{k=1,\dots,M}$ subject to eq. (2.1).

More precisely, let λ denote a small scaling parameter. By omitting the hard scale Q from now on, the momentum scalings are then:

$$p_i^\mu = (p_i \cdot \bar{\beta}_i, p_i \cdot \beta_i, \mathbf{p}_{i\perp}) \sim (1, \lambda^{a_i}, \lambda^{a_i/2}) \quad \text{for } i = 1, \dots, K; \quad (2.1a)$$

$$q_j^\mu \sim 1 \quad (\text{all components}) \quad \text{for } j = 1, \dots, L; \quad (2.1b)$$

$$l_k^\mu = (l_k \cdot \bar{\beta}'_k, l_k \cdot \beta'_k, \mathbf{l}_{k\perp}) \sim \lambda^{b_k} (1, \lambda^{c_k}, \lambda^{c_k/2}) \quad \text{for } k = 1, \dots, M; \quad (2.1c)$$

$$p_{i_1} \cdot p_{i_2} \sim 1, \quad l_{k_1} \cdot l_{k_2} \sim \lambda^{b_{k_1} + b_{k_2}}, \quad p_{i_1} \cdot l_{k_2} \sim \lambda^{b_{k_2}} \quad \text{for } i_1 \neq i_2, k_1 \neq k_2. \quad (2.1d)$$

Note that the wide-angle nature is encoded in eq. (2.1d), indicating that the lightlike vectors $\beta_1, \dots, \beta_K, \beta'_1, \dots, \beta'_M$ are all along distinct directions. The exponents a_i, b_k, c_k can be taken from the following sets:

$$a_i \in \mathbb{N}_+^\infty \equiv \mathbb{N}_+ \cup \{+\infty\} = \{1, 2, \dots, +\infty\}; \quad (2.2a)$$

$$b_k \in \mathbb{N}_+ = \{1, 2, \dots\}; \quad (2.2b)$$

$$c_k \in \mathbb{N}^\infty \equiv \mathbb{N} \cup \{+\infty\} = \{0, 1, \dots, +\infty\}. \quad (2.2c)$$

Note that the value $+\infty$ implies that p_i^μ and l_k^μ can be exactly lightlike, i.e., $p_i^2 = 0$ and $l_k^2 = 0$ for some i, k .

We define the *virtuality expansion* as the expansion in the parameter λ . All the examples discussed in section 1 are special cases of the virtuality expansion. The general configuration is illustrated in figure 3.

2.2 Momentum modes

We now formalize the momentum modes that are relevant in the virtuality expansion.

Notation of Modes.

Unless otherwise specified, we use the roman letter X to denote a general momentum mode. The full set of modes in the virtuality expansion follows certain patterns. To describe

them, we begin with three basic types:

$$\text{Hard mode } (H): \quad k_H^\mu \sim 1 \quad (\text{all its components}); \quad (2.3a)$$

$$\text{Collinear-}i \text{ mode } (C_i): \quad k_{C_i}^\mu = (k_{C_i} \cdot \bar{\beta}_i, k_{C_i} \cdot \beta_i, \mathbf{k}_{C_i \perp}) \sim (1, \lambda, \lambda^{1/2}); \quad (2.3b)$$

$$\text{Soft mode } (S): \quad k_S^\mu \sim \lambda \quad (\text{all its components}). \quad (2.3c)$$

As we will propose in section 4 and justify in section 5.3, all momentum modes considered in this paper can be denoted by $S^m C_i^n$, where $(m, n) \in \mathbb{N}^2$. The mode $S^m C_i^n$ can be regarded as the Hadamard product of m soft modes and n collinear- i modes.³ A momentum k_X^μ in the mode $X = S^m C_i^n$ scales as

$$k_X^\mu = (k_X \cdot \bar{\beta}_i, k_X \cdot \beta_i, \mathbf{k}_\perp) \sim (\lambda^m, \lambda^{m+n}, \lambda^{m+n/2}). \quad (2.4)$$

For a given momentum k , we use $\mathcal{X}(k)$ to denote its corresponding momentum mode. For a given edge $e \in \mathcal{G}$, we use $\mathcal{X}(e)$ to denote the mode of its line momentum. Later in section 3.2, we will use the same notation to denote the modes of certain subgraphs of \mathcal{G} .

Under this construction, the external momenta in (2.1) belong to the following modes:

$$\begin{aligned} \mathcal{X}(p_i) &: C_i, C_i^2, C_i^3, \dots, C_i^\infty; \\ \mathcal{X}(q_j) &: H; \\ \mathcal{X}(l_k) &: S, SC_i, SC_i^2, S^2, \dots, SC_i^\infty, \dots. \end{aligned} \quad (2.5)$$

Note that the mode C_i^∞ means that p_i^μ is precisely parallel to β_i^μ . In this way, all modes from the external kinematics can be expressed in the form $S^m C_i^n$, with $(m, n) \in (\mathbb{N}^\infty)^2$.

Virtuality Degree of a Mode.

For a given mode X , we denote its *virtuality degree* by $\mathcal{V}(X)$, defined as the power of λ in k_X^2 , where k_X is an X -mode momentum:

$$\mathcal{V}(X) = a, \quad \text{if } k_X^2 \sim \lambda^a. \quad (2.6)$$

It follows that $\mathcal{V}(S^m C_i^n) = 2m + n$.

Note that if the line momentum of an edge e , k_e^μ , is in the X mode, then its corresponding Lee-Pomeransky parameter x_e (see section 2.3) scales as:

$$x_e \sim \lambda^{-\mathcal{V}(X)}, \quad (2.7)$$

which is due to $x_e \sim (k_e^2)^{-1}$, a fact we will emphasize again in section 2.3.

³The special case $(m, n) = (0, 0)$ corresponds to the hard mode H .

Harder and Softer Modes.

We define a partial order of the modes as follows. Given two distinct modes X_1 and X_2 , we say X_1 is *harder than* X_2 , or X_2 is *softer than* X_1 , if for some vectors v we have

$$k_{X_1} \cdot v \gg k_{X_2} \cdot v, \quad (2.8)$$

and for *all* vectors w , we have

$$k_{X_1} \cdot w \gtrsim k_{X_2} \cdot w, \quad (2.9)$$

where “ \gtrsim ” means either “ \gg ” or “ \sim ”. In momentum space, this implies that the range of $k_{X_1}^\mu$ is a proper superset of the range of $k_{X_2}^\mu$. If X_1 is neither harder nor softer than X_2 , we call X_1 and X_2 *overlapping*.

For example, S is softer than C_i , which is clear from their scalings:

$$k_S^\mu \sim (\lambda, \lambda, \lambda), \quad k_{C_i}^\mu \sim (1, \lambda, \lambda^{1/2}). \quad (2.10)$$

More generally, if $X_1 = S^{m_1} C_i^{n_1}$ and $X_2 = S^{m_2} C_i^{n_2}$ with the same i , then X_1 is harder than X_2 if and only if $m_1 \leq m_2$ and $m_1 + n_1 \leq m_2 + n_2$. If instead $X_1 = S^{m_1} C_i^{n_1}$ and $X_2 = S^{m_2} C_j^{n_2}$ with $i \neq j$, then X_1 is harder than X_2 if and only if $m_1 + n_1 \leq m_2$.

A crucial property is that if X_1 is harder than X_2 , then $\mathcal{V}(X_1) < \mathcal{V}(X_2)$. Note that the converse does not hold: for example, $\mathcal{V}(S) = 2 < \mathcal{V}(C_i^3) = 3$, but S is not harder than C_i^3 .

2.3 Parametric representation, polytope, and spanning (2-)trees

We consider a massless Feynman integral dimensionally regularized in $D = 4 - 2\epsilon$ dimensions:

$$\mathcal{I}(\mathcal{G}) \equiv \mathcal{C} \cdot \int \prod_{i=1}^L \frac{d^D k_i}{i\pi^{D/2}} \prod_{e \in \mathcal{G}} \frac{1}{D_e^{\nu_e}}, \quad (2.11)$$

where \mathcal{C} is an overall factor, L is the number of independent loop momenta, and e represents the edges of the graph \mathcal{G} . In the scope of this work, we consider exclusively massless propagators, so $D_e = l_e^2 + i0$ here, with l_e^μ the line momentum of e . Below, we discuss the Lee-Pomeransky parameterization of \mathcal{I} , which allows us to relate the leading terms in the expansion to

- (1) points on the “lower facets” of a constructed polytope $\Delta(\mathcal{G})$,
- (2) the minimum spanning (2-)trees of \mathcal{G} .

These relations are the foundation of our later analyses.

Lee-Pomeransky Parameterization.

For convenience, we use \mathbf{s} to denote the set of scalar products formed among the external momenta of \mathcal{G} , so \mathcal{I} is a function of \mathbf{s} . The Lee-Pomeransky representation of $\mathcal{I}(\mathbf{s})$ reads [26]

$$\mathcal{I}(\mathbf{s}) = \mathcal{C}' \cdot \int_0^\infty \left(\prod_{e \in \mathcal{G}} \frac{dx_e}{x_e} \right) \cdot \left(\prod_{e \in \mathcal{G}} x_e^{\nu_e} \right) \cdot \left(\mathcal{P}(\mathbf{x}; \mathbf{s}) \right)^{-D/2}, \quad (2.12)$$

where the overall factor $\mathcal{C}' \equiv \frac{\Gamma(D/2)}{\Gamma((L+1)D/2 - \sum_{e \in \mathcal{G}} \nu_e) \prod_{e \in \mathcal{G}} \Gamma(\nu_e)} \mathcal{C}$. In the integrand above, we have used \mathbf{x} to denote the set of Lee-Pomeransky parameters x_1, \dots, x_N , with N being the number of edges of \mathcal{G} . $\mathcal{P}(\mathbf{x}; \mathbf{s})$ is called the Lee-Pomeransky polynomial, defined as

$$\mathcal{P}(\mathbf{x}; \mathbf{s}) \equiv \mathcal{U}(\mathbf{x}) + \mathcal{F}(\mathbf{x}; \mathbf{s}), \quad (2.13)$$

where $\mathcal{U}(\mathbf{x})$ and $\mathcal{F}(\mathbf{x}; \mathbf{s})$ are the first and second Symanzik polynomials, respectively:

$$\mathcal{U}(\mathbf{x}) = \sum_{T^1} \prod_{e \notin T^1} x_e, \quad \mathcal{F}(\mathbf{x}; \mathbf{s}) = \sum_{T^2} (-Q_{T^2}^2) \prod_{e \notin T^2} x_e. \quad (2.14)$$

The notations T^1 and T^2 denote a *spanning tree* and a *spanning 2-tree* of the graph \mathcal{G} , respectively. The momentum $Q_{T^2}^\mu$ is the total momentum flowing between the components of T^2 , and $Q_{T^2}^2$ is referred to as the *kinematic factor* of T^2 .

In contrast to the momentum representation, where each region is characterized by the scaling of loop momenta, in the Lee-Pomeransky representation each region R is characterized by the scaling of the parameters:⁴

$$x_e \sim \lambda^{v_e} \quad \forall e \in \mathcal{G}. \quad (2.15)$$

Let us remark that a key relation between the Lee-Pomeransky parameter x_e and the line momentum k_e (for massless e) is [27]

$$x_e \sim (k_e^2)^{-1} \sim \lambda^{-\mathcal{V}(X)}, \quad (2.16)$$

where X is the momentum mode of k_e and $\mathcal{V}(X)$ is its virtuality degree defined in section 2.2. This relation enables a translation between the momentum and parametric descriptions of a given region. If the scalings of k_e^μ are known, the scaling of x_e follows immediately from the above. Conversely, given the scalings of x_e , the scaling of k_e^2 is obtained directly; the scalings of the components of k_e^μ can then be deduced from momentum conservation, Landau equations, etc., a process that is sometimes nontrivial [24] but always feasible.

We now return to the Lee-Pomeransky-parameter description of a region, (2.15). Each term of $\mathcal{P}(\mathbf{x}; \mathbf{s})$, denoted by $s \cdot x_1^{r_1} x_2^{r_2} \cdots x_N^{r_N}$ with s being the kinematic coefficient, scales as

$$s \cdot x_1^{r_1} x_2^{r_2} \cdots x_N^{r_N} \sim \lambda^{v_1 r_1 + \cdots + v_N r_N + r_{N+1}}, \quad \text{if } s \sim \lambda^{r_{N+1}}. \quad (2.17)$$

The leading terms in the expansion then correspond to those with the minimum value of $v_1 r_1 + \cdots + v_N r_N + r_{N+1}$. Below we will construct a polytope Δ corresponding to the Feynman integral and see that the leading terms are located on the “lower facets” of $\Delta(\mathcal{G})$.

⁴More precisely, (2.15) describes the scaling behavior of facet regions. For hidden regions, one generally has $x_e = \mathcal{O}(\lambda^{v_e})$ with additional constraints on \mathbf{x} [12], which we do not investigate in this work.

Polytope and Lower Facets

Let us map each individual term $s \cdot x_1^{r_1} x_2^{r_2} \cdots x_N^{r_N}$ to a specific point \mathbf{r} in the $(N + 1)$ -dimensional space as follows:

$$s \cdot x_1^{r_1} x_2^{r_2} \cdots x_N^{r_N} \rightarrow \mathbf{r} \equiv (r_1, r_2, \dots, r_N, r_{N+1}) \quad \text{if } s \sim \lambda^{r_{N+1}}. \quad (2.18)$$

Next, we construct a polytope $\Delta(\mathcal{G})$, defined as the *convex hull* of all these points obtained from above.

A crucial observation is the correspondence between the leading terms in a region R and a certain *lower facet* of $\Delta(\mathcal{G})$, denoted by f_R . By “facet”, we refer to those N -dimensional boundaries of $\Delta(\mathcal{G})$, and “lower facets” refer to those facets whose inward-pointing normal vectors have a positive $(N + 1)$ -th entry. To see why this correspondence holds, first note that the points \mathbf{r} corresponding to the leading terms must span an N -dimensional space; otherwise, scaleless integrals would appear in the expansion. We denote this space by f_R . To see why f_R must be a lower facet of $\Delta(\mathcal{G})$, observe from (2.17) that those \mathbf{r} must all have the same, minimum value of

$$\mathbf{v} \cdot \mathbf{r} = v_1 r_1 + \cdots + v_N r_N + r_{N+1},$$

where \mathbf{v} has been defined as the following $(N + 1)$ -dimensional vector:

$$\mathbf{v} \equiv (v_1, \dots, v_N; 1). \quad (2.19)$$

On the one hand, the minimum value of $\mathbf{v} \cdot \mathbf{r}$ suggests that f_R must lie on the boundary of $\Delta(\mathcal{G})$, with \mathbf{v} normal to f_R and pointing into the polytope. On the other hand, the $(N + 1)$ -th entry of \mathbf{v} is positive (equal to 1). Thus f_R is a lower facet.

Weighted Graph and Minimum Spanning (2-)trees.

The leading terms in the expansion can also be related to the minimum spanning (2-)trees of \mathcal{G} . Let us begin by defining a weighted graph in general. We associate each edge $e \in \mathcal{G}$ with a real number $w(e)$, which we refer to as the *weight* of e . We then define the weight of a spanning tree T^1 or a spanning 2-tree T^2 as follows:

- $w(T^1)$ is the sum over $w(e)$ where e is *not* in T^1 ;
- $w(T^2)$ is the sum over $w(e)$ where e is *not* in T^2 , plus a *kinematic contribution* b if the kinematic factor $Q_{T^2}^2$ is $\mathcal{O}(\lambda^b)$.

Note that we exclude those spanning 2-trees with $Q_{T^2}^2 = 0$, as they do not appear in the \mathcal{F} polynomial. Summarizing the above, for each term of $\mathcal{P}(\mathbf{x}; \mathbf{s})$ the weight of its corresponding spanning (2-)tree T is

$$w(T) \equiv \sum_{e \notin T} w(e) + b \quad \text{if } s \sim \lambda^b. \quad (2.20)$$

Among all such T , we select those with the smallest weight and call them the *minimum spanning (2-)trees* of \mathcal{G} .

Recall that in the massless case, each power r_e in a term $s \cdot x_1^{r_1} x_2^{r_2} \cdots x_N^{r_N}$ of $\mathcal{P}(\mathbf{x}; \mathbf{s})$ is either 0 or 1. Setting $w(e) = v_e$ in eq. (2.20), we see that the minimum spanning (2-)trees of \mathcal{G} all minimize $\mathbf{v} \cdot \mathbf{r}$, the exact quantity that characterizes leading terms as discussed earlier. In this sense, every leading \mathcal{U} term corresponds to a minimum spanning tree of \mathcal{G} , and every leading \mathcal{F} term corresponds to a minimum spanning 2-tree of \mathcal{G} .

To clarify the notation above: for each edge $e \in \mathcal{G}$, we have let $\mathcal{V}(\mathcal{X}(e))$ denote the virtuality degree of its line-momentum mode, v_e the corresponding component of the region vector or the power of λ in the scaling of x_e , and $w(e)$ the weight assigned to it. These quantities are simply related by:

$$v_e = w(e) = -\mathcal{V}(\mathcal{X}(e)). \quad (2.21)$$

With this construction, the identification of regions can then be formulated as follows. *We aim to find all possible scalings of the Lee–Pomeransky parameters x_1, \dots, x_N such that the points associated with the minimum spanning (2-)trees of \mathcal{G} are sufficient to span a lower facet of the polytope $\Delta(\mathcal{G})$.* This is the core methodology of the region analysis in this paper.

3 Algebraic and graphical structure of modes

This section provides a more comprehensive examination of the structure of momentum modes from two perspectives. In section 3.1, we begin by introducing two fundamental operations, \wedge and \vee , defined on any two given modes, and explore several of their algebraic properties. Then, in section 3.2, we assign to each edge and vertex in a given region a specific mode and develop the concepts of mode subgraphs and mode components, which can be seen as fundamental building blocks of each region.

3.1 The \wedge and \vee operations

In section 2.2, we defined a partially ordered set (poset) of momentum modes ordered by the “softer than” (or “harder than”) relation. We will now define two operations on these modes, which correspond to the mathematical concepts of the *join* and *meet* within this poset.

For any two given modes X_1 and X_2 , we define

- $X_1 \wedge X_2$: the hardest mode that is softer than or equal to both X_1 and X_2 ;
- $X_1 \vee X_2$: the softest mode that is harder than or equal to both X_1 and X_2 .

These operations are well-defined: among all modes simultaneously softer than or equal to both X_1 and X_2 , there exists a unique hardest one; similarly, among all modes simultaneously harder than or equal to both, there exists a unique softest one. Explicit expressions confirming this are derived below.

Two properties follow immediately from the definition. First, both the operations \wedge and \vee satisfy *commutativity*:

$$X_1 \wedge X_2 = X_2 \wedge X_1, \quad X_1 \vee X_2 = X_2 \vee X_1. \quad (3.1)$$

Second, if X_1 is softer (harder) than X_2 , we have $X_1 \wedge X_2 = X_1$ (X_2), and if X_1 and X_2 are overlapping, then $X_1 \wedge X_2$ is softer than both X_1 and X_2 , while $X_1 \vee X_2$ is harder than both X_1 and X_2 .

We now derive explicit expressions for overlapping X_1 and X_2 .

We start from the case where the modes X_1 and X_2 are possibly (soft-)collinear to the same direction β_i , i.e., $X_1 = S^{m_1} C_i^{n_1}$ and $X_2 = S^{m_2} C_i^{n_2}$. In this case, one can assume $m_1 > m_2$ and $m_1 + n_1 < m_2 + n_2$ without loss of generality. Let us further denote $X_1 \wedge X_2 = S^{m_3} C_i^{n_3}$. From the text below (2.10), we must have $m_3 \leq m_1$ and $m_3 + n_3 \leq m_2 + n_2$, yielding the following candidates:

$$\begin{aligned} (m_3, n_3) &= (m_1, m_2 + n_2 - m_1), & \rightarrow & S^{m_1} C_i^{m_2+n_2-m_1}; \\ (m_3, n_3) &= (m_1 + 1, m_2 + n_2 - m_1 - 1), & \rightarrow & S^{m_1+1} C_i^{m_2+n_2-m_1-1}; \\ &\dots & &\dots \end{aligned}$$

The hardest mode from above is $S^{m_1} C_i^{m_2+n_2-m_1}$, so we have $X_1 \wedge X_2 = S^{m_1} C_i^{m_2+n_2-m_1}$. Similarly, $X_1 \vee X_2 = S^{m_2} C_i^{m_1+n_1-m_2}$. Note that these results hold when $m_1 = m_2$ and/or $m_1 + n_1 = m_2 + n_2$ as well.

We then consider the case where X_1 and X_2 are (soft-)collinear to distinct directions, i.e., $X_1 = S^{m_1} C_i^{n_1}$ and $X_2 = S^{m_2} C_j^{n_2}$ with $i \neq j$. Here, without loss of generality, we suppose $m_1 + n_1 \leq m_2 + n_2$. If we further have $m_1 + n_1 \leq m_2$, then X_1 is harder than X_2 , and we automatically have $X_1 \wedge X_2 = S^{m_2} C_j^{n_2}$ and $X_1 \vee X_2 = S^{m_1} C_i^{n_1}$.

If $m_2 \leq m_1 + n_1$ instead, let us denote $X_1 \wedge X_2 = S^{m_3} C_k^{n_3}$, which must be simultaneously softer than X_1 and X_2 . If $k = j$, then we need $m_1 + n_1 \leq m_3$ and $m_2 + n_2 \leq m_3 + n_3$ (from the text below (2.10)), whose solutions and corresponding modes are:

$$\begin{aligned} (m_3, n_3) &= (m_1 + n_1, m_2 + n_2 - m_1 - n_1), & \rightarrow & S^{m_1+n_1} C_j^{m_2+n_2-m_1-n_1}; \\ (m_3, n_3) &= (m_1 + n_1 + 1, m_2 + n_2 - m_1 - n_1 - 1), & \rightarrow & S^{m_1+n_1+1} C_j^{m_2+n_2-m_1-n_1-1}; \\ &\dots & &\dots \end{aligned}$$

among which the hardest mode is $S^{m_1+n_1} C_j^{m_2+n_2-m_1-n_1}$. If $k \neq j$ otherwise, then the only requirement we need is $m_3 \geq m_2 + n_2$ ($\geq m_1 + n_1$ automatically). The hardest mode satisfying this condition is $S^{m_2+n_2}$, which is softer than (or equal to, if $m_1 + n_1 = m_2 + n_2$) the mode $S^{m_1+n_1} C_j^{m_2+n_2-m_1-n_1}$. Therefore, we can always write $X_1 \wedge X_2 = S^{m_1+n_1} C_j^{m_2+n_2-m_1-n_1}$ in the case of $m_2 \leq m_1 + n_1$.

It remains to work out the mode $X_1 \vee X_2$ under the condition $m_2 \leq m_1 + n_1$, which further depends on the values of m_1 and m_2 . Let us consider the subcase $m_1 \leq m_2$ first and denote $X_1 \vee X_2 \equiv S^{m_4} C_\ell^{n_4}$. For $\ell = i$, requiring that $S^{m_4} C_\ell^{n_4}$ is harder than both $S^{m_1} C_i^{n_1}$ and $S^{m_2} C_j^{n_2}$ leads to $m_4 + n_4 \leq \min\{m_2, m_1 + n_1\} = m_2$ and $m_4 \leq m_1$ (from the text

below (2.10)). The solutions and corresponding modes are then:

$$\begin{aligned}
(m_4, n_4) &= (m_1, m_2 - m_1), & \rightarrow & S^{m_1} C_i^{m_2 - m_1}; \\
(m_4, n_4) &= (m_1 - 1, m_2 - m_1 + 1), & \rightarrow & S^{m_1 - 1} C_i^{m_2 - m_1 + 1}; \\
&\dots & &\dots
\end{aligned}$$

among which the softest mode is $S^{m_1} C_i^{m_2 - m_1}$. For $\ell \neq i$, requiring $S^{m_4} C_\ell^{n_4}$ to be harder than both $S^{m_1} C_i^{m_1}$ and $S^{m_2} C_j^{m_2}$ leads to only $m_4 + n_4 \leq m_1$. The hardest mode allowed is then S^{m_1} , which is softer than (or equal to, if $m_1 = m_2$) the mode $S^{m_1} C_j^{m_2 - m_1}$. As a result, we have $X_1 \vee X_2 = S^{m_1} C_i^{m_2 - m_1}$ for $m_1 \leq m_2$. Similarly, $X_1 \vee X_2 = S^{m_2} C_j^{m_1 - m_2}$ for $m_1 \geq m_2$.

The results are summarized in the following theorem.

Theorem 3.1. *Any two overlapping modes $X_1 = S^{m_1} C_i^{n_1}$ and $X_2 = S^{m_2} C_j^{n_2}$ fall into one of the following cases, with the corresponding expressions of $X_1 \wedge X_2$ and $X_1 \vee X_2$, up to swapping $1 \leftrightarrow 2$:*

1. $i = j$, $m_2 < m_1 \leq m_1 + n_1 < m_2 + n_2$:

$$X_1 \wedge X_2 = S^{m_1} C_i^{m_2 + n_2 - m_1} \text{ and } X_1 \vee X_2 = S^{m_2} C_i^{m_1 + n_1 - m_2}.$$

2. $i \neq j$, $m_1 \leq m_2 \leq m_1 + n_1 \leq m_2 + n_2$:

$$X_1 \wedge X_2 = S^{m_1 + n_1} C_j^{m_2 + n_2 - m_1 - n_1} \text{ and } X_1 \vee X_2 = S^{m_1} C_i^{m_2 - m_1}.$$

3. $i \neq j$, $m_2 \leq m_1 \leq m_1 + n_1 \leq m_2 + n_2$:

$$X_1 \wedge X_2 = S^{m_1 + n_1} C_j^{m_2 + n_2 - m_1 - n_1} \text{ and } X_1 \vee X_2 = S^{m_2} C_j^{m_1 - m_2}.$$

Theorem 3.1 can be regarded as an alternative definition of the \wedge and \vee operations for overlapping modes. Tables 1 and 2 list the results of these operations for several typical examples of X_1 and X_2 . The tables are only half filled, as the remaining entries follow from the commutativity of the operations, eq. (3.1).

So far we have shown that $X_1 \wedge X_2$ and $X_1 \vee X_2$ are well and uniquely defined for any two modes X_1 and X_2 . With this construction, the poset of modes is indeed a *lattice*, a crucial mathematical concept in order theory [28–30].

One immediate proposition is the *associativity* of \wedge and \vee , respectively:

$$(X_1 \wedge X_2) \wedge X_3 = X_1 \wedge (X_2 \wedge X_3), \quad (X_1 \vee X_2) \vee X_3 = X_1 \vee (X_2 \vee X_3). \quad (3.2)$$

To see this, let us denote $X_a = (X_1 \wedge X_2) \wedge X_3$ and $X_b = X_1 \wedge (X_2 \wedge X_3)$. By definition, X_a is simultaneously softer than or equal to X_1 , X_2 , and X_3 , thus it is also softer than or equal to $X_2 \wedge X_3$. Since X_b is the hardest mode that is simultaneously softer than or equal to both X_1 and $X_2 \wedge X_3$, we know that X_a is softer than or equal to X_b . The same logic in reverse shows X_b is softer than or equal to X_a . Thus $X_a = X_b$. The proof for \vee is analogous.

Associativity implies that $X_1 \wedge \dots \wedge X_n$ ($X_1 \vee \dots \vee X_n$) is exactly the hardest (softest) mode that is softer (harder) than or equal to all of X_1, \dots, X_n simultaneously.

\wedge	H	C_i	C_j	S	C_i^2	C_j^2	SC_i	SC_j	C_i^3	C_j^3
H	H	C_i	C_j	S	C_i^2	C_j^2	SC_i	SC_j	C_i^3	C_j^3
C_i		C_i	S	S	C_i^2	SC_j	SC_i	SC_j	C_i^3	SC_j^2
C_j			C_j	S	SC_j	C_j^2	SC_i	SC_j	SC_i^2	C_j^3
S				S	SC_i	SC_j	SC_i	SC_j	SC_i^2	SC_j^2
C_i^2					C_i^2	S^2	SC_i	S^2	C_i^3	S^2C_j
C_j^2						C_j^2	S^2	SC_j	S^2C_i	C_j^3
SC_i							SC_i	S^2	SC_i^2	S^2C_j
SC_j								SC_j	S^2C_i	SC_j^2
C_i^3									C_i^3	S^3
C_j^3										C_j^3

Table 1. Examples of the \wedge operation of momentum modes, where we assume $i \neq j$. Only the diagonal and upper-right portion of the table is shown; the remaining entries can be obtained using the commutativity of \wedge .

\vee	H	C_i	C_j	S	C_i^2	C_j^2	SC_i	SC_j	C_i^3	C_j^3
H	H	H	H	H	H	H	H	H	H	H
C_i		C_i	H	C_i	C_i	H	C_i	C_i	C_i	H
C_j			C_j	C_j	H	C_j	C_j	C_j	H	C_j
S				S	C_i	C_j	S	S	C_i	C_j
C_i^2					C_i^2	H	C_i^2	C_i	C_i^2	H
C_j^2						C_j^2	C_j	C_j^2	H	C_j^2
SC_i							SC_i	S	C_i^2	C_j
SC_j								SC_j	SC_i	C_j^2
C_i^3									C_i^3	H
C_j^3										C_j^3

Table 2. Examples of the \vee operation of momentum modes, where we assume $i \neq j$. Only the diagonal and upper-right portion of the table is shown; the remaining entries can be obtained using the commutativity of \vee .

One may wonder whether \wedge and \vee satisfy the distributive laws. The answer is *no*: taking $X_1 = SC_1$, $X_2 = SC_2$, and $X_3 = C_3^3$ (distinct directions), we have

$$(X_1 \wedge X_2) \vee X_3 = C_3^2 \neq C_3 = (X_1 \vee X_3) \wedge (X_2 \vee X_3), \quad (3.3)$$

$$(X_1 \vee X_2) \wedge X_3 = SC_3^2 \neq S^2C_3 = (X_1 \wedge X_3) \vee (X_2 \wedge X_3).$$

The observation above shows one difference between (\wedge, \vee) and (\cap, \cup) from set theory. The following theorem, meanwhile, describes a more striking distinction.

Theorem 3.2. For any set of modes $\{X_1, \dots, X_n\}$ with $n \geq 3$, there exist $a, b, c, d \in \{1, \dots, n\}$ such that

$$X_a \wedge X_b = X_1 \wedge \dots \wedge X_n, \quad X_c \vee X_d = X_1 \vee \dots \vee X_n. \quad (3.4)$$

In other words, to obtain $X_1 \wedge \dots \wedge X_n$ ($X_1 \vee \dots \vee X_n$) we can simply take two representatives of this set, X_a and X_b (X_c and X_d), and $X_a \wedge X_b$ ($X_c \vee X_d$) is the same mode.

Proof. To begin, note that it suffices to prove the theorem if we show the existence of $X_a \wedge X_b$ for $n = 3$, because the corresponding modes can be identified recursively for any larger n .

We next focus on the first equation of (3.4) and consider the special case where $X_i = C_i^{n_i}$ for $i = 1, 2, 3$.⁵ Among the three integers $\{n_i\}$, we take the largest two of them, n_a and n_b with $a, b \in \{1, 2, 3\}$. For example,

- $X_1 = C_1, X_2 = C_2^2, X_3 = C_3^2 \quad \Rightarrow \quad (a, b) = (2, 3);$
- $X_1 = C_1, X_2 = C_2, X_3 = C_3^2 \quad \Rightarrow \quad (a, b) = (1, 3) \text{ or } (2, 3).$

Without loss of generality, we can further assume $n_a \leq n_b$. It then follows that

$$X_a \wedge X_b = S^{n_a} C_b^{n_b - n_a} = X_1 \wedge X_2 \wedge X_3. \quad (3.5)$$

The second equality is because $S^{n_a} C_b^{n_b - n_a}$ is already softer than the third mode.

For any generic mode $X = S^m C_i^n$, there exists two collinear modes C_i^{m+n} and C_j^m ($j \neq i$), such that $X = C_i^{m+n} \wedge C_j^m$. We can thus use this decomposition to rewrite $X_1 \wedge X_2 \wedge X_3$ as the \wedge operation of 6 collinear modes, which equals the \wedge of two of them (denoted as $C_a^{n_a}$ and $C_b^{n_b}$) from the analysis above. The mode $C_a^{n_a} \wedge C_b^{n_b}$, meanwhile, also equals the \wedge of two modes generating $C_a^{n_a}$ and $C_b^{n_b}$. We thus complete the proof of the first equation of (3.4).

We finally show the existence of $c, d \in \{1, 2, 3\}$ such that $X_c \vee X_d = X_1 \vee \dots \vee X_n$. We first assume $X_i = S^{m_i} C_i^{n_i}$ with distinct $i = 1, 2, 3$. Similar as above, we take c and d such that m_c and m_d are the smallest among $\{m_1, m_2, m_3\}$, with $m_c \geq m_d$. Similar as above,

$$X_c \vee X_d = S^{m_d} C_d^{m_c - m_d} = X_1 \vee X_2 \vee X_3. \quad (3.6)$$

Thus the second equation of (3.4) is justified under this assumption.

It remains to consider the possibility that some overlapping modes in $\{X_1, \dots, X_n\}$ are (soft-)collinear along the same direction, i.e., $X_1 = S^{m_1} C_i^{n_1}$ and $X_2 = S^{m_2} C_i^{n_2}$ with the relation $m_2 < m_1 \leq m_1 + n_1 < m_2 + n_2$ (case 1 of theorem 3.1). In this case, however, one can always modify X_1 into a direction-independent mode $S^{m_1+n_1}$, because

$$S^{m_1+n_1} \vee S^{m_2} C_i^{n_2} = S^{m_1} C_i^{n_1} \vee S^{m_2} C_i^{n_2} (= S^{m_2} C_i^{m_1+n_1-m_2}), \quad (3.7)$$

as verified directly from the explicit expressions. The directions are now effectively distinct, so eq. (3.5) applies. \square

⁵Here we have taken all the collinear directions distinct, because if two modes are collinear to the same direction, then one of them is either softer or harder than the other. The mode $X_1 \wedge X_2 \wedge X_3$ then automatically reduces to the \wedge operation of two representatives that are collinear to distinct directions.

We remark that the choice of X_a and X_b in eq. (3.4) may not be unique. For example,

$$C_i \wedge C_j = C_1 \wedge \cdots \wedge C_n (= S), \quad C_i \vee C_j = C_1 \vee \cdots \vee C_n (= H), \quad (3.8)$$

for any $i, j \in \{1, \dots, n\}$ with $i \neq j$.

The following theorem relates the virtuality degrees of modes under the \wedge and \vee operations, revealing a particular elegance of the mode algebra:

Theorem 3.3. *Given any two modes X_1 and X_2 , their virtuality degrees can be related to those of $X_1 \wedge X_2$ and $X_1 \vee X_2$ simply as follows:*

$$\mathcal{V}(X_1) + \mathcal{V}(X_2) = \mathcal{V}(X_1 \wedge X_2) + \mathcal{V}(X_1 \vee X_2). \quad (3.9)$$

Proof. The equality reduces to a trivial relation $\mathcal{V}(X_1) + \mathcal{V}(X_2) = \mathcal{V}(X_1) + \mathcal{V}(X_2)$ if X_1 is softer or harder than X_2 . For overlapping X_1 and X_2 , the relation follows directly from theorem 3.1. For instance, in case 1 there, $\mathcal{V}(X_1) = 2m_1 + n_1$, $\mathcal{V}(X_2) = 2m_2 + n_2$, $\mathcal{V}(X_1 \wedge X_2) = m_1 + m_2 + n_2$, and $\mathcal{V}(X_1 \vee X_2) = m_1 + m_2 + n_1$. The remaining two cases are verified similarly. Hence, eq. (3.9) always holds. \square

A simple nontrivial example is $X_i = C_i$ for $i = 1, 2$. Here $X_1 \wedge X_2 = S$ and $X_1 \vee X_2 = H$, and eq. (3.9) reduces to $1 + 1 = 2 + 0$.

The relation (3.9) can be generalized to three or more modes, as stated in the following corollary.

Corollary 3.3.1. *Given any modes X_1, \dots, X_n ($n \geq 2$), we have*

$$\mathcal{V}(X_1) + \cdots + \mathcal{V}(X_n) \leq \mathcal{V}(X_1 \wedge X_2) + \cdots + \mathcal{V}(X_{n-1} \wedge X_n) + \mathcal{V}(X_1 \vee \cdots \vee X_n). \quad (3.10)$$

Proof. We show (3.10) by induction. This inequality at the special case of $n = 2$ reduces to eq. (3.9). Suppose it holds at $n = k$, then for $n = k + 1$, we have

$$\begin{aligned} \mathcal{V}(X_1) + \cdots + \mathcal{V}(X_{k+1}) &\leq \mathcal{V}(X_1 \wedge X_2) + \cdots + \mathcal{V}(X_{k-1} \wedge X_k) + \mathcal{V}(X_1 \vee \cdots \vee X_k) + \mathcal{V}(X_{k+1}) \\ &= \mathcal{V}(X_1 \wedge X_2) + \cdots + \mathcal{V}(X_{k-1} \wedge X_k) + \mathcal{V}((X_1 \vee \cdots \vee X_k) \wedge X_{k+1}) + \mathcal{V}(X_1 \vee \cdots \vee X_{k+1}) \\ &\leq \mathcal{V}(X_1 \wedge X_2) + \cdots + \mathcal{V}(X_{k-1} \wedge X_k) + \mathcal{V}(X_k \wedge X_{k+1}) + \mathcal{V}(X_1 \vee \cdots \vee X_{k+1}). \end{aligned} \quad (3.11)$$

In the first line above, we have applied the induction hypothesis. In the second line, we have used eq. (3.9) by regarding $X_1 \vee \cdots \vee X_k$ as a single mode. In the third line, we have used the defining property of \wedge and \vee operations: since the mode $X_1 \vee \cdots \vee X_k$ is harder than or equal to X_k , the mode $(X_1 \vee \cdots \vee X_k) \wedge X_{k+1}$ is harder than or equal to $X_k \wedge X_{k+1}$, thus $\mathcal{V}((X_1 \vee \cdots \vee X_k) \wedge X_{k+1}) \leq \mathcal{V}(X_k \wedge X_{k+1})$. \square

For general n , the mathematical induction above can be viewed as the following recursive procedure.

1, Apply theorem 3.3 to two selected modes X_1, X_2 and obtain

$$\mathcal{V}(X_1) + \mathcal{V}(X_2) = \mathcal{V}(X_1 \wedge X_2) + \mathcal{V}(X_1 \vee X_2). \quad (3.12)$$

2, Apply theorem 3.3 to three selected modes X_1, X_2, X_3 and obtain

$$\mathcal{V}(X_1 \vee X_2) + \mathcal{V}(X_3) = \mathcal{V}((X_1 \vee X_2) \wedge X_3) + \mathcal{V}(X_1 \vee X_2 \vee X_3).$$

Since $\mathcal{V}((X_1 \vee X_2) \wedge X_3) \leq \mathcal{V}(X_2 \wedge X_3)$, we have, in combination with eq. (3.12),

$$\mathcal{V}(X_1) + \mathcal{V}(X_2) + \mathcal{V}(X_3) \leq \mathcal{V}(X_1 \wedge X_2) + \mathcal{V}(X_2 \wedge X_3) + \mathcal{V}(X_1 \vee X_2 \vee X_3). \quad (3.13)$$

3, Apply theorem 3.3 to four selected modes $X_1, X_2, X_3, X_4, \dots$

It follows from above that the inequality in (3.10) comes purely from

$$\mathcal{V}((X_1 \vee X_2) \wedge X_3) \leq \mathcal{V}(X_2 \wedge X_3), \quad \mathcal{V}((X_1 \vee X_2 \vee X_3) \wedge X_4) \leq \mathcal{V}(X_3 \wedge X_4), \quad \dots$$

Therefore, the equality in (3.10) holds if and only if all the equalities in the $n - 1$ relations above hold. In fact, this is equivalent to a more general condition, which we state as another corollary of theorem 3.3.

Corollary 3.3.2. *The equality in (3.10) holds if and only if all the following conditions hold:*

$$\begin{aligned} (X_{i_1} \vee X_{i_2}) \wedge X_{i_3} &= X_{i_2} \wedge X_{i_3}, \\ (X_{i_1} \vee X_{i_2} \vee X_{i_3}) \wedge X_{i_4} &= X_{i_3} \wedge X_{i_4}, \\ &\dots \\ (X_{i_1} \vee \dots \vee X_{i_{n-1}}) \wedge X_{i_n} &= X_{i_{n-1}} \wedge X_{i_n}, \end{aligned} \quad (3.14)$$

with $\{i_1, \dots, i_n\}$ being any permutation of $\{1, \dots, n\}$ such that for each $k \in \{1, \dots, n\}$, the set $\{i_1, \dots, i_k\}$ consists of k consecutive integers.

Proof. The relations (3.12), (3.13), etc., hold for any permutation $\{1, \dots, n\} \rightarrow \{i_1, \dots, i_n\}$. However, when they are chained together to obtain (3.10), the right-hand side of the final inequality becomes

$$\mathcal{V}(X_{i_1} \wedge X_{i_2}) + \mathcal{V}(X_{i_2} \wedge X_{i_3}) + \dots + \mathcal{V}(X_{i_{n-1}} \wedge X_{i_n}).$$

For this sum to equal $\sum_{j=1}^{n-1} \mathcal{V}(X_j \wedge X_{j+1})$ (the desired right-hand side of (3.10)), every pair (i_{m-1}, i_m) appearing in the sum must be a pair of consecutive integers j and $j + 1$. That is, $i_k = \min\{i_1, \dots, i_{k-1}\} - 1$ or $i_k = \max\{i_1, \dots, i_{k-1}\} + 1$ for each $k \in \{2, \dots, n\}$. This is precisely the condition that $\{i_1, \dots, i_k\}$ consists of k consecutive integers, with

$$\begin{aligned} \mathcal{V}((X_{i_1} \vee X_{i_2}) \wedge X_{i_3}) &= \mathcal{V}(X_{i_2} \wedge X_{i_3}), \\ \mathcal{V}((X_{i_1} \vee X_{i_2} \vee X_{i_3}) \wedge X_{i_4}) &= \mathcal{V}(X_{i_3} \wedge X_{i_4}), \\ &\dots \\ \mathcal{V}((X_{i_1} \vee \dots \vee X_{i_{n-1}}) \wedge X_{i_n}) &= \mathcal{V}(X_{i_{n-1}} \wedge X_{i_n}). \end{aligned} \quad (3.15)$$

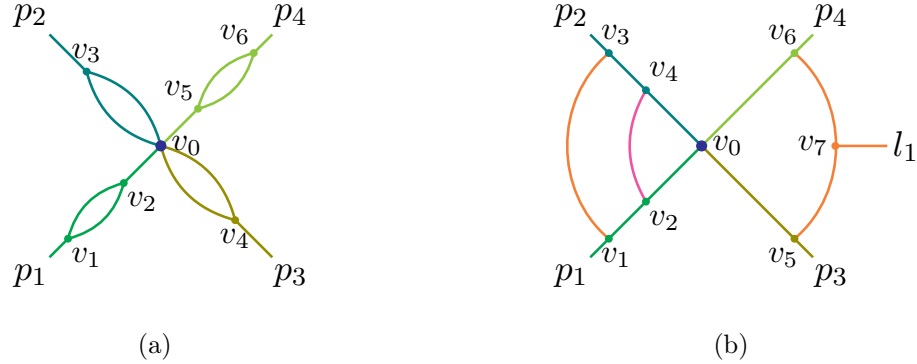


Figure 4. Two examples illustrating some special cases of mode subgraphs, where the external momenta and internal vertices are explicitly specified. (a): the H subgraph Γ_H consists of the vertex v_0 only. (b): Γ_H consists of the vertex v_0 only; additionally, the S^2 subgraph Γ_{S^2} consists of two connected components.

Note that the relations above are equivalent to eq. (3.14). Conversely, if any equality above becomes “ $<$ ” instead (i.e., some mode on the left-hand side of eq. (3.14) is harder than the mode on the right-hand side), the strict inequality would hold in (3.10). \square

Later in section 6.2, we will see the essential role theorem 3.3 and its corollaries play in characterizing general leading \mathcal{F} terms in any given expansion, as a necessity in deriving the region structure.

3.2 Mode subgraphs

We begin with the notion of graph adjacency. Two graphs Γ_1 and Γ_2 are called *adjacent* if there exists a vertex $v \in \Gamma_1$ and an edge $e \in \Gamma_2$ (or vice versa) such that v is an endpoint of e .

Mode subgraphs are defined as subgraphs formed by edges of a unique mode. For each given mode X , the corresponding X -mode subgraph—or simply X subgraph, denoted Γ_X —is defined to consist of the following edges and vertices:

- edges whose line momenta are in the X mode;
- vertices whose adjacent line momenta k_a^μ satisfy $\bigvee_a \mathcal{X}(k_a) = X$.

Note that an X subgraph may consist of a single vertex, and it may have several disconnected components. Two examples are shown in figure 4. In figure 4a we require each edge to be collinear to a certain p_i , with $p_i^2 \sim \lambda$ for $i = 1, 2, 3, 4$. In figure 4b we require the **rhodamine** edges to be in the S mode, the **orange** edges in the S^2 mode, and each solid edge collinear to a certain p_i , with $p_i^2 = 0$ for $i = 1, 2, 3, 4$ and $l_1^\mu \sim \lambda^2$. The mode subgraphs for these examples

are listed below (where we use e_{ij} to indicate the edge connecting v_i and v_j):

Figure 4a: $\Gamma_H = (\{v_0\}, \emptyset)$, $\Gamma_{C_1} = (\{v_1, v_2\}, \{e'_{12}, e''_{12}, e_{02}\})$, ...

Figure 4b: $\Gamma_H = (\{v_0\}, \emptyset)$, $\Gamma_{C_1^2} = (\{v_1\}, \{e_{12}\})$, $\Gamma_{C_1} = (\{v_2\}, \{e_{02}\})$, ...

$\Gamma_S = (\emptyset, \{e_{24}\})$, $\Gamma_{S^2} = (\emptyset, \{e_{13}\}) \cup (\{v_7\}, \{e_{57}, e_{67}\})$.

Note that the edges e'_{12} and e''_{12} denote the two distinct edges connecting v_1 and v_2 in figure 4a. In both examples, Γ_H consists of a single vertex v_0 . In figure 4b, Γ_{S^2} has two connected components, which are aside “U” above.

For a given mode subgraph Γ , we denote its corresponding mode by $\mathcal{X}(\Gamma)$ or $\mathcal{X}(\Gamma')$ for any subgraph $\Gamma' \subset \Gamma$. By assigning edges and vertices into different mode subgraphs as described, we obtain the following two properties.

1. $\Gamma_1 \cap \Gamma_2 = \emptyset$ for any two mode subgraphs γ_1 and γ_2 . In other words, the entire graph \mathcal{G} is a *disjoint union* of mode subgraphs.
2. Two adjacent mode subgraphs cannot have overlapping modes.

The first property follows by construction. assume the contrary: a vertex $v \in \Gamma_1$ is an endpoint of an edge $e \in \Gamma_2$, with $\mathcal{X}(\Gamma_1)$ overlapping with $\mathcal{X}(\Gamma_2)$. By definition, $\mathcal{X}(v) = \mathcal{X}(\Gamma_1)$. At the same time, $\mathcal{X}(v)$ must be equal to or harder than $\mathcal{X}(\Gamma_1) \vee \mathcal{X}(\Gamma_2)$, which is (strictly) harder than either $\mathcal{X}(\Gamma_1)$ or $\mathcal{X}(\Gamma_2)$ because these modes overlap. This yields a contradiction. Hence, adjacent mode subgraphs must have non-overlapping modes.

From this, we can make another observation: for a mode subgraph Γ_X , any vertex $v \notin \Gamma_X$ that is adjacent to Γ_X must correspond to a mode harder than X . This observation motivates the construction of *contracted mode subgraphs*. A *contracted X subgraph*, denoted $\tilde{\Gamma}_X$, is obtained from Γ_X by introducing an auxiliary vertex and identifying it with all vertices of other mode subgraphs that are adjacent to Γ_X .

Let us illustrate this concept with a few examples. In figure 4a, the only vertex not belonging to Γ_{C_1} but adjacent to it is the hard vertex v_0 . To obtain $\tilde{\Gamma}_{C_1}$, we simply replace v_0 by the auxiliary vertex of $\tilde{\Gamma}_{C_1}$. So we have

$$\tilde{\Gamma}_{C_1} = \Gamma_{C_1} \cup \{\text{auxiliary vertex}\},$$

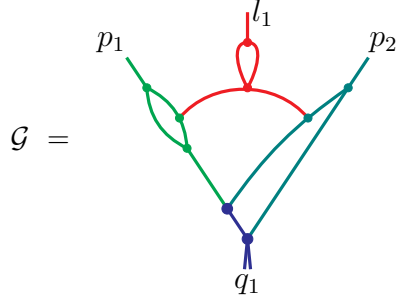
and the same conclusion for the C_2, C_3, C_4 subgraphs.

As a slightly more involved example, consider figure 4b. The vertices not belonging to Γ_S but adjacent to it are v_2 and v_4 . To construct $\tilde{\Gamma}_S$, we identify these vertices with an auxiliary vertex. Similarly, $\tilde{\Gamma}_{S^2}$ can be obtained. The graphs $\tilde{\Gamma}_S$ and $\tilde{\Gamma}_{S^2}$ are depicted below, with v_* representing their auxiliary vertices.

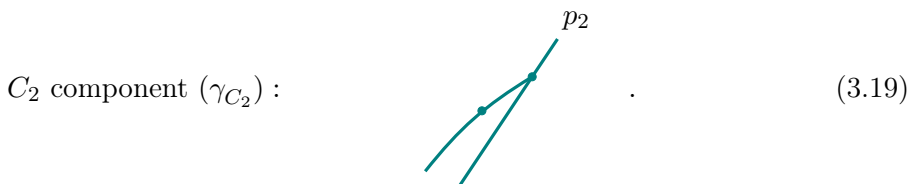
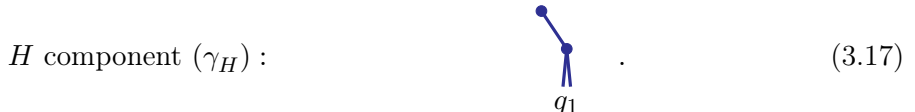
$$\tilde{\Gamma}_S = \text{Diagram of } \tilde{\Gamma}_S \text{ (pink loop with } v_*\text{)} ; \quad \tilde{\Gamma}_{S^2} = \text{Diagram of } \tilde{\Gamma}_{S^2} \text{ (orange double loop with } v_*\text{ and } l_1\text{)} . \quad (3.16)$$

For a given mode X , an X -mode component (or for simplicity, X component) is a subgraph of Γ_X that becomes a one-vertex irreducible (1VI) component of $\tilde{\Gamma}_X$. We use γ_X to denote general mode components. For example, figure 4b contains one S -mode component and two S^2 -mode components, as a direct conclusion from (3.16).

Let us understand this key concept from the following example:



In this graph, the mode subgraphs are marked in distinct colors. The H subgraph is in **blue**, the C_1 subgraph is in **green**, the C_2 subgraph is in **teal**, and the S subgraph is in **red**. The mode components are as follows.



One can verify that each of the mode components above does correspond to a 1VI component of the contracted mode subgraph.

Note that each individual mode component must be connected (a property we will use in section 6), because distinct connected components of Γ_X do not lie in the same 1VI component of $\tilde{\Gamma}_X$.

To end this section, we note a theorem that relates contracted mode subgraphs to minimum spanning trees of \mathcal{G} , as proved in ref. [24].

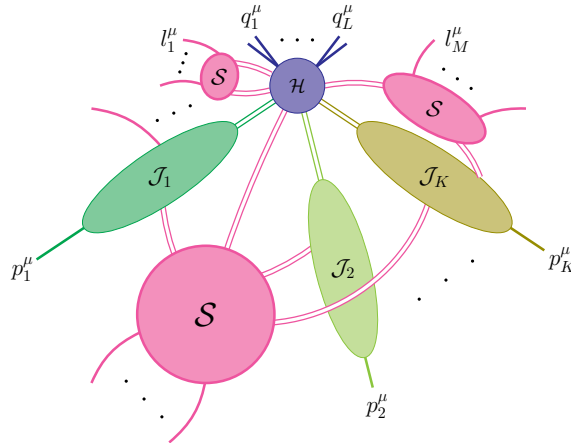


Figure 5. The fundamental pattern for facet regions in the virtuality expansion of massless wide-angle scattering. The graph comprises a connected hard subgraph \mathcal{H} , jet subgraphs $\mathcal{J}_1, \dots, \mathcal{J}_K$, and a soft subgraph \mathcal{S} . Off-shell external momenta q_1, \dots, q_L attach exclusively to \mathcal{H} . Each on-shell external momentum p_i attaches to its jet \mathcal{J}_i (if nonempty) or directly to \mathcal{H} (otherwise). Doubled lines represent any number of edges.

Theorem 3.4. *Let \mathcal{G} be a weighted graph such that for every $n \in \mathbb{N}$ the graph $\bigcup_{w(X) \geq -n} \Gamma_X$ (where $w(X) = -\mathcal{V}(X)$) is connected. Then, for any T^1 being a spanning tree of \mathcal{G} ,*

$$\tilde{\gamma}_X \cap T^1 \text{ is a spanning tree of } \tilde{\gamma}_X \text{ } (\forall \text{ mode } X) \Leftrightarrow T^1 \text{ is a minimum spanning tree of } \mathcal{G}.$$

This theorem will be used as follows. In section 5.1, we will see that the condition of the theorem, $\bigcup_{w(X) \geq -n} \Gamma_X$ for any $n \in \mathbb{N}$, is indeed satisfied as a consequence of the ‘First Connectivity Requirement’. Then, because every leading \mathcal{U} term corresponds to a minimum spanning tree of \mathcal{G} , it follows immediately that $\tilde{\gamma}_X \cap T^1$ is a spanning tree of $\tilde{\gamma}_X$ for each X . This gives a graph-theoretical perspective for characterizing leading \mathcal{U} terms and paves the way for a similar characterization of leading \mathcal{F} terms, which will be detailed in section 6.2.

4 The fundamental pattern

This section introduces the fundamental pattern that governs facet regions at all orders in the virtuality expansion of wide-angle kinematics, eq. (2.1). The pattern rests on two natural assumptions, which will be stated and justified.

In any such expansion, the relevant regions typically include a *hard region* where all loop momenta are hard, and several *infrared regions* where some loop momenta are collinear, soft, or in other infrared modes (as defined in section 2.2). All these regions conform to the fundamental pattern shown in figure 5.

In this pattern, the hard scattering of external momenta $\{p_i\}_{i=1}^K$ and $\{q_j\}_{j=1}^L$ occurs within a single connected hard subgraph \mathcal{H} with off-shell total momentum. Collinear line momenta (those parallel to a given p_i) flow through the corresponding jet subgraph \mathcal{J}_i . In

other words, large ($\mathcal{O}(1)$) momentum components thus traverse \mathcal{H} and the jets, while small momenta (vanishing in the infrared limit) are exchanged via the soft subgraph \mathcal{S} . The off-shell legs $\{q_j\}$ attach only to \mathcal{H} ; on-shell legs $\{p_i\}$ attach to \mathcal{J}_i (if $\mathcal{J}_i \neq \emptyset$) or \mathcal{H} directly (otherwise); soft external momenta $\{l_k\}_{k=1}^M$ may attach to \mathcal{H} , the jets $\mathcal{J} \equiv \bigcup_{i=1}^K \mathcal{J}_i$, and \mathcal{S} .

We emphasize the notational distinction: calligraphic letters $(\mathcal{H}, \mathcal{J}_i, \mathcal{S})$ denote subgraphs, while roman letters (H, C_i, S, \dots) denote momentum modes.

At this stage, we provisionally allow hard loops within $\mathcal{J} \cup \mathcal{S}$, although they will later be excluded by the ‘‘First Connectivity Theorem’’ (theorem 5.1). The subgraphs \mathcal{H} , \mathcal{J} , and \mathcal{S} are thus related to mode components as follows. \mathcal{H} consists solely of H components; each \mathcal{J}_i is the union of $C_i^{n_i}$ components ($n_i \in \mathbb{N}_+$) and possibly some H components; and S is the union of $S^m C_k^n$ components ($m \in \mathbb{N}_+$, $n \in \mathbb{N}$, k unrestricted) and possibly H components.

The fundamental pattern relies on the following assumptions.⁶

1. Infrared regions all correspond to singularities of the Feynman integrand, i.e., solutions of the Landau equations, whose configurations can be described by figure 5.
2. Configurations where the hard scattering occurs at multiple positions (Landshoff scattering) are not relevant to facet regions.

These assumptions are empirically well supported by numerous examples, though a fully rigorous proof remains elusive. In the remainder of this section, we explain why both are natural from physical and mathematical perspectives.

Infrared regions and Landau equations.

Let us demonstrate why the configuration in figure 5 is natural for infrared regions from the perspective of the Landau equations. If the Feynman integrand remains entirely regular as $\lambda \rightarrow 0$ in (2.1), expanding in the hard region alone would suffice to reproduce the full asymptotic series. However, when the integrand possesses singularities that cannot be avoided by contour deformation, contributions from neighborhoods of those singularities become essential, meaning additional infrared regions must be included.

It is known that all such singularities are captured by the Landau equations [31–33]. The physical solutions of the Landau equations (those with $\alpha_e \in [0, 1]$) admit a classical picture known as the *Coleman–Norton interpretation* [34]. For wide-angle scattering, this classical picture is precisely the structure shown in figure 5, provided the hard subgraph is connected—a point we will justify later. Therefore, figure 5 is a natural pattern for infrared regions.

Note that the Coleman–Norton interpretation, as a consequence of the Landau equations, already imposes strong constraints on the region structure. For example, once two jets depart from a hard subgraph, the vertices belonging to distinct jets are widely separated, so no short-distance propagators can connect them. Consequently, the structure in figure 6a cannot

⁶Besides these assumptions, one may wonder why it is legitimate to take $m, n \in \mathbb{N}$ in $S^m C_i^n$ —for example, why cannot the ‘‘semihard mode’’ $(\lambda^{1/2}, \lambda^{1/2}, \lambda^{1/2})$ be relevant. This follows from the ‘‘infrared-compatibility requirement’’, as we will explain later in section 5.3.

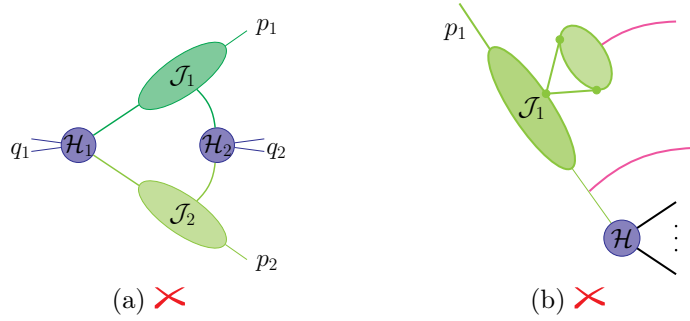


Figure 6. Configurations that cannot be solutions of the Landau equations because they do not conform with the Coleman–Norton interpretation. (a) short-distance propagators (those within \mathcal{H}_2) connecting vertices from two jets after scattering at \mathcal{H}_1 in advance. (b) the existence of a “vacuum bubble” within the jet \mathcal{J}_1 .

correspond to a solution of the Landau equations and thus does not represent a region. As another example, configurations containing a “vacuum bubble” within a jet (possibly connected by soft edges) also violate the Coleman–Norton interpretation. Therefore, figure 6b cannot be part of any region. These pathological configurations have been implicitly excluded in the fundamental pattern.

Another implication from the Landau equations is the absence of the Glauber mode (i.e., $(\lambda^a, \lambda^b, \lambda^c)$ with $a+b > 2c$) in \mathcal{S} . This is because in the wide-angle kinematics, one can always deform the integration contour to avoid pinches in the Glauber scaling [35].

Absence of Landshoff scattering configurations.

The Landau equations do not require the hard subgraph \mathcal{H} to be connected in general. Actually, hard scattering can occur at multiple disconnected locations, a pattern known as *Landshoff scattering* [36]. A three-loop example of two-to-two Landshoff scattering is shown in figure 7a. Here, the incoming momenta p_1 and p_2 split, scatter separately at the hard subgraphs \mathcal{H}_1 and \mathcal{H}_2 , and then merge into the outgoing momenta p_3 and p_4 . On top of this graph, one can also add soft momenta mediating between the \mathcal{H} and \mathcal{J} subgraphs. At higher loops, patterns with three or more connected components of \mathcal{H} can also arise.

We emphasize that Landshoff scattering *does* correspond to singularities of the Feynman integrand and can yield valid regions in the asymptotic expansion. For example, figure 7a has been verified in ref. [11] as a hidden regions in the “on-shell expansion”. What we demonstrate below, however, is that these configurations do *not* correspond to facet regions.

To see this, a crucial observation is that when the hard scattering occurs at a single \mathcal{H} , the $\mathcal{O}(1)$ components of line momenta from distinct jets are independent of each other. In contrast, in the Landshoff-scattering pattern, those components are correlated, imposing extra constraints on the scaling of the Lee–Pomeransky parameters. As a result, the Lee–Pomeransky-parameter description of facet regions, eq. (2.15), is not sufficient here.

For example, in figure 7a, the $\mathcal{O}(1)$ components of all the k_i , namely $k_i \cdot \bar{\beta}_i$, must approach

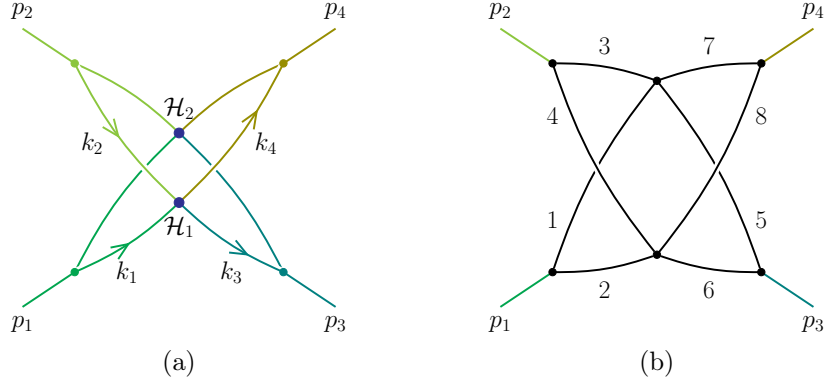


Figure 7. A three-loop $2 \rightarrow 2$ Landshoff scattering graph in the wide-angle kinematics, where the two hard-scattering components are \mathcal{H}_1 and \mathcal{H}_2 . (a) the momentum configuration, with different types of green representing different jets. (b) the parameterization of the edges for (4.2).

the same value in the infrared limit [37]. Assuming $p_i^2 \sim \lambda$, we have

$$\frac{k_i \cdot \bar{\beta}_i}{p_i \cdot \bar{\beta}_i} - \frac{k_j \cdot \bar{\beta}_j}{p_j \cdot \bar{\beta}_j} \sim \sqrt{\lambda} \text{ for any } i \neq j. \quad (4.1)$$

In the parametric representation, this additional constraint becomes [11]

$$\frac{x_1}{x_2} - \frac{x_3}{x_4} \sim \frac{x_3}{x_4} - \frac{x_5}{x_6} \sim \frac{x_5}{x_6} - \frac{x_7}{x_8} \sim \sqrt{\lambda}, \quad (4.2)$$

with the parameterization of edges shown in figure 7b. Note that each x_i is $\mathcal{O}(\lambda^{-1})$, so each individual ratio in (4.2) is $\mathcal{O}(1)$, while their differences scale as $\sqrt{\lambda}$. This explains why (2.15) alone is insufficient to characterize the region.

Based on the above, we propose that Landshoff scatterings cannot be characterized by the facet-region scaling behavior (2.15) in general. Therefore, each facet region must feature a single connected hard subgraph, as in figure 5.

5 Further requirements of the mode subgraphs

The fundamental pattern (figure 5) alone is far from sufficient to determine the complete list of regions. Typically, a given graph admits infinitely many configurations consistent with the fundamental pattern, because loops in \mathcal{S} have modes of the form $S^m C_i^m$, and we can make m arbitrarily large without violating momentum conservation. Even when all relevant modes in a graph are specified in advance, the number of configurations may still vastly exceed the number of actual regions, as many configurations are actually scaleless and therefore do not contribute to the asymptotic expansion. Hence, a crucial task is to derive a set of graph-theoretic rules that impose further constraints on the mode subgraphs, thereby providing a necessary and sufficient condition for a configuration to be a valid region.

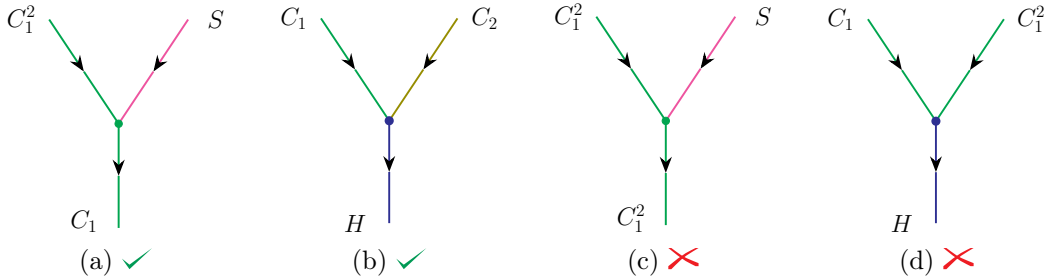


Figure 8. Some examples where the connection of mode subgraphs satisfies momentum conservation (in (a) and (b), marked with \checkmark) or violates momentum conservation (in (c) and (d), marked with \times).

As we will see, these constraints fall into two categories: *connectivity* and *infrared compatibility*—concepts that will be explained in detail. In section 5.1, we present the connectivity requirements, which comprise the First and Second Connectivity Theorems. In section 5.2, we describe the infrared-compatibility requirement. These requirements impose strong constraints not only on the connection of mode subgraphs, but also on the momentum modes allowed for a given external kinematics, as we demonstrate in section 5.3. In particular, we point out that the virtuality expansion *never features “cascading modes”*. Finally, in section 5.4 we summarize the subgraph requirements and illustrate how they match the known results for some special cases of virtuality expansion.

5.1 The connectivity requirements

As the name suggests, the connectivity requirements govern how the mode subgraphs in the fundamental pattern (figure 5) are interconnected.

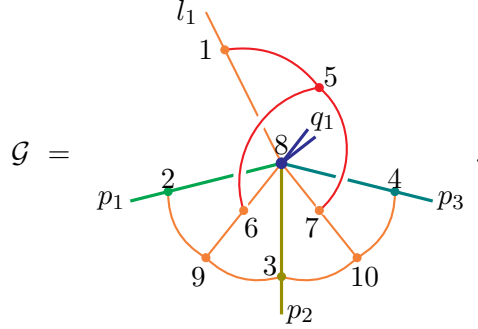
To begin, we note that momentum conservation already imposes implicit constraints on the connectivity of mode subgraphs. At any vertex v , we partition the incident line momenta into two nonempty sets $\{k_1, \dots, k_a\}$ (incoming) and $\{k_{a+1}, \dots, k_b\}$ (outgoing). Their modes then satisfy

$$\mathcal{X}(k_1) \vee \dots \vee \mathcal{X}(k_a) = \mathcal{X}(k_{a+1}) \vee \dots \vee \mathcal{X}(k_b).$$

Consequently, the configurations in figures 8a and 8b are allowed, whereas those in figures 8c and 8d are forbidden and thus cannot appear in any region. We will incorporate these constraints implicitly into the fundamental pattern rather than stating them as an independent requirement.

We now investigate a more subtle connectivity property. We observe that the union of all X -mode subgraphs with $\mathcal{V}(X)$ below any specific value is connected. Likewise, the union of all X -mode subgraphs with X harder than any specific mode is connected. As an explicit

example, consider the following region of the graph \mathcal{G} :



Here, the external kinematics consist of a C_1^2 -mode momentum p_1 , a C_2 -mode momentum p_2 , a C_3^2 -mode momentum p_3 , an off-shell (hard-mode) momentum q_1 , and an SC_4 -mode momentum (soft emission) l_1 . The vertices are labeled 1–10. The mode subgraphs are colored as follows: H mode (blue), C_1^2 mode (green), C_2 mode (olive), C_3^2 mode (teal), SC_i modes with $i = 1, 3, 4$ (orange), and S^2 mode (red). In other words,

$$\begin{aligned}\Gamma_H &= (\{v_8\}, \emptyset), & \Gamma_{C_2^2} &= (\{v_2\}, \{e_{28}\}), & \Gamma_{C_3} &= (\{v_3\}, \{e_{38}\}), & \Gamma_{C_4^2} &= (\{v_4\}, \{e_{48}\}), \\ \Gamma_{SC_1} &= (\{v_1\}, \{e_{18}\}), & \Gamma_{SC_2} &= (\{v_6, v_9\}, \{e_{29}, e_{69}, e_{39}, e_{68}\}), \\ \Gamma_{SC_4} &= (\{v_7, v_{10}\}, \{e_{4;10}, e_{7;10}, e_{3;10}, e_{78}\}), & \Gamma_{S^2} &= (\{v_5\}, \{e_{51}, e_{56}, e_{57}\}).\end{aligned}$$

The notation e_{ij} above denotes the edge connecting v_i and v_j . Let us now consider certain types of subgraphs of \mathcal{G} . The first type is $\bigcup_{\mathcal{V}(X) \leq n} \Gamma_X$:

$$\begin{aligned}\bigcup_{\mathcal{V}(X) \leq 0} \Gamma_X &= \text{blue line}, & \bigcup_{\mathcal{V}(X) \leq 1} \Gamma_X &= \bigcup_{\mathcal{V}(X) \leq 2} \Gamma_X = \text{green line}, \\ & & & \text{olive line}, \\ \bigcup_{\mathcal{V}(X) \leq 3} \Gamma_X &= \text{green line with orange loops}, & \bigcup_{\mathcal{V}(X) \leq 4} \Gamma_X &= \mathcal{G}. \tag{5.1}\end{aligned}$$

The second type is $\bigcup_{X' \text{ not softer than } X} \Gamma_{X'}$:

$$\begin{aligned}
\bigcup_{X' \text{ not softer than } H} \Gamma_{X'} &= \text{[Diagram of a blue double line with a blue dot at the vertex]} , \\
\bigcup_{X' \text{ not softer than } C_1^2} \Gamma_{X'} &= \text{[Diagram of a green line with a blue dot at the vertex, a vertical yellow line, and a red line branching off]} , \\
\bigcup_{X' \text{ not softer than } SC_1} \Gamma_{X'} &= \text{[Diagram of a green line with a blue dot at the vertex, a vertical yellow line, and an orange loop attached to the vertical line]} , \\
\bigcup_{X' \text{ not softer than } S^2} \Gamma_{X'} &= \text{[Diagram of a green line with a blue dot at the vertex, a vertical yellow line, and a red line branching off]} , \\
\Gamma_X &= \text{[Diagram of a green line with a blue dot at the vertex, a vertical yellow line, and an orange loop attached to the vertical line]} ,
\end{aligned}$$

(5.2)

The third type is $\bigcup_{X' \text{ harder than } X} \Gamma_{X'}$. By considering all possible modes X , we obtain the same four graphs as above. It is straightforward to verify that all these graphs are connected. In fact, this connectedness is a general requirement for any region of any graph to yield a scaleful expanded integral. This property is formalized as the *First Connectivity Theorem*.

Theorem 5.1 (First Connectivity Theorem). *For any region, the following subgraphs of \mathcal{G} must all be connected:*

- 1, $\bigcup_{\mathcal{V}(X) \leq n} \Gamma_X$ for any $n \in \mathbb{N}$,
- 2, $\bigcup_{X' \text{ not softer than } X} \Gamma_{X'}$ for any mode X ,
- 3, $\bigcup_{X' \text{ harder than } X} \Gamma_{X'}$ for any mode X .

The significance of this theorem is that once the connectedness of \mathcal{H} is confirmed (as part of the assumptions of the fundamental region pattern in figure 5), all other graphs in statement 1 with $n \in \mathbb{N}_+$ are automatically connected as well. With this said, configurations such as a hard loop inside a jet (figure 9a), or a soft loop surrounded by softer ones (figure 9b), etc., are all excluded from the regions by this theorem.

To prove theorem 5.1, a key observation is that the connectedness of the graphs in 1 automatically implies that of the graphs in 2 and 3. We formulate it as the following lemma.

Lemma 5.2. *If all the graphs $\bigcup_{\mathcal{V}(X) \leq n} \Gamma_X$ are connected ($n = 0, 1, 2, \dots$), then the following graphs are also connected.*

- $\bigcup_{X' \text{ not softer than } X} \Gamma_{X'}$ for any mode X ,
- $\bigcup_{X' \text{ harder than } X} \Gamma_{X'}$ for any mode X .

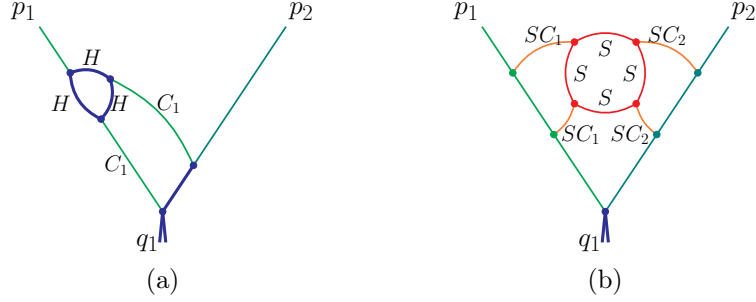


Figure 9. Examples of configurations that are scaleless and thus not facet regions due to the First Connectivity Theorem. (a): a hard loop (blue) inside a jet. (b): an S -mode loop (red) surrounded by softer edges.

Proof. Let us fix an arbitrary mode X_0 and consider the graph

$$\mathcal{G}_0 := \bigcup_{X' \text{ not softer than } X_0} \Gamma_{X'}.$$

Let v_1 and v_2 be any two vertices in \mathcal{G}_0 , and set $n_0 = \max\{\mathcal{V}(\mathcal{X}(v_1)), \mathcal{V}(\mathcal{X}(v_2))\}$. Since $\bigcup_{\mathcal{V}(X) \leq n} \Gamma_X$ is connected for any $n \in \mathbb{N}$, there exists a path $P_0 \subset \bigcup_{\mathcal{V}(X) \leq n_0} \Gamma_X$ connecting v_1 and v_2 . Every edge and vertex in P_0 has a mode X satisfying $\mathcal{V}(X) \leq n_0$. Since n_0 is the maximum of the virtuality degrees of v_1 and v_2 , no element in P_0 can be softer than X_0 . Therefore, P_0 is entirely contained within \mathcal{G}_0 , indicating that \mathcal{G}_0 is connected.

Now, to prove the connectedness of the remaining graphs, assume for contradiction, i.e., for some mode X , the graph $\mathcal{G} := \bigcup_{X' \text{ harder than } X} \Gamma_{X'}$ is disconnected. Among all such modes, choose X_* to be one with the smallest virtuality degree. By this minimality, the graph

$$\mathcal{G}_* := \bigcup_{X' \text{ harder than } X_*} \Gamma_{X'}$$

must consist of at least two connected components. One contains the hard subgraph \mathcal{H} . The other, denoted as γ_* , is necessarily a mode component (defined in section 3.2) with $\mathcal{X}(\gamma_*)$ harder than X_* . Let us pick a vertex $v_* \in \gamma_*$ and denote $n_* = \mathcal{V}(\mathcal{X}(\gamma_*))$. Since the graph $\bigcup_{\mathcal{V}(X) \leq n_*} \Gamma_X$ is connected, there exists a path P_* in this graph connecting v_* to \mathcal{H} . Meanwhile, since the two subgraphs γ_* and \mathcal{H} are disconnected from each other, the path must at some point leave the component γ_* . The first edge on P_* that lies outside γ_* is then an edge e_* not in \mathcal{G}_* but adjacent to γ_* (i.e., $e_* \in P_* \setminus \mathcal{G}_*$).

We now examine the mode of e_* :

- because $e_* \in P_*$, we have $\mathcal{V}(\mathcal{X}(e_*)) \leq n_* = \mathcal{V}(\mathcal{X}(\gamma_*))$;
- because $e_* \notin \mathcal{G}_*$, the mode $\mathcal{X}(e_*)$ is not harder than $\mathcal{X}(\gamma_*)$.

These relations force $\mathcal{X}(e_*)$ and $\mathcal{X}(\gamma_*)$ to be overlapping with each other. However, as established in section 3.2, adjacent mode components cannot have overlapping modes. This contradiction shows that our initial assumption was false; therefore, every graph $\bigcup_{X' \text{ harder than } X} \Gamma_{X'}$ is connected. \square

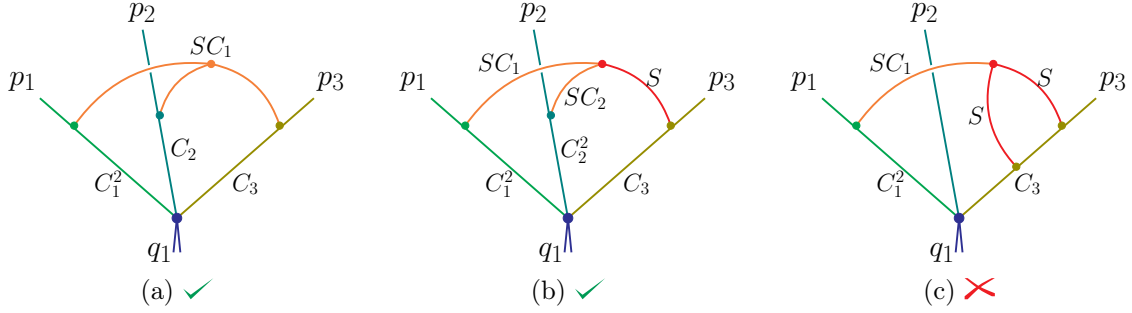


Figure 10. Two regions (a) and (b) of the same graph, and a non-region configuration (c) of a similar graph. In all these configurations, the external momenta satisfy $p_1^2 \sim p_2^2 \sim \lambda^2$, $p_3^2 \sim \lambda$, and $q_1^2 \sim 1$.

Given these arguments, proving theorem 5.1 reduces to establishing the connectedness of the graphs in 1, which still remains technically involved. A detailed demonstration of this fact is provided in section 6.1.

We now consider another essential observation: for each mode subgraph γ , its mode $\mathcal{X}(\gamma)$ should be “derivable” from either the harder neighbors or softer neighbors (including external momenta) of γ . That is, we expect $\mathcal{X}(\gamma)$ to be equal to either of the following:

- (1) $\bigwedge_i \mathcal{X}(\gamma_i)$, where γ_i are those adjacent to γ with harder weights,
- (2) $\bigvee_i \mathcal{X}(k_i)$, where k_i are those external momenta entering γ , or line momenta of softer-mode subgraphs adjacent to γ .

To illustrate, consider the three examples in figure 10, where the mode of each edge is specified. Their external momenta all satisfy $p_1^2 \sim p_2^2 \sim \lambda^2$, $p_3^2 \sim \lambda$, and $q_1^2 \sim 1$. All these configurations satisfy momentum conservation and theorem 5.1. One can further verify that figures 10a and 10b also meet the requirement stated above. For example, the SC_1 subgraph in figure 10a is adjacent to the harder-mode subgraphs $\gamma_{C_1^2}$, γ_{C_2} , and γ_{C_3} . By definition,

$$SC_1 = C_1^2 \wedge C_2 \wedge C_3.$$

The S subgraph in figure 10b is adjacent to softer-mode subgraphs γ_{SC_1} and γ_{SC_2} , and by definition,

$$S = SC_1 \vee SC_2.$$

In contrast, figure 10c contains a mode subgraph S that satisfies neither condition (1) nor (2) above, so it does not correspond to a valid region.

We now make two remarks. First, by theorem 3.2, in either $\bigwedge_i \mathcal{X}(\gamma_i)$ or $\bigvee_i \mathcal{X}(k_i)$, one can always choose exactly two representatives from the index set. Second, the requirement that γ is adjacent to γ_1, \dots , as described above, can actually be loosened to a generalized concept “relevant” (to be defined in section 5.2.2). We now formulate this relaxed connectivity requirement as the *Second Connectivity Theorem*.

Theorem 5.3 (Second Connectivity Theorem). *Each mode subgraph γ must satisfy at least either of the following conditions:*

- 1, γ is relevant to two harder-mode subgraphs γ_1 and γ_2 , with $\mathcal{X}(\gamma) = \mathcal{X}(\gamma_1) \wedge \mathcal{X}(\gamma_2)$;
- 2, two momenta k_1 and k_2 , from the external kinematics and/or relevant softer-mode subgraphs, enter γ , with $\mathcal{X}(\gamma) = \mathcal{X}(k_1) \vee \mathcal{X}(k_2)$.

The proof of this theorem will be deferred to the end of section 6.2.

5.2 The infrared-compatibility requirement

For any given region, its mode components must not only satisfy the connectivity requirements but also acquire their corresponding infrared scalings from the external kinematics, either directly or indirectly, otherwise the expanded integral would remain scaleless. This additional requirement, called the *infrared-compatibility requirement*, exhibits a particularly interesting “message-delivery pattern”. In the following, we first introduce the basic idea and then formulate the requirement precisely.

5.2.1 Basic idea: delivery of infrared scalings

Below we discuss possible mechanisms a mode component γ acquires its infrared scaling. We shall collate the mechanisms with some typical examples, which motivates the message-delivery pattern.

Mechanism 1.

The most straightforward way for a mode component γ to obtain its infrared scaling is from the external momenta directly. This happens when the total external momentum entering γ is precisely in the mode $\mathcal{X}(\gamma)$. In this case, one can construct a unitarity cut through γ , with the total incoming external momenta on one side. The momentum flowing across the cut is then of the mode $\mathcal{X}(\gamma)$.

An example is shown in figure 11, where the external momenta modes are C_1-C_4 . The mode subgraph Γ_H is colored **blue**, Γ_{C_1} **green**, and Γ_{C_2} **olive**. There are four mode components labeled in figure 11a: one C_1 component (γ_1), two C_2 components (γ_2 and γ_3), and one H component (γ_4). Each γ_i obtains its momentum scaling directly from the external kinematics, with the corresponding unitarity cut indicated in figure 11b. One can verify that the external momentum flowing across each cut has the same mode as the corresponding component. In other words, $\gamma_1-\gamma_4$ acquire their infrared scalings from the external kinematics.

Mechanism 2.

Suppose, for instance, that γ_1 and γ_2 have already acquired their infrared scalings from the external kinematics as above, i.e., external momenta entering γ_1 and γ_2 have the modes $\mathcal{X}(\gamma_1)$ and $\mathcal{X}(\gamma_2)$, respectively. Then any γ that is adjacent to both γ_1 and γ_2 and satisfying $\mathcal{X}(\gamma) = \mathcal{X}(\gamma_1) \wedge \mathcal{X}(\gamma_2)$ would also acquire its infrared scaling. In other words, such a

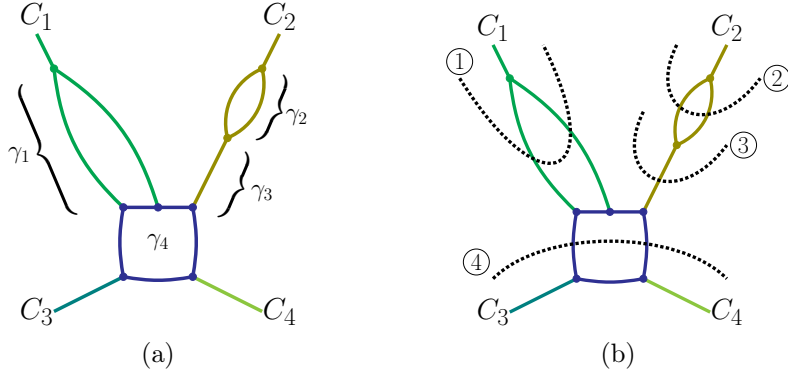


Figure 11. An example showing the case where all the mode components acquire their infrared scalings from the external kinematics. (a): the mode components $\gamma_1-\gamma_4$. (b): the unitarity cuts across the mode components, each isolating some external momentum.

γ acquires its scaling from two “harder-mode neighbors”, rather than from any $\mathcal{X}(\gamma)$ -mode external momentum.

The previously discussed figure 10a is an example, where the C_1^2 and C_3 components have already obtained their scalings from the external kinematics (recall $\mathcal{X}(p_1) = C_1^2$ and $\mathcal{X}(p_3) = C_3$ there), and the SC_1 component (note that $SC_1 = C_1^2 \wedge C_3$), which is adjacent to both, thereby obtains its infrared scaling as well.

Mechanism 3.

In certain situations, γ can acquire its infrared scaling from only a single (rather than multiple as in Mechanism 2) “harder-mode neighbor”. The simplest example illustrating this is the region in figure 2c, where $p_1^2 \sim \lambda$ while $p_2^2 = p_3^2 = 0$. Consider γ as the soft component exchanged among \mathcal{J}_1 , \mathcal{J}_2 , and \mathcal{J}_3 . Only \mathcal{J}_1 acquires its infrared scaling directly from the external momentum p_1 . The soft component γ , however, can still acquire its own scaling in this topology. Afterwards, it can in turn deliver scaling to the other jets (\mathcal{J}_2 and \mathcal{J}_3) adjacent to it, effectively acting as a “messenger”. Thus, the initial scaling from p_1 is propagated through the graph via γ .

Let us further recall that figures 2a and 2b both correspond to scaleless integrals. From this, one can tentatively conclude that soft components adjacent to three or more jets can act as messengers, while those adjacent to only two or fewer jets cannot. In fact, for configurations involving only modes H , C , and S , this has already been justified in section 4 of ref. [24].

In general, the infrared scaling of a mode component γ can also be acquired after several rounds of the delivery of infrared scaling. This is why we call it a “message-delivery pattern”. Consider, for example, the two configurations in figure 12, where $p_1^2 \sim \lambda$ while $p_i^2 = 0$ for all $i \neq 1$. As one can verify, figure 12a yields a scaleful integral while figure 12b is scaleless. From the perspective of the mechanisms above, in figure 12a the infrared scaling from p_1 can be delivered to all mode components via messengers (which are the three soft components γ_a , γ_b , and γ_c , each adjacent to three or more jets). In contrast, in figure 12b one soft component

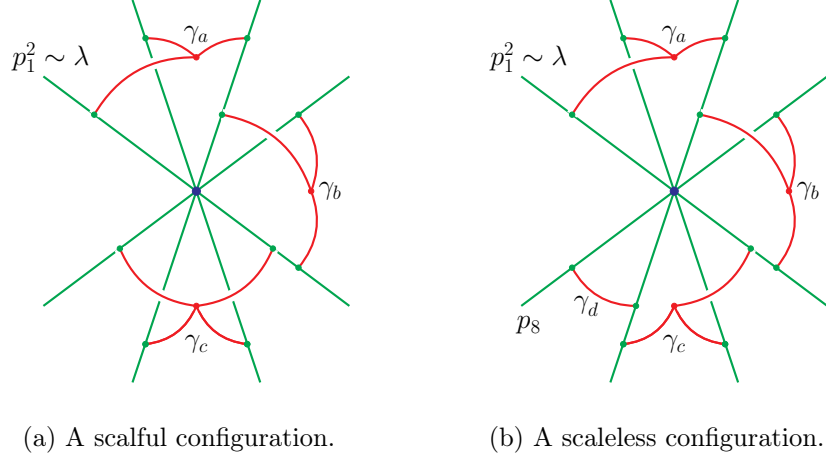


Figure 12. Two examples demonstrating the “message-delivery” mechanism. In these $4 \rightarrow 4$ scattering configurations, the external momentum p_1 has a small virtuality ($p_1^2 \sim \lambda$) while all other p_i are strictly on-shell ($p_i^2 = 0$ for $i \neq 1$). Green lines represent distinct collinear modes, and red curves represent the soft mode. The left example (a) corresponds to a scaleful expanded integral, whereas the right example (b) is scaleless. This difference arises because the “infrared message”, i.e., the small virtuality p_1^2 , can be delivered by the “messengers” to all other jets in (a), but not to \mathcal{J}_8 in (b).

γ_d is adjacent to exactly two jets, thus cannot acquire their infrared scalings through the message-delivery pattern.

As we will see, the preceding examples illustrate three distinct mechanisms by which a mode component can acquire its infrared scaling: (1) from the external kinematics directly, (2) from two harder-mode neighbors directly, and (3) from one harder-mode neighbor via a messenger. In the following, we formalize them on a rigorous footing for all-order analysis.

5.2.2 Formal constructions and statement

Motivated by the examples above, we now introduce a series of definitions to formulate the infrared-compatibility requirement.

Marginal Softness.

We start with a key relation between momentum modes. X_1 is called *marginally softer than* X_2 , if X_1 is softer than X_2 yet some components of the momentum k_{X_1} are of the same scale as the corresponding components of k_{X_2} . Alternatively, this means the leading contribution of $(k_{X_1} + k_{X_2})^2$ retains a dependence on k_{X_1} .

For example, the mode S is marginally softer than C_1 , whereas S^2 is not, as is evident

fact from the expansion of $(k_S + k_{C_1})^2$ and $(k_{S^2} + k_{C_1})^2$:

$$(k_S + k_{C_1})^2 = \underbrace{k_{C_1}^2}_{\mathcal{O}(\lambda)} + \underbrace{2k_{C_1} \cdot k_S}_{\mathcal{O}(\lambda)} + \underbrace{k_S^2}_{\mathcal{O}(\lambda^2)} \sim k_{C_1}^2 + 2k_{C_1} \cdot k_S, \quad \rightarrow \text{dependent on } k_S; \quad (5.3a)$$

$$(k_{S^2} + k_{C_1})^2 = \underbrace{k_{C_1}^2}_{\mathcal{O}(\lambda)} + \underbrace{2k_{C_1} \cdot k_{S^2}}_{\mathcal{O}(\lambda^2)} + \underbrace{k_{S^2}^2}_{\mathcal{O}(\lambda^4)} \sim k_{C_1}^2, \quad \rightarrow \text{independent of } k_{S^2}. \quad (5.3b)$$

A given mode can be marginally softer than several others. For example, S^2 is marginally softer than both SC_i and C_i^2 for any i . More generally, the modes for which S^m is marginally softer are precisely those of the form $S^{m-m'}C_i^{m'}$ with $m' \in \{1, \dots, m\}$.

Relevance of Mode Components.

We now extend this idea from modes to mode components γ_1 and γ_2 . We say γ_1 is relevant to γ_2 if the following conditions hold:

1. $\mathcal{X}(\gamma_1)$ is marginally softer than $\mathcal{X}(\gamma_2)$.
2. There exists a path P connecting γ_1 to γ_2 , such that for any two elements (edges or vertices) $a, b \in P$ where a is closer to γ_1 than b is, we have that $\mathcal{X}(a)$ is softer than or equal to $\mathcal{X}(b)$.

To illustrate this concept, recall the example in figure 10b. There, either SC_i component ($i = 1, 2$) is relevant to the C_i^2 and C_3 components. Notice that although an SC_i component is not adjacent to the C_3 component, they are connected via an S component, and along the path $SC_i \rightarrow S \rightarrow C_3$, the modes become progressively harder. The S component, in contrast, is relevant to the C_3 component only.

Messengers.

We now formulate the notion of messengers. Motivated by the examples in section 5.2.1, it acts as a soft “core” mediating infrared scaling among three or more harder-mode components.

Formally, a degree- m messenger, denoted by $\Gamma^{[m]}$, is a connected subgraph satisfying

1. The mode of every edge and vertex in $\Gamma^{[m]}$ is of the form $S^m C_i^{n_i}$, with $n_i \in \mathbb{N}$.
2. $\Gamma^{[m]}$ is relevant to *three or more* distinct mode components γ_i , such that
 - $\mathcal{X}(\gamma_i) = S^{m-m_i} C_i^{m_i+n_i}$ with $m_i \in \{1, \dots, m\}$, and for at least one i we have $n_i = 0$;
 - the total external momentum entering γ_i has mode $S^{m-m_i} C_i^{m_i+n_i+n'_i}$, with $n'_i \in \mathbb{N}^\infty$.

To understand this, consider the examples in figure 13, which show six degree- m messengers $\Gamma^{[m]}$ (dashed curves, with $m = 1$ in (a), (b), (d), and (e), while $m = 3$ in (c) and (f)), together with the $S^{m-m_i} C_i^{m_i+n_i}$ components $\Gamma^{[m]}$ is relevant to (solid lines). For simplicity, we show cases where $\Gamma^{[m]}$ is relevant to exactly three such components; configurations with four or

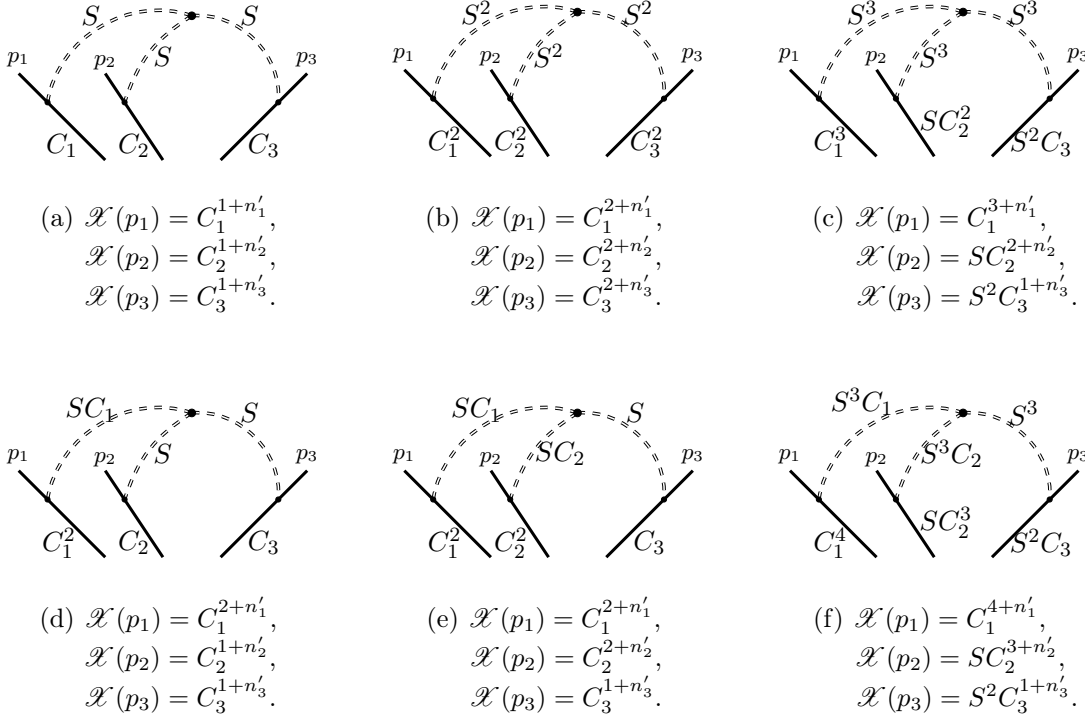


Figure 13. Six examples of messengers (represented by dashed curves) and their relevant $S^{m-m_i}C_i^{m_i+n_i}$ components (solid lines). The modes of the edges are specified in each sub-figure, and those of the external momenta p_1, p_2, p_3 are specified in the caption, with $n'_i \in \{0, 1, \dots, +\infty\}$.

more are analogous. The modes of the edges are specified in the figure, and those of the external momenta p_1, p_2, p_3 are specified in the caption, with $n'_i \in \mathbb{N}^\infty$.

Let us go through some representatives in figure 13. Figure 13a generalizes the aforementioned example of figure 2c (where we have $n'_1 = 0$ and $n'_2 = n'_3 = +\infty$). Figure 13c shows that the m_i in $S^{m-m_i}C_i^{m_i+n_i}$ components can have different values, and in this example, we have $m_1 = 3, m_2 = 2, m_3 = 1$, and $n_1 = n_2 = n_3 = 0$. Figure 13d shows that a messenger can consist of multiple mode components, and here, it consists of an SC_1 and an S components.

The general configuration of $\Gamma^{[m]}$, together with its relevant harder-mode components $\gamma_1, \dots, \gamma_I$ ($I \geq 3$), is depicted in figure 14.

Infrared Compatibility.

With the preceding constructions in place, we now define the central concept of infrared compatibility. The definition is recursive: a mode component γ is called *infrared compatible*, if it satisfies at least one of the conditions below (where ‘already confirmed’ components are those previously established as infrared compatible in the recursion):

- 1, the partial sum over momenta entering γ , which are exclusively from the external kinematics and already confirmed infrared-compatible subgraphs, is of the mode $\mathcal{X}(\gamma)$;

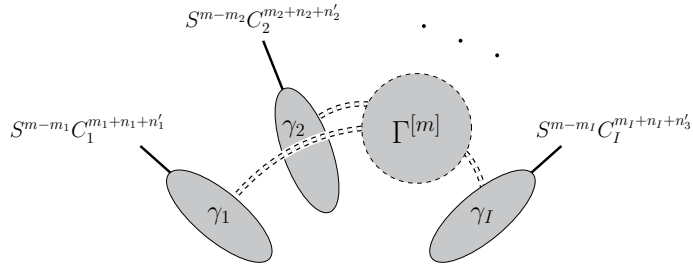


Figure 14. The general configuration of a degree- m messenger $\Gamma^{[m]}$ and its relevant components $\gamma_1, \dots, \gamma_I$ ($I \geq 3$). All modes inside $\Gamma^{[m]}$ are of the form $S^m C_i^{m_i}$ ($i \in \{1, \dots, I\}$). For each i , γ_i has the mode $S^{m-m_i} C_i^{m_i+n_i}$, and its external momentum mode is specified in the figure.

- 2, $\mathcal{X}(\gamma) = S^m$, and γ is contained in a degree- m messenger and relevant to some mode component γ_0 that is already confirmed infrared compatible;
- 3, $\mathcal{X}(\gamma) = S^m C_i^n$ ($n \in \mathbb{N}$), and γ is relevant to two mode components γ_1 and γ_2 that are already confirmed infrared compatible, with $\mathcal{X}(\gamma) = \mathcal{X}(\gamma_1) \wedge \mathcal{X}(\gamma_2)$.

The recursive nature of this definition is essential: the infrared compatibility of a component may depend on prior confirmation of others (typically, starting from components directly tied to external kinematics and propagating inward).

The elegance of this concept lies in the fact that, once the connectivity requirements are satisfied, infrared compatibility provides a necessary and sufficient condition for the expanded integral to be scaleful.

Theorem 5.4. *All mode components are infrared compatible.*

This theorem will be proved in section 6.3. At this point, let us verify its content from the aforementioned examples. The soft components in figures 2a and 2b are not infrared compatible (failing all three conditions above, and recursion does not occur), whereas all mode components in figure 2c are. This distinguishes the valid region in the latter case. As a more nontrivial illustration, all mode components in figure 12a become infrared compatible through the recursive process (with scaling propagating via the messengers $\gamma_a, \gamma_b, \gamma_c$). In contrast, figure 12b contains two non-infrared-compatible components: (1) the S component γ_d , and (2) the C_i component adjacent only to γ_d (and not to $\gamma_a, \gamma_b, \gamma_c$). Accordingly, the former is a valid region while the latter is not. Some other examples are provided in sections 7.1 and 7.2.

5.3 Implications from the infrared-compatibility requirement

The infrared-compatibility requirement is strong: it constrains not only the connections among subgraphs but also the mode structure. Moreover, it automatically implies the Second Connectivity Theorem. We discuss these consequences in this subsection.

As a first corollary of theorem 5.4, the ‘‘resolution’’ of the set of possible modes is fixed by the external kinematics.

Corollary 5.4.1. *If all the external momentum modes are in the form $S^m C_i^n$ with $m, n \in k\mathbb{N}$ (for a fixed $k \in \{2, 3, \dots\}$) and arbitrary i , then all the modes occurring in \mathcal{G} must be of this form as well.*

This explains why the momentum modes in the virtuality expansion (eq. (2.1)) can always be expressed as $S^m C_i^n$ with $m, n \in \mathbb{N}$. For example, suppose that for some kinematics satisfying eq. (2.1), there existed a region containing the “semihard” mode $S^{1/2} \equiv (\lambda^{1/2}, \lambda^{1/2}, \lambda^{1/2})$. Rescaling $\lambda \rightarrow \lambda^2$ would produce a configuration in which all external momentum modes are of the form $S^m C_i^n$ with $m, n \in \{2, 4, \dots\}$, while an S mode (i.e., S^1) would appear internally. Such a configuration is forbidden by the corollary, so the $S^{1/2}$ mode cannot actually occur in the virtuality expansion. The same argument excludes any other modes $S^m C_i^n$ for which $(m, n) \notin \mathbb{N}^2$

Proof. We prove the corollary by induction. In the process of verifying the infrared compatibility of any mode component γ , if all those previously confirmed infrared-compatible mode subgraphs have modes of the form $S^m C_i^n$ with $m, n \in \mathbb{N}$, then the three infrared-compatibility conditions force $\mathcal{X}(\gamma)$ to be of the same form as well. \square

Another essential implication from the infrared-compatibility requirement is the *absence of cascading modes* in the virtuality expansion. By *cascading modes*, we mean the phenomenon in which, for fixed external kinematics, the number of distinct momentum modes required to describe the regions grows unbounded (e.g., increasingly softer modes like S^k for arbitrarily large k) as the loop order increases. This has been observed in certain asymptotic expansions involving multiple on-shell massive momenta [24, 38] or on-shell spacelike-collinear momenta [39]. In contrast, within the scope of this work, i.e., the virtuality expansion in wide-angle kinematics (eq. (2.1)), cascading modes never occur.

Corollary 5.4.2. *For any fixed external kinematics satisfying eq. (2.1), the number of distinct momentum modes occurring at the amplitude level is bounded, independently of the loop order.*

Proof. Consider the modes of all partial sums (of one or more momenta) among the external momenta, which have nonzero virtuality:

$$S^{m_1} C_{i_1}^{n_1}, S^{m_2} C_{i_2}^{n_2}, \dots, S^{m_r} C_{i_r}^{n_r}, \quad (5.4)$$

where $n_1, \dots, n_r \neq +\infty$. Define an index

$$\kappa \equiv \max\{m_1 + n_1, \dots, m_r + n_r\}. \quad (5.5)$$

Every mode in (5.4), which corresponds to a partial sum of the external momenta, is harder than or equal to S^κ .

The proof proceeds by induction on the recursive confirmation of infrared compatibility (theorem 5.4). Components confirmed first (those directly tied to external kinematics) have modes harder than or equal to S^κ . At any stage, if all previously confirmed components satisfy

this bound, then any newly confirmed component (via any of the three infrared-compatibility conditions) inherits scaling from harder or equally soft sources and thus also satisfies the bound. Consequently, no mode component can be softer than S^κ , independent of loop order. This proves the absence of cascading modes. \square

The proof above also shows the softest possible mode S^κ associated with the given external kinematics. This information will prove useful for deriving the complete list of regions directly from our structural understanding, as discussed in section 5.4 and in later multiloop applications (section 7). Finally, we note that theorem 5.4 is strictly stronger than theorem 5.3.

Corollary 5.4.3. *If all mode components are infrared compatible, then the Second Connectivity Theorem (theorem 5.3) necessarily holds.*

Proof. Consider any mode component γ . Its infrared compatibility must be confirmed via one of the three conditions. If it is confirmed through condition 1 or 3, the statement of the Second Connectivity Theorem is automatically satisfied. If it is confirmed through condition 2, then γ has mode S^m and is contained in a degree- m messenger $\Gamma^{[m]}$. By the definition of messengers, $\Gamma^{[m]}$ is relevant to three or more distinct mode components γ_i (denoted $\gamma_1, \dots, \gamma_a$ with $a \geq 3$ for simplicity), where $\mathcal{X}(\gamma_i) = S^{m-m_i} C_i^{m_i+n_i}$ and one of the following holds:

- at least two of the n_1, \dots, n_a are zero;
- exactly one of the n_1, \dots, n_a is zero.

In both cases, γ fulfills the Second Connectivity Theorem. In the first case, there exist indices $i, j \in \{1, \dots, a\}$ with $n_i = n_j = 0$. The corresponding components γ_i and γ_j then have modes $S^{m-m_i} C_i^{m_i}$ and $S^{m-m_j} C_j^{m_j}$, respectively. γ is then relevant to both γ_i and γ_j , with $\mathcal{X}(\gamma) = \mathcal{X}(\gamma_i) \wedge \mathcal{X}(\gamma_j)$, which satisfies (the first part of) the Second Connectivity Theorem. In the second case, at least two indices $i, j \in \{1, \dots, a\}$ satisfy $n_i, n_j \neq 0$. By definition, $\Gamma^{[m]}$ contains components γ'_i and γ'_j that are relevant to γ_i and γ_j , respectively. We then have $\mathcal{X}(\gamma'_i) = S^m C_i^{m_i}$ and $\mathcal{X}(\gamma'_j) = S^m C_j^{m_j}$. Consequently, $\mathcal{X}(\gamma) = \mathcal{X}(\gamma'_i) \vee \mathcal{X}(\gamma'_j)$, which meets (the second part of) the Second Connectivity Theorem. \square

5.4 Summary and matching to known expansions

For better legibility, we collect the subgraphs requirements discussed in the preceding subsections and restate them below as the central conclusion of this work.

For any configuration consistent with the fundamental pattern (figure 5), it is a region *if and only if* both of the following conditions hold:

- 1, the graph $\bigcup_{\mathcal{V}(X) \leq n} \Gamma_X$ is connected for any $n \in \mathbb{N}$;
- 2, all mode components are infrared compatible.

Note that the second and third statements of the First Connectivity Theorem (theorem 5.1) are not included above because they follow from the first statement, as shown in lemma 5.2. Likewise, the Second Connectivity Theorem (theorem 5.3) is omitted because it is a consequence of the infrared-compatibility requirement, as established in corollary 5.4.3.

We now compare the subgraph requirements derived for the general virtuality expansion with those known for certain special cases. One typical expansion is the *on-shell expansion*, defined by the kinematics

$$p_i^2 \sim \lambda \quad (i = 1, \dots, K), \quad q_j^2 \sim 1 \quad (j = 1, \dots, L), \quad p_{i_1} \cdot p_{i_2} \sim 1 \quad (i_1 \neq i_2). \quad (5.6)$$

This corresponds to assigning each external momentum p_i in the virtuality expansion (2.1) into the C_i mode, while omitting all soft external momenta l_k .

Another similar expansion is the *soft expansion*, defined by

$$\begin{aligned} p_i^2 = 0 \quad (i = 1, \dots, K), \quad q_j^2 \sim 1 \quad (j = 1, \dots, L), \quad l_k^2 = 0 \quad (k = 1, \dots, M), \\ p_{i_1} \cdot p_{i_2} \sim 1 \quad (i_1 \neq i_2), \quad p_i \cdot l_k \sim q_j \cdot l_k \sim \lambda, \quad l_{k_1} \cdot l_{k_2} \sim \lambda^2 \quad (k_1 \neq k_2). \end{aligned} \quad (5.7)$$

In comparison with the on-shell expansion above, here all p_i are exactly on shell (i.e., in the C_i^∞ mode), and we include soft external momenta l_1, \dots, l_M , each exactly on-shell (i.e., in the SC_k^∞ mode).

All-order prescriptions for the region structures of these expansions have been derived in ref. [24]. A rigorous proof exists for the on-shell expansion regions, while the subgraph requirements for the soft expansion regions have been derived assuming a specific set of momentum modes. These derivations, however, are lengthy and technical, and apply only to those special expansions. Below, we demonstrate that from the understanding of region structures developed in this work, those results can be obtained from a surprisingly concise proof.

A first observation is that the softest possible mode in these expansions is S , independent of loop order. This follows from the proof of no cascading modes (corollary 5.4.2). For generic on-shell-expansion kinematics, the modes of all possible partial sums of external momenta are H and C_i (any i); for generic soft-expansion kinematics, they are H , C_i , and S . In both cases, the index κ from corollary 5.4.2 equals 1, confirming that S is the softest possible mode.

The fundamental pattern, figure 5, then reduces to figure 15a for the on-shell expansion, and figure 15b for the soft expansion. In these patterns, the jet \mathcal{J}_i contains only C_i -mode components, and \mathcal{S} contains only S -mode components. The First Connectivity Theorem is automatically satisfied.

Now consider additional constraints on the mode subgraphs. For both patterns in figure 15, the Second Connectivity Theorem requires:

- (1) momentum flowing into every 1VI component of \mathcal{H} has the hard mode;
- (2) momentum flowing into every 1VI component of \mathcal{J}_i has the C_i mode;
- (3) if an S component is attached by zero or one soft external momentum, then it must be adjacent to two or more jets.

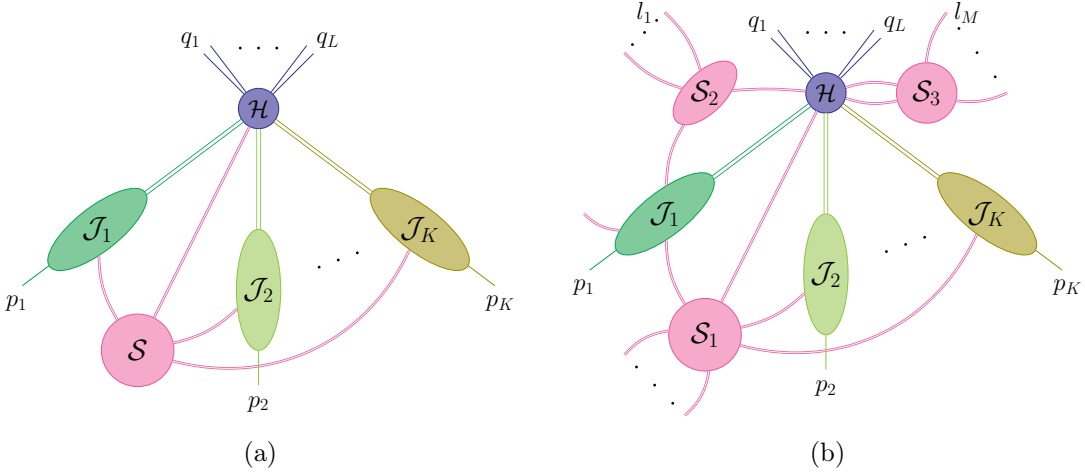


Figure 15. Generic facet regions in (a) the on-shell expansion and (b) the soft expansion.

The infrared-compatibility requirement further imposes:

- (4) every mode component is infrared compatible.

These requirements can be further simplified as follows. For the on-shell expansion, (1) and (2) are unchanged. Since there are no soft external momenta, (3) can be reduced to “every S component is adjacent to two or more distinct jets”. When these hold, all mode components are automatically infrared compatible, rendering (4) redundant.

For the soft expansion, (1)–(3) are unchanged. When these hold, (4) reduces to “all C_i components are infrared compatible”, which suffices to ensure that all S components are infrared compatible as well. These simplified requirements agree completely with those in previous works.

6 Proof of the subgraph requirements

This section, as the most technical part of this paper, aims to show that the subgraph requirements listed in section 5.4 are necessary and sufficient for any configuration of figure 5 to be a region. We begin by establishing some notation. For each term $s \cdot x_1^{r_1} x_2^{r_2} \dots x_N^{r_N}$ of $\mathcal{P}(\mathbf{x}; \mathbf{s})$, we use \mathbf{x}^r to represent it, and $T(\mathbf{r})$ to represent its corresponding spanning (2-)tree.

Our analysis will be based on two fundamental criteria for a given region R , which we term the *facet criterion* and the *minimum-weight criterion*.

Facet criterion: up to rescaling, the region vector \mathbf{v}_R is the unique vector normal to the facet f_R .

Minimum-weight criterion: for any leading term \mathbf{x}^r and any other term $\mathbf{x}^{r'}$ (including non-leading ones), we have $w(T(\mathbf{r})) \leq w(T(\mathbf{r}'))$.

The weight for spanning (2-)trees is defined in eq. (2.20). These criteria follow directly from the defining properties of lower facets and leading polynomials and help justify the subgraph requirements by repeatedly applying proof by contradiction. That is, to establish a given graph-theoretical property, we assume it is violated and exhaustively consider the possible configurations. Contradictions with either fundamental criterion above then rules out the violation, thus proving the property. The following lemma exemplifies this methodology.

Lemma 6.1. *Suppose γ is a mode component contained in $\mathcal{G}' \subseteq \mathcal{G}$ (where \mathcal{G}' can be either the entire Feynman graph or any of its subgraphs), such that $\mathcal{X}(\gamma)$ is harder than any of its adjacent edges, then for any leading term where \mathcal{G}' appears as a spanning tree T^1 , the graph $\gamma \cap T^1$ is a tree subgraph.*

Proof. As T^1 is a tree, the graph $\gamma \cap T^1$ contains no loops. It then remains to show its connectedness. Assume, for contradiction, that $\gamma \cap T^1$ is disconnected. Because γ itself is connected (by definition of a mode component), there must exist an edge $e \in \gamma \setminus T^1$ (i.e., in γ but not in T^1) connecting two distinct components of $\gamma \cap T^1$.

The graph $T^1 \cup e$ then contains a unique loop. This loop must include at least one edge e' that is adjacent to γ . We can now construct a new spanning tree

$$T'^1 \equiv T^1 \cup e \setminus e',$$

whose weight is given by

$$w(T'^1) = w(T^1) + w(e') - w(e). \quad (6.1)$$

Recall $w(e)$ denotes the weight associated with edge e , as defined in section 2.3. By the lemma's hypothesis, $\mathcal{X}(\gamma)$ is harder than $\mathcal{X}(e')$, which implies $w(e) > w(e')$. Therefore, $w(T'^1) < w(T^1)$, contradicting the minimum-weight criterion. This contradiction forces us to conclude that $\gamma \cap T^1$ is indeed connected, and hence a tree. \square

Using this same methodology, the following subsections will present more sophisticated analyses of the region structure. In section 6.1 we show the First Connectivity Theorem (theorem 5.1). Next we investigate the general structure of the leading terms in section 6.2. We shall classify them into certain types and characterize each type by its mode component structures, which allows for an immediate proof of the Second Connectivity Theorem (theorem 5.3). Having established the connectivity theorems, we proceed to show in section 6.3 that the infrared-compatibility requirement is necessary (theorem 5.4) and sufficient. To improve legibility, illustrative examples will accompany the key technical proofs.

6.1 Proof of the First Connectivity Theorem

Recall that in section 5.1, we have shown that the First Connectivity Theorem can be proved once those graphs of type 1 in its statement are proved connected. In what follows, we shall see their connectedness by contradiction.

Specifically, consider a mode component γ_* such that all the edges and vertices adjacent to γ_* have larger virtualities than $\mathcal{V}(\mathcal{X}(\gamma_*))$. As adjacent subgraphs cannot be overlapping with each other (see section 3.2), this further implies that all the edges adjacent to γ_* are softer than $\mathcal{X}(\gamma_*)$. By definition, the hard subgraph \mathcal{H} satisfies this condition, and the First Connectivity Theorem is equivalent to the statement that no other such γ_* would exist.

In principle, γ_* can consist of only a single vertex, but we only need to consider the cases where γ_* contains edges. The reason is, if one have managed to show that any such γ_* leads to a scaleless integral, then contracting γ_* to a single vertex amounts to removing its propagators from the integrand, and the integral would remain scaleless.

From now on, we assume the existence of such a nontrivial γ_* ($\neq \mathcal{H}$) in a given region R . We aim at proving the following statement:

$$\boxed{\text{The graph } T(\mathbf{r}) \cap \gamma_* \text{ is a spanning tree of } \gamma_*, \text{ for any leading term } \mathbf{x}^r.} \quad (6.2)$$

This, in turn, will imply a homogeneity condition as an additional constraint on the dimension of f_R . Let us use $\mathbf{n}_\gamma(\mathbf{r})$ to denote the degree of the parameters associated with the edges of γ in \mathbf{x}^r . Equivalently, $\mathbf{n}_\gamma(\mathbf{r})$ equals the number of edges of γ that are absent in the spanning (2-)tree $T(\mathbf{r})$. The homogeneity condition reads:

$$\mathbf{n}_{\gamma_*}(\mathbf{r}) = L(\gamma_*), \text{ for any leading term } \mathbf{x}^r. \quad (6.3)$$

The resulting expanded integral will therefore be scaleless. This contradicts the fundamental premise that the expansion procedure yields scaleful contributions for the region R . Consequently, our assumption that a nontrivial mode component $\gamma_* \neq \mathcal{H}$ with the stated property exists in R must be false. This establishes the connectedness of the graphs of type 1, completing the proof.

Proof of statement (6.2). To start with, note that $T(\mathbf{r}) \cap \gamma_*$ contains no loops. So the later analyses will focus on showing the connectedness of $T(\mathbf{r}) \cap \gamma_*$.

Let us consider the possibility that the graph $T(\mathbf{r}) \cap \gamma_*$ contains multiple connected components. From lemma 6.1, such a possibility is excluded if all the vertices of $T(\mathbf{r}) \cap \gamma_*$ lie in the same tree component. Therefore, \mathbf{x}^r can only be a leading \mathcal{F} term, and γ_* intersects both components of $T(\mathbf{r})$, which we shall denote by $T^2(\mathbf{r})$ from now on.

Since γ_* is itself connected, there exists an edge $e_0 \in \gamma_* \setminus T^2(\mathbf{r})$ whose endpoints, v_A and v_B , lie in the two distinct components of $T^2(\mathbf{r})$. We denote these components by $t(\mathbf{r}; A)$ and $t(\mathbf{r}; B)$, respectively. We will now exhaust the possible configurations of $T^2(\mathbf{r})$ and exclude them one by one.

- I. If the entire graph \mathcal{G} has an off-shell external momentum q_j^μ with $q_j^2 \sim 1$, then without loss of generality, we may assume it attached to $t(\mathbf{r}; A)$. The configuration of $T^2(\mathbf{r})$ is then shown in figure 16a, where we have used a dashed line to emphasize that $e_0 \notin T^2(\mathbf{r})$. From v_A to q_j^μ there is a unique path $P_A \subset t(\mathbf{r}; A)$, and since the edges attaching to γ_*

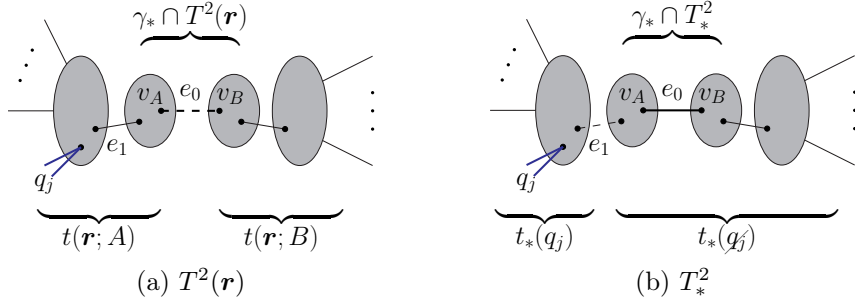


Figure 16. The comparison of the two spanning 2-trees, $T^2(\mathbf{r})$ and T_*^2 , in case **I**, where each blob represents a tree subgraph. The two components of each spanning 2-tree is specified. The two blobs in the middle, which v_A and v_B belongs to, are contained in γ_* .

are all softer than $\mathcal{X}(\gamma_*)$, there must be an edge $e_1 \in P_A$ with $w(e_1) < w(e_0)$. We can now construct the following spanning 2-tree (see figure 16b):

$$T_*^2 \equiv T^2(\mathbf{r}) \cup e_0 \setminus e_1. \quad (6.4)$$

The weight of T_*^2 then satisfies

$$w(T_*^2) \leq w(T^2(\mathbf{r})) + w(e_1) - w(e_0) < w(T^2(\mathbf{r})). \quad (6.5)$$

The first inequality follows because $Q_{T_*^2}^2 \gtrsim Q_{T^2(\mathbf{r})}^2$ (recall that Q_{T^2} denotes the total momentum flowing between the components of T^2); therefore, the kinematic contribution to $w(T_*^2)$ —which is the power of λ in $Q_{T_*^2}^2$, see eq. (2.20)—cannot exceed the kinematic contribution to $w(T^2(\mathbf{r}))$. A detailed justification is provided in appendix A.1. The second inequality uses $w(e_1) < w(e_0)$, which holds by construction. Inequality (6.5) thus contradicts the minimum-weight criterion, ruling out the presence of any off-shell external momenta.

If no external momenta is off shell, there must exist four or more p_i , and one component of $T^2(\mathbf{r})$ must be attached by at least two of them. Now we suppose p_1 and p_2 are attached to $t(\mathbf{r}; A)$, and define two specific paths $P_1, P_2 \subset t(\mathbf{r}; A)$, which connect v_A to the external momenta p_1 and p_2 respectively. By construction, both paths start from v_A , possibly sharing some initial edges and vertices (which constitute a sub-path $P_1 \cap P_2$), before diverging and ending at p_1 and p_2 . We now inspect whether or not $P_1 \cap P_2$ is contained in γ_* (equivalently, whether P_1 and P_2 separate inside or outside γ_*).

II. For $P_1 \cap P_2 \not\subset \gamma_*$, which means that P_1 and P_2 separate *outside* γ_* , there must exist an edge $e_1 \in P_1 \cap P_2$ that is adjacent to γ_* , as is shown in figure 17a. By construction, $w(e_1) < w(e_0)$. We can thus follow the analysis in case **I** above to construct another spanning 2-tree, $T_*^2 \equiv T^2(\mathbf{r}) \cup e_0 \setminus e_1$ (see figure 17b), with $w(T_*^2) < w(T^2(\mathbf{r}))$ due to the same reason as (6.5). (Note that the only difference between this case and case **I** is

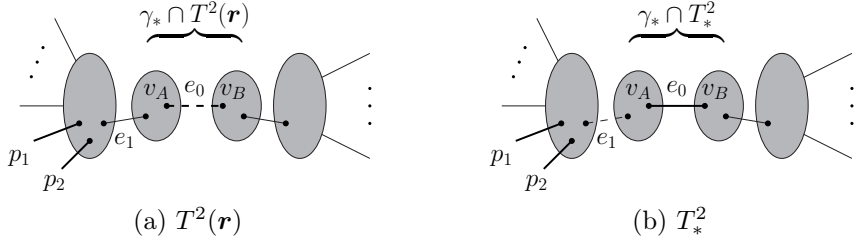


Figure 17. The comparison of the two spanning 2-trees, $T^2(\mathbf{r})$ and T_*^2 , in case **II**.

that q_j is replaced by p_1 and p_2 .) The same violation of the minimum-weight criterion then excludes this possibility as well.

From the preceding analyses, the remaining possible configurations of $T^2(\mathbf{r})$ require that $P_1 \cap P_2 \subset \gamma_*$, i.e., the paths P_1, P_2, \dots (possibly some other paths) separate at some vertex *within* γ_* before ending at p_1, p_2, \dots , respectively. To further rule out these configurations, we consider the location of the hard subgraph \mathcal{H} . First, we argue that \mathcal{H} *cannot* have nonzero intersections with both $t(\mathbf{r}; A)$ and $t(\mathbf{r}; B)$ simultaneously.

III. If both $\mathcal{H} \cap t(\mathbf{r}; A) \neq \emptyset$ and $\mathcal{H} \cap t(\mathbf{r}; B) \neq \emptyset$, there is then an edge $e_H \in \mathcal{H} \setminus T^2(\mathbf{r})$ connecting the two components of $T^2(\mathbf{r})$. The spanning tree $T^1(\mathbf{r}_1) \equiv T^2(\mathbf{r}) \cup e_H$ has the weight

$$w(T^1(\mathbf{r}_1)) = w(T^2(\mathbf{r})) - w(e_H) - \mathcal{V}(Q_{T^2(\mathbf{r})}) \leq w(T^2(\mathbf{r})), \quad (6.6)$$

where we have used $w(e_H) = 0$ and $\mathcal{V}(Q_{T^2(\mathbf{r})}) \in \mathbb{N}$ in the inequality. From the minimum-weight criterion, the equality must hold, immediately indicating: (1) $\mathcal{V}(Q_{T^2(\mathbf{r})}) = 0$, i.e., the momentum flowing between the components of $T^2(\mathbf{r})$ is $\mathcal{O}(1)$; (2) $\mathbf{x}^{\mathbf{r}_1}$ is a leading \mathcal{U} term because $w(T^1(\mathbf{r}_1)) = w(T^2(\mathbf{r}))$.

Let us then add e_0 to the spanning tree $T^1(\mathbf{r}_1)$ and obtain a graph $T^1(\mathbf{r}_1) \cup e_0$. From the defining property of spanning trees, there is a unique loop in this graph. This loop, by construction, simultaneously contains $e_H \in \mathcal{H}$ and $e_0 \in \gamma_*$. Since \mathcal{H} is not adjacent to γ_* (recall that all the edges adjacent to γ_* are softer than $\mathcal{X}(\gamma_*)$), this loop must also contain some edge e_1 that is adjacent to γ_* , with $w(e_1) < w(e_0)$. Then the following spanning tree $T^1(\mathbf{r}') \equiv T^1(\mathbf{r}_1) \cup e_0 \setminus e_1$ has a smaller weight:

$$w(T^1(\mathbf{r}')) = w(T^1(\mathbf{r}_1)) + w(e_1) - w(e_0) < w(T^1(\mathbf{r}_1)). \quad (6.7)$$

The minimum-weight criterion is again violated, ruling out this possibility.

Therefore, all the \mathcal{H} vertices must simultaneously lie in either $t(\mathbf{r}; A)$ or $t(\mathbf{r}; B)$, and from now on, we assume they are in $t(\mathbf{r}; A)$.

A more detailed depiction of $T^2(\mathbf{r})$ is then shown in figure 18a. Here, m on-shell external momenta p_1, \dots, p_m are attached to $t(\mathbf{r}; A)$, and n others p_{m+1}, \dots, p_{m+n} to $t(\mathbf{r}; B)$, with

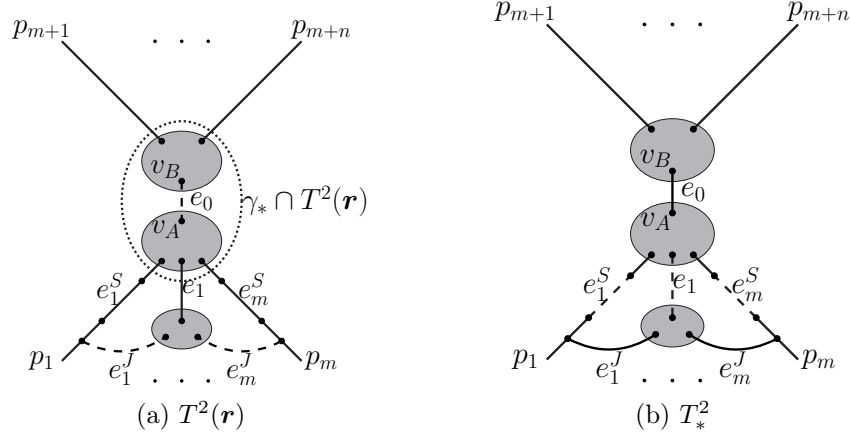


Figure 18. The comparison of the two spanning 2-trees, $T^2(\mathbf{r})$ and T_*^2 , in case **IV**. The subgraph $\gamma_* \cap T^2(\mathbf{r})$ is enclosed by the dotted curve. The three gray blobs, from top to bottom, represent $\gamma_* \cap t(\mathbf{r}; B)$, $\gamma_* \cap t(\mathbf{r}; A)$, and $\mathcal{H} \cap t(\mathbf{r}; A)$, respectively.

$m+n \geq 4$. The m paths in $t(\mathbf{r}; A)$ from v_A to each p_i ($1 \leq i \leq m$) share no edges outside γ_* for any two of them. Similarly, the n paths in $t(\mathbf{r}; B)$ from v_B to each p_{m+i} ($1 \leq i \leq n$) share no edges outside γ_* for any two of them. The subgraph $\mathcal{H} \cap t(\mathbf{r}; A)$, which by lemma 6.1 is a tree (more precisely, a spanning tree of \mathcal{H}), forms part of $t(\mathbf{r}; A)$.⁷ We denote this scenario as the final case **IV** and analyze it below.

IV. For each external momentum p_i ($i = 1, \dots, m+n$), let P_i be the path in $T^2(\mathbf{r})$ that connects p_i to a vertex of $v_A \in \gamma_*$. We now demonstrate that at least two of these paths must contain edges from \mathcal{S} , by considering the possible locations of γ_* .

- $\gamma_* \subset \mathcal{S}$. Since any path in \mathcal{G} connecting an external momentum p_i to a vertex in γ_* must include a soft edge adjacent to γ_* , in this case, all paths P_1, \dots, P_{m+n} contain edges from \mathcal{S} .
- $\gamma_* \subset \mathcal{J}_{i_0}$ for a specific i_0 . In this case, a path connecting p_i (for any $i \neq i_0$) to γ_* must either (1) pass through the hard subgraph \mathcal{H} , or (2) contain a soft edge. Since $\mathcal{H} \cap t(\mathbf{r}; A)$ is connected (as established previously), at most one of these paths can intersect \mathcal{H} . With three or more such paths in the set $\{P_i\}_{i \neq i_0}$, this means at least two of them must fulfill condition (2) and therefore contain soft edges.

We thus conclude from both scenarios that at least two paths P_i contain soft edges.

In figure 18a, let us assume that P_1 and P_m are two of these paths (the subsequent logic can apply identically to the other type of choices, i.e., P_1 and P_{m+1}), with e_1^S and e_m^S being the soft edges that are adjacent to \mathcal{J}_1 and \mathcal{J}_m respectively. In the entire graph \mathcal{G} ,

⁷Here we have drawn $\mathcal{H} \cap t(\mathbf{r}; A)$ attached to γ_* . Actually, it could also be attached to one of the “ p_i branches” ($i = 1, \dots, m$), but the subsequent analysis would be identical, so we do not treat this case separately.

consider the path in \mathcal{J}_1 which carries the soft momentum flow from e_1^S to \mathcal{H} . On this path, there exists an edge $e_1^J \in \mathcal{J}_1 \setminus T^2(\mathbf{r})$, whose endpoints are in the P_1 and $\mathcal{H} \cap t(\mathbf{r}; A)$ respectively. Similarly, there exists an edge $e_m^J \in \mathcal{J}_m \setminus T^2(\mathbf{r})$, whose endpoints are in P_m and $\mathcal{H} \cap t(\mathbf{r}; A)$ respectively. Since e_1^J (e_m^J) is a jet edge carrying the soft momentum in e_1^S (e_m^S), we have two inequalities $w(e_1^S) < w(e_1^J)$ and $w(e_m^S) < w(e_m^J)$.

Meanwhile, consider the path in $t(\mathbf{r}; A)$ which connects $\gamma_* \cap t(\mathbf{r}; A)$ and $\mathcal{H} \cap t(\mathbf{r}; A)$, which must contain an edge e_1 such that $w(e_1) < w(e_0)$. (This follows from the same reasoning as cases **I-III**.) We can then consider the following spanning 2-tree

$$T_*^2 \equiv T^2(\mathbf{r}) \cup (e_0 \cup e_1^J \cup e_m^J) \setminus (e_1 \cup e_1^S \cup e_m^S), \quad (6.8)$$

as is shown in figure 18b, with the momentum between its two components being $p_1 + p_m$, which is off shell. Its weight satisfies

$$\begin{aligned} w(T_*^2) &\leq w(T^2(\mathbf{r})) + w(e') + w(e_1^S) + w(e_2^S) - w(e_0) - w(e_1^J) - w(e_2^J) \\ &< w(T^2(\mathbf{r})). \end{aligned} \quad (6.9)$$

In the first inequality, we have used that $(p_1 + p_m)^2 \sim \mathcal{O}(1)$, implying that the kinematic contribution to $w(T_*^2)$ is zero; meanwhile, the kinematic contribution to $w(T^2(\mathbf{r}))$ is either zero or positive by definition. In the second inequality, we have employed the previously derived inequalities, $w(e') < w(e_0)$, $w(e_1^S) < w(e_1^J)$, and $w(e_2^S) < w(e_2^J)$. Therefore, the minimum-weight criterion is also violated in this case.

In conclusion, we have excluded all possible configurations of $T^2(\mathbf{r})$ under the assumption that $T(\mathbf{r}) \cap \gamma_*$ contains multiple connected components, thus proving the statement (6.2). \square

With $T(\mathbf{r}) \cap \gamma_*$ confirmed a spanning tree for any leading term \mathbf{x}^r , a homogeneity condition from eq. (6.3) arises, imposing as an additional reduction of the dimension of f_R and making the expanded integral scaleless. Therefore, such a γ_* cannot exist, and we have finally proved the First Connectivity Theorem.

Let us end this subsection by going through an example to see how our reasoning above works. Consider the aforementioned configuration in figure 9b, in which the First Connectivity Theorem is violated due to the S loop in the middle. By denoting this S component as γ_* , one can verify through direct inspection that the graph $T(\mathbf{r}) \cap \gamma_*$ is a spanning tree of γ_* for any leading term \mathbf{x}^r ; thus, a homogeneity condition arises and its corresponding expanded integral is scaleless. One can also see the tree structure of $T(\mathbf{r}) \cap \gamma_*$ without examining all the leading terms. Suppose there exists a leading \mathcal{F} term \mathbf{x}^r , for which the graph $T(\mathbf{r}) \cap \gamma_*$ is disconnected. One can then construct another spanning 2-tree with a smaller weight, thereby

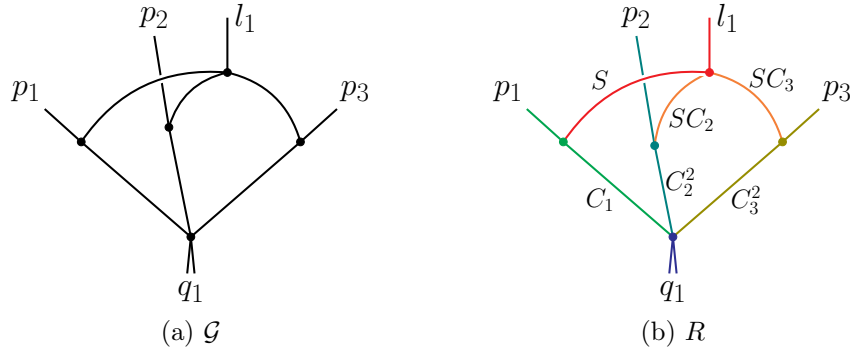
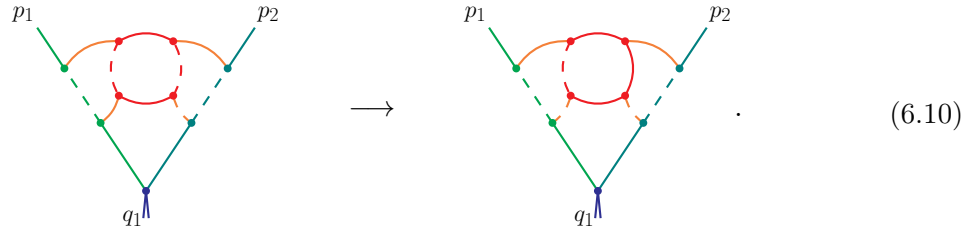


Figure 19. A two-loop graph \mathcal{G} and one of its regions R .

violating the minimal-weight criterion. For example,



This modification is precisely from the analysis of case **I** in our proof of statement (6.2). As a result, such an \mathbf{x}^r does not exist in the leading polynomial.

6.2 Structures of leading terms

To further investigate region structures, we need to understand the expressions of the leading terms in an arbitrary virtuality expansion. Generally, the number of leading terms with respect to a given region can be large, but as we will show, they can all be characterized graphically in terms of the spanning (2-)tree structures of the mode components.

We begin with the two-loop example in figure 19, where \mathcal{G} is the Feynman graph and the external momenta p_1, p_2, p_3, q_1, l_1 are in the modes C_1, C_2^2, C_3^2, H , and S , respectively. For this kinematics, R is one of the admissible regions (as can be verified by explicit computation). The modes of the internal edges are indicated by color: C_1 edges are **green**, C_2^2 edges are **teal**, C_3^2 edges are **olive**, S edges are **red**, and SC_1 and SC_2 edges are **orange**.

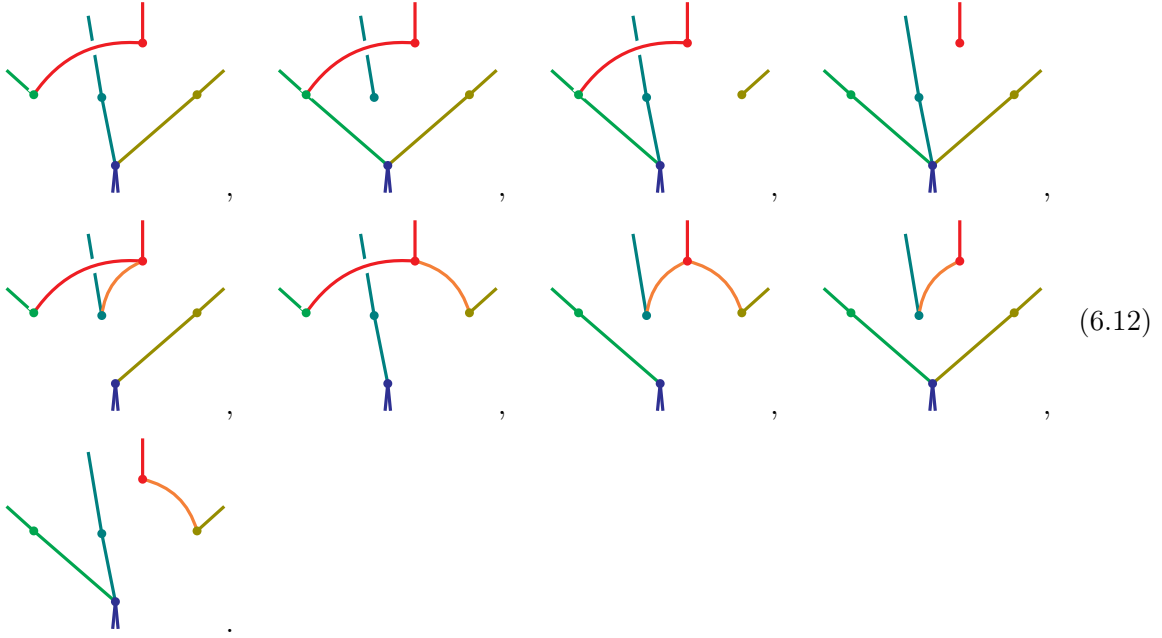
From now on, we will use the superscript “ (R) ” to denote terms that are leading in the region R . That is, $\mathcal{U}^{(R)}$ and $\mathcal{F}^{(R)}$ represent the leading \mathcal{U} and \mathcal{F} polynomials, respectively.

We now consider the leading terms associated with R and list their corresponding spanning

(2-)trees. There is a unique $\mathcal{U}^{(R)}$ term,



together with nine $\mathcal{F}^{(R)}$ terms,



This example provides a first indication that the $\mathcal{F}^{(R)}$ terms are intrinsically more intricate than the $\mathcal{U}^{(R)}$ terms. Later, we will further classify the $\mathcal{F}^{(R)}$ terms and show how each class can be generally characterized by the mode components of R .

6.2.1 $\mathcal{U}^{(R)}$ terms

We start by considering general $\mathcal{U}^{(R)}$ terms. As they correspond to the minimum spanning trees of \mathcal{G} where the weight of each edge is given by \mathbf{v}_R , we can combine theorems 3.4 and 5.1 (both proved already) to obtain the following:

Lemma 6.2. *If \mathbf{x}^r is a $\mathcal{U}^{(R)}$ term, then each graph $\gamma \cap T^1(\mathbf{r})$, where γ denotes any mode component, is a spanning tree of $\tilde{\gamma}$. That is,*

$$\mathcal{U}^{(R)} : \mathbf{n}_\gamma(\mathbf{r}) = L(\tilde{\gamma}) \text{ for any mode component } \gamma. \quad (6.13)$$

Recall that $\mathbf{n}_\gamma(\mathbf{r})$ denotes the degree of those parameters associated with the edges of γ in \mathbf{x}^r ; or equivalently, the number of edges of γ that are absent in the spanning (2-)tree $T(\mathbf{r})$.

Conversely, by combining an arbitrary choice of spanning trees from all mode components, we obtain a minimum spanning tree of \mathcal{G} , which corresponds to a $\mathcal{U}^{(R)}$ term. To formalize this, let $\mathbf{x}^{[\gamma]}$ denote the parameters associated with the edges of γ . Then the leading polynomial $\mathcal{U}^{(R)}(\mathbf{x})$ can be factorized as follows:

$$\mathcal{U}^{(R)}(\mathbf{x}) = \prod_{\gamma} \mathcal{U}_{\gamma}(\mathbf{x}^{[\gamma]}), \quad (6.14)$$

where $\mathcal{U}_{\gamma}(\mathbf{x}^{[\gamma]})$ is the polynomial containing only $\mathbf{x}^{[\gamma]}$ and corresponding to a certain spanning tree of $\tilde{\gamma}$. This factorization identity has been discussed previously in ref. [27].

6.2.2 Classification of $\mathcal{F}^{(R)}$ terms

In contrast to the previous cases, the structure of a generic spanning 2-tree T^2 corresponding to an $\mathcal{F}^{(R)}$ term is significantly more complex. To analyze it systematically, we first classify general $\mathcal{F}^{(R)}$ terms into two types, based on the following key property regarding the edges connecting the two components of T^2 .⁸

Lemma 6.3. *For any edge $e \in \mathcal{G} \setminus T^2$ whose endpoints are in the two components of T^2 respectively, its weight must satisfy $w(e) \leq -\mathcal{V}(Q_{T^2})$, where Q_{T^2} denotes the momentum flowing between the two components of T^2 .*

Proof. By definition, the graph $T^2 \cup e$ is a spanning tree of \mathcal{G} , which must correspond to a \mathcal{U} term. This \mathcal{U} term has the weight

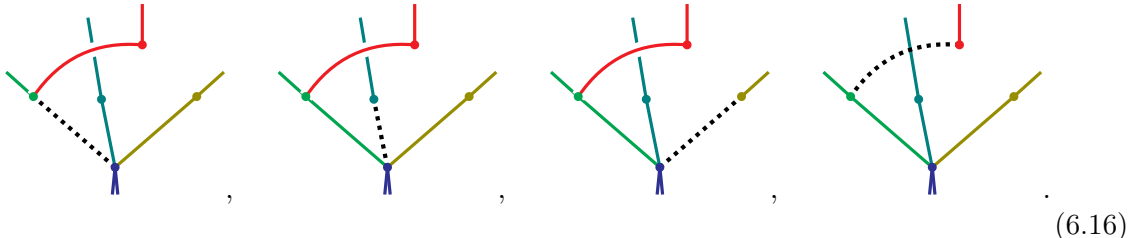
$$w(T^2) - w(e) - \mathcal{V}(Q_{T^2}). \quad (6.15)$$

Based on the minimum-weight criterion, the expression above must be greater than or equal to $w(T^2)$. This directly leads to $w(e) \leq -\mathcal{V}(Q_{T^2})$. \square

Building on this observation, we classify general $\mathcal{F}^{(R)}$ terms into the following two types.

- **Type-I ($\mathcal{F}_I^{(R)}$):** there exists an edge $e \in \mathcal{G} \setminus T^2$ whose endpoints are in the two components of T^2 respectively, such that $w(e) = -\mathcal{V}(Q_{T^2})$.
- **Type-II ($\mathcal{F}_{II}^{(R)}$):** for any edge $e \in \mathcal{G} \setminus T^2$ whose endpoints are in the two components of T^2 respectively, we have $w(e) < -\mathcal{V}(Q_{T^2})$.

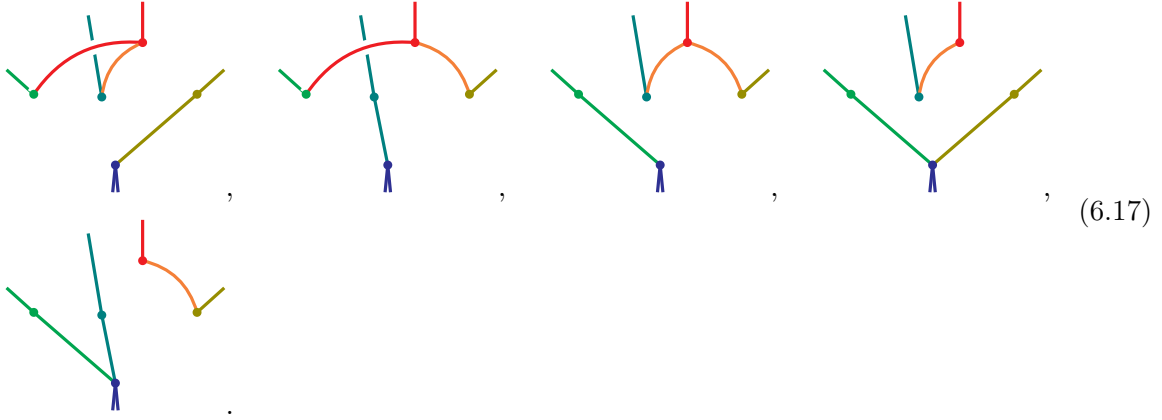
Let us recall the previous example in (6.12) to better understand these notions. There are four $\mathcal{F}_I^{(R)}$ terms, which are:



⁸By “edges connecting the two components of T^2 ”, we refer to those edges whose endpoints are in the two components of T^2 , respectively. These edges themselves do not belong to T^2 by definition.

In each graph above, we have used black dotted lines to label the edge e whose endpoints lie in the two components respectively and for which $w(e) = -\mathcal{V}(Q_{T^2})$. (In general, there can be multiple such e .) From left to right, their corresponding modes are C_1 , C_2^2 , C_3^2 , and S .

The remaining five graphs in (6.12) are $\mathcal{F}_{\text{II}}^{(R)}$ terms:



For each of these five spanning 2-trees, the total momentum flowing between its components is harder than the momentum of any edge connecting those components. For example, in the fourth graph, a C_2^2 -mode external momentum p_2 and an S -mode external momentum l_1 attach to the same component, yielding a total momentum in the mode C_2 (because $C_2^2 \vee S = C_2$) that flows between the components of T^2 . Meanwhile, there are three edges connecting the two components of the spanning 2-tree, whose associated modes are S , C_2^2 , and SC_3 respectively, all softer than C_2 .

In what follows, we analyze the general structure of each type of $\mathcal{F}^{(R)}$ term.

6.2.3 $\mathcal{F}_{\text{I}}^{(R)}$ terms

For any given $\mathcal{F}_{\text{I}}^{(R)}$ term \mathbf{x}^r , adding to $T^2(\mathbf{r})$ the edge e —which connects the two components of $T^2(\mathbf{r})$ and satisfies $w(e) = -\mathcal{V}(Q_{T^2(\mathbf{r})})$ —yields a spanning tree. One can verify that this spanning tree has the same weight as $T^2(\mathbf{r})$ and therefore corresponds to a $\mathcal{U}^{(R)}$ term. For example, adding the dotted line in each graph of (6.16) produces the $\mathcal{U}^{(R)}$ term in (6.11). This correspondence between $\mathcal{F}_{\text{I}}^{(R)}$ and $\mathcal{U}^{(R)}$ terms automatically allows us to characterize general $\mathcal{F}_{\text{I}}^{(R)}$ terms via mode components, similar to lemma 6.2.

Lemma 6.4. *If \mathbf{x}^r is an $\mathcal{F}_{\text{I}}^{(R)}$ term, then there exists a corresponding mode component γ' with $\mathcal{X}(\gamma') = \mathcal{X}(Q_{T^2(\mathbf{r})})$, such that (1) $\gamma' \cap T^2(\mathbf{r})$ is a spanning 2-tree of $\tilde{\gamma}'$; (2) for all other mode components $\gamma \neq \gamma'$, $\gamma \cap T^2(\mathbf{r})$ is a spanning tree of $\tilde{\gamma}$. That is,*

$$\mathcal{F}_{\text{I}}^{(R)} : \quad \mathbf{n}_{\gamma'} = L(\tilde{\gamma}') + 1, \quad \mathbf{n}_{\gamma} = L(\tilde{\gamma}) \quad \forall \gamma \neq \gamma'. \quad (6.18)$$

From now on, we will use $\mathbf{n}_{\gamma'}$ to represent $\mathbf{n}_{\gamma'}(\mathbf{r})$ unless \mathbf{x}^r refers to one specific term. Similar to eq. (6.14), the sum of $\mathcal{F}_{\text{I}}^{(R)}$ terms sharing the same kinematic factor $(-s)$ factorizes

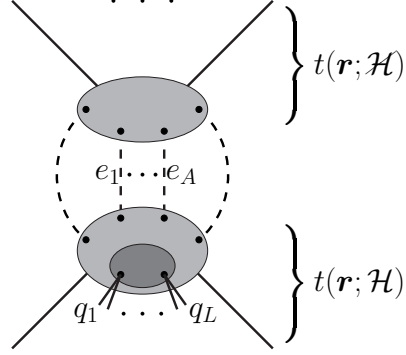


Figure 20. The configuration of $T^2(\mathbf{r})$ where $x^{\mathbf{r}}$ is an $\mathcal{F}_{\text{II}}^{(R)}$ term. The top and bottom gray blobs represent $t(\mathbf{r}; \mathcal{H})$ and $t(\mathbf{r}; \mathcal{H})$ respectively, and the dark gray blob contained in $t(\mathbf{r}; \mathcal{H})$ represents $\mathcal{H} \cap t(\mathbf{r}; \mathcal{H})$. Among the dashed edges that connect $t(\mathbf{r}; \mathcal{H})$ and $t(\mathbf{r}; \mathcal{H})$, a certain subset $\{e_1, \dots, e_A\}$ is selected accordingly (see the description above lemma 6.5).

as follows:

$$\mathcal{F}_{\text{I}}^{(R)}(\mathbf{x}) = (-s) \cdot \mathcal{F}_{\gamma'}(\mathbf{x}^{[\gamma']}) \cdot \prod_{\gamma \neq \gamma'} \mathcal{U}_{\gamma}(\mathbf{x}^{[\gamma]}), \quad (6.19)$$

where γ' is determined by $(-s)$ such that the virtuality of the mode $\mathcal{X}(\gamma')$ is exactly s . The terms in the polynomial $\mathcal{F}_{\gamma'}(\mathbf{x}^{[\gamma']})$ correspond to certain spanning 2-trees of $\tilde{\gamma}'$ for which the total momenta flowing between their components are of mode $\mathcal{X}(\gamma')$.

6.2.4 $\mathcal{F}_{\text{II}}^{(R)}$ terms

Most complexities arise in characterizing the $\mathcal{F}_{\text{II}}^{(R)}$ terms. To begin, for any given $\mathcal{F}_{\text{II}}^{(R)}$ term $\mathbf{x}^{\mathbf{r}}$, we consider the positions of the hard vertices. A first observation is that they must all lie in the same component of $T^2(\mathbf{r})$. To see this, consider the contrary, i.e., suppose hard vertices lie in both components of $T^2(\mathbf{r})$. Since \mathcal{H} is connected, there must be an edge $e^{[H]} \in \mathcal{H}$ with endpoints in the two components of $T^2(\mathbf{r})$ respectively. We then have, from the definition of $\mathcal{F}_{\text{II}}^{(R)}$ terms, that $0 = w(e^{[H]}) < -\mathcal{V}(Q(\mathbf{r}))$, which cannot hold since $\mathcal{V}(Q(\mathbf{r})) \in \mathbb{N}$.

With this observation, let us denote the components of $T^2(\mathbf{r})$ by $t(\mathbf{r}; \mathcal{H})$ (containing all the hard vertices) and $t(\mathbf{r}; \mathcal{H})$ (containing no hard vertices), as shown in figure 20. Among all the edges in $\mathcal{G} \setminus T^2(\mathbf{r})$ that connect $t(\mathbf{r}; \mathcal{H})$ and $t(\mathbf{r}; \mathcal{H})$, we select those whose modes are *not softer* than any others, and denote them as e_1, \dots, e_A . For example, suppose the set of edges connecting $t(\mathbf{r}; \mathcal{H})$ and $t(\mathbf{r}; \mathcal{H})$ are in the modes C_2^2 , S , SC_3 , and C_4^3 respectively; then the set $\{e_1, \dots, e_A\}$ includes those edges whose modes are C_2^2 , S , and C_4^3 (those in the mode SC_3 are not included because SC_3 is softer than S).

In general, e_1, \dots, e_A possess the following properties.

Lemma 6.5. *The edges e_1, \dots, e_A , as constructed above, must satisfy:*

- (1) $A \geq 2$;

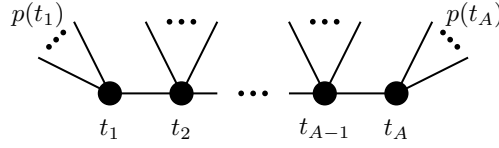


Figure 21. The schematic structure of the tree graph $t(\mathbf{r}; \mathcal{H})$, where the nodes represent the subtrees t_1, \dots, t_A (possibly with some attached branches) and are aligned by the $A - 1$ paths in $t(\mathbf{r}; \mathcal{H})$. The sum of external momenta attached to t_a is $\mathfrak{p}(t_a)$, which can generally be zero for $a \neq 1, A$.

(2) $\Gamma_X \cap t(\mathbf{r}; \mathcal{H}) = \emptyset$, where Γ_X is the X -mode subgraph, with X being harder than $\mathcal{X}(e_a)$ for some $a \in \{1, \dots, A\}$.

Proof. To see (1), note that from the definition of $\mathcal{F}_{\text{II}}^{(R)}$ terms, we have

$$w(e_1), \dots, w(e_A) < -\mathcal{V}(Q(\mathbf{r})) \quad \text{and} \quad \bigvee_{a=1}^A \mathcal{X}(e_a) = \mathcal{X}(Q(\mathbf{r})), \quad (6.20)$$

which cannot be simultaneously satisfied for $A = 1$. So $A \geq 2$.

We prove (2) by contradiction. Suppose the mode X is harder than a specific $\mathcal{X}(e_a)$, and $\Gamma_X \cap t(\mathbf{r}; \mathcal{H}) \neq \emptyset$. It then follows that the subgraph $\bar{\Gamma}_X$, which is defined as the union of Γ_X and all the harder-mode subgraphs, overlaps with both $t(\mathbf{r}; \mathcal{H})$ and $t(\mathbf{r}; \mathcal{H})$. That is,

$$\bar{\Gamma}_X \cap t(\mathbf{r}; \mathcal{H}) \neq \emptyset, \quad \bar{\Gamma}_X \cap t(\mathbf{r}; \mathcal{H}) \neq \emptyset. \quad (6.21)$$

From theorem 5.1, $\bar{\Gamma}_X$ is connected, so there must be some edges $\bar{e} \in \bar{\Gamma}_X \setminus T^2(\mathbf{r})$ connecting the two components of $T^2(\mathbf{r})$. The mode $\mathcal{X}(e_a)$ is then softer than $\mathcal{X}(\bar{e})$, which contradicts the defining property of the set e_1, \dots, e_A : the edge e_a should not have been an element of the set $\{e_1, \dots, e_A\}$ by construction. Therefore, we must have $\Gamma_X \cap t(\mathbf{r}; \mathcal{H}) = \emptyset$. \square

For each $a = 1, \dots, A$, we now define a corresponding tree subgraph $t_a \subset t(\mathbf{r}; \mathcal{H})$ such that: (1) it contains one endpoint of e_a , and (2) its edges and vertices are all of the same mode $\mathcal{X}(e_a)$. The tree graph $t(\mathbf{r}; \mathcal{H})$ thus contains A distinct subtrees t_1, \dots, t_A ⁹, which are connected by paths within $t(\mathbf{r}; \mathcal{H})$. In fact, t_1, \dots, t_A are not only connected but also *aligned* by these paths—a property that we will specify as a corollary of lemma 6.5.

Corollary 6.5.1. *The subtrees t_1, \dots, t_A are aligned by these paths. That is, $t(\mathbf{r}; \mathcal{H})$ can be represented by figure 21 where the nodes represent t_1, \dots, t_A (possibly with some attached branches), and each line represents a path connecting them. Furthermore, denoting the sum of external momenta attached to t_a by $\mathfrak{p}(t_a)$, we have*

$$\mathcal{X}(\mathfrak{p}(t_1)) \vee \mathcal{X}(\mathfrak{p}(t_A)) = \mathcal{X}(\mathfrak{p}(t_1)) \vee \dots \vee \mathcal{X}(\mathfrak{p}(t_A)). \quad (6.22)$$

⁹If multiple edges e_a correspond to the same subtree t_a , the distinct subtrees are $t_1, \dots, t_{A'}$ with $A' \leq A$. Meanwhile, the following analysis applies equally in this case, so we shall not treat it separately.

Proof. From theorem 3.2, there exist $a_1, a_2 \in \{1, \dots, A\}$, such that

$$\mathcal{X}(\mathbf{p}(t_{a_1})) \vee \mathcal{X}(\mathbf{p}(t_{a_2})) = \mathcal{X}(\mathbf{p}(t_1)) \vee \dots \vee \mathcal{X}(\mathbf{p}(t_A)). \quad (6.23)$$

There is a unique path $P_{a_1 a_2} \subset t(\mathbf{r}; \mathcal{H})$ that connects t_{a_1} and t_{a_2} . Let us consider the possibility that there is a third subtree t_b (with $b \neq a_1, a_2$) that does not intersect with $P_{a_1 a_2}$, i.e., $P_{a_1 a_2} \cap t_b = \emptyset$. In this case, one can construct another spanning 2-tree whose weight is lower than $w(T^2(\mathbf{r}))$ as follows. First, by construction there exists an edge e_b whose endpoints are in $t(\mathbf{r}; \mathcal{H})$ and $t(\mathbf{r}; \mathcal{H})$ respectively, such that $\mathcal{X}(e_b) = \mathcal{X}(t_b)$. Second, there is a unique path $P'_b \subset t(\mathbf{r}; \mathcal{H})$ connecting t_b to $P_{a_1 a_2}$. The mode of one specific edge $e'_b \in P'_b$, which is adjacent to t_b , must be softer than $\mathcal{X}(t_b)$, otherwise the statement (2) in lemma 6.5 would be violated. We thus have $w(e'_b) < w(e_b)$. Third, the spanning 2-tree $T'^2 \equiv T^2(\mathbf{r}) \cup e_b \setminus e'_b$ does not disconnect $P_{a_1 a_2}$, thus its kinematic factor is as large as that of $T^2(\mathbf{r})$ according to eq. (6.23). Combining these three observations, we obtain

$$w(T'^2) = w(T^2(\mathbf{r})) + w(e'_b) - w(e_b) < w(T^2(\mathbf{r})), \quad (6.24)$$

which is a violation to the minimum-weight criterion.

This analysis indicates that the path $P_{a_1 a_2}$ must intersect *all* the subtrees t_1, \dots, t_A . This is possible only if $t(\mathbf{r}; \mathcal{H})$ has the structure shown in figure 21, with t_{a_1} and t_{a_2} at the endpoints (i.e., t_1 and t_A as shown in figure 21), which directly yields eq. (6.22). \square

One can examine the examples in (6.17) and see that they are consistent with corollary 6.5.1. For each spanning 2-tree there, the component $t(\mathbf{r}; \mathcal{H})$ (the one not attached by the off-shell external momentum) conforms to the structure in figure 21. For example, in the third term of (6.17), the three subtrees t_1 (teal), t_2 (red), and t_3 (olive) are aligned by two paths (orange). In contrast, the spanning 2-tree shown below does not correspond to any $\mathcal{F}_{II}^{(R)}$ term and therefore does not appear in (6.17), because the four subtrees of $t(\mathbf{r}; \mathcal{H})$ are not aligned by the paths:



Following the proof above, one can obtain three other spanning 2-trees (which are precisely the first three terms of (6.17)) whose weights are smaller than the spanning 2-tree above.

From the preceding conclusions, one can denote the paths described in corollary 6.5.1 by $P_{1,2}, \dots, P_{A-1,A}$, where $P_{a,a+1}$ connects the subtrees t_a and t_{a+1} . To further analyze the substructure of $P_{a,a+1}$, we label its edges in order as e_1^a, \dots, e_i^a , such that e_1^a is adjacent to t_a , e_2^a is adjacent to e_1^a , and so on, with e_i^a adjacent to t_{a+1} . If there exist indices i_1, i_2 with $1 \leq i_1 < i_2 \leq i$ such that the mode $\mathcal{X}_{i_1 i_2} \equiv \mathcal{X}(e_{i_1}^a) = \mathcal{X}(e_{i_1+1}^a) = \dots = \mathcal{X}(e_{i_2-1}^a)$ is harder

than both $\mathcal{X}(e_{i_1-1}^a)$ and $\mathcal{X}(e_{i_2}^a)$, we identify a corresponding subtree in $t(\mathbf{r}; \mathcal{H})$ that contains the edges $e_{i_1}^a, \dots, e_{i_2-1}^a$ and whose edges and vertices all have the same mode $\mathcal{X}_{i_1 i_2}$.

We then include all such additional subtrees (if any) in the original set $\{t_1, \dots, t_A\}$ and obtain a larger set. By construction, these trees remain aligned by the paths in $t(\mathbf{r}; \mathcal{H})$. For simplicity, we shall still use t_1, \dots, t_A to denote them with an enlarged A . Note that after this operation, statement (1) of lemma 6.5 and corollary 6.5.1 still apply. Meanwhile, statement (2) of lemma 6.5 no longer applies; nevertheless, we will not use it in the subsequent analysis.

With the set $\{t_1, \dots, t_A\}$ extended as above, from now on we call t_1, \dots, t_A the *characteristic subtrees* of the $\mathcal{F}_{\text{II}}^{(R)}$ term $\mathbf{x}^{\mathbf{r}}$. The following corollary investigates the structure of their connecting paths, $P_{1,2}, \dots, P_{A-1,A}$.

Corollary 6.5.2. *Each $P_{a,a+1}$ contains a single sub-path whose edges all have the same mode, which is equal to or softer than $\mathcal{X}(t_a) \wedge \mathcal{X}(t_{a+1})$; all the other edges in $P_{a,a+1}$ (if any) are of harder modes.*

Proof. For each $a \in \{1, \dots, A\}$, we denote the edges of $P_{a,a+1}$ in a certain order as e_1^a, \dots, e_i^a , such that e_1^a is adjacent to t_a , e_2^a is adjacent to e_1^a , etc., and e_j^a is adjacent to t_{a+1} . From our construction above, there exist i_1, i_2 with $1 \leq i_1 < i_2 \leq i$, such that

- $\mathcal{X}(e_b^a)$ is equal to or harder than $\mathcal{X}(e_{b+1}^a)$, for $b = 1, \dots, i_1 - 1$;
- $\mathcal{X}(e_b^a) = \mathcal{X}(e_{b+1}^a)$, for $b = i_1, \dots, i_2 - 1$;
- $\mathcal{X}(e_b^a)$ is equal to or softer than $\mathcal{X}(e_{b+1}^a)$, for $b = i_2, \dots, i - 1$;

In other words, the softest edges in $P_{a,a+1}$ are $e_{i_1}^a, \dots, e_{i_2-1}^a$, which form a sub-path of $P_{a,a+1}$. Their mode must be simultaneously softer than $\mathcal{X}(t_a)$ and $\mathcal{X}(t_{a+1})$, thus equal to or softer than $\mathcal{X}(t_a) \wedge \mathcal{X}(t_{a+1})$. \square

Another crucial property is that edges adjacent to a characteristic subtree t_a cannot be in any mode harder than $\mathcal{X}(t_a)$. A more precise description is given by the following lemma.

Lemma 6.6. *For any edge $e \in \mathcal{G}$ adjacent to a characteristic subtree t_a , the following holds:*

1. *If both endpoints of e lie in $t(\mathbf{r}; \mathcal{H})$, then $\mathcal{X}(e)$ is softer than $\mathcal{X}(t_a)$.*
2. *If one endpoint of e is in $t(\mathbf{r}; \mathcal{H})$ and the other is in $t(\mathbf{r}; \mathcal{H})$, then $\mathcal{X}(e)$ is softer than or equal to $\mathcal{X}(t_a)$.*
3. *There exists at least one such edge e with endpoints in $t(\mathbf{r}; \mathcal{H})$ and $t(\mathbf{r}; \mathcal{H})$, respectively, for which $\mathcal{X}(e) = \mathcal{X}(t_a)$.*

Note that the statements above are already justified by lemma 6.5 for the edges e_1, \dots, e_A defined at the beginning of our $\mathcal{F}^{(R)}$ -term analysis. Here, we argue that they continue to hold after $\{t_1, \dots, t_A\}$ has been extended to the set of characteristic subtrees as described.

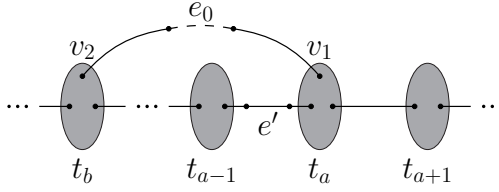


Figure 22. The configuration of $t(r; H)$ of case (1) in the proof of lemma 6.6. The gray blobs represent the subtrees t_b , t_{a-1} , t_a , and t_{a+1} . The endpoints of e_0 are directly connected to t_a and t_b , respectively. The edge e' belongs to the path $P_{a-1,a}$.

Proof. We first show that $\mathcal{X}(e)$ cannot be harder than $\mathcal{X}(t_a)$. Otherwise, by the First Connectivity Theorem (theorem 5.1), there would exist a path in \mathcal{G} connecting t_a and H whose edges all have modes harder than $\mathcal{X}(t_a)$. Starting from one endpoint v_1 that is adjacent to t_a , this path, denoted as P_0 , must first reach a vertex v_2 that lies in either (1) another characteristic subtree t_b ¹⁰, or (2) the other component of $T^2(r)$, which is $t(r; H)$. Below we demonstrate that both possibilities would violate the minimum-weight criterion.

In case (1), there is an edge $e_0 \in P_0 \setminus t(r; H)$ such that $t(r; H) \cup e_0$ contains a path through e_0 , connecting v_1 and v_2 . However, a unique path already exists within $t(r; H)$ connecting v_1 and v_2 , which must pass through either $P_{a-1,a}$ or $P_{a,a+1}$. (Figure 22 illustrates the configuration where $e' \in P_{a-1,a}$.) Consequently, $t(r; H) \cup e_0$ contains a loop. Within this loop, there is an edge $e' \in P_{a-1,a} \cup P_{a,a+1}$ for which $\mathcal{X}(e')$ is softer than $\mathcal{X}(t_a)$. We now construct another spanning 2-tree $T_0^2 \equiv T^2(r) \cup e_0 \setminus e'$, whose weight is given by

$$w(T_0^2) = w(T^2(r)) + w(e') - w(e_0) < w(T^2(r)), \quad (6.26)$$

where we have used the aforementioned fact that $\mathcal{X}(e')$ is softer than $\mathcal{X}(e_0)$ softer than $\mathcal{X}(t_a)$, from which $w(e') < w(e_0)$. The minimum-weight criterion is thus violated.

For case (2), there exists an edge $e_0 \in P_0$ whose endpoints are in $t(r; H)$ and $t(r; H)$, respectively. Note that $\mathcal{X}(v_1)$ is harder than $\mathcal{X}(t_a)$, thus $v_1 \notin t_a$, and v_1 must not disconnect t_a , as is shown in figure 23. This implies the existence of another edge $e' \in t_a$, such that the spanning 2-tree $T_0^2 \equiv T^2(r) \cup e_0 \setminus e'$, with a weight given by

$$w(T_0^2) = w(T^2(r)) + w(e') - w(e_0) < w(T^2(r)). \quad (6.27)$$

As in case (1), the minimum-weight criterion is violated.

Therefore, for all e adjacent to t_a , $\mathcal{X}(e)$ is either equal to or softer than $\mathcal{X}(t_a)$. Note that if both endpoints of e are in $t(r; H)$, $\mathcal{X}(e)$ can only be softer than $\mathcal{X}(t_a)$ otherwise it would be absorbed into t_a . The first two statements of the lemma are then proved.

Finally, the First Connectivity Theorem indicates that the modes $\mathcal{X}(e)$ cannot be all softer than $\mathcal{X}(t_a)$. In other words, there exists at least one specific edge e with $\mathcal{X}(e) = \mathcal{X}(t_a)$.

¹⁰We also include in this case the possibility that v_2 lies in one of the $A - 1$ connecting paths of $t(r; H)$, for which the same analysis would apply.

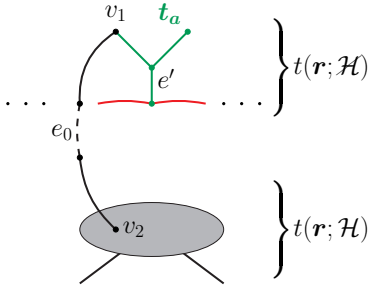


Figure 23. The configuration of $T^2(\mathbf{r})$ of case (2) in the proof of lemma 6.6. In the component $t(\mathbf{r}; \mathcal{H})$, the characteristic subtree t_a is marked in green, while its adjacent paths are marked in red. The vertex v_1 , which is one endpoint of the path P_0 , does not belong to and cannot disconnect t_a .

From the first two statements, its endpoints must be in $t(\mathbf{r}; \mathcal{H})$ and $t(\mathbf{r}; \mathcal{H})$ respectively. The third statement is also proved. \square

So far, the pattern of $T^2(\mathbf{r})$ has been clarified as follows. It consists of two components, $t(\mathbf{r}; \mathcal{H})$ and $t(\mathbf{r}; \mathcal{H})$, where all the hard vertices are contained in $t(\mathbf{r}; \mathcal{H})$. In the component $t(\mathbf{r}; \mathcal{H})$, there are A characteristic subtrees t_1, \dots, t_A aligned by $A - 1$ paths $P_{1,2}, \dots, P_{A-1,A}$. For each $a \in \{1, \dots, A\}$, there exists some edge $e_a \in \mathcal{G} \setminus T^2(\mathbf{r})$, whose endpoints are in t_a and $t(\mathbf{r}; \mathcal{H})$, respectively, with $\mathcal{X}(e_a) = \mathcal{X}(t_a)$. For each $a \in \{1, \dots, A - 1\}$, all the edges of the path $P_{a,a+1}$ are softer than either $\mathcal{X}(t_a)$ or $\mathcal{X}(t_{a+1})$. From now on, we refer to the softest mode on the path $P_{a,a+1}$ —that is, the mode of the edges in the sub-path identified in corollary 6.5.2—as the *characteristic mode* of $P_{a,a+1}$ and denote it as \widehat{X}_a . The following lemma relates $\widehat{X}_1, \dots, \widehat{X}_{A-1}$ and $\mathcal{X}(t_1), \dots, \mathcal{X}(t_A)$.

Lemma 6.7. *The characteristic modes $\hat{X}_1, \dots, \hat{X}_{A-1}$ and the modes $\mathcal{X}(t_1), \dots, \mathcal{X}(t_A)$ satisfy the following relations:*

1. $\widehat{X}_a = \mathcal{X}(t_a) \wedge \mathcal{X}(t_{a+1})$ for $a = 1, \dots, A-1$;
2. $\mathcal{X}(t_a) = \widehat{X}_{a-1} \vee \widehat{X}_a$ for $a = 2, \dots, A-1$.

This lemma reveals a particularly elegant property of $t(\mathbf{r}; \mathcal{H})$. The characteristic mode of the path $P_{a,a+1}$ can be determined by its neighboring characteristic subtrees, t_a and t_{a+1} , via the \wedge operation. Conversely, the mode of each “internal” characteristic subtree t_a (with $a \in \{2, \dots, A-1\}$) is determined by the characteristic modes of its two adjacent paths, $P_{a-1,a}$ and $P_{a,a+1}$, via the \vee operation.

Proof. Before we justify the two relations, we first point out that the mode $\mathcal{X}(\mathbf{p}(t_a))$ is softer than or equal to $\mathcal{X}(t_a)$ (recall that $\mathbf{p}(t_a)$ refers to the sum of external momenta entering t_a). Otherwise, there would exist some edge adjacent to t_a whose mode is harder than $\mathcal{X}(t_a)$, which contradicts lemma 6.6.

To justify 1, we modify $T^2(\mathbf{r})$ into a specific spanning tree as follows. For each t_a , we include to $T^2(\mathbf{r})$ the edge e_a (see the paragraph above this lemma, and note the relation

$\mathcal{X}(e_a) = \mathcal{X}(t_a)$; for each path $P_{a,a+1}$, we delete any one edge \tilde{e}_a that is of its characteristic mode \hat{X}_a . This operation includes A more edges to $T^2(\mathbf{r})$ and delete $A - 1$ edges from $T^2(\mathbf{r})$, turning it into a spanning tree of \mathcal{G} . Let us denote the corresponding \mathcal{U} term as $\mathbf{x}^{r'}$.

On the one hand, from the minimum-weight criterion, $w(T^1(\mathbf{r}')) \geq w(T^2(\mathbf{r}))$, where the equal sign holds if and only if $\mathbf{x}^{r'}$ is a $\mathcal{U}^{(R)}$ term.

On the other hand, by construction we have

$$\begin{aligned}
w(T^1(\mathbf{r}')) &= w(T^2(\mathbf{r})) - \sum_{i=1}^A w(e_a) + \sum_{a=1}^{A-1} w(\tilde{e}_a) - \mathcal{V}(\mathcal{X}(\mathbf{p}(t_1)) \vee \cdots \vee \mathcal{X}(\mathbf{p}(t_A))) \\
&= w(T^2(\mathbf{r})) + \sum_{a=1}^A \mathcal{V}(\mathcal{X}(t_a)) - \sum_{a=1}^{A-1} \mathcal{V}(\hat{X}_a) - \mathcal{V}(\mathcal{X}(\mathbf{p}(t_1)) \vee \cdots \vee \mathcal{X}(\mathbf{p}(t_A))) \\
&\leq w(T^2(\mathbf{r})) + \sum_{i=1}^A \mathcal{V}(\mathcal{X}(t_a)) - \sum_{a=1}^{A-1} \mathcal{V}(\mathcal{X}(t_a) \wedge \mathcal{X}(t_{a+1})) - \mathcal{V}(\mathcal{X}(\mathbf{p}(t_1)) \vee \cdots \vee \mathcal{X}(\mathbf{p}(t_A))) \\
&\leq w(T^2(\mathbf{r})) + \sum_{i=1}^A \mathcal{V}(\mathcal{X}(t_a)) - \sum_{a=1}^{A-1} \mathcal{V}(\mathcal{X}(t_a) \wedge \mathcal{X}(t_{a+1})) - \mathcal{V}(\mathcal{X}(t_1) \vee \cdots \vee \mathcal{X}(t_A)) \\
&\leq w(T^2(\mathbf{r})). \tag{6.28}
\end{aligned}$$

We now explain each line in (6.28). The first line expresses the defining property of $w(T^1(\mathbf{r}'))$: to obtain it from $w(T^2(\mathbf{r}))$, one subtracts the weights of the included edges $\{e_a\}_{a=1,\dots,A}$, adds the weights of the deleted edges $\{\tilde{e}_a\}_{a=1,\dots,A-1}$, and subtracts the kinematic factor of $T^2(\mathbf{r})$, which is $\mathcal{V}(\mathcal{X}(\mathbf{p}(t_1)) \vee \cdots \vee \mathcal{X}(\mathbf{p}(t_A)))$. In the second line, the edge weights are substituted with their virtuality degrees, i.e., $w(e) = -\mathcal{V}(\mathcal{X}(e))$; we have also employed $\mathcal{X}(e_a) = \mathcal{X}(t_a)$. In the third line, we have used the fact that the characteristic mode \hat{X}_a is either equal to or softer than $\mathcal{X}(t_a) \wedge \mathcal{X}(t_{a+1})$ (see corollary 6.5.2), which implies $\mathcal{V}(\hat{X}_a) \geq \mathcal{V}(\mathcal{X}(t_a) \wedge \mathcal{X}(t_{a+1}))$ for each $a = 1, \dots, A - 1$. In the fourth line, we have used the aforementioned property that $\mathcal{X}(\mathbf{p}(t_a))$ is softer than or equal to $\mathcal{X}(t_a)$, from which $\mathcal{V}(\mathcal{X}(\mathbf{p}(t_1)) \vee \cdots \vee \mathcal{X}(\mathbf{p}(t_A))) \geq \mathcal{V}(\mathcal{X}(t_1) \vee \cdots \vee \mathcal{X}(t_A))$. Finally, in the last line, we have employed corollary 3.3.1.

In comparison with the previous conclusion that $w(T^1(\mathbf{r}')) \geq w(T^2(\mathbf{r}))$, we must have

$$w(T^1(\mathbf{r}')) = w(T^2(\mathbf{r})),$$

which further indicates that every equality in (6.28) must hold. The mode \hat{X}_a is then precisely $\mathcal{X}(t_a) \wedge \mathcal{X}(t_{a+1})$. In other words, the softest edge in $P_{a,a+1}$ is of the mode $\mathcal{X}(t_a) \wedge \mathcal{X}(t_{a+1})$. We have thus justified the first statement.

To see why the second statement is true, note that from above,

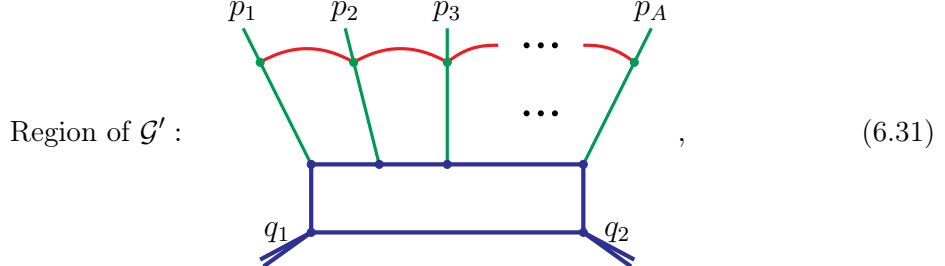
$$\hat{X}_{a-1} \vee \hat{X}_a = (\mathcal{X}(t_{a-1}) \wedge \mathcal{X}(t_a)) \vee (\mathcal{X}(t_a) \wedge \mathcal{X}(t_{a+1})). \tag{6.29}$$

The mode $\mathcal{X}(t_a)$ is harder than both brackets on the right-hand side above. Therefore, $\mathcal{X}(t_a)$ must be equal to or harder than $\hat{X}_{a-1} \vee \hat{X}_a$. Below we aim to rule out the possibility that $\mathcal{X}(t_{a_0})$ is harder than $\hat{X}_{a_0-1} \vee \hat{X}_{a_0}$ for some $a_0 \in \{2, \dots, A - 1\}$.

As we have demonstrated above, all the equalities hold in (6.28), from which we have

$$\sum_{a=1}^A \mathcal{V}(\mathcal{X}(t_a)) = \sum_{a=1}^{A-1} \mathcal{V}(\mathcal{X}(t_a) \wedge \mathcal{X}(t_{a+1})) + \mathcal{V}(\mathcal{X}(t_1) \vee \cdots \vee \mathcal{X}(t_A)). \quad (6.30)$$

Meanwhile, let us construct the following graph \mathcal{G}' , which can be regarded as a simplified version of \mathcal{G} , and consider a specific region:

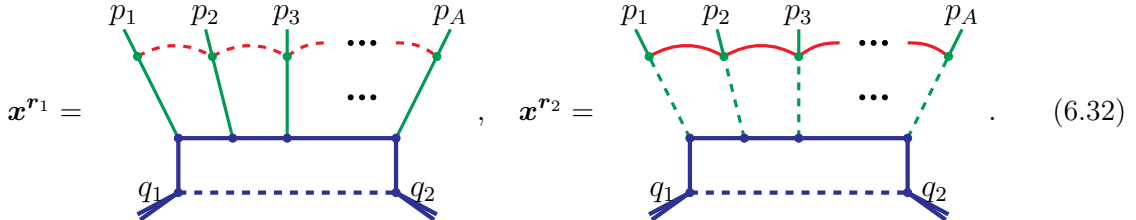


The external momenta are chosen with the following modes:

$$\mathcal{X}(q_1) = \mathcal{X}(q_A) = H, \quad \mathcal{X}(p_1) = \mathcal{X}(t_1), \quad \mathcal{X}(p_A) = \mathcal{X}(t_A), \quad \mathcal{X}(p_i) = \widehat{X}_{i-1} \vee \widehat{X}_i \quad (i = 2, \dots, A-1).$$

In the region above, the blue edges are all hard, the green edges are in the same mode of their corresponding p_i , respectively, and the modes of the red edges (from left to right) are $\widehat{X}_1, \dots, \widehat{X}_{A-1}$, respectively. One can verify the existence of this region directly, by applying the weight-solving algorithm that will be introduced later in section 6.3 (which is independent of the analysis in this lemma). For simplicity, we will not show it here.

We then consider the following two terms in the Symanzik polynomials:



The first term, \mathbf{x}^{r_1} , corresponds to a spanning tree that is consistent with (6.13). It is thus a $\mathcal{U}^{(R)}$ term. The second term, \mathbf{x}^{r_2} , corresponds to a spanning 2-tree and is by definition an $\mathcal{F}_{\text{II}}^{(R)}$ term. (In fact, it is an $\mathcal{F}_{\text{II}}^{(R)}$ term, as we will see later.) By comparing their weights, we have

$$\begin{aligned} w(T^2(\mathbf{r}_2)) &\geq w(T^1(\mathbf{r}_1)) \\ &= w(T^2(\mathbf{r}_2)) + \sum_{a=1}^A \mathcal{V}(\mathcal{X}(p_a)) - \sum_{a=1}^{A-1} \mathcal{V}(\widehat{X}_a) - \mathcal{V}(\mathcal{X}(t_1) \vee \cdots \vee \mathcal{X}(t_A)) \\ &> w(T^2(\mathbf{r}_2)) + \sum_{a=1}^A \mathcal{V}(\mathcal{X}(t_a)) - \sum_{a=1}^{A-1} \mathcal{V}(\mathcal{X}(t_a) \wedge \mathcal{X}(t_{a+1})) - \mathcal{V}(\mathcal{X}(t_1) \vee \cdots \vee \mathcal{X}(t_A)). \end{aligned} \quad (6.33)$$

To see the last strict inequality, recall our assumption that there is an a_0 with $\mathcal{X}(t_{a_0})$ harder than $\widehat{X}_{a_0-1} \vee \widehat{X}_{a_0}$, from which $\mathcal{V}(\mathcal{X}(t_{a_0})) < \mathcal{V}(\widehat{X}_{a_0-1} \vee \widehat{X}_{a_0}) = \mathcal{V}(\mathcal{X}(p_a))$. However, (6.33) would then yield the following inequality

$$\sum_{i=1}^A \mathcal{V}(\mathcal{X}(t_a)) < \sum_{a=1}^{A-1} \mathcal{V}(\mathcal{X}(t_a) \wedge \mathcal{X}(t_{a+1})) + \mathcal{V}(\mathcal{X}(t_1) \vee \cdots \vee \mathcal{X}(t_A)), \quad (6.34)$$

contradicting eq. (6.30). As a result, $\mathcal{X}(t_a) = \widehat{X}_{a-1} \vee \widehat{X}_a$ must hold for all a . The second statement is thus proved as well. \square

Let us now check the statement of lemma 6.7 by inspecting the third term of (6.17), i.e.,



where $A = 3$, and the modes $\mathcal{X}(t_1) = C_2^2$, $\mathcal{X}(t_2) = S$, $\mathcal{X}(t_3) = C_3^2$, $\widehat{X}_1 = SC_2$, and $\widehat{X}_2 = SC_3$ have been specified. For this example, the relation $\widehat{X}_a = \mathcal{X}(t_a) \wedge \mathcal{X}(t_{a+1})$ becomes

$$SC_1 = C_1^2 \wedge S, \quad SC_2 = S \wedge C_2^2. \quad (6.36)$$

Meanwhile, the relation $\mathcal{X}(t_a) = \widehat{X}_{a-1} \vee \widehat{X}_a$ becomes

$$S = SC_1 \vee SC_2. \quad (6.37)$$

These relations all hold by definition, serving as a check for lemma 6.7.

From the proof above, eq. (6.30) must hold for any $\mathcal{F}_{\text{II}}^{(R)}$ term. That is, the equality in (3.10) must hold if we take $\{X_1, \dots, X_n\} = \{\mathcal{X}(t_1), \dots, \mathcal{X}(t_A)\}$. A necessary and sufficient condition for this equality can be immediately obtained from corollary 3.3.2, which we summarize into the corollary below.

Corollary 6.7.1. *Each $\mathcal{F}_{\text{II}}^{(R)}$ term satisfies*

$$\begin{aligned} (\mathcal{X}(t_{a_1}) \vee \mathcal{X}(t_{a_2})) \wedge \mathcal{X}(t_{a_3}) &= \mathcal{X}(t_{a_2}) \wedge \mathcal{X}(t_{a_3}), \\ (\mathcal{X}(t_{a_1}) \vee \mathcal{X}(t_{a_2}) \vee \mathcal{X}(t_{a_3})) \wedge \mathcal{X}(t_{a_4}) &= \mathcal{X}(t_{a_3}) \wedge \mathcal{X}(t_{a_4}), \\ &\dots \\ (\mathcal{X}(t_{a_1}) \vee \cdots \vee \mathcal{X}(t_{a_{A-1}})) \wedge \mathcal{X}(t_{a_A}) &= \mathcal{X}(t_{a_{A-1}}) \wedge \mathcal{X}(t_{a_A}), \end{aligned} \quad (6.38)$$

with $\{a_1, \dots, a_A\}$ being any permutation of $\{1, \dots, A\}$, such that for each $k \in \{1, \dots, A\}$, the set $\{a_1, \dots, a_k\}$ consists of k consecutive integers.

In the entire graph \mathcal{G} , we now denote the mode component containing the subtree t_a as γ'_a (for $a = 1, \dots, A$), and the mode component containing the softest (characteristic-mode) edges in $P_{a,a+1}$ as γ''_a (for $a = 1, \dots, A-1$). These subgraphs have certain structures in $T^2(\mathbf{r})$, as described in the following corollary.

Corollary 6.7.2. *The subgraphs γ'_a ($a = 1, \dots, A$) and γ''_a ($a = 1, \dots, A-1$), as defined above, satisfy:*

- each $\tilde{\gamma}'_a \cap T^2(\mathbf{r})$ is a spanning 2-tree of $\tilde{\gamma}'_a$;
- each $\tilde{\gamma}''_a \cap T^2(\mathbf{r})$ contains a single loop of $\tilde{\gamma}''_a$.

Proof. We first show that the graph $\tilde{\gamma}'_a \cap T^2(\mathbf{r})$ has two connected components. By definition, $\tilde{\gamma}'_a \cap T^2(\mathbf{r})$ is obtained from $\gamma'_a \cap T^2(\mathbf{r})$ by contracting to a single vertex all the harder-mode vertices which $\gamma'_a \cap T^2(\mathbf{r})$ is adjacent to. From lemma 6.6, such vertices do not exist in $t(\mathbf{r}; \mathcal{H})$. Therefore, the contraction does not change the structure of $\gamma'_a \cap t(\mathbf{r}; \mathcal{H})$, which will remain as a tree subgraph, disconnected from $\tilde{\gamma}'_a \cap t(\mathbf{r}; \mathcal{H})$.

We next verify that $\tilde{\gamma}'_a \cap t(\mathbf{r}; \mathcal{H})$ contains no loops in order to show the first statement. Since $t(\mathbf{r}; \mathcal{H})$ is a tree graph, a loop in $\tilde{\gamma}'_a \cap t(\mathbf{r}; \mathcal{H})$ can only arise if γ'_a is adjacent to two (or more) harder-mode vertices $v_1, v_2 \in t(\mathbf{r}; \mathcal{H})$, and $\gamma'_a \cap t(\mathbf{r}; \mathcal{H})$ contains a (unique) path P_1 that connects v_1 and v_2 . (After contracting v_1 and v_2 to the same vertex, the path P_1 turns into a closed loop.) To exclude this possibility, let us consider the union of mode subgraphs $\bar{\Gamma}_* \equiv \cup_X \Gamma_X$ with X harder than $\mathcal{X}(\gamma'_a)$, which is connected according to theorem 5.1. It then follows that there is another path $P_2 \subset \bar{\Gamma}_*$ joining v_1 and v_2 , and furthermore, there is an edge $e_* \in P_2$ such that $t(\mathbf{r}; \mathcal{H}) \cup e_*$ contains a loop that shares some edges with P_1 . Let us denote any one of such edges by e' . The following spanning 2-tree

$$T'^2 \equiv T^2(\mathbf{r}) \cup e_* \setminus e' = t(\mathbf{r}; \mathcal{H}) \cup (t(\mathbf{r}; \mathcal{H}) \cup e_* \setminus e')$$

has the same kinematic factor as $T^2(\mathbf{r})$. Meanwhile, its weight is

$$w(T'^2) = w(T^2(\mathbf{r})) + w(e') - w(e_*) < w(T^2(\mathbf{r})), \quad (6.39)$$

where we have used the defining property that $\mathcal{X}(e')$ is softer than that $\mathcal{X}(e_*)$, from which $w(e') < w(e_*)$. The minimum-weight criterion is thus violated, indicating the absence of loops in $\tilde{\gamma}'_a \cap t(\mathbf{r}; \mathcal{H})$. The first statement in the lemma is proved.

Finally, let us consider the second statement. For each a , since $\gamma''_a \cap T^2(\mathbf{r})$ contains no loops, any given loop in $\tilde{\gamma}''_a \cap T^2(\mathbf{r})$ must have the following origin: a path in $\gamma''_a \cap T^2(\mathbf{r})$ has endpoints that are harder than $\mathcal{X}(\gamma''_a)$, thus a loop is formed after these endpoints are identified as the same vertex. Recall that γ''_a is defined as the mode component containing the softest edges in $P_{a,a+1}$, which, according to lemma 6.7, form a *single* sub-path of $P_{a,a+1}$. The two endpoints of this sub-path hence belongs to harder-mode subgraphs, which, in forming $\tilde{\gamma}''_a$, are identified as a single vertex. A unique loop in $\tilde{\gamma}''_a$ is then generated. The proof is then completed. \square

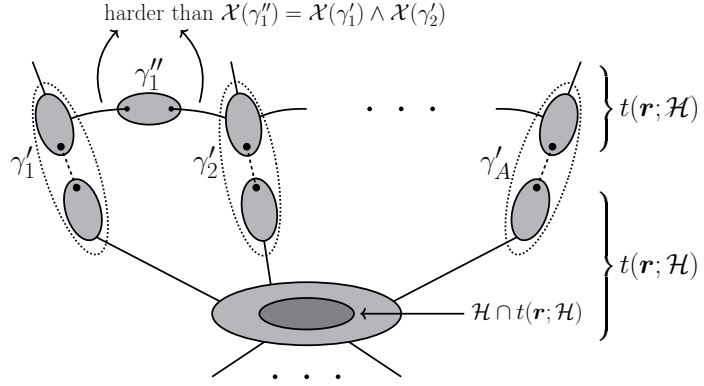


Figure 24. General structure of an $\mathcal{F}_{\text{II}}^{(R)}$ term \mathbf{x}^r , where the spanning 2-tree $T^2(\mathbf{r})$ consists of the components $t(\mathbf{r}; \mathcal{H})$ and $t(\mathbf{r}; \mathcal{H})$. Gray blobs represent tree subgraphs, with the dark gray blob being $\mathcal{H} \cap t(\mathbf{r}; \mathcal{H})$. The mode components γ'_a ($a = 1, \dots, A$), encircled by dotted curves, have their intersections $\gamma'_a \cap t(\mathbf{r}; \mathcal{H})$ connected by paths $P_{a,a+1}$. Each sub-path $\gamma''_a \cap P_{a,a+1}$ has the characteristic mode of $P_{a,a+1}$, which is $\mathcal{X}(\gamma'_a) \wedge \mathcal{X}(\gamma'_{a+1})$, with its endpoints belonging to harder-mode subgraphs.

With the results of corollary 6.7.2, we immediately have:

$$\mathfrak{n}_{\gamma'_a} = L(\tilde{\gamma}'_a) + 1, \quad \text{for } a = 1, \dots, A; \quad (6.40a)$$

$$\mathfrak{n}_{\gamma''_a} = L(\tilde{\gamma}''_a) - 1, \quad \text{for } a = 1, \dots, A - 1. \quad (6.40b)$$

We have clarified the general structure of the $\mathcal{F}_{\text{II}}^{(R)}$ terms \mathbf{x}^r as follows. To recapitulate, the spanning 2-tree $T^2(\mathbf{r})$ can be represented by figure 24, which consists of two components $t(\mathbf{r}; \mathcal{H})$ and $t(\mathbf{r}; \mathcal{H})$. The component $t(\mathbf{r}; \mathcal{H})$ contains all the hard vertices. The other component, $t(\mathbf{r}; \mathcal{H})$, can be seen as A distinct subgraphs $\gamma'_a \cap t(\mathbf{r}; \mathcal{H})$ (with $a = 1, \dots, A$) aligned by $A - 1$ paths $P_{a,a+1}$ (with $a = 1, \dots, A - 1$). Each gray blob in the figure represents a tree subgraph. The graph $\tilde{\gamma}'_a \cap T^2(\mathbf{r})$ is a spanning 2-tree of $\tilde{\gamma}'_a$. The softest edges on each $P_{a,a+1}$ are of the mode $\mathcal{X}(\gamma'_a) \wedge \mathcal{X}(\gamma'_{a+1})$ (the characteristic mode of $P_{a,a+1}$), forming a sub-path of $P_{a,a+1}$. By denoting the mode component containing this sub-path as γ''_a (with $a = 1, \dots, A - 1$), the graph $\tilde{\gamma}''_a \cap T^2(\mathbf{r})$ contains a single loop of $\tilde{\gamma}''_a$.

To characterize the mode structure of $t(\mathbf{r}; \mathcal{H})$, we define its *reduced form* as a sequence of A nodes aligned by $A - 1$ paths (see figure 25). One can thus see the nodes as the characteristic subtrees t_1, \dots, t_A , and the paths as $P_{1,2}, \dots, P_{A-1,A}$. The characteristic subtree modes $\mathcal{X}(t_1), \dots, \mathcal{X}(t_A)$ are indicated on the corresponding nodes. Similarly, the characteristic modes $\hat{X}_1, \dots, \hat{X}_{A-1}$ are indicated on the corresponding paths. These modes satisfy the relations given in lemma 6.7.

We emphasize that the external momenta of $t(\mathbf{r}; \mathcal{H})$ are implicit in the reduced form, subject to certain constraints. In proving lemma 6.7, we have demonstrated that the mode of the total external momentum attached to t_a , which we denote by $\mathcal{X}(\mathbf{p}(t_a))$, must be softer than or equal to $\mathcal{X}(t_a)$. It is also possible that some t_a have no external momenta attached;



Figure 25. The reduced form of $t(\mathbf{r}; \mathcal{H})$, where the A nodes represent the subtrees t_1, \dots, t_A , and the $A - 1$ paths aligning them represent the paths $P_{1,2}, \dots, P_{A-1,A}$. Here we have omitted any branches and external momenta attached to them. Below each t_a , we label its mode $\mathcal{X}(t_a)$, and above each $P_{a,a+1}$, we label its characteristic mode \hat{X}_a .

however, according to corollary 6.5.1, t_1 and t_A must have at least one for each of them, satisfying eq. (6.22).

So far, we have characterized $\mathcal{F}_{\text{II}}^{(R)}$ terms by their subgraph structures via eq. (6.40), analogous to the previous characterizations of $\mathcal{U}^{(R)}$ and $\mathcal{F}_{\text{I}}^{(R)}$ terms in eqs. (6.13) and (6.18), respectively. Before proceeding to a summary of these results, we note that the modes $\mathcal{X}(\gamma'_a)$ and $\mathcal{X}(\gamma''_a)$ can be further constrained. To this end, we begin from the following lemma.

Lemma 6.8. *The modes $\mathcal{X}(t_a)$ ($a = 1, \dots, A$) are restricted to the following forms: there exist an index $b \in \{1, \dots, A\}$ and distinct directions $i \neq j$, such that*

$$\mathcal{X}(t_a) = S^{m_a} C_i^{n_a} \text{ for } a \in \{1, \dots, b\}, \text{ and } \mathcal{X}(t_a) = S^{m_a} C_j^{n_a} \text{ for } a \in \{b + 1, \dots, A\},$$

with the exponents satisfying

$$m_1 + n_1 > m_2 + n_2 > \dots > m_b + n_b, \text{ and } m_{b+1} + n_{b+1} < \dots < m_A + n_A.$$

Before going through a proof, we first discuss the meaning of this lemma by illustrating some concrete examples in figure 26. Each figure represents the reduced form of a $t(\mathbf{r}; \mathcal{H})$, where (a)–(d) have $A = 2$, (e)–(g) have $A = 3$, (h) and (i) have $A = 4$, and (j) has $A = 5$. One can verify the statement of lemma 6.8 directly through these examples. Consider, for instance, case (h), where

$$\mathcal{X}(t_1) = C_1^4, \quad \mathcal{X}(t_2) = SC_1^2, \quad \mathcal{X}(t_3) = S^2, \quad \mathcal{X}(t_4) = C_2^3. \quad (6.41)$$

Each mode above is of the form $S^m C_1^n$ or $S^m C_2^n$ (for $\mathcal{X}(t_3) = S^2$, we may regard it as belonging to both forms by taking $n = 0$), while the values $m + n$ satisfy $m_1 + n_1 > m_2 + n_2 > m_3 + n_3$ and $m_3 + n_3 < m_4 + n_4$. The characteristic modes of the paths,

$$\hat{X}_1 = SC_1^3, \quad \hat{X}_2 = S^2 C_1, \quad \hat{X}_3 = S^2 C_2, \quad (6.42)$$

are related to the subtree modes $\{\mathcal{X}(t_a)\}_{a=1,2,3,4}$ via the relations in lemma 6.7.

Below we prove lemma 6.8.

Proof. We first exclude an unwanted pattern. Suppose three consecutive characteristic subtrees t_1, t_2, t_3 all have modes of the same direction i :

$$\mathcal{X}(t_1) = S^{m_1} C_i^{n_1}, \quad \mathcal{X}(t_2) = S^{m_2} C_i^{n_2}, \quad \mathcal{X}(t_3) = S^{m_3} C_i^{n_3},$$

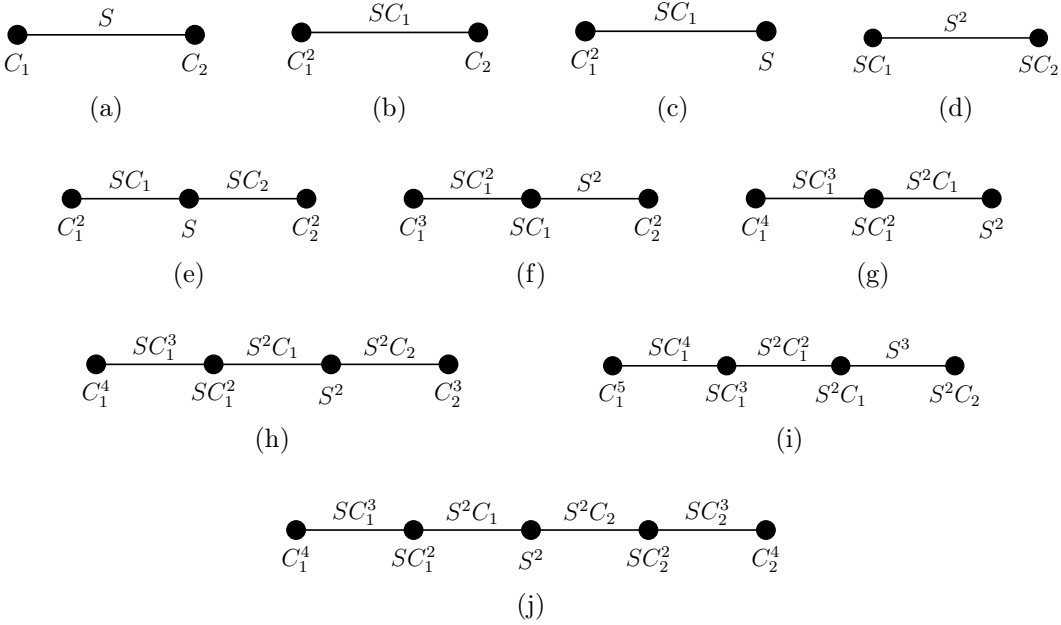


Figure 26. Some examples of reduced forms of $t(r; \mathcal{H})$, with the modes $\mathcal{X}(t_a)$ and \widehat{X}_a specified.

with $m_1 + n_1 < m_2 + n_2$ and $m_3 + n_3 < m_2 + n_2$. We show this cannot occur for a generic $\mathcal{F}_{\text{II}}^{(R)}$ term.

From corollary 6.7.1, the following condition must hold

$$(S^{m_1} C_i^{n_1} \vee S^{m_2} C_i^{n_2}) \wedge S^{m_3} C_i^{n_3} = S^{m_2} C_i^{n_2} \wedge S^{m_3} C_i^{n_3}. \quad (6.43)$$

Applying the \wedge and \vee rules from theorem 3.1 gives

$$(S^{m_1} C_i^{n_1} \vee S^{m_2} C_i^{n_2}) \wedge S^{m_3} C_i^{n_3} = S^{m_3} C_i^{\max\{m_1+n_1, m_3+n_3\}-m_3}, \quad (6.44a)$$

$$S^{m_2} C_i^{n_2} \wedge S^{m_3} C_i^{n_3} = S^{m_3} C_i^{m_2+n_2-m_3}. \quad (6.44b)$$

By construction, $\max\{m_1 + n_1, m_3 + n_3\} < m_2 + n_2$, so the right-hand sides cannot be equal. Hence, we must have either $m_1 + n_1 < m_2 + n_2 < m_3 + n_3$ or $m_1 + n_1 > m_2 + n_2 > m_3 + n_3$. The same reasoning extends to any chain of consecutive subtrees $t_{a+1}, t_{a+2}, \dots, t_{a+b}$ ($b \geq 2$) with modes of the same direction i :

$$\mathcal{X}(t_{a+1}) = S^{m_{a+1}} C_i^{n_{a+1}}, \quad \mathcal{X}(t_{a+2}) = S^{m_{a+2}} C_i^{n_{a+2}}, \quad \dots, \quad \mathcal{X}(t_{a+b}) = S^{m_{a+b}} C_i^{n_{a+b}}.$$

For such a chain one of the following two ordering patterns must hold:

- (1) $m_{a+1} + n_{a+1} < \dots < m_{a+b} + n_{a+b}$ and $m_{a+1} > \dots > m_{a+b}$,
- (2) $m_{a+1} + n_{a+1} > \dots > m_{a+b} + n_{a+b}$ and $m_{a+1} < \dots < m_{a+b}$.

The two cases are related by reversing the order of the subtrees; we may therefore assume, without loss of generality, that $m_{a+1} + n_{a+1} > \dots > m_{a+b} + n_{a+b}$ (case (2)). Theorem 3.1 then yields

$$\mathcal{X}(t_{a+1}) \vee \dots \vee \mathcal{X}(t_{a+b}) = S^{m_{a+1}} C_i^{m_{a+b} + n_{a+b} - m_{a+1}}. \quad (6.45)$$

Now let t_{a+1}, \dots, t_{a+b} be *all* the characteristic subtrees whose modes can be written as $S^m C_i^n$. If any other characteristic subtrees remain, they must have a different direction $j \neq i$ and lie either before t_{a+1} or after t_{a+b} . That leads to the following two possibilities.

Possibility 1: $\mathcal{X}(t_a) = S^{m_a} C_j^{n_a}$ for some $j \neq i$. Corollary 6.7.1 requires

$$(\mathcal{X}(t_{a+1}) \vee \dots \vee \mathcal{X}(t_{a+b})) \wedge \mathcal{X}(t_a) = \mathcal{X}(t_{a+1}) \wedge \mathcal{X}(t_a). \quad (6.46)$$

Using (6.45) and theorem 3.1, both sides of (6.46) can be evaluated. With the abbreviation $\sigma_\ell \equiv m_\ell + n_\ell$ we obtain

$$\begin{aligned} (\mathcal{X}(t_{a+1}) \vee \dots \vee \mathcal{X}(t_{a+b})) \wedge \mathcal{X}(t_a) &= S^{m_{a+1}} C_i^{m_{a+b} + n_{a+b} - m_{a+1}} \wedge S^{m_a} C_j^{n_a} \\ &= \begin{cases} S^{\sigma_{a+b}} C_j^{\sigma_a - \sigma_{a+b}} & \text{for } m_{a+b} + n_{a+b} \leq m_a + n_a, \\ S^{\sigma_a} C_i^{\sigma_{a+b} - \sigma_a} & \text{for } m_a + n_a \leq m_{a+b} + n_{a+b}, \end{cases} \end{aligned} \quad (6.47)$$

where we have defined $\sigma_a \equiv m_a + n_a$ throughout this proof for simplicity. Meanwhile,

$$\begin{aligned} \mathcal{X}(t_{a+1}) \wedge \mathcal{X}(t_a) &= S^{m_{a+1}} C_i^{n_{a+1}} \wedge S^{m_a} C_j^{n_a} \\ &= \begin{cases} S^{\sigma_{a+1}} C_j^{\sigma_a - \sigma_{a+1}} & \text{for } m_{a+1} + n_{a+1} \leq m_a + n_a, \\ S^{\sigma_a} C_i^{\sigma_{a+1} - \sigma_a} & \text{for } m_a + n_a \leq m_{a+1} + n_{a+1}. \end{cases} \end{aligned} \quad (6.48)$$

Because $i \neq j$ and $\sigma_{a+1} > \sigma_{a+b}$, the two expressions above would never coincide. Eq. (6.46) cannot be satisfied. Therefore, a subtree of direction j cannot appear *before* the aforementioned sequence of direction- i subtrees t_{a+1}, \dots, t_{a+b} . In other words, $a = 0$.

Possibility 2: $\mathcal{X}(t_{a+b+1}) = S^{m_{a+b+1}} C_j^{n_{a+b+1}}$ for some $j \neq i$. Corollary 6.7.1 requires

$$(\mathcal{X}(t_{a+1}) \vee \dots \vee \mathcal{X}(t_{a+b})) \wedge \mathcal{X}(t_{a+b+1}) = \mathcal{X}(t_{a+b}) \wedge \mathcal{X}(t_{a+b+1}). \quad (6.49)$$

A direct computation analogous to the previous one shows that (6.49) holds identically, regardless of the ordering of σ_{a+b} and σ_{a+b+1} :

$$\begin{aligned} (\mathcal{X}(t_{a+1}) \vee \dots \vee \mathcal{X}(t_{a+b})) \wedge \mathcal{X}(t_{a+b+1}) &= S^{m_{a+1}} C_i^{m_{a+b} + n_{a+b} - m_{a+1}} \wedge S^{m_{a+b+1}} C_j^{n_{a+b+1}} \\ &= \begin{cases} S^{\sigma_{a+b}} C_j^{\sigma_{a+b+1} - \sigma_{a+b}} & \text{for } m_{a+b} + n_{a+b} \leq m_{a+b+1} + n_{a+b+1} \\ S^{\sigma_{a+b+1}} C_i^{\sigma_{a+b} - \sigma_{a+b+1}} & \text{for } m_{a+b+1} + n_{a+b+1} \leq m_{a+b} + n_{a+b} \end{cases} \\ &= \mathcal{X}(t_{a+b}) \wedge \mathcal{X}(t_{a+b+1}), \end{aligned} \quad (6.50)$$

That is, a subtree of a different direction j may appear only *after* the sequence of direction- i subtrees t_{a+1}, \dots, t_{a+b} .

We can repeat the same analysis for the new direction j and obtain the following conclusion: all subtrees t_1, \dots, t_A must be partitioned into at most two contiguous sequences, each containing subtrees of a single direction. Furthermore, within each sequence the values $\sigma_a = m_a + n_a$ are *strictly monotonic*; the sequence containing t_1 has σ_a strictly decreasing, while the other sequence (if it exists) has σ_a strictly increasing. This is precisely the statement of the lemma. \square

As a final remark, the external momenta attached to t_a ($a = 1, \dots, A$), which we have denoted as $\mathbf{p}(t_a)$, must satisfy:

- $\mathcal{X}(\mathbf{p}(t_a))$ is equal to or softer than $\mathcal{X}(t_a)$;
- $\mathbf{p}(t_1), \mathbf{p}(t_A) \neq 0$, while other $\mathbf{p}(t_a)$ ($a = 2, \dots, A-1$) can be zero.;
- $\mathcal{X}(t_1) \vee \mathcal{X}(t_A) = \mathcal{X}(\mathbf{p}(t_1)) \vee \mathcal{X}(\mathbf{p}(t_A))$.

These properties are automatic from the lemmas above.

6.2.5 Summary

Let us summarize all the main results for the leading-term structure, which we have obtained so far, and formulate them into the following theorem.

Theorem 6.9. *For any given region R , the leading terms \mathbf{x}^r can be characterized as follows:*

- $\mathcal{U}^{(R)}$ term: each graph $\gamma \cap T^1(\mathbf{r})$, where γ denotes any mode component, is a spanning tree of $\tilde{\gamma}$. That is,

$$\mathbf{n}_\gamma = L(\tilde{\gamma}) \text{ for any mode component } \gamma. \quad (6.51)$$

- $\mathcal{F}_I^{(R)}$ term: there exists a corresponding mode component γ' with $\mathcal{X}(\gamma') = \mathcal{X}(Q(\mathbf{r}))$, such that (1) $\gamma' \cap T^2(\mathbf{r})$ is a spanning 2-tree of $\tilde{\gamma}'$; (2) for any other mode component $\gamma \neq \gamma'$, the graph $\gamma \cap T^2(\mathbf{r})$ is a spanning tree of $\tilde{\gamma}$. That is,

$$\mathbf{n}_{\gamma'} = L(\tilde{\gamma}') + 1, \quad \mathbf{n}_\gamma = L(\tilde{\gamma}) \quad \forall \gamma \neq \gamma'. \quad (6.52)$$

- $\mathcal{F}_{II}^{(R)}$ term: the spanning 2-tree $T^2(\mathbf{r})$ can be represented by figure 24, with mode components satisfying

$$\begin{aligned} \mathcal{X}(\gamma_a'') &= \mathcal{X}(\gamma_a') \wedge \mathcal{X}(\gamma_{a+1}'), \quad \text{for } a = 1, \dots, A-1, \\ \mathcal{X}(\gamma_a') &= \mathcal{X}(\gamma_{a-1}'') \vee \mathcal{X}(\gamma_a'') \quad \text{for } a = 2, \dots, A-1, \\ \mathbf{n}_{\gamma_1'} &= L(\tilde{\gamma}_1') + 1, \dots, \mathbf{n}_{\gamma_A'} = L(\tilde{\gamma}_A') + 1, \\ \mathbf{n}_{\gamma_1''} &= L(\tilde{\gamma}_1'') - 1, \dots, \mathbf{n}_{\gamma_{A-1}''} = L(\tilde{\gamma}_{A-1}'') - 1, \\ \mathbf{n}_\gamma &= L(\tilde{\gamma}), \quad \forall \gamma \notin \{\gamma_1', \dots, \gamma_A'\} \cup \{\gamma_1'', \dots, \gamma_{A-1}''\}. \end{aligned} \quad (6.53)$$

Furthermore, the modes of $\{\gamma_a'\}_{a=1, \dots, A}$ and $\{\gamma_a''\}_{a=1, \dots, A-1}$ are restricted by lemma 6.8.

This theorem will play an essential role in validating the infrared-compatibility requirement. Additionally, the Second Connectivity Theorem (theorem 5.3) admits a concise proof, which we present to conclude this subsection.

6.2.6 Proof of the Second Connectivity Theorem

Again, we proceed by contradiction. Suppose γ is a mode component that satisfies neither condition in theorem 5.3. We will show that for any leading term \mathbf{x}^r , the subgraph $\tilde{\gamma} \cap T(\mathbf{r})$ is always a spanning tree of $\tilde{\gamma}$, thereby inducing a homogeneity condition that renders the expanded integral scaleless.

From theorem 6.9, $\tilde{\gamma} \cap T(\mathbf{r})$ is a spanning tree of $\tilde{\gamma}$ as long as \mathbf{x}^r belongs to $\mathcal{U}^{(R)}(\mathbf{x})$ or $\mathcal{F}_I^{(R)}(\mathbf{x}; \mathbf{s})$. For \mathbf{x}^r being an $\mathcal{F}_{II}^{(R)}$ term, the only possibility for a different $\tilde{\gamma} \cap T(\mathbf{r})$ is that $\gamma \in \{\gamma'_1, \dots, \gamma'_n, \gamma''_1, \dots, \gamma''_{n-1}\}$. However, each γ''_i meets condition 1 of theorem 5.3: it is relevant to two harder-mode subgraphs γ'_i and γ'_{i+1} , with $\mathcal{X}(\gamma''_i) = \mathcal{X}(\gamma'_i) \wedge \mathcal{X}(\gamma'_{i+1})$. Meanwhile, each γ'_i meets condition 2 of theorem 5.3: there are two momenta $k_{i,1}, k_{i,2}$ —sourced from the external kinematics and/or softer-mode subgraphs relevant to γ'_i —entering γ'_i , such that $\mathcal{X}(\gamma'_i) = \mathcal{X}(k_{i,1}) \vee \mathcal{X}(k_{i,2})$. Therefore, γ can belong to neither $\{\gamma'_i\}$ nor $\{\gamma''_i\}$, and $\tilde{\gamma} \cap T(\mathbf{r})$ must be a spanning tree of $\tilde{\gamma}$ as well. This completes the proof of the Second Connectivity Theorem.

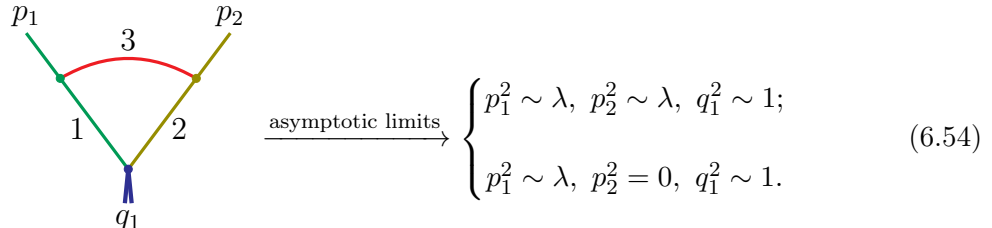
6.3 The infrared-compatibility requirement

This section demonstrates that for a configuration R satisfying the connectivity requirements, the infrared-compatibility requirement is both necessary and sufficient for R to be a region. This is equivalent to showing that the corresponding lower face f_R , which is spanned by all leading terms, is an N -dimensional space, where N is the number of edges in \mathcal{G} .

There have been previous analyses in this direction for the on-shell expansion [27] and soft expansion [24]; they aim to determine the dimension of f_R by identifying independent vectors within it: R is a (facet) region if and only if one can find N independent vectors. Here, in contrast, we shall employ an equivalent but formally more concise approach, namely, to investigate whether the space normal to f_R is one dimensional.

This can be achieved by solving for the edge weights $\{w_e\}_{e \in \mathcal{G}}$ from the leading polynomial. Specifically, each term that is leading in the expansion with respect to R yields a linear equation constraining these weights. Given the complete set of these constraints, the condition that f_R is N dimensional is then equivalent to the uniqueness of the solution for $\{w_e\}$.

Let us see this from the following two configurations of the one-loop form factor, with the external momenta in two distinct asymptotic limits:



$$\xrightarrow{\text{asymptotic limits}} \begin{cases} p_1^2 \sim \lambda, p_2^2 \sim \lambda, q_1^2 \sim 1; \\ p_1^2 \sim \lambda, p_2^2 = 0, q_1^2 \sim 1. \end{cases} \quad (6.54)$$

The edges e_1 , e_2 , and e_3 are in the C_1 , C_2 , and S modes respectively. This configuration, as has been explained in section 1, is a region for the first asymptotic limit ($p_1^2 \sim \lambda$, $p_2^2 \sim \lambda$, $q_1^2 \sim 1$), but not for the second one ($p_1^2 \sim \lambda$, $p_2^2 = 0$, $q_1^2 \sim 1$).

This conclusion can be derived by solving for the edge weights. Recall that we use \mathbf{x}^r to represent a term $s \cdot x_1^{r_1} \cdots x_N^{r_N}$ where $s \sim \lambda^{r_N+1}$. If \mathbf{x}^r is a leading term, we have:

$$\sum_{i=1}^N r_i \cdot w_{e_i} + r_{N+1} = w_{\mathcal{G}}, \quad (6.55)$$

where $w_{\mathcal{G}}$ is called the leading weight, which is the same for all leading terms. From now on, we will refer to eq. (6.55) as the *characteristic equation* of \mathbf{x}^r . For the first asymptotic limit, the leading terms and their characteristic equations are:

$$\begin{aligned} x_3 &\rightarrow w_{e_3} = w_{\mathcal{G}}; \\ (-p_1^2)x_1x_3 &\rightarrow w_{e_1} + w_{e_3} + 1 = w_{\mathcal{G}}; \\ (-p_2^2)x_2x_3 &\rightarrow w_{e_2} + w_{e_3} + 1 = w_{\mathcal{G}}; \\ (-q_1^2)x_1x_2 &\rightarrow w_{e_1} + w_{e_2} = w_{\mathcal{G}}. \end{aligned} \quad (6.56)$$

There is a unique solution to the equations above: $(w_{e_1}, w_{e_2}, w_{e_3}) = (-1, -1, -2)$, which confirms that the configuration is a region in this limit. In contrast, for the second limit, we only have three (instead of four) leading terms, corresponding to a subset of the equations above:

$$\begin{aligned} x_3 &\rightarrow w_{e_3} = w_{\mathcal{G}}; \\ (-p_1^2)x_1x_3 &\rightarrow w_{e_1} + w_{e_3} + 1 = w_{\mathcal{G}}; \\ (-q_1^2)x_1x_2 &\rightarrow w_{e_1} + w_{e_2} = w_{\mathcal{G}}. \end{aligned} \quad (6.57)$$

Here the solution is no longer unique: $(w_{e_1}, w_{e_2}, w_{e_3}) = (-1, -1 + a, -2 + a)$ contains a free parameter $a \in \mathbb{R}$. This means that the space normal to f_R is at least two dimensional, so f_R is at most $N - 1$ dimensional, and the configuration is not a region in this limit.

In the following, we will apply this method to generic Feynman graphs in the wide-angle kinematics. In section 6.3.1, we show the sufficiency of the infrared-compatibility requirement: with this requirement fulfilled, one can specify the unique solution of $(w_{e_1}, \dots, w_{e_N})$ based on the leading-term characteristic equations, using a weight-solving algorithm we shall provide. In section 6.3.2, we show the necessity of the infrared-compatibility requirement by contradiction: once it is not fulfilled, the solution always contains a free parameter $a \in \mathbb{R}$.

6.3.1 Proof of sufficiency

We first introduce a lemma regarding the edge weights within the same mode component.

Lemma 6.10. *For any mode component γ , the characteristic equations with respect to the $\mathcal{U}^{(R)}$ terms constrain all edge weights in γ to be equal. Consequently, solving for one of them automatically determines the others.*

This lemma has been stated and proved (as theorem 1) in ref. [27]; for brevity, we omit the proof here. From this, by setting all the edge weights in a mode component equal, all the characteristic equations for the $\mathcal{U}^{(R)}$ terms reduce to a single one. To solve for all edge weights in \mathcal{G} , it is therefore sufficient to solve for one arbitrary edge weight from each mode component. We now present a recursive procedure that accomplishes this, which we refer to as the *weight-solving algorithm*.

Weight-solving algorithm

Step 1. By comparing the characteristic equations from specific $\mathcal{U}^{(R)}$ and $\mathcal{F}_I^{(R)}$ terms, solve the edge weight of any γ for which the partial momentum—sourced exclusively from the external kinematics—is $\mathcal{X}(\gamma)$.

Step 2. If edges with unsolved weights remain, compare specific $\mathcal{F}_{II}^{(R)}$ terms to solve the weight of any 1VI component $\tilde{\gamma}$ satisfying one of the following conditions:

- $\mathcal{X}(\gamma) = S^m$, and γ is contained in a degree- m messenger and relevant to some weight-solved mode component γ_1 ;
- $\mathcal{X}(\gamma) = S^m C_i^n$ ($n \in \mathbb{N}$), and γ is relevant to two weight-solved mode components γ_1 and γ_2 , with $\mathcal{X}(\gamma) = \mathcal{X}(\gamma_1) \wedge \mathcal{X}(\gamma_2)$.

Step 3. If edges with unsolved weights remain, attach to any vertex of those γ (from the previous step) an $\mathcal{X}(\gamma)$ -mode external momentum.

Step 4+. Repeat Steps 1–3 until all edge weights are solved.

Recall the definition of infrared compatibility from section 5.2.2, which is closely related to the procedure described above. In fact, the weight-solving algorithm provides a concrete representation of how the condition of infrared compatibility “propagates” through the subgraphs. Specifically, if the process of solving for weights by comparing certain leading terms, as outlined in Steps 1 and 2, proceeds successfully, then fulfilling the infrared-compatibility requirement (i.e., all the mode components are infrared compatible) guarantees that the procedure will terminate with all edge weights solved. This constitutes the core idea of our proof.

The purpose of Step 3 is to induce the recursive procedure by enabling the repetition of Steps 1 and 2 on the modified graph. A crucial subtlety, however, arises here: attaching an additional external momentum to \mathcal{G} can generate new leading terms, hence new characteristic equations constraining the weights $\{w_e\}$. We must therefore demonstrate that these new equations are (linearly) *dependent* on the original ones; otherwise, the addition of such an external momentum would change the dimension of f_R , invalidating the whole proof.

Consequently, the remainder of this section will demonstrate:

- (1) how the edge weights can be solved as indicated in Steps 1 and 2;

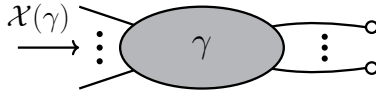


Figure 27. The configuration of a mode component γ , whose total external momentum is in the mode $\mathcal{X}(\gamma)$. The circled vertices are those belonging to harder-mode subgraphs, hence not in γ .

(2) why the additional characteristic equations from Step 3 can be determined by the original ones.

Starting from Step 1, let us consider any given 1VI component $\tilde{\gamma}$, whose total external momentum is of the mode $\mathcal{X}(\gamma)$. The configuration of γ can then be described by figure 27, where the circled vertices are those belonging to harder-mode subgraphs (hence not in γ), which are identified as a single vertex in $\tilde{\gamma}$.

Among all the terms of $\mathcal{P}^{(R)}$, we choose two typical ones as follows. The first, \mathbf{x}^{r_1} , is a $\mathcal{U}^{(R)}$ term. From lemma 6.2, $\tilde{\gamma} \cap T^1(\mathbf{r}_1)$ is a spanning tree of $\tilde{\gamma}$. Since the total external momentum flowing through $\tilde{\gamma}$ is of the mode $\mathcal{X}(\gamma)$, we can always choose \mathbf{x}^{r_1} such that there is one edge $e \in \gamma \cap T^1(\mathbf{r}_1)$, with the momentum flowing through e of the mode $\mathcal{X}(\gamma)$. Based on this, we can further construct an \mathcal{F} term \mathbf{x}^{r_2} , such that $T^2(\mathbf{r}_2) = T^1(\mathbf{r}_1) \setminus e$. It follows from eq. (6.19) that \mathbf{x}^{r_2} is an $\mathcal{F}_I^{(R)}$ term.

One can then examine the characteristic equations for \mathbf{x}^{r_1} and \mathbf{x}^{r_2} . Their differences lie in a w_e term (which the \mathbf{x}^{r_2} equation possesses while the \mathbf{x}^{r_1} equations does not) and their kinematic contributions (the r_{N+1} term in eq. (6.55), which is 0 for $\mathbf{r} = \mathbf{r}_1$ while $\mathcal{V}(\mathcal{X}(\gamma))$ for $\mathbf{r} = \mathbf{r}_2$). By subtracting these equations, we obtain

$$0 = w_e + \mathcal{V}(\mathcal{X}(\gamma)) \Leftrightarrow w_e = -\mathcal{V}(\mathcal{X}(\gamma)). \quad (6.58)$$

The weight of any edge $e \in \gamma$ is then solved equally as $-\mathcal{V}(\mathcal{X}(\gamma))$, as the content of Step 1.

Now suppose some edges have unsolved weights at this point. We proceed to Step 2. Since all the mode components are infrared compatible, the definition in section 5.2.2 guarantees that at least one component γ satisfying the condition in Step 2 must exist. We now explain how to solve for the weight of edges from such a γ , which we denote by w_γ from now on.

Let us consider the first case of Step 2. As the degree- m messenger $\Gamma^{[m]}$ is defined to be relevant to three or more mode components, one of which is γ_1 , three possibilities occur:

- (a) γ is relevant to ≥ 3 mode components (γ_1 and another two or more);
- (b) γ is relevant to 2 mode components (γ_1 and another one);
- (c) γ is relevant to 1 mode component (γ_1).

These three possibilities can be represented by figure 28, where for simplicity let us omit all additional loop structures. The analysis below would also apply in the existence of more complicated structures. For each possibility, $\Gamma^{[m]}$ is relevant to the mode components γ_i

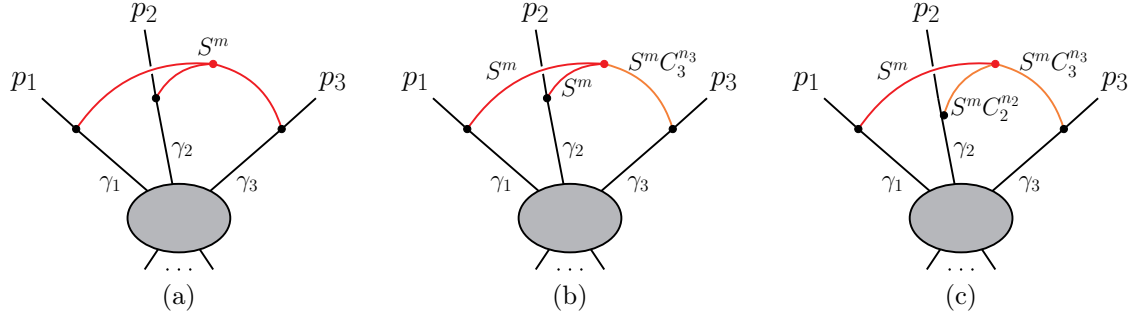


Figure 28. Three representative configurations for the S^m component γ within the messenger $\Gamma^{[m]}$, represented by red curves. The subgraphs γ_i ($i = 1, 2, 3$) are the mode components to which $\Gamma^{[m]}$ is relevant, and the p_i ($i = 1, 2, 3$) are their respective external momenta. Further loop structures within γ_i ($i = 1, 2, 3$) are omitted. The gray blob represents the remaining part of \mathcal{G} .

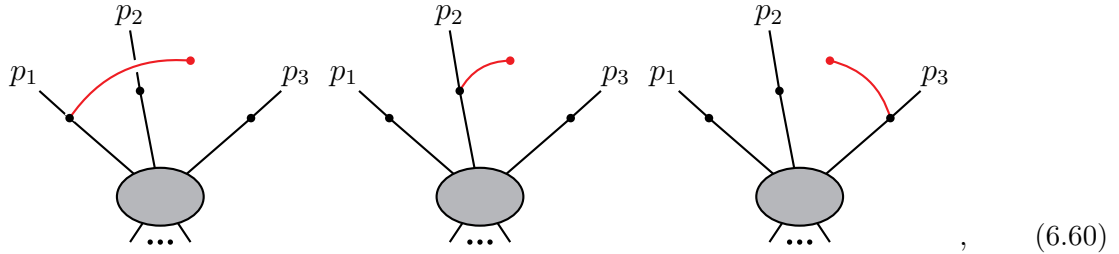
($i = 1, 2, 3$), and p_i are their external momenta respectively. In particular, γ_1 is the mode subgraph whose edge weights have been solved in Step 1. Below we shall analyze what modes γ_i and p_i can possibly have.

In figure 28a, the S^m component is relevant to γ_1 , γ_2 , and γ_3 by construction. Each mode $\mathcal{X}(\gamma_i)$ is of the form $S^{m-m_i} C_i^{m_i}$. Since the edge weights of γ_1 have been solved in Step 1, its external momentum p_1 must be of the mode $\mathcal{X}(\gamma_1)$. We therefore have

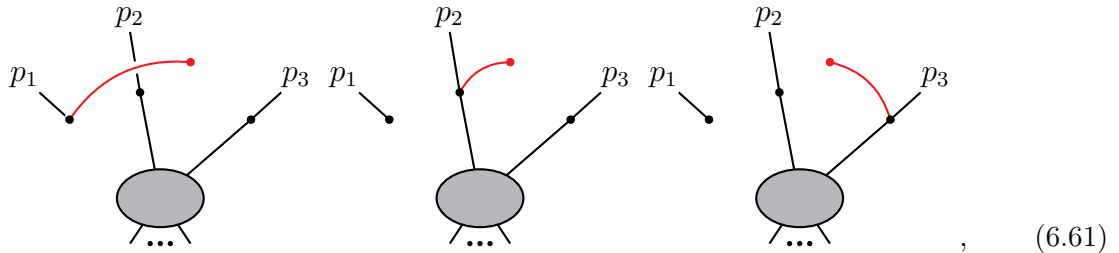
$$\mathcal{X}(\gamma_1) = S^{m-m_1} C_1^{m_1}, \quad \mathcal{X}(\gamma_2) = S^{m-m_2} C_2^{m_2}, \quad \mathcal{X}(\gamma_3) = S^{m-m_3} C_3^{m_3}; \quad (6.59a)$$

$$\mathcal{X}(p_1) = S^{m-m_1} C_1^{m_1}, \quad \mathcal{X}(p_2) = S^{m-m_2} C_2^{m_2+n'_2}, \quad \mathcal{X}(p_3) = S^{m-m_3} C_3^{m_3+n'_3}. \quad (6.59b)$$

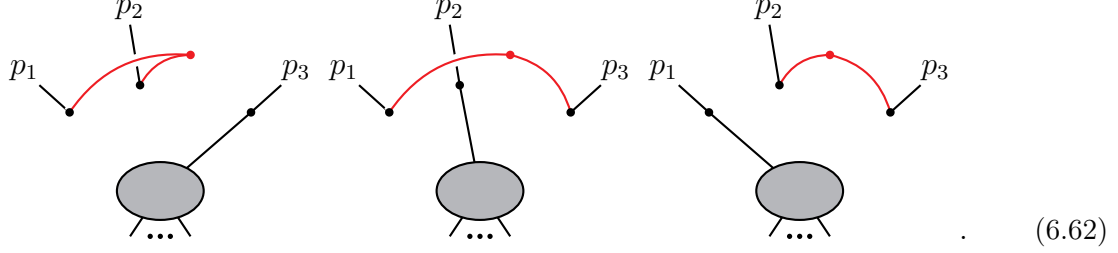
From section 6.2, the leading polynomial contains the following $\mathcal{U}^{(R)}$ terms



$\mathcal{F}_1^{(R)}$ terms



and $\mathcal{F}_{\text{II}}^{(R)}$ terms



Note that the gray blobs in (6.60)-(6.62) represent certain tree subgraphs. By comparing the characteristic equations of the $\mathcal{U}^{(R)}$ and $\mathcal{F}_{\text{I}}^{(R)}$ terms, we have set $w_{e_1} = -\mathcal{V}(\mathcal{X}(\gamma_1))$ as in eq. (6.58), as the content of Step 1.

The kinematic coefficient for the $\mathcal{F}_{\text{II}}^{(R)}$ terms, from eq. (6.59), are of the following scales:

$$(p_1 + p_2)^2 \sim \lambda^{2m-m_1-m_2}, \quad (p_1 + p_3)^2 \sim \lambda^{2m-m_1-m_3}, \quad (p_2 + p_3)^2 \sim \lambda^{2m-m_2-m_3}, \quad (6.63)$$

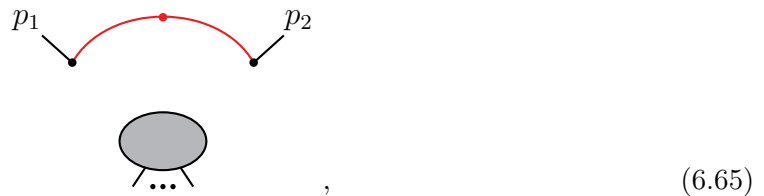
which can be derived from the \vee -operation rule (see theorem 3.1). We then consider the characteristic equations of the $\mathcal{F}_{\text{II}}^{(R)}$ terms and compare them with those of the $\mathcal{U}^{(R)}$ terms. In detail, the differences between the first $\mathcal{U}^{(R)}$ and $\mathcal{F}_{\text{II}}^{(R)}$ terms lie in the terms w_{γ_1} and w_{γ_2} (present in the $\mathcal{U}^{(R)}$ -term equation but absent from the $\mathcal{F}_{\text{II}}^{(R)}$ -term equation), a w_{γ} term (present in the $\mathcal{F}_{\text{II}}^{(R)}$ -term equation but absent from the $\mathcal{U}^{(R)}$ -term equation), and the kinematic contribution (which is 0 for the $\mathcal{U}^{(R)}$ term and $2m - m_1 - m_2$ for the $\mathcal{F}_{\text{II}}^{(R)}$ term). The sum over these contributions must be zero, which yields one equation.

By comparing the $\mathcal{U}^{(R)}$ term and the other two $\mathcal{F}_{\text{II}}^{(R)}$ terms, we obtain another two equations. We then have:

$$\left. \begin{aligned} w_{\gamma_1} + w_{\gamma_2} - w_{\gamma} + (2m - m_1 - m_2) &= 0 \\ w_{\gamma_1} + w_{\gamma_3} - w_{\gamma} + (2m - m_1 - m_3) &= 0 \\ w_{\gamma_2} + w_{\gamma_3} - w_{\gamma} + (2m - m_2 - m_3) &= 0 \end{aligned} \right\} \Rightarrow w_{\gamma} = -2m. \quad (6.64)$$

Furthermore, from the above we obtain $w_{\gamma_2} = -2m + m_2$ and $w_{\gamma_3} = -2m + m_3$. These weights are determined by repeatedly applying Step 1 in subsequent recursions. In this manner, we have solved for w_{γ} , completing Step 2. For the other two cases shown in figures 28b and 28c, nearly identical analyses yield w_{γ} , which are detailed in appendix A.2.

Now we consider the second case of Step 2, where γ is relevant to two weight-solved mode components γ_1 and γ_2 (and possibly other mode components), with $\mathcal{X}(\gamma) = \mathcal{X}(\gamma_1) \wedge \mathcal{X}(\gamma_2)$. This case can be represented by figure 29. We denote $\mathcal{X}(\gamma) = S^m C_i^n$ (note that $n = 0$ is possible), $\mathcal{X}(\gamma_1) = S_1^m C_1^{n_1}$, and $\mathcal{X}(\gamma_2) = S_2^m C_2^{n_2}$. The following $\mathcal{F}_{\text{II}}^{(R)}$ term exists:



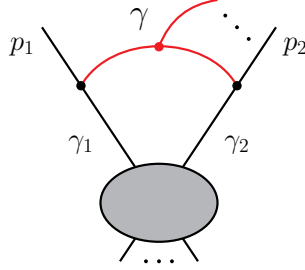


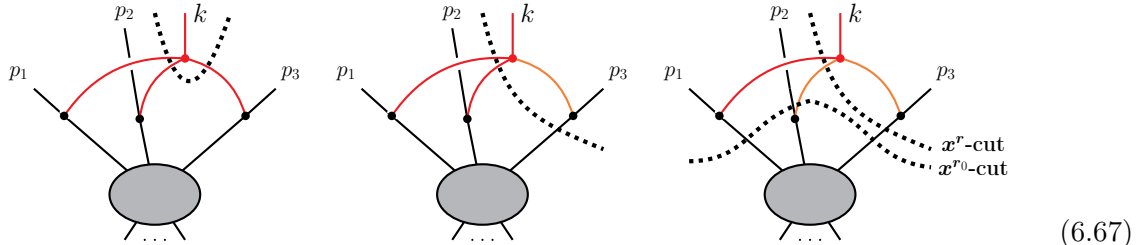
Figure 29. The second case of γ in Step 2, represented by the red curves. Further loop structures within γ_1 , γ_2 , and γ are omitted.

where the gray blob represents certain tree structures. Note that the momentum flowing between the two components of this spanning 2-tree is of the mode $\mathcal{X}(\gamma_1) \vee \mathcal{X}(\gamma_2)$.¹¹ Comparing the characteristic equations of this $\mathcal{F}_{\text{II}}^{(R)}$ term and the $\mathcal{U}^{(R)}$ terms yields

$$\begin{aligned} 0 &= w_{\gamma_1} + w_{\gamma_2} - w_{\gamma} + \mathcal{V}(\mathcal{X}(\gamma_1) \vee \mathcal{X}(\gamma_2)) \\ &= -\mathcal{V}(\mathcal{X}(\gamma_1)) - \mathcal{V}(\mathcal{X}(\gamma_2)) - w_{\gamma} + \mathcal{V}(\mathcal{X}(\gamma_1) \vee \mathcal{X}(\gamma_2)) \quad \Rightarrow \quad w_{\gamma} = \mathcal{V}(\mathcal{X}(\gamma_1) \wedge \mathcal{X}(\gamma_2)), \end{aligned} \quad (6.66)$$

where lemma 3.3 has been applied. We have thus justified Step 2 completely.

We proceed to Step 3 of the weight-solving algorithm, where the operation is to attach some additional external momenta to the vertices of those γ in Step 2. For example, this operation modifies the three configurations in figure 28 into the following (at this moment let us ignore the dotted curves, which are for later use):



As we have explained, additional terms can be introduced to the original leading polynomial, and we must confirm that their corresponding characteristic equations can be obtained from the original ones.

To this end, let us inspect the structure of these extra leading terms. A first observation is that they can only be $\mathcal{F}^{(R)}$ terms, because $\mathcal{U}^{(R)}$ terms correspond to minimum spanning trees of \mathcal{G} , the set of which does not depend on the external momenta. Let us then take any of these terms, denote it as \mathbf{x}^r , and suppose the total momentum flowing between the components of $T^2(\mathbf{r})$ to be in the mode X_* . Since k is one of the external momenta, $\mathcal{X}(k)$ must be either equal to or softer than X_* . We now consider these possibilities.

¹¹By definition, the mode is $\mathcal{X}(p_1) \vee \mathcal{X}(p_2)$. Since the edge weights of γ_1 and γ_2 have been solved in Step 1, we must also have $\mathcal{X}(p_1) = \mathcal{X}(\gamma_1)$ and $\mathcal{X}(p_2) = \mathcal{X}(\gamma_2)$ here.

For $\mathcal{X}(k)$ equal to X_* , the external momentum k is the hardest one among all attached to the same component of $T^2(\mathbf{r})$. The extra $\mathcal{F}^{(R)}$ term, which does not exist in the original Symanzik polynomial, must then be an $\mathcal{F}_I^{(R)}$ term. The first graph in (6.67) is an example, where the dotted curve represents the unitarity cut separating the two components of $T^2(\mathbf{r})$. Subtracting the characteristic equation of this $\mathcal{F}_I^{(R)}$ term from those of the $\mathcal{U}^{(R)}$ terms yields the trivial identity $w_\gamma - w_{\gamma'} = 0$. Hence, these additional $\mathcal{F}^{(R)}$ terms do not produce independent characteristic equations.

For $\mathcal{X}(k)$ softer than X_* , we can in fact sharpen the statement: $\mathcal{X}(k)$ must be *marginally softer than X_** (a concept defined in section 5.2.2). If it were not marginally softer, another external momentum attached to the same component would dominate the total momentum transfer, causing the term to already appear in the original $\mathcal{F}^{(R)}$ polynomial. One example is the second graph in (6.67), where $\mathcal{X}(k) = \mathcal{X}(\gamma) = S^m$, which is marginally softer than the total momentum $p_3 + k$ flowing across the unitarity cut, whose mode is $X_* = S^{m-m_3} C_3^{m_3}$ (can be obtained from eq. (6.59)).

In general, let the total momentum flowing between the components of $T^2(\mathbf{r})$ be $k + p'$, where the external momenta k and p' are both attached to $t(\mathbf{r}; \mathcal{H})$ (defined in section 6.2.4), with k added in Step 3 and p' from the original kinematics. In our previous example, the second graph in (6.67), $p' = p_3$. As argued above, the mode $\mathcal{X}(k)$ is marginally softer than $X_* = \mathcal{X}(k) \vee \mathcal{X}(p')$, and therefore, $\mathcal{X}(k)$ is overlapping with $\mathcal{X}(p')$.¹² To demonstrate that the characteristic equation of this $\mathcal{F}^{(R)}$ term is linearly dependent on the original equations, we now state a key property concerning the virtuality degrees of general modes, captured by the following lemma.

Lemma 6.11. *Let $X_1 = S^{m_1} C_i^{n_1}$ and $X_2 = S^{m_2} C_i^{n_2}$ with $m_1 + n_1 = m_2 + n_2$, then for any $X_3 = S^{m_3} C_j^{n_3}$ (with $j \neq i$) such that both X_1 and X_2 are overlapping with X_3 , we have*

$$\mathcal{V}(X_1 \vee X_3) - \mathcal{V}(X_1) = \mathcal{V}(X_2 \vee X_3) - \mathcal{V}(X_2). \quad (6.68)$$

Proof. By employing theorem 3.1, we have

$$\mathcal{V}(X_i) = 2m_i + n_i, \quad \mathcal{V}(X_i \vee X_3) = m_i + m_3 \quad \text{for } i = 1, 2. \quad (6.69)$$

Therefore, $\mathcal{V}(X_1 \vee X_3) - \mathcal{V}(X_1) = m_3 - m_1 - n_1 = m_3 - m_2 - n_2 = \mathcal{V}(X_2 \vee X_3) - \mathcal{V}(X_2)$. \square

We aim to employ lemma 6.11 to illustrate that any new $\mathcal{F}_{II}^{(R)}$ term \mathbf{x}^r arising from k corresponds to an original $\mathcal{F}_{II}^{(R)}$ term \mathbf{x}^{r_0} , such that they have the same characteristic equation.

As noted earlier, the external momenta attached to $t(\mathbf{r}; \mathcal{H})$ are k and p' , where p' originates from the original external kinematics and $\mathcal{X}(p')$ overlaps with $\mathcal{X}(k)$. A direct inspection of figures 28 and 29, which exhaust all possible configurations of γ in Step 2, reveals that there always exists another external momentum p_0 attached to a mode component γ_0 whose weight w_{γ_0} was solved as $-\mathcal{V}(\mathcal{X}(p_0))$ in Step 1, such that:

¹²Here we do not need to consider the possibility that $\mathcal{X}(k)$ is marginally softer than $\mathcal{X}(p')$, because in this case, having an additional k does not affect any original characteristic equations.

- (1) $\mathcal{X}(p_0)$ is overlapping with $\mathcal{X}(p')$;
- (2) There is another $\mathcal{F}^{(R)}$ term \mathbf{x}^{r_0} with both p' and p_0 attached to the $t(\mathbf{r}_0; \mathcal{H})$.

For example, in the third graph of (6.67), we have $p' = p_3$, $p_0 = p_1$, $\gamma_0 = \gamma_1$, and the unitarity cuts corresponding to \mathbf{x}^r and \mathbf{x}^{r_0} are labeled “ \mathbf{x}^r -cut” and “ \mathbf{x}^{r_0} -cut”, respectively. The characteristic equations of \mathbf{x}^r and \mathbf{x}^{r_0} read:

$$\begin{aligned}\mathbf{x}^r : \quad & w_\gamma + \mathcal{V}(\mathcal{X}(k) \vee \mathcal{X}(p')) + \dots = 0; \\ \mathbf{x}^{r_0} : \quad & w_{\gamma_0} + \mathcal{V}(\mathcal{X}(p_0) \vee \mathcal{X}(p')) + \dots = 0.\end{aligned}\tag{6.70}$$

Here the terms represented by “ \dots ” are identical. Recall that the weights $w_{\gamma_0} = -\mathcal{V}(\mathcal{X}(p_0))$ and $w_\gamma = -\mathcal{V}(\mathcal{X}(k))$ have already been determined in Steps 1 and 2. Applying lemma 6.11 with $X_1 = \mathcal{X}(p_0)$, $X_2 = \mathcal{X}(k)$, and $X_3 = \mathcal{X}(p')$ shows that the two equations in (6.70) are indeed equivalent. In other words, the characteristic equation for \mathbf{x}^r can always be derived from that of an original leading term \mathbf{x}^{r_0} . This confirms that Step 3 introduces *no* new independent characteristic equations beyond those obtained in previous steps.

With this established, one can iterate Steps 1–3 until all edge weights are solved—a process guaranteed to terminate provided all mode components are infrared compatible, as demonstrated earlier. This completes the proof of the sufficiency of the infrared-compatibility requirement.

6.3.2 Proof of necessity

We now show the necessity of the infrared-compatibility requirement. We will see that once it is not fulfilled in a configuration, the solution of the edge weights from the set of leading-term characteristic equations, (6.55), will always contain a free parameter $a \in \mathbb{R}$. Such freedom would render the expanded integral scaleless and exclude the configuration from the region list.

To proceed, we consider a specific subgraph Γ_Δ composed exclusively of non-infrared-compatible mode components, with the following properties after every component in $\mathcal{G} \setminus \Gamma_\Delta$ has been set to infrared compatible:

- 1, *none* of the components in Γ_Δ becomes infrared compatible;
- 2, setting *any* single component in Γ_Δ to infrared compatible causes *all* the others to become infrared compatible as a consequence.

In other words, Γ_Δ is a “minimal piece” of the complete set of non-infrared-compatible components. The first condition means that the infrared compatibility of Γ_Δ cannot be induced from outside. The second condition means that no proper subset of Γ_Δ has this property.

Three examples of Γ_Δ are shown in figure 30, where the edges belonging to Γ_Δ are drawn bold and dash-dotted. Each configuration in figure 30 yields a scaleless integral because certain mode components are not infrared compatible; Γ_Δ is a particular subset of those components. In figure 30a, the non-infrared-compatible components are the S and C_1 edges, and the only

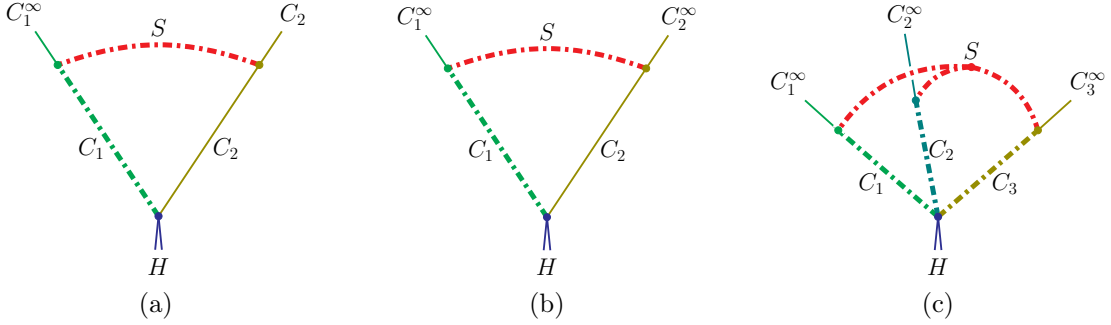


Figure 30. Three examples of Γ_Δ ; its edges are drawn bold and dash-dotted. In each configuration the whole integral is scaleless because the infrared-compatibility requirement is not satisfied.

possible Γ_Δ is their union (together with their shared vertex), because setting either edge infrared compatible automatically makes the other infrared compatible. In figure 30b, none of the edges are infrared compatible, but Γ_Δ cannot be the union of all three edges because it can be reduced: one can set the C_2 edge infrared compatible without forcing the other two to become infrared compatible. Consequently, in this case Γ_Δ consists of the S and C_1 edges (and their shared vertex). In figure 30c, none of the edges are infrared compatible, and a degree-1 messenger (defined in section 5.2.2) is present. Hence, setting any single mode component infrared compatible forces all the others to become infrared compatible. As a result, Γ_Δ must be the union of all these edges.

Note that in a given scaleless configuration, the choice of Γ_Δ may not be unique. For example, in figure 30b, Γ_Δ was chosen as the union of the S and C_1 edges, and their shared vertex. Due to symmetry, it could equally be chosen in the other direction, consisting of the S and C_2 edges, and their shared vertex.

Two fundamental structures within Γ_Δ are already visible from these examples. First, if a component $\gamma \subset \Gamma_\Delta$ is an S^M component that also serves as a degree- M messenger (like the S component in figure 30c), then all $S^m C_i^{M-m}$ components to which γ is relevant (such as the C_i components in figure 30c, where $(m, M) = (0, 1)$) must also lie inside Γ_Δ . Second, for each such $S^m C_i^{M-m}$ component, if another S^M component is relevant to it but not part of a degree- M messenger (as are the S components in figures 30a and 30b), it must also belong to Γ_Δ . In the following, we will put these statements on a rigorous footing to construct a general Γ_Δ , and demonstrate its consistency with the definition.

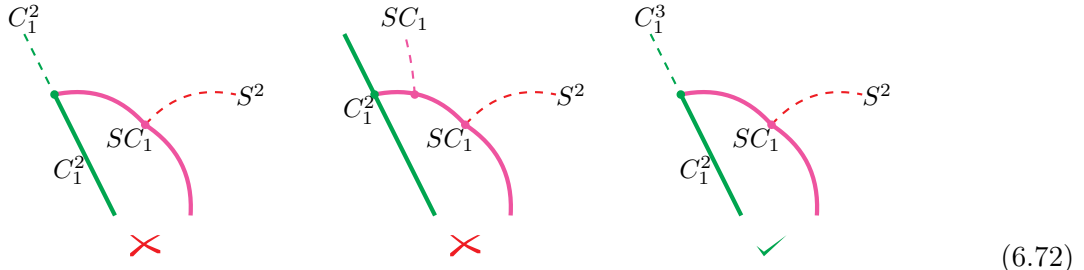
To begin, pick any S^M component $\gamma_A \subset \Gamma_\Delta$ that is contained in a degree- M messenger. (If no such γ_A exists, we skip the steps that involve it.) By definition, γ_A must be relevant to some $S^m C_i^n$ components with $m + n = M$. All of these $S^m C_i^n$ components must belong to Γ_Δ ; otherwise, declaring all the components in $\mathcal{G} \setminus \Gamma_\Delta$ infrared compatible would make some of them infrared compatible, further making γ_A infrared compatible (as we have seen in analyzing the three possibilities in figure 28), which contradicts the definition of Γ_Δ . We denote the union of all such γ_A by $\Gamma_{[\mathcal{S}_A]}$, with “ \mathcal{S}_A ” indicating specific subgraphs of \mathcal{S} . By

construction, the edges and vertices of $\Gamma_{[S_A]}$ are all in the same mode S^M .

Now consider the $S^m C_i^n$ components $\Gamma_{[S_A]}$ is relevant to. Suppose they involve directions $i = 1, \dots, I$ ($I \geq 1$), and for each i , the hardest mode among them is $S^{m_i} C_i^{n_i}$ ($m_i + n_i = M$). We then group the components into the following subgraphs:

$$\begin{aligned}\Gamma_{[\mathcal{SJ}_1]} &:= \gamma_{S^{m_1} C_1^{n_1}} \cup \gamma_{S^{m_1+1} C_1^{n_1-1}} \cup \dots \cup \gamma_{S^{m_1+n_1-1} C_1}, \\ \Gamma_{[\mathcal{SJ}_2]} &:= \gamma_{S^{m_2} C_2^{n_2}} \cup \gamma_{S^{m_2+1} C_2^{n_2-1}} \cup \dots \cup \gamma_{S^{m_2+n_2-1} C_2}, \\ &\dots \\ \Gamma_{[\mathcal{SJ}_I]} &:= \gamma_{S^{m_I} C_I^{n_I}} \cup \gamma_{S^{m_I+1} C_I^{n_I-1}} \cup \dots \cup \gamma_{S^{m_I+n_I-1} C_I}.\end{aligned}\tag{6.71}$$

The subscript “[\mathcal{SJ}_i]” indicates that the edges and vertices of $\Gamma_{[\mathcal{SJ}_i]}$ are in $\mathcal{S} \cup \mathcal{J}_i$. A key observation about the external momentum entering $\Gamma_{[\mathcal{SJ}_i]}$ is that its mode must be of the form $S^{m_i} C_i^{n_i+n'_i}$, with $n'_i \in \mathbb{N}_+ \cup \{\infty\}$. This is the only form that ensures: (1) no mode component inside $\Gamma_{[\mathcal{SJ}_i]}$ is infrared compatible, and (2) momentum conservation is consistent with the wide-angle kinematics in (2.1). The examples below for $M = 2$ illustrate this point, showing three different configurations of $\Gamma_{[\mathcal{SJ}_1]}$ and the momenta attached to them. In the figures, thick solid lines represent $\Gamma_{[\mathcal{SJ}_1]}$, the red dashed line labeled “ S^2 ” denotes the momentum from $\Gamma_{[S_A]}$ entering $\Gamma_{[\mathcal{SJ}_1]}$, and the remaining dashed line represents the external momentum of $\Gamma_{[\mathcal{SJ}_1]}$, whose mode is C_1^2 in the first example, SC_1 in the second, and C_1^3 in the third.



The first configuration is not possible because the external momentum entering $\Gamma_{[\mathcal{SJ}_1]}$ is of the mode C_1 . This would render the C_1 component of $\Gamma_{[\mathcal{SJ}_1]}$ infrared compatible, violating the defining property of Γ_Δ . The second configuration is also impossible: by momentum conservation, the C_1 component would require a p_1 -type external momentum input (see (2.1a)), which cannot coexist with the SC_1^2 external momentum in our wide-angle kinematics, (2.1d). The third configuration, in contrast, is possible: the mode components in $\Gamma_{[\mathcal{SJ}_1]}$ could become infrared compatible only after $\Gamma_{[S_A]}$ is set infrared compatible.

Similarly, there can be external momenta attached directly to a given γ_A . Denote the total momentum entering γ_A as $\mathbf{p}(\gamma_A)$.¹³ By momentum conservation, the mode $\mathcal{X}(\mathbf{p}(\gamma_A))$ cannot be harder than or overlapping with S^M , and in fact, we can sharpen this requirement:

¹³More generally, $\mathbf{p}(\gamma_A)$ can also include those line momenta of softer infrared-compatible subgraphs entering γ_A . The analysis here applies equally to that case.

$\mathcal{X}(\mathfrak{p}(\gamma_A))$ must be equal to or softer than $S^{M'}$ for some $M' > M$. If this were not the case, $\mathcal{X}(\mathfrak{p}(\gamma_A))$ would be of the form $S^M C_j^{n_j}$ with $j \notin \{1, \dots, I\}$, making $\mathfrak{p}(\gamma_A)$ relevant to every $\Gamma_{[\mathcal{S}\mathcal{J}_i]}$. The $S^{m_i} C_i^{n_i}$ components inside $\Gamma_{[\mathcal{S}\mathcal{J}_i]}$ would become infrared compatible due to its external momentum flow, again violating the definition of Γ_Δ .

So far we have identified the following subgraphs within Γ_Δ : $\Gamma_{[\mathcal{S}_A]}, \Gamma_{[\mathcal{S}\mathcal{J}_1]}, \dots, \Gamma_{[\mathcal{S}\mathcal{J}_I]}$. In addition, let us define a further subgraph $\Gamma_{[\mathcal{S}_B]}$ consisting of the following mode components:

- the S^M components, each relevant to precisely one $\Gamma_{[\mathcal{S}\mathcal{J}_i]}$;
- the $S^M C_j^{n'_j}$ components ($j \notin \{1, \dots, I\}$ and $n'_j \in \mathbb{N}_+$), each relevant to one or more of $\Gamma_{[\mathcal{S}_A]}, \Gamma_{[\mathcal{S}\mathcal{J}_1]}, \dots, \Gamma_{[\mathcal{S}\mathcal{J}_I]}$.

As in the analysis above, any external momentum entering such a component (if present) must be equal to or softer than $S^{M'}$, for some $M' > M$. For simplicity, we do not repeat the analysis here.

Crucially, $\Gamma_{[\mathcal{S}_B]}$ must itself be contained in Γ_Δ . Suppose, for contradiction, that an $S^M C_j^{n'_j}$ component relevant to $\Gamma_{[\mathcal{S}\mathcal{J}_1]}$ lies in $\mathcal{G} \setminus \Gamma_\Delta$ instead. After we set the whole of $\mathcal{G} \setminus \Gamma_\Delta$ infrared compatible, this component becomes infrared compatible, and the total momentum flowing into $\Gamma_{[\mathcal{S}\mathcal{J}_1]}$ would acquire mode $S^{m_1} C_1^{n_1}$, thereby rendering $\Gamma_{[\mathcal{S}\mathcal{J}_1]}$ infrared compatible as well. This contradicts the definition of Γ_Δ . Hence $\Gamma_{[\mathcal{S}_B]} \subset \Gamma_\Delta$.

We finalize our construction for Γ_Δ at this point, and obtain its pattern in figure 31. We color the subgraphs as follows: $\Gamma_{[\mathcal{S}\mathcal{J}_i]}$ are drawn in different shades of **green**, $\Gamma_{[\mathcal{S}_A]}$ in **red**, and $\Gamma_{[\mathcal{S}_B]}$ in **rhodamine**. The edges of Γ_Δ are drawn dash-dotted, and its complement $\mathcal{G} \setminus \Gamma_\Delta$ in **gray**. It remains to verify that the constructed subgraph of \mathcal{G} satisfies the definition of Γ_Δ . In other words, the collection $\{\Gamma_{[\mathcal{S}\mathcal{J}_1]}, \dots, \Gamma_{[\mathcal{S}\mathcal{J}_I]}, \Gamma_{[\mathcal{S}_A]}, \Gamma_{[\mathcal{S}_B]}\}$ should comprise all subgraphs of Γ_Δ precisely. This is established by the following lemma.

Lemma 6.12. *The graph Γ_Δ constructed above satisfies the following conditions.*

1. *For every mode component $\gamma_B \subset \Gamma_{[\mathcal{S}_B]}$, there exist two mode components $\gamma_1 \subset \Gamma_\Delta$ and $\gamma_2 \subset \mathcal{G} \setminus \Gamma_\Delta$, such that γ_B is relevant to them both, and $\mathcal{X}(\gamma_B) = \mathcal{X}(\gamma_1) \wedge \mathcal{X}(\gamma_2)$.*
2. *No mode component in Γ_Δ would become infrared compatible even if all the mode components in $\mathcal{G} \setminus \Gamma_\Delta$ are infrared compatible.*
3. *For every mode component $\gamma' \subset \Gamma_{[\mathcal{S}\mathcal{J}_i]}$ that is softer than $S^{m_i} C_i^{n_i}$, there exists a mode component $\gamma'' \subset \mathcal{G} \setminus \Gamma_\Delta$, such that γ' is relevant to γ'' , and $\mathcal{X}(\gamma') = S^{m_i} C_i^{n_i} \wedge \mathcal{X}(\gamma'')$.*
4. *Suppose all mode components in $\mathcal{G} \setminus \Gamma_\Delta$ are infrared compatible. Then setting any single mode component in Γ_Δ infrared compatible forces all other mode components in Γ_Δ to become infrared compatible.*

Proof. We have shown that the total momentum entering γ_B , sourced exclusively from the external kinematics or from softer infrared-compatible subgraphs entering γ_B , must be equal to

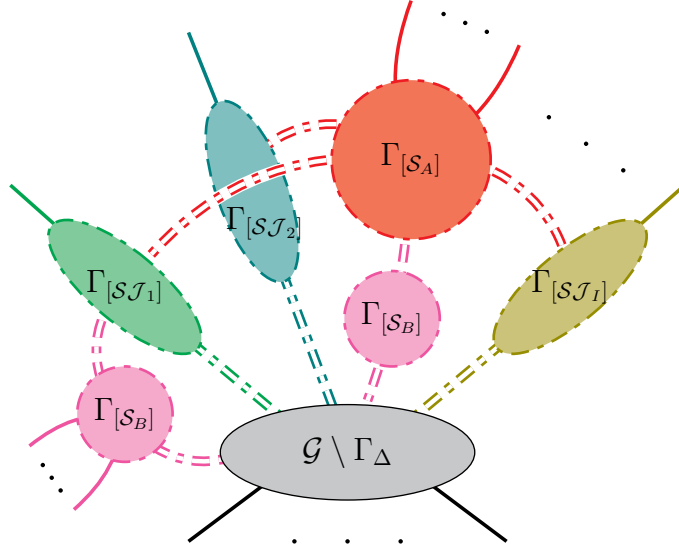


Figure 31. Illustration of the general structure of Γ_Δ (the union of colored subgraphs, whose edges are dash-dotted) and $\mathcal{G} \setminus \Gamma_\Delta$ (the gray blob). Double lines indicate multiple connections. Here $\Gamma_{[S_A]}$ is shown as a single component, and $\Gamma_{[S_B]}$ consists of two components: one adjacent to $\Gamma_{[S_J1]}$ and $\mathcal{G} \setminus \Gamma_\Delta$, and the other adjacent to $\Gamma_{[S_A]}$ and $\mathcal{G} \setminus \Gamma_\Delta$. The analysis regarding this pattern applies equally to more general configurations of $\Gamma_{[S_A]}$ and $\Gamma_{[S_B]}$.

or softer than $S^{M'}$ for some $M' > M$. Consequently, condition 2 of the Second Connectivity Theorem (theorem 5.3) applies to γ_B . That is, γ_B must be adjacent to two harder-mode subgraphs γ_1 and γ_2 such that $\mathcal{X}(\gamma_B) = \mathcal{X}(\gamma_1) \wedge \mathcal{X}(\gamma_2)$.

Given the known mode structure of Γ_Δ , one can directly verify that γ_1 and γ_2 cannot both lie inside Γ_Δ . Nor can they both belong to $\mathcal{G} \setminus \Gamma_\Delta$; otherwise, setting $\mathcal{G} \setminus \Gamma_\Delta$ infrared compatible would also make γ_B infrared compatible. Hence, one of them must be contained in Γ_Δ with the other in $\mathcal{G} \setminus \Gamma_\Delta$. This completes the proof of the first statement.

We next investigate when an $S^m C_i^n$ component $\gamma_{S^m C_i^n} \subset \Gamma_{[S_Ji]}$ can become infrared compatible. According to the definition of infrared compatibility, two scenarios are possible:

- (1) There exist two softer-mode subgraphs γ_a and γ_b , both relevant to $\gamma_{S^m C_i^n}$ and already confirmed infrared compatible, with $S^m C_i^n = \mathcal{X}(\gamma_a) \vee \mathcal{X}(\gamma_b)$.
- (2) γ is relevant to two harder-mode subgraphs γ_a and γ_b that are both confirmed infrared compatible, with $S^m C_i^n = \mathcal{X}(\gamma_a) \wedge \mathcal{X}(\gamma_b)$.

For the first case, a key observation is that the relation $S^m C_i^n = \mathcal{X}(\gamma_a) \vee \mathcal{X}(\gamma_b)$ forces $\mathcal{X}(\gamma_a)$ and $\mathcal{X}(\gamma_b)$ to take the following forms (up to an exchange):

$$\begin{aligned} \mathcal{X}(\gamma_a) &= S^{m+n'} C_i^{n-n'} \quad (n' \leq n) \quad \text{or} \quad S^{m+n} C_j^{n'_j} \quad (j \neq i, n'_j \in \mathbb{N}_+), \\ \mathcal{X}(\gamma_b) &= S^m C_i^{n''} \quad (n'' \geq n+1). \end{aligned} \tag{6.73}$$

Similarly, for the second case, $S^m C_i^n = \mathcal{X}(\gamma_a) \wedge \mathcal{X}(\gamma_b)$ implies the following form:

$$\begin{aligned}\mathcal{X}(\gamma_a) &= S^{m-m'} C_i^{n+m'} \quad (m' \leq m), \\ \mathcal{X}(\gamma_b) &= S^m C_i^{n''} \quad (n'' \leq n-1).\end{aligned}\tag{6.74}$$

Both eqs. (6.73) and (6.74) follow from theorem 3.1, as we will detail in appendix A.3.

From our construction of Γ_Δ , no matter which case above we take, γ_a have been included in Γ_Δ already. This indicates that $\gamma_{S^m C_i^n}$ can become infrared compatible only if some specific mode component in Γ_Δ has been set infrared compatible. In other words, the infrared compatibility of $\mathcal{G} \setminus \Gamma_\Delta$ alone *cannot* induce that of $\gamma_{S^m C_i^n}$. The same analyses can be made for the other mode components in Γ_Δ . We have thus proved the second statement.

The proof of the third statement follows a line of reasoning very similar to that of the first one. From the external momentum structure of γ' and the Second Connectivity Theorem, γ' must be adjacent to two harder-mode subgraphs γ_1 and γ'' satisfying $\mathcal{X}(\gamma') = \mathcal{X}(\gamma_1) \wedge \mathcal{X}(\gamma'')$. Since $\mathcal{X}(\gamma') = S^{m_i+m'_i} C_i^{n_i-m'_i}$ with $0 \leq m'_i \leq n_i - 1$ here, eq. (6.74) can be employed to indicate that either $\mathcal{X}(\gamma_1)$ or $\mathcal{X}(\gamma'')$ is equal to $S^{m_i} C_i^{n_i}$. Choosing $\mathcal{X}(\gamma_1) = S^{m_i} C_i^{n_i}$ and noting the mode structure of Γ_Δ , we conclude that γ'' must lie inside $\mathcal{G} \setminus \Gamma_\Delta$. This establishes the third statement.

To show the fourth statement, assume that all mode components in $\mathcal{G} \setminus \Gamma_\Delta$ are already infrared compatible. We will show that once any single additional component in Γ_Δ is made infrared compatible, all the remaining components in Γ_Δ become infrared compatible as well.

First, we demonstrate that making any component in a given $\Gamma_{[\mathcal{S}\mathcal{J}_i]}$ infrared compatible forces every other component in that $\Gamma_{[\mathcal{S}\mathcal{J}_i]}$ to become infrared compatible. On the one hand, by the third statement (already proved), setting the $S^{m_i} C_i^{n_i}$ component infrared compatible renders all other components of $\Gamma_{[\mathcal{S}\mathcal{J}_i]}$ —those with modes $S^{m_i+1} C_i^{n_i-1}$, $S^{m_i+2} C_i^{n_i-2}$, \dots , $S^{m_i+n_i-1} C_i$ —infrared compatible. On the other hand, if we instead set any $S^{m_i+k} C_i^{n_i-k}$ component (with $1 \leq k \leq n_i - 1$) infrared compatible, the sum of its momentum with the external momenta entering the $S^{m_i} C_i^{n_i}$ component acquires mode $S^{m_i} C_i^{n_i}$, which in turn forces the $S^{m_i} C_i^{n_i}$ component to become infrared compatible.

Then, we show that infrared compatibility propagates among $\Gamma_{[\mathcal{S}\mathcal{J}_i]}$, $\Gamma_{[\mathcal{S}_A]}$, and $\Gamma_{[\mathcal{S}_B]}$. From the defining properties of messengers and infrared compatibility, setting any mode component in $\Gamma_* \equiv \Gamma_{[\mathcal{S}_A]} \cup \Gamma_{[\mathcal{S}\mathcal{J}_1]} \cup \dots \cup \Gamma_{[\mathcal{S}\mathcal{J}_I]}$ makes all the others in Γ_* infrared compatible. By the first statement (already proved), this also forces $\Gamma_{[\mathcal{S}_B]}$ to become infrared compatible. Conversely, if we set any mode component in $\Gamma_{[\mathcal{S}_B]}$ infrared compatible, then some components of Γ_* would acquire external momentum of precisely its mode, thus becoming infrared compatible. After this step, the previous argument can be iterated.

Collectively, these observations establish the fourth statement. \square

Before proceeding, we illustrate two more nontrivial examples of Γ_Δ in figure 32, where every external momentum and edge is labeled with its mode. In each example, every edge belongs to some non-infrared-compatible mode component, and those belonging to Γ_Δ are drawn bold and dash-dotted.

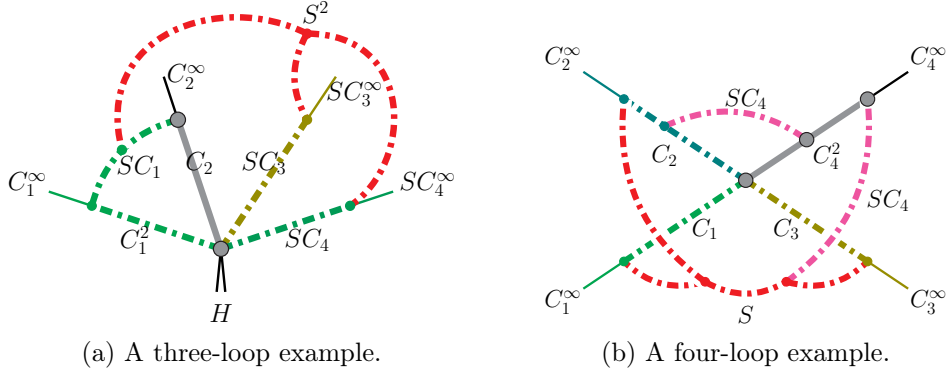


Figure 32. Two examples of Γ_Δ whose edges are drawn bold and dash-dotted, and colored according to figure 31.

We have color-coded the edges and vertices according to the general pattern shown in figure 31. In figure 32a, we have $M = 2$, and the degree-2 messenger, which is precisely $\Gamma_{[S_A]}$ here, is relevant to $\Gamma_{[S_{\mathcal{J}_i}]}$ with $i = 1, 3, 4$. The graph $\Gamma_{[S_{\mathcal{J}_1}]}$ consists of a C_1 component and an SC_1 component, $\Gamma_{[S_{\mathcal{J}_3}]}$ consists of an SC_3 component, and $\Gamma_{[S_{\mathcal{J}_4}]}$ consists of an SC_4 component. The subgraph $\Gamma_{[S_B]}$ is empty in this configuration.

In figure 32b, we have $M = 1$, and the degree-1 messenger $\Gamma_{[S_A]}$ is relevant to $\Gamma_{[S_{\mathcal{J}_i}]}$ with $i = 1, 2, 3$. Each $\Gamma_{[S_{\mathcal{J}_i}]}$ consists of C_i components only. The subgraph $\Gamma_{[S_B]}$ consists of two SC_4 components in this configuration.

Now that the structure of Γ_Δ has been clarified, we show that if $\Gamma_\Delta \neq \emptyset$ in a configuration R , there exists a free parameter $a \in \mathbb{R}$ among the edge weights. This is sufficient to prove the necessity of the infrared-compatibility requirement. Concretely, while $w_e = -\mathcal{V}(\mathcal{X}(e))$ for each $e \in \mathcal{G}$ is one solution to the characteristic equations, we may also deform the weights as follows:

$$\begin{aligned} w_e &\rightarrow -\mathcal{V}(\mathcal{X}(e)) + a, \text{ for each } e \in \Gamma_{[S_{\mathcal{J}_1}]} \cup \dots \cup \Gamma_{[S_{\mathcal{J}_I}]} \cup \Gamma_{[S_B]}; \\ w_e &\rightarrow -\mathcal{V}(\mathcal{X}(e)) + 2a, \text{ for each } e \in \Gamma_{[S_A]}. \end{aligned} \quad (6.75)$$

The space normal to the lower face f_R is thus at least one dimensional.

To see this, we must understand the structure of the leading-term characteristic equations. As remarked below lemma 6.10, setting all edge weights in a mode component equal reduces all characteristic equations for the $\mathcal{U}^{(R)}$ terms to a single equation, which determines the overall weight of the entire graph. The characteristic equations from the $\mathcal{F}^{(R)}$ terms are then needed to determine individual edge weights. Specifically, to solve for the weight w_e of an edge, we require those $\mathcal{F}^{(R)}$ terms in which $e \in \gamma'$ in eq. (6.52), or $e \in \{\gamma'_1, \dots, \gamma'_A\} \cup \{\gamma''_1, \dots, \gamma''_{A-1}\}$ in eq. (6.53). Since each $\mathcal{F}^{(R)}$ term can be expressed as a unitarity cut of the entire graph, to solve for the weights w_e with $e \in \Gamma_\Delta$ we must consider those unitarity cuts passing through Γ_Δ . Let us discuss all the possible cases, some of which are illustrated in figure 33.

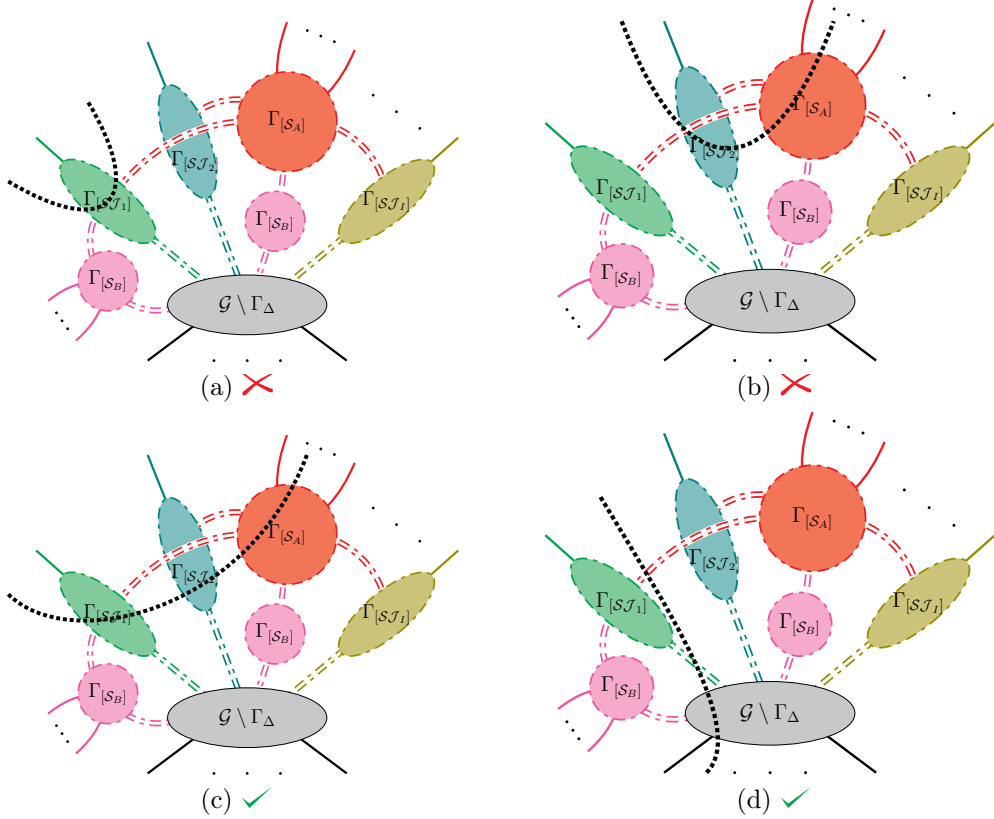


Figure 33. Some typical \mathcal{F} -term unitarity cuts passing through Γ_Δ . We argue that (a) and (b) cannot correspond to any $\mathcal{F}^{(R)}$ term (marked with “ \times ”) while (c) and (d) can (marked with “ \checkmark ”).

First, there cannot be any $\mathcal{F}^{(R)}$ -term unitarity cut that isolates only the external momentum of a single $\Gamma_{[S\mathcal{J}_i]}$ (see figure 33a). Otherwise, it would correspond to an $\mathcal{F}_I^{(R)}$ term, and the difference between its characteristic equation and the $\mathcal{U}^{(R)}$ -term characteristic equation would determine some edge weights in $\Gamma_{[S\mathcal{J}_i]}$, contradicting to the fact that no mode component in Γ_Δ is infrared compatible. Out of the same reason, no $\mathcal{F}^{(R)}$ -term unitarity cut can isolate only the external momenta of $\Gamma_{[S_A]}$ or $\Gamma_{[S_B]}$.

This reasoning can be extended to rule out those $\mathcal{F}^{(R)}$ -term unitarity cuts, which isolate the external momentum of a single $\Gamma_{[S\mathcal{J}_i]}$ together with some external momenta from the graph $\Gamma_{[S_A]} \cup \Gamma_{[S_B]}$ (see figure 33b). This is because those external momenta of $\Gamma_{[S_A]} \cup \Gamma_{[S_B]}$ are not relevant to $\Gamma_{[S\mathcal{J}_i]}$ (recall that they must be equal to or softer than $S^{M'}$ with some $M' > M$, as demonstrated earlier). Therefore, if such a unitarity cut did correspond to an $\mathcal{F}^{(R)}$ -term, removing all the external momenta of $\Gamma_{[S_A]} \cup \Gamma_{[S_B]}$ would also lead to an $\mathcal{F}^{(R)}$ -term, leading back to the configuration in figure 33a, which has already been ruled out.

From the observations above, each possible unitarity cut must correspond to an $\mathcal{F}_{II}^{(R)}$ term and satisfy one of the following:

- (1) it isolates the external momenta of multiple $\Gamma_{[S\mathcal{J}_i]}$ (see figure 33c);

(2) it isolates the external momenta of a single $\Gamma_{[\mathcal{S}\mathcal{J}_i]}$ together with some other external momenta in $\mathcal{G} \setminus \Gamma_\Delta$ (see figure 33d).

We now analyze these two cases separately. For case (1), from lemma 6.8, which constrains the mode structure of generic $\mathcal{F}_{\text{II}}^{(R)}$ terms, implies that the unitarity cut must pass through precisely two of the $\Gamma_{[\mathcal{S}\mathcal{J}_i]}$ graphs. Furthermore, a path in $\Gamma_{[\mathcal{S}_A]}$ must connect their external momenta in the spanning 2-tree. Figure 33c illustrates the pattern where these are $\Gamma_{[\mathcal{S}\mathcal{J}_1]}$ and $\Gamma_{[\mathcal{S}\mathcal{J}_2]}$. Theorem 6.9 then gives

$$\mathfrak{n}_{\gamma_{[\mathcal{S}\mathcal{J}_1]}} = L(\tilde{\Gamma}_{[\mathcal{S}\mathcal{J}_1]}) + 1, \quad \mathfrak{n}_{\gamma_{[\mathcal{S}\mathcal{J}_2]}} = L(\tilde{\Gamma}_{[\mathcal{S}\mathcal{J}_2]}) + 1, \quad \mathfrak{n}_{\gamma_{[\mathcal{S}_A]}} = L(\tilde{\Gamma}_{[\mathcal{S}_A]}) - 1. \quad (6.76)$$

In other words, compared with the $\mathcal{U}^{(R)}$ -term characteristic equation, the characteristic equation for this $\mathcal{F}_{\text{II}}^{(R)}$ term contains two additional terms w_{e_1} and w_{e_2} (with $e_1 \in \Gamma_{[\mathcal{S}\mathcal{J}_1]}$ and $e_2 \in \Gamma_{[\mathcal{S}\mathcal{J}_2]}$) and one fewer term w_{e_A} (with $e_A \in \Gamma_{[\mathcal{S}_A]}$). Under the edge-weight deformation in (6.75), $w_{e_1} \rightarrow w_{e_1} + a$, $w_{e_2} \rightarrow w_{e_2} + a$, and $w_{e_A} \rightarrow w_{e_A} + 2a$. This characteristic equation remains to hold.

For case (2), similarly, the unitarity cut passes through one $\Gamma_{[\mathcal{S}\mathcal{J}_i]}$, and the external momentum of this $\Gamma_{[\mathcal{S}\mathcal{J}_i]}$ is connected to another external momentum attached to $\mathcal{G} \setminus \Gamma_\Delta$ by a path in $\Gamma_{[\mathcal{S}_B]}$. Figure 33d illustrates the pattern for $i = 1$. From theorem 6.9, we then have

$$\mathfrak{n}_{\gamma_{[\mathcal{S}\mathcal{J}_1]}} = L(\tilde{\Gamma}_{[\mathcal{S}\mathcal{J}_1]}) + 1, \quad \mathfrak{n}_{\gamma_{[\mathcal{S}_B]}} = L(\tilde{\Gamma}_{[\mathcal{S}_B]}) - 1. \quad (6.77)$$

Again, compared with the $\mathcal{U}^{(R)}$ -term characteristic equation, the characteristic equation for this $\mathcal{F}_{\text{II}}^{(R)}$ term contains two additional terms w_{e_1} and w_{e_2} (with $e_1 \in \Gamma_{[\mathcal{S}\mathcal{J}_1]}$ and $e_2 \in \mathcal{G} \setminus \Gamma_\Delta$) and one fewer term w_{e_B} (with $e_B \in \Gamma_{[\mathcal{S}_B]}$). It remains to hold under the edge-weight deformation in (6.75), where $w_{e_1} \rightarrow w_{e_1} + a$ and $w_{e_B} \rightarrow w_{e_B} + a$.

Let us summarize our analysis and results above. We have shown that if the infrared-compatibility requirement is not satisfied in a configuration, a subgraph $\Gamma_\Delta \subset \mathcal{G}$ can always be identified, such that the leading-term characteristic equations do not have a unique solution, because they still hold under the deformation shown in (6.75). Thus, the expanded integral would be scaleless, and this configuration is not a region. We have then proved the necessity of the infrared-compatibility requirement.

7 Verification with more multiloop examples

In this section, we test our understanding of region structures through several multiloop examples. We begin with a three-loop two-to-two scattering graph in section 7.1. The associated expansion contains 81 regions; we explain how these arise from the fundamental pattern in section 4 while satisfying all subgraph requirements in section 5. Next, in section 7.2, we consider a more complicated six-loop graph that contributes to the one-to-three decay process with an additional soft emission, and we examine its 199 regions.

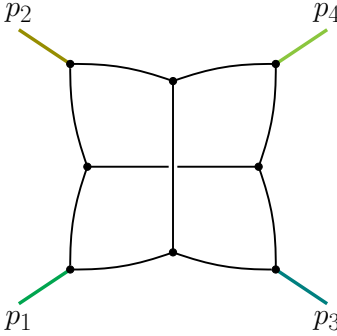


Figure 34. A three-loop graph contributing to the two-to-two scattering $p_1 + p_2 \rightarrow p_3 + p_4$.

Finally, we note that although the present work is formulated for massless Feynman integrals, the extension to massive cases could be straightforward. In particular, with only minor adaptations, our analysis can be applied to a recent study of $gg \rightarrow HH$ [25], which involves massive integrals, and it automatically reproduces the results obtained there. We demonstrate this extension in section 7.3.

7.1 A three-loop example: two-to-two scattering

In this subsection, we analyze the region structure of the three-loop graph shown in figure 34. It represents a two-to-two scattering process. For the asymptotic expansion, we assign the following modes to the external momenta, which are color coded accordingly in the figure:

$$\mathcal{X}(p_1) = C_1, \quad \mathcal{X}(p_2) = C_2^2, \quad \mathcal{X}(p_3) = C_3^\infty, \quad \mathcal{X}(p_4) = C_4^\infty. \quad (7.1)$$

That is, the momenta p_i ($i = 1, 2, 3, 4$) lie along distinct lightcones, with $p_1^2 \sim \lambda$, $p_2^2 \sim \lambda^2$, and $p_3^2 = p_4^2 = 0$. In this kinematic setup, a straightforward verification by computer codes yields 81 distinct (facet) regions, each expressed in parameter space (see section 2.3 for the parametric representation of regions). Below, we shall derive the momentum-space interpretations of these regions directly from our understanding of region structures, and confirm that they match the output of the computer codes exactly.

Before proceeding, we note that figure 34 exhibits a *unique hidden region* in which hard scattering occurs in two disconnected subgraphs: the horizontal and vertical central rungs [11, 12]. This Landshoff-type configuration does not correspond to any facet region and therefore cannot be derived directly from the geometric method, but it gives an essential contribution to the asymptotic expansion, as verified by recent analytic results [40]. Nevertheless, in this work, we restrict our analysis solely to facet regions.

First, let us derive the regions containing the softest mode(s) in the expansion. From section 5.3, the possibly softest mode is $S^{\max_i\{m_i+n_i\}}$, where the index i goes through those external modes $S^{m_i}C_i^{n_i}$ with $n_i \neq \infty$. From eq. (7.1), we have

$$i \in \{1, 2\}, \quad m_1 = m_2 = 0, \quad n_1 = 1, \quad n_2 = 2. \quad (7.2)$$

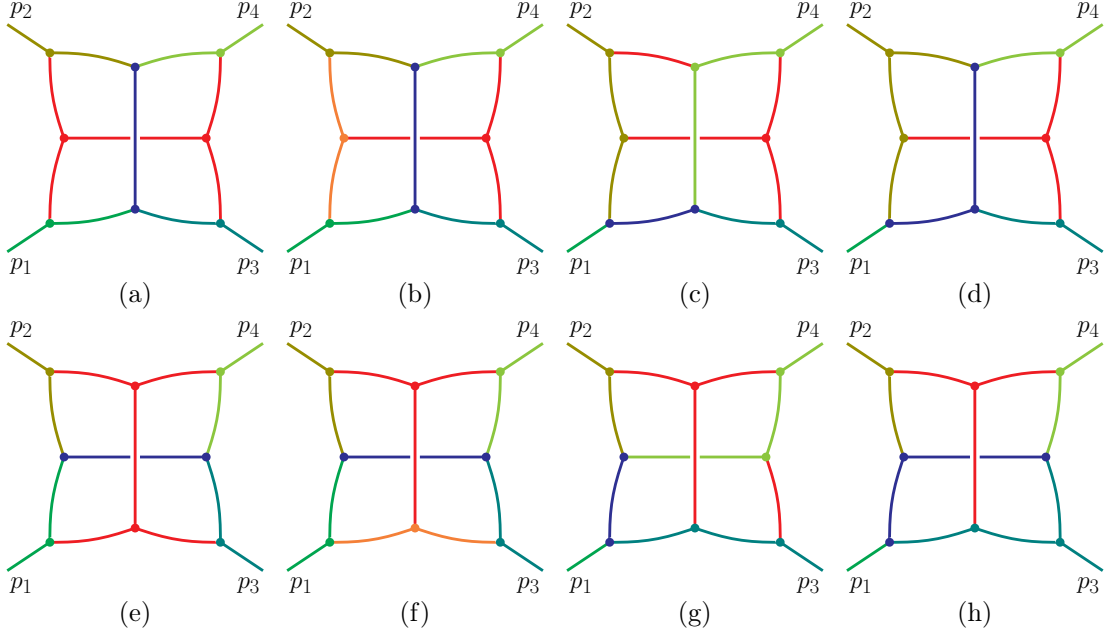


Figure 35. The 8 regions of figure 34 characterized by the S^2 mode.

Thus $\max_i\{m_i + n_i\} = 2$, and the possibly softest mode is S^2 .

We now exhaust all configurations of figure 34 that satisfy (1) the fundamental pattern (figure 5), (2) the subgraph requirements, and (3) the condition that the S^2 component (denoted by γ_{S^2}) is nonempty.¹⁴ There are 8 such configurations, shown in figure 35. In accordance with the external modes, we adopt the following color scheme throughout this subsection: H mode (**blue**), C_1 mode (**green**), C_2^n mode (**olive**) with $n \in \{1, 2\}$, C_3^n mode (**teal**) with $n \in \mathbb{N}_+$, C_4^n mode (**lime**) with $n \in \mathbb{N}_+$, SC_i modes with $i \in \{2, 3, 4\}$ (**orange**), and S^2 mode (**red**).

One can directly verify that all the subgraph requirements are satisfied in each region. For example, in figure 35a, the First Connectivity Theorem holds because all subgraphs of the form $\bigcup_{\gamma_{\mathcal{V}(X)} \leq n} \Gamma_X$ (with $n = 0, 1, 2, 3, 4$) are connected. Moreover, each mode component is infrared compatible, as can be checked in the following sequence:

- (1) γ_{C_1} and $\gamma_{C_2^2}$ (because the external momenta p_1 and p_2 , which carry precisely the modes C_1 and C_2^2 respectively, enter them respectively);
- (2) γ_{S^2} (since it is a degree-2 messenger relevant to $\gamma_{C_2^2}$, $\gamma_{C_3^2}$, $\gamma_{C_4^2}$, and $\gamma_{C_2^2}$ was already confirmed infrared compatible in the previous step);

¹⁴In practice, the most efficient procedure is first to enumerate all fundamental patterns containing a γ_{S^2} and satisfying the connectivity requirements, and then to discard those that fail the infrared-compatibility requirement.

(3) $\gamma_{C_3^2}$ and $\gamma_{C_4^2}$ (because the total momentum entering each of them—summed from the external kinematics and previously confirmed infrared-compatible components—belongs to mode C_3^2 or C_4^2 , respectively).

Next, we determine the regions where the softest mode(s) are of the form SC_i for some i . A key observation is that the only possible such mode is SC_2 . To see why, note that no external momentum has mode SC_i . Then by the Second Connectivity Theorem (theorem 5.3), any SC_i component must be relevant to two harder-mode components γ_{X_1} and γ_{X_2} with $SC_i = X_1 \wedge X_2$. From the \wedge operation rule (theorem 3.1), one of X_1 or X_2 must be C_i^2 . Because $\mathcal{X}(p_1) = C_1$, which is already harder than C_1^2 , there cannot be a C_1^2 mode component, ruling out $i = 1$. If $i = 3$, then the region would contain both an SC_3 component γ_{SC_3} and a C_3^2 component $\gamma_{C_3^2}$, both of which must be infrared compatible (theorem 5.4). This, however, leads to a circular dependency:

- For $\gamma_{C_3^2}$ to be infrared compatible, the component γ_{SC_3} (whose momentum enters $\gamma_{C_3^2}$) must be confirmed infrared compatible first.
- For γ_{SC_3} to be infrared compatible, it must be relevant to two already confirmed infrared-compatible components; since one of them must be $\gamma_{C_3^2}$, this in turn requires $\gamma_{C_3^2}$ to be infrared compatible first.

Hence the infrared-compatibility requirement cannot be satisfied when an SC_3 component is present. The same reasoning excludes SC_4 components. We therefore conclude that in this scenario the unique softest mode is SC_2 , which substantially simplifies the enumeration of regions.

For configurations with a single edge in \mathcal{H} , there are 15 regions, shown in figure 36, where we have colored the S mode in **rhodamine**. One can verify that in each case the orange-colored mode is indeed SC_2 . Moreover, all subgraph requirements are satisfied. For example, the mode components in figure 36b are infrared compatible, as confirmed by the following sequence:

- (1) γ_{C_1} and $\gamma_{C_2^2}$ (from the external momenta p_1 and p_2);
- (2) γ_{SC_2} (since it is relevant to γ_{C_1} and $\gamma_{C_2^2}$, with $SC_2 = C_1 \wedge C_2^2$);
- (3) γ_{C_3} and γ_{C_4} (via the momentum flow from p_3 , p_4 , and γ_{SC_2});
- (4) γ_S (since it is relevant to γ_{C_3} and γ_{C_4} , with $S = C_3 \wedge C_4$);
- (5) γ_H (via momentum flow from γ_{C_1} and γ_{C_3} , or from $\gamma_{C_2^2}$ and γ_{C_4}).

This pattern of establishing infrared compatibility applies to most of the other regions in figure 36. When a particular mode component is absent (for example, $\gamma_{C_4^2} = \emptyset$ in figure 36c), we simply omit it.

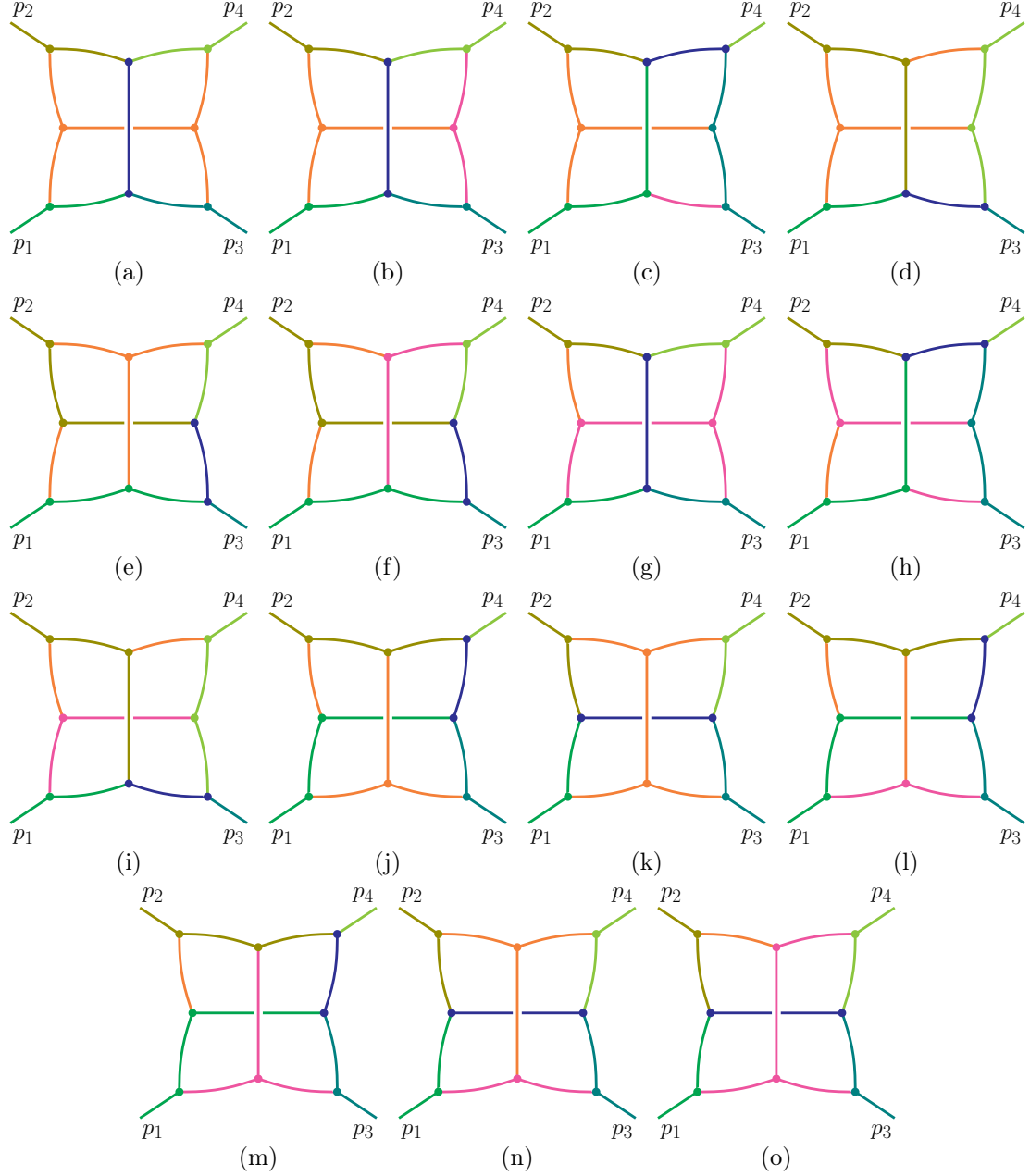


Figure 36. The 15 regions of figure 34 characterized by the SC_2 mode with a single edge in \mathcal{H} .

An exception is figure 36m. There, steps (1) and (2) above still hold. Next, observe that the γ_S component is relevant to three harder-mode components: γ_{C_1} , γ_{C_2} , and γ_{C_3} , whose external momentum modes are C_1 , C_2^2 , and C_3^∞ , respectively. Hence γ_S satisfies the conditions of a degree-1 messenger, and it is infrared compatible due to the already-established infrared compatibility of γ_{C_1} . The remaining components (γ_{C_2} , γ_{C_3} , and γ_H) can then be shown to be

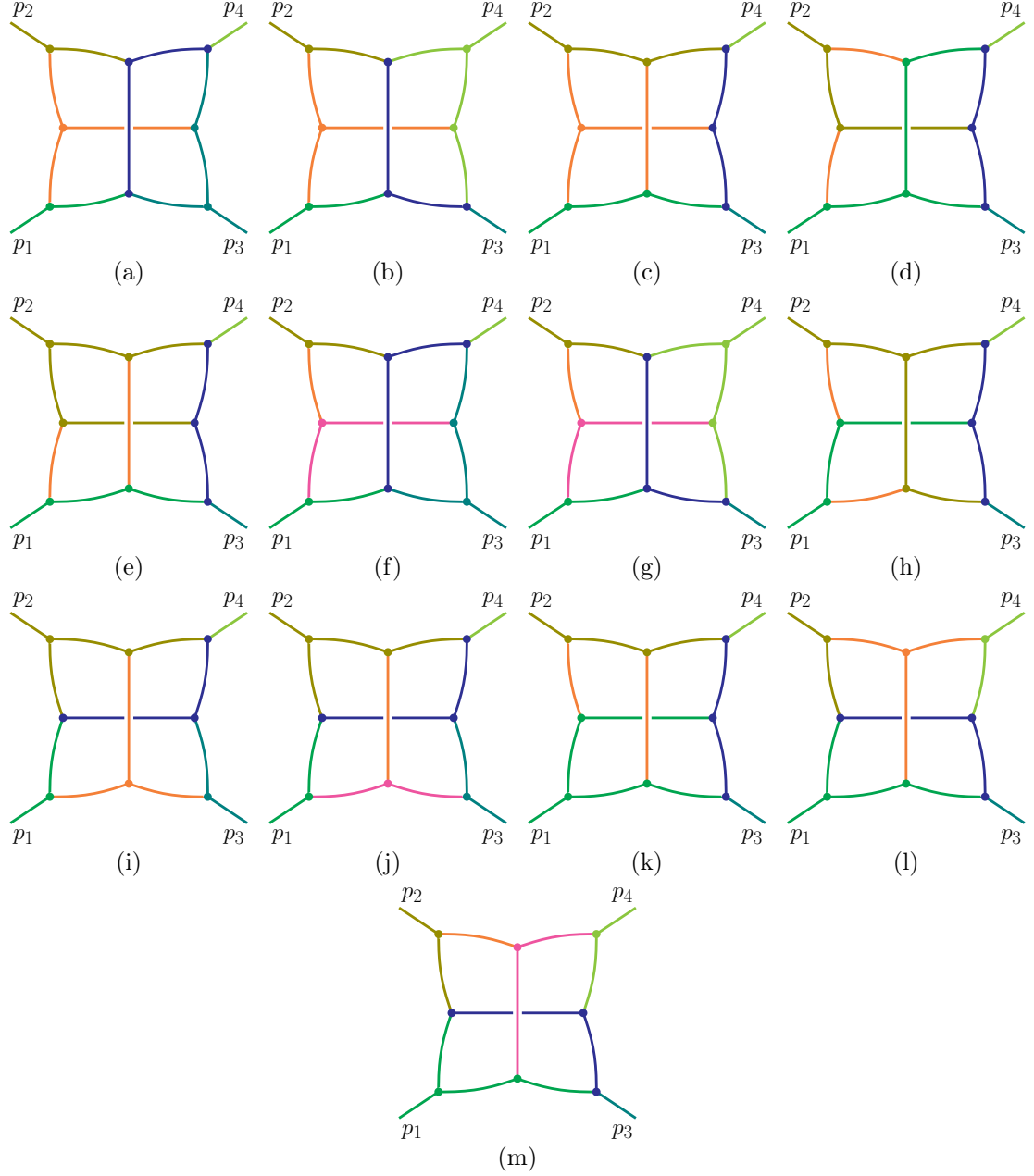


Figure 37. The 13 regions of figure 34 characterized by the SC_2 mode with two edges in \mathcal{H} .

infrared compatible via their momentum flows.

For the remaining regions characterized by the SC_2 mode, 13 of them have exactly two edges in \mathcal{H} (see figure 37); 14 of them have three or more edges in \mathcal{H} (see figure 38). For each of these regions, the verification of the subgraph requirements follows similarly as before, which we do not elaborate here for simplicity. So far we have come up with all those regions

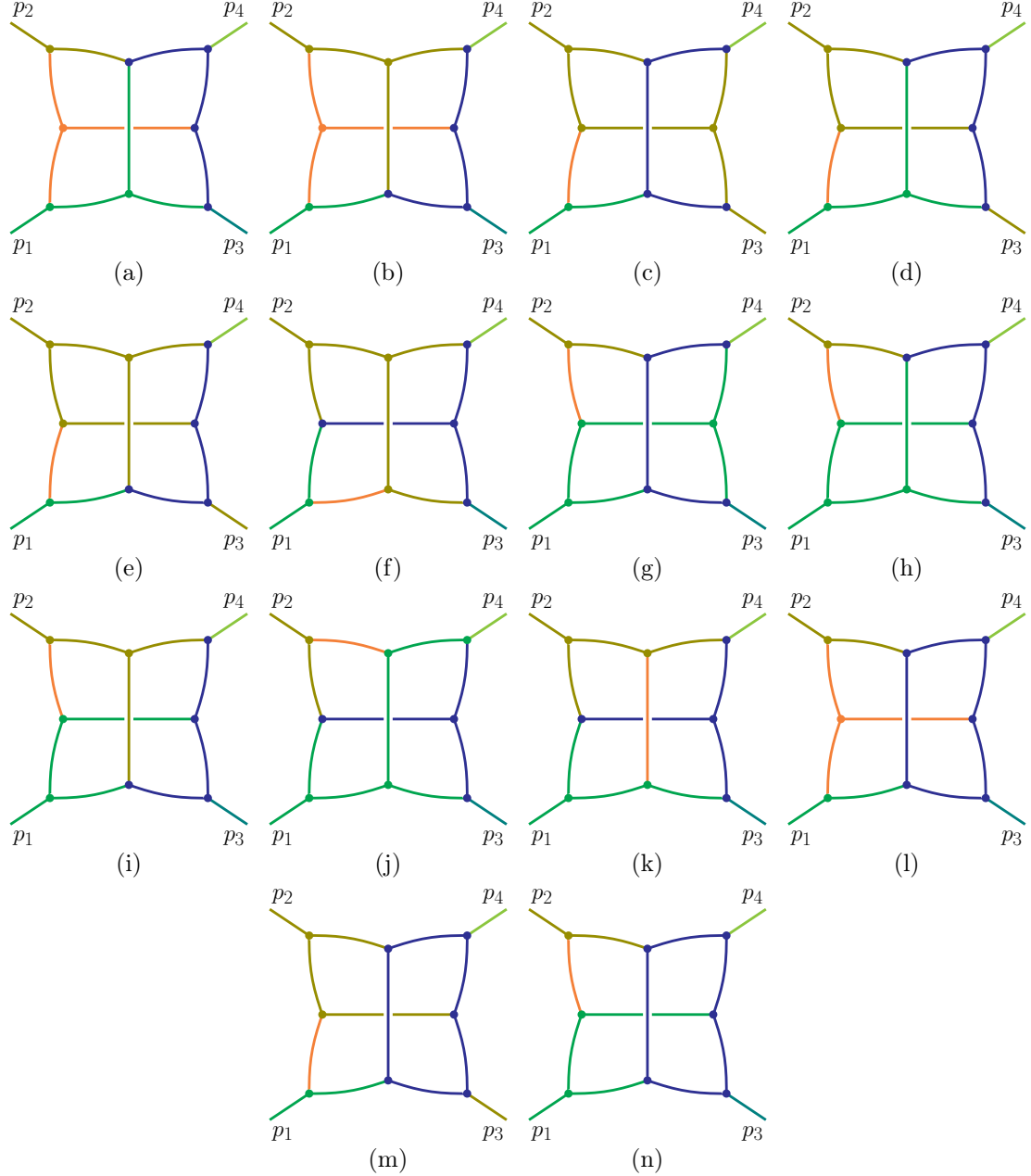


Figure 38. The 14 regions of figure 34 characterized by the $\textcolor{red}{SC}_2$ mode with ≥ 3 edges in \mathcal{H} .

featuring the modes S^2 and/or SC_i .

Then, we determine the regions characterized by the mode S . That is, in each such region, there is a nonempty S component γ_S , and no modes are softer than S . There are 15 such regions in total, shown in figure 39.

Special attention is required for figures 39g and 39j. While they appear identical due to

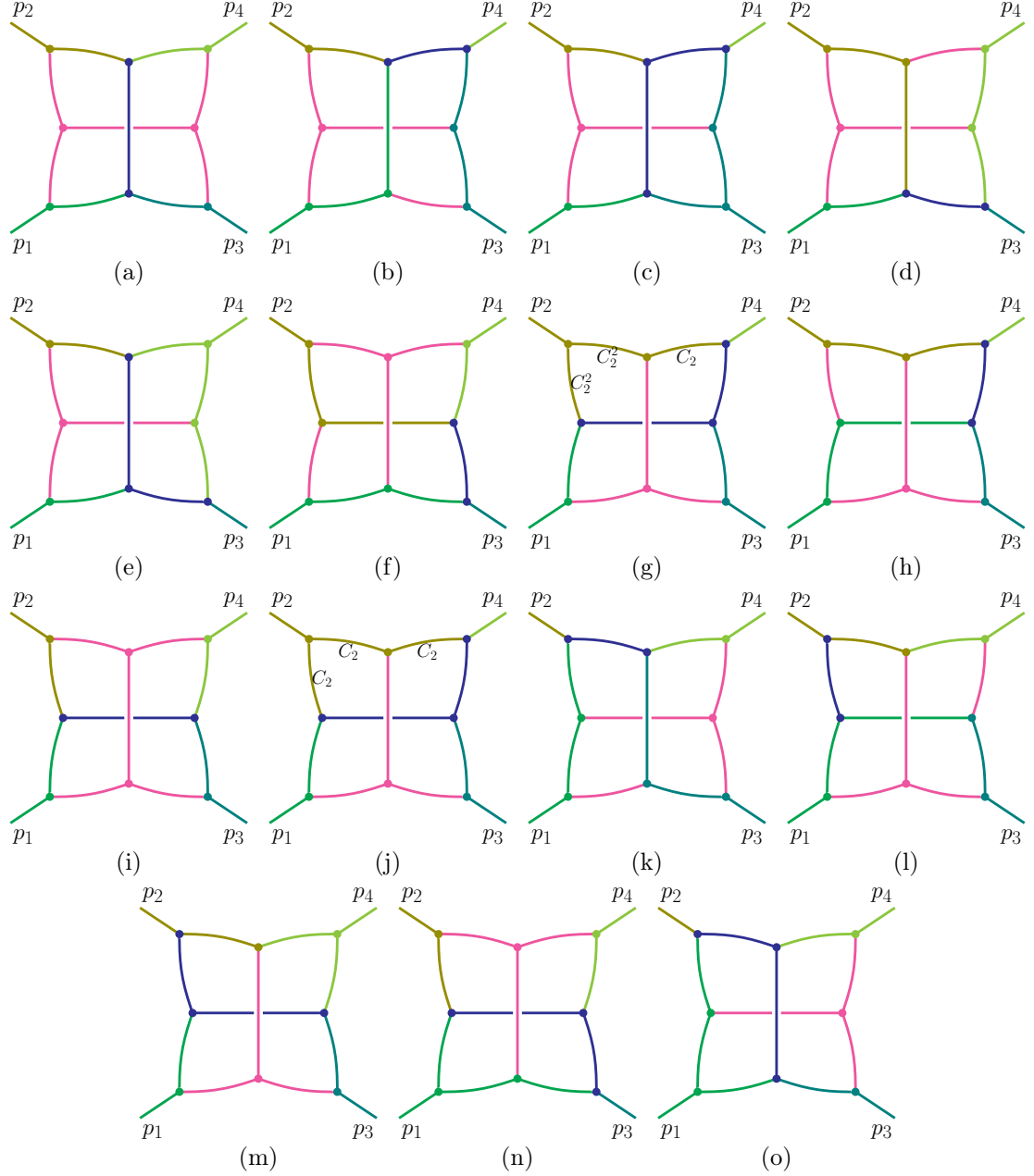


Figure 39. The 15 regions of figure 34 characterized by the $\textcolor{blue}{S}$ mode.

our shared use of **olive** for both C_2 and C_2^2 modes, they represent distinct configurations. In figure 39g, the two edges adjacent to p_2 are in the C_2^2 mode, whereas in figure 39j they are in the C_2 mode. Both configurations satisfy all subgraph requirements and are therefore valid regions in the expansion. For example, in figure 39g, $\gamma_{C_2^2}$ is infrared compatible due to the external momentum p_2 (which is in the C_2 mode), while in figure 39j, γ_{C_2} becomes infrared

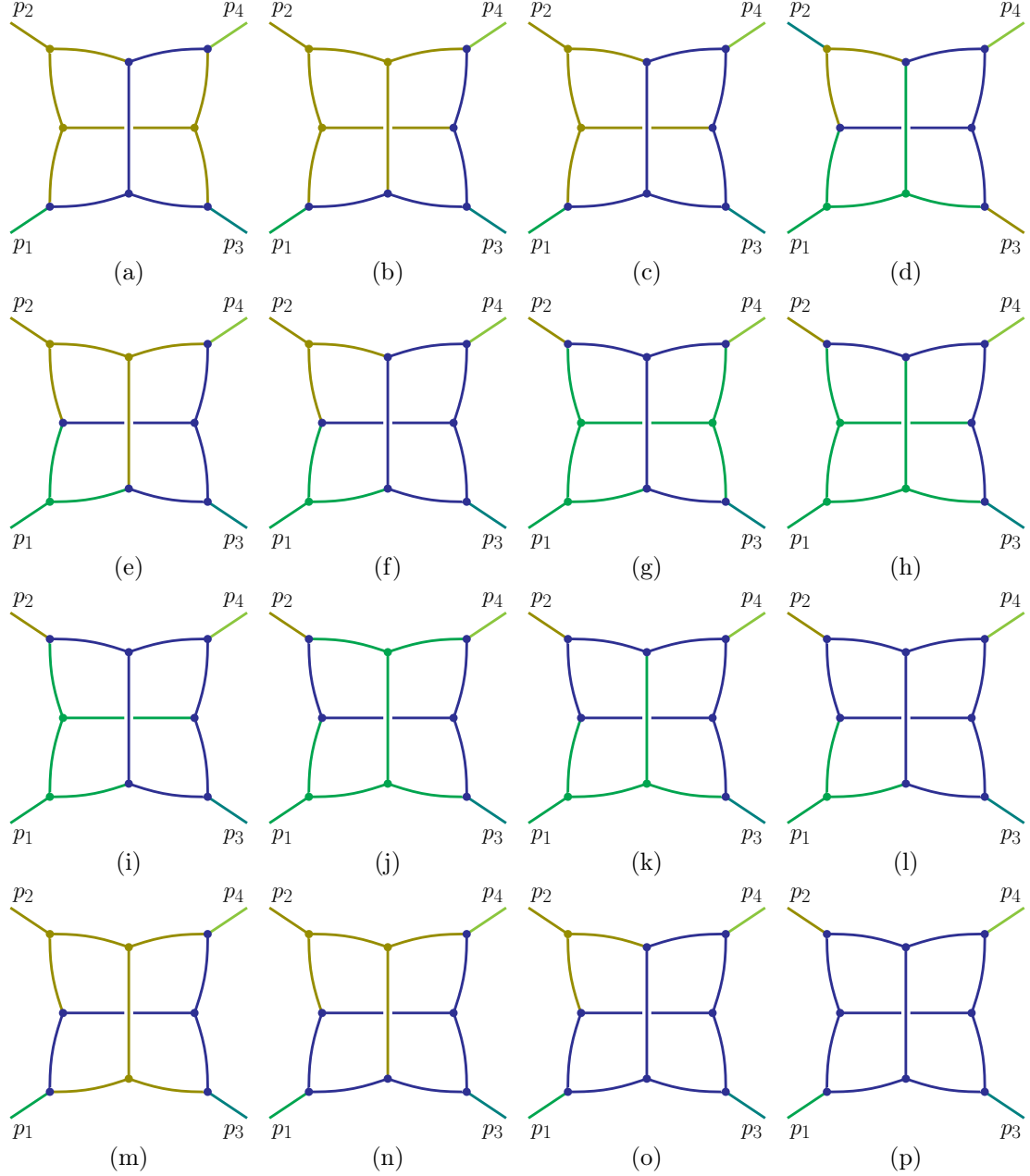


Figure 40. The 16 regions of figure 34 with only the hard and collinear (including C_2^2) modes.

compatible via the momentum flow from p_2 and the S component (which is confirmed infrared compatible in advance).

Finally, we derive the regions with only the hard and collinear (including C_2^2) modes. Note that in this situation, there cannot be any C_3 or C_4 component, otherwise the infrared-compatibility requirement would be violated (recall that $\mathcal{X}(p_3) = C_3^\infty$ and $\mathcal{X}(p_4) = C_4^\infty$,

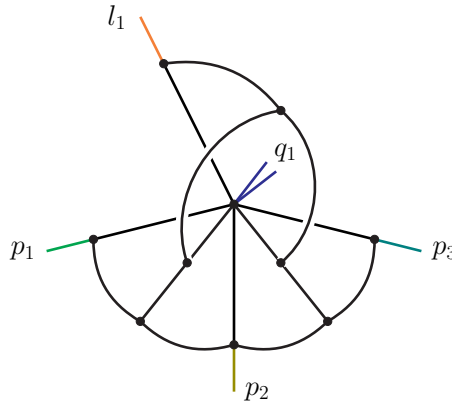


Figure 41. A six-loop graph contributing to the one-to-three decay process with a soft emission, i.e., $q_1 \rightarrow p_1 + p_2 + p_3 + l_1$.

which do not carry the modes C_3 or C_4). There are 16 such regions, depicted in figure 40. The last one, figure 40p, is the hard region.

We have thus derived all the regions of figure 34 in the associated virtuality expansion. The total number of regions is

$$8 + 13 + 15 + 14 + 15 + 16 = 81, \quad (7.3)$$

which matches the count obtained from `pySecDec`. One can further translate these regions from momentum space to parameter space using the relation in eq. (2.16), again finding perfect agreement.

7.2 A six-loop example: one-to-three decay plus a soft emission

In this subsection, we consider the six-loop graph in figure 41. It represents a one-to-three decay process with an additional soft emission ($q_1 \rightarrow p_1 + p_2 + p_3 + l_1$). For the asymptotic expansion, we assign the following modes to the external momenta and color them accordingly in the figure:

$$\mathcal{X}(p_1) = C_1^\infty, \quad \mathcal{X}(p_2) = C_2, \quad \mathcal{X}(p_3) = C_3^\infty, \quad \mathcal{X}(l_1) = SC_4, \quad \mathcal{X}(q_1) = H. \quad (7.4)$$

In this kinematic setup, a straightforward verification by codes yields 199 distinct regions (expressed in parameter space). Below, we derive their momentum-space interpretations based on our understanding.

We start from those regions with the softest mode(s). Following the same reasoning as in section 7.1, the possibly softest mode is $S^{\max_i\{m_i+n_i\}} = S^2$. In order that a nonempty S^2 component (i.e., $\gamma_{S^2} \neq \emptyset$) satisfies the infrared-compatibility requirement (theorem 5.4), it must acquire its infrared scaling from its harder-mode neighbors that have already been confirmed infrared compatible. Among all possible harder-mode neighbors of γ_{S^2} , only one of them, γ_{SC_4} , can become infrared compatible in advance due to the SC_4 -mode external

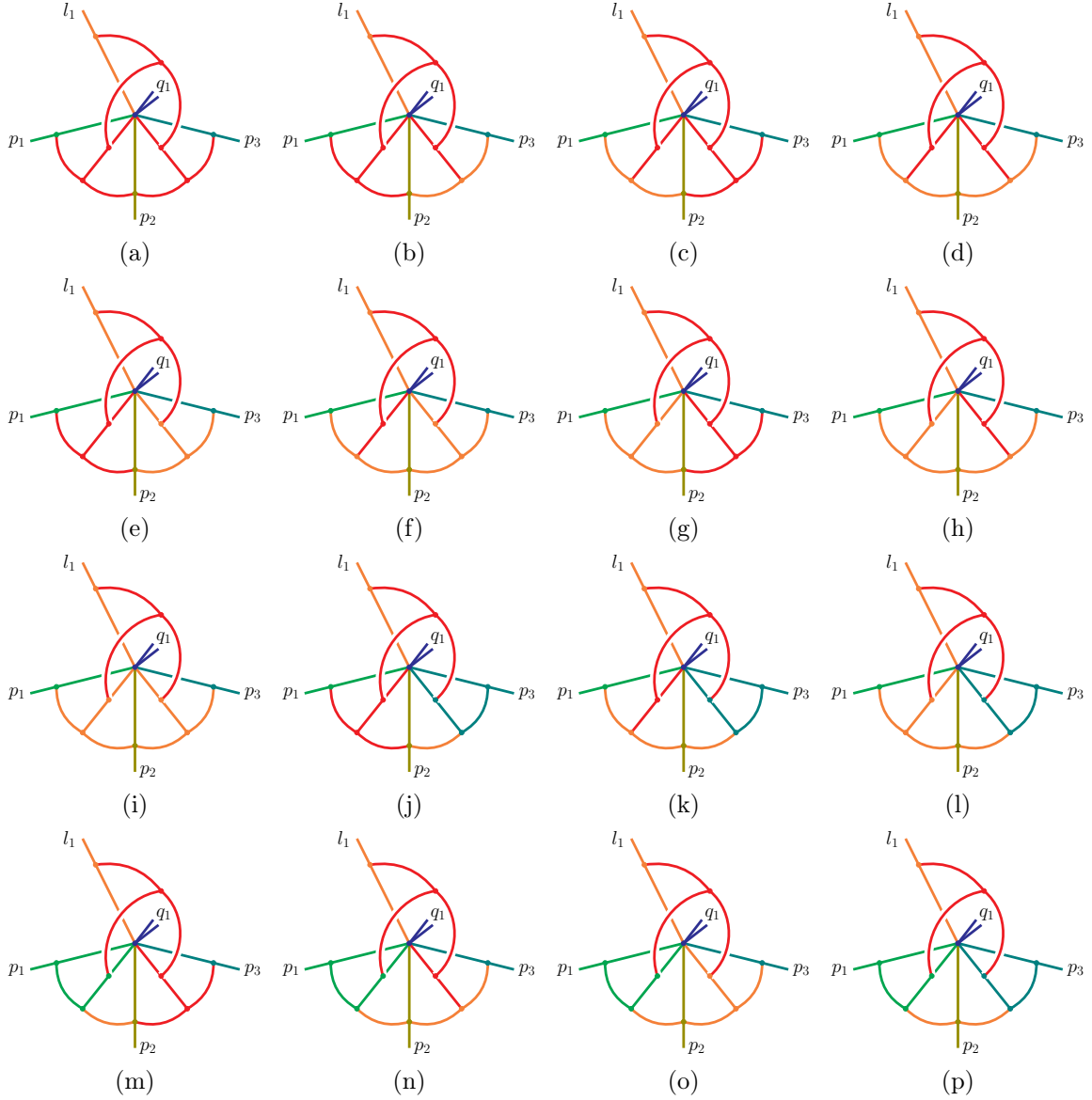


Figure 42. The 16 regions of figure 41, which are characterized by the S^2 mode with all three jets J_1, J_2, J_3 nonempty ($\gamma_{C_1}, \gamma_{C_2}, \gamma_{C_3} \neq \emptyset$).

momentum l_1 . That is, the infrared compatibility of γ_{S^2} is assured only if it exist as a degree-2 messenger, simultaneously relevant to nonempty mode components $\gamma_{C_1^2}$, $\gamma_{C_3^2}$, and γ_{SC_4} . It then follows that the jet components $\gamma_{C_1}, \gamma_{C_3} \neq \emptyset$, containing C_1^2 and C_3^2 modes respectively.

In this situation, let us further assume that $\gamma_{C_2} \neq \emptyset$, for which 16 regions are allowed, as depicted in figure 42. In accordance with the external modes, here (and throughout this subsection) we color the mode subgraphs as follows: H mode (blue), C_1^2 mode (green), C_2 mode (olive), C_3^2 mode (teal), SC_i modes with $i = 1, 3, 4$ (orange), and S^2 mode (red).

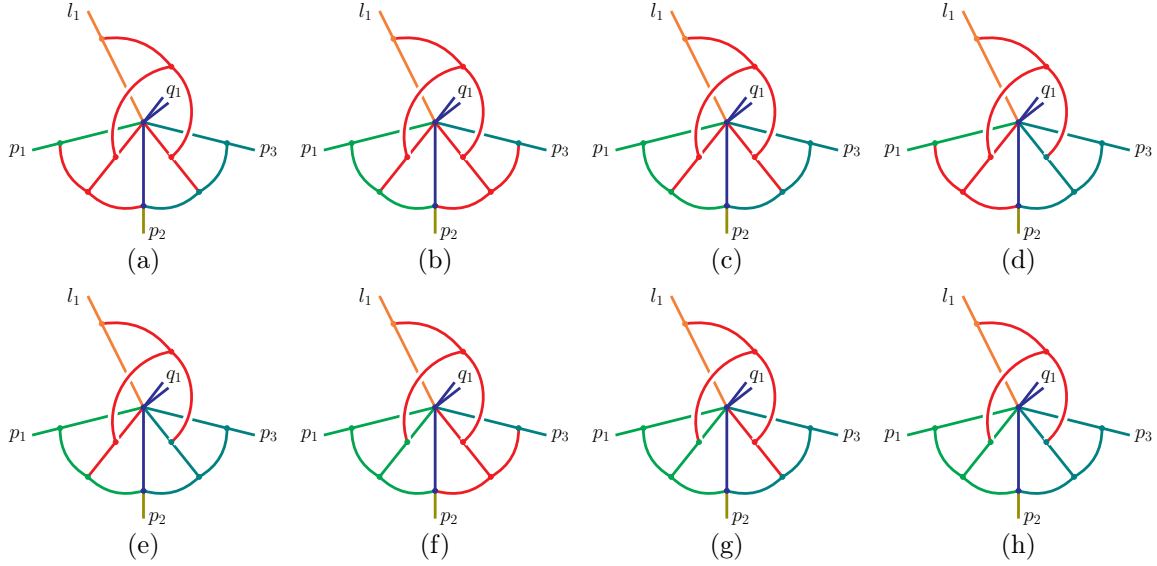


Figure 43. The 8 regions of figure 41, which are characterized by the S^2 mode with $\mathcal{J}_1, \mathcal{J}_3 \neq \emptyset$ and $\mathcal{J}_2 = \emptyset$.

One can verify that for each of these regions, all subgraph requirements are satisfied. In particular, to satisfy the infrared-compatibility requirement, mode components are confirmed to be infrared compatible in the following sequence:

- (1) γ_{SC_4} and γ_{C_2} (from the external momenta l_1 and p_2);
- (2) γ_{S^2} (as it is a messenger relevant to γ_{SC_4} component);
- (3) $\gamma_{C_1^2}$ and $\gamma_{C_3^2}$ (via the momentum flow from p_1 , p_3 , and γ_{S^2});
- (4) γ_{SC_1} and γ_{SC_3} (since they are relevant to either $\gamma_{C_1^2}$ or $\gamma_{C_3^2}$, and to γ_{C_2}).

Conversely, any other configuration with $\gamma_{S^2} \neq \emptyset$ and $\gamma_{C_1}, \gamma_{C_2}, \gamma_{C_3} \neq \emptyset$ would violate at least one subgraph requirement, thus not appearing in figure 42.

For configurations with $\gamma_{S^2} \neq \emptyset$ and $\gamma_{C_2} = \emptyset$ (in other words, p_2 is attached to \mathcal{H} directly), there are 8 regions, as shown in figure 43. Identical to the region structure in figure 42, here γ_{S^2} still acts as a degree-2 messenger, which is relevant to γ_{SC_4} , γ_{C_1} , and γ_{C_3} . One difference lies in the absence of SC_1 and SC_3 components, i.e., $\gamma_{SC_1} = \gamma_{SC_3} = \emptyset$. This is due to the infrared-compatibility requirement: since $\gamma_{C_2} = \emptyset$ here, any nonempty γ_{SC_1} or γ_{SC_3} would not be infrared compatible.

Next, we consider regions characterized by SC_i modes; namely, regions whose softest modes are SC_1 , SC_3 , and/or SC_4 . A key observation is that only the SC_4 mode can appear in such regions. To see why, suppose for example that $\gamma_{SC_1} \neq \emptyset$. Since there are no external momenta of mode SC_1 , the infrared-compatibility requirement would force γ_{SC_1} to be relevant

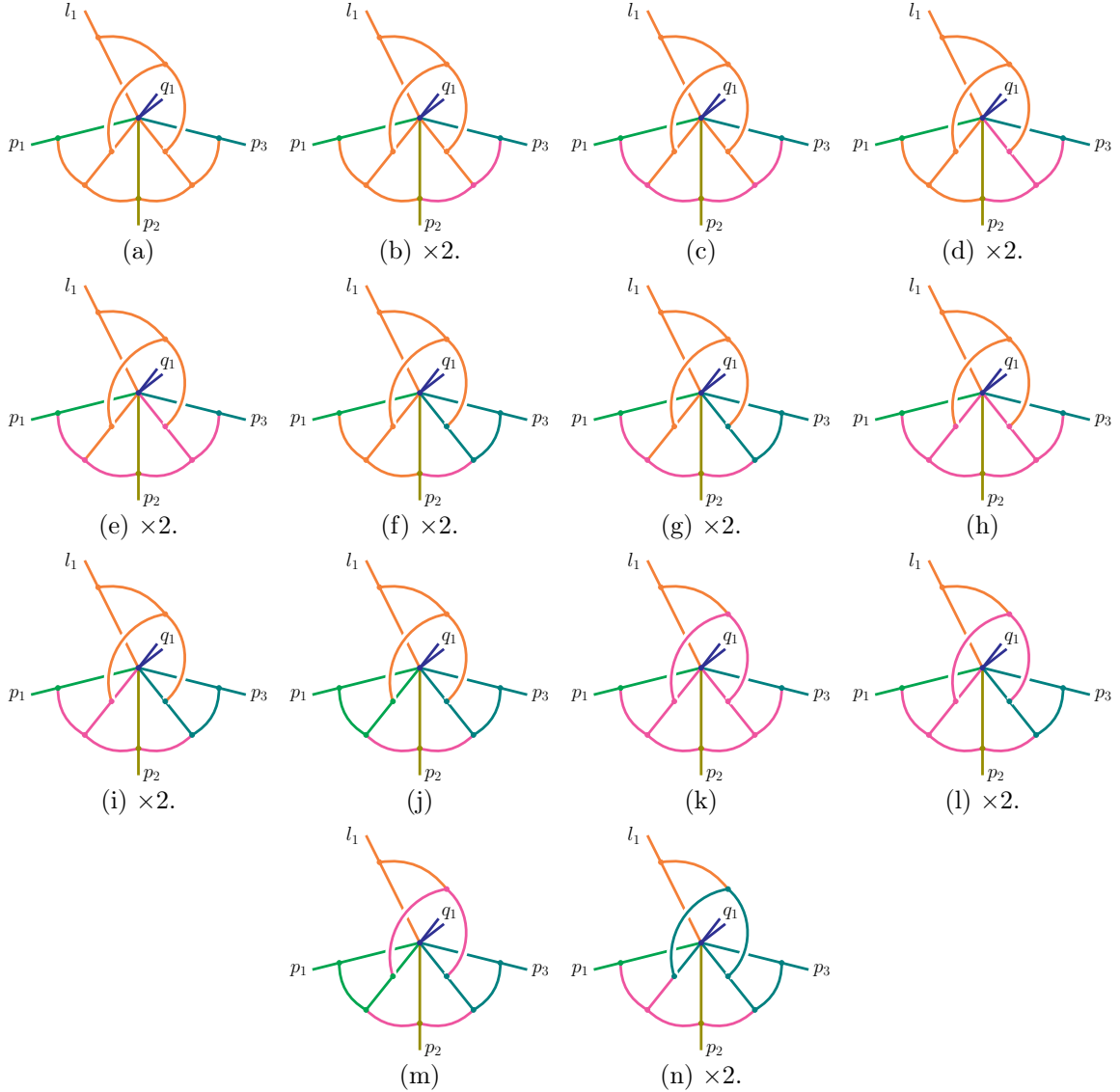


Figure 44. The 22 regions of figure 41 characterized by the SC_4 mode and with all three jets $\mathcal{J}_1, \mathcal{J}_2, \mathcal{J}_3$ nonempty. The color **rhodamine** represents the S mode. Only 14 distinct diagrams are shown explicitly; the remaining 8 are obtained by applying the reflection $1 \leftrightarrow 3$ to those with “ $\times 2$ ”.

to two already infrared-compatible components, which must include a $\gamma_{C_1^2}$. However, the infrared compatibility of $\gamma_{C_1^2}$ requires the confirmation of infrared compatibility of γ_{SC_1} in advance, which leads to a similar circular dependency discussed in section 7.1. In other words, γ_{SC_1} cannot satisfy the infrared-compatibility requirement. Therefore, all regions of this type contain the SC_4 mode, while SC_1 modes for $i = 1, 2, 3$ are absent.

Following the analysis above, we first examine configurations where $\mathcal{J}_1, \mathcal{J}_2$, and \mathcal{J}_3 are all nonempty (from now on, we use \mathcal{J}_i to represent the mode component γ_{C_i}). There are 22

such regions, shown in figure 44, where we have colored the S mode in **rhodamine**. For each of them, the external momentum l_1 must be relevant to both \mathcal{J}_1 and \mathcal{J}_3 . Since

$$\mathcal{X}(l_1) \vee \mathcal{X}(p_1) = SC_4 \vee C_1^\infty = C_1, \quad \mathcal{X}(l_1) \vee \mathcal{X}(p_3) = SC_4 \vee C_3^\infty = C_3, \quad (7.5)$$

only C_1 and C_3 modes are allowed in \mathcal{J}_1 and \mathcal{J}_3 , respectively. Note that l_1 can enter some S component before reaching \mathcal{J}_1 or \mathcal{J}_3 .

Only 14 of the 22 regions are explicitly shown in figure 44. Due to symmetry, the remaining 8 regions can be obtained by applying the reflection $1 \leftrightarrow 3$ (i.e., $p_1 \leftrightarrow p_3$ and $C_1 \leftrightarrow C_3$) to those marked “ $\times 2$ ”.

For configurations with $\mathcal{J}_1, \mathcal{J}_2 \neq \emptyset$ and $\mathcal{J}_3 = \emptyset$, there are 22 regions, 16 of which are presented in figure 45 due to page limit. Nevertheless, the remaining 6 follow very similar structures. In these regions, since \mathcal{J}_3 is empty, l_1 only needs to be relevant to \mathcal{J}_1 , and like above, it can enter some S component before reaching \mathcal{J}_1 .

By applying the reflection $1 \leftrightarrow 3$ to the regions in figure 45, we obtain another 22 regions in which $\mathcal{J}_1 = \emptyset$ and $\mathcal{J}_2, \mathcal{J}_3 \neq \emptyset$.

For the configurations with $\mathcal{J}_1, \mathcal{J}_3 \neq \emptyset$ and $\mathcal{J}_2 = \emptyset$, there are 16 regions. 10 of them are explicitly shown in figures 46a–46j, while the remaining 6 can be obtained by applying the reflection $1 \leftrightarrow 3$ to the graphs marked “ $\times 2$ ”.

For the configurations with $\mathcal{J}_1 \neq \emptyset$ and $\mathcal{J}_2, \mathcal{J}_3 = \emptyset$, there are 9 regions, shown in figures 46k–46s. By applying the reflection $1 \leftrightarrow 3$ to these graphs, we obtain another 9 regions corresponding to $\mathcal{J}_3 \neq \emptyset$ and $\mathcal{J}_1, \mathcal{J}_2 = \emptyset$.

For the configurations with $\mathcal{J}_2 \neq \emptyset$ and $\mathcal{J}_1, \mathcal{J}_3 = \emptyset$, there are 15 regions, where 10 are explicitly shown in figures 47a–47j, with the remaining obtainable by applying the reflection $1 \leftrightarrow 3$ to those marked “ $\times 2$ ”.

For the configurations with $\mathcal{J}_1, \mathcal{J}_2, \mathcal{J}_3 = \emptyset$, there are 5 regions, where 4 are shown in figures 47k–47n, with the remaining one obtained from figure 47l by reflecting $1 \leftrightarrow 3$.

So far we have examined all the regions containing S^2 and/or SC_i modes. An interesting feature is that in those regions characterized by the SC_4 mode, some S components can also exist, only if two or more jets ($\mathcal{J}_1, \mathcal{J}_2, \mathcal{J}_3$) are nonempty. This is consistent with the Second Connectivity Theorem (theorem 5.3), because there is only one mode softer than S , thus condition 2 of the theorem cannot apply to any given S component γ_S . In other words, γ_S must be relevant to harder-mode components, which can only be from nonempty jets.

Then, we consider regions characterized by the S mode; namely, regions in which the softest mode is S . In this case, the remaining modes can only be H or C_i (with $i = 1, 2, 3$ if $\mathcal{J}_i \neq \emptyset$). Let us first consider those configurations with $\mathcal{J}_1, \mathcal{J}_2, \mathcal{J}_3 \neq \emptyset$. Since $\mathcal{X}(p_1) = C_1^\infty$ and $\mathcal{X}(p_3) = C_3^\infty$, in order that \mathcal{J}_1 and \mathcal{J}_3 satisfy the infrared-compatibility requirement, either of the following must be satisfied.

- (1) The external momentum l_1 is relevant to both \mathcal{J}_1 and \mathcal{J}_3 , simultaneously making them infrared compatible.

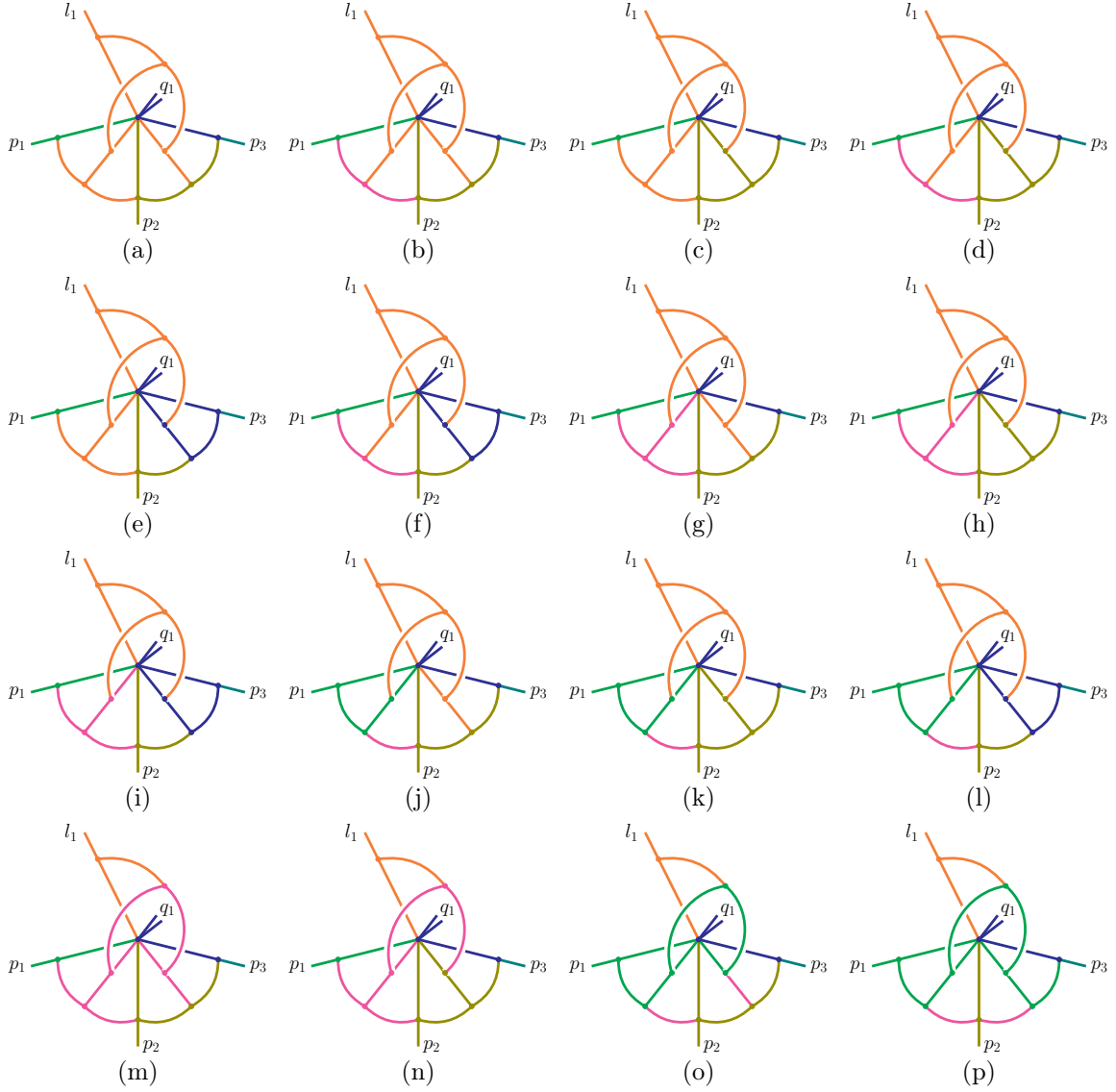


Figure 45. 16 of the 22 regions of figure 41, which are characterized by the SC_4 mode with $\mathcal{J}_1, \mathcal{J}_2 \neq \emptyset$ and $\mathcal{J}_3 = \emptyset$.

- (2) The external momentum l_1 is relevant to \mathcal{J}_1 (\mathcal{J}_3), making it infrared compatible, while there is an S component acting as a degree-1 messenger that is relevant to both jets, thus making the other infrared compatible.

Following this idea, we come up with 8 such regions, 5 of which are explicitly shown in figure 48. The first row, figures 48a–48c, follow from (1) above, while the second row, figure 48d and 48e, follow from (2).

For the regions without three jets, we observe that for each of them, there must be precisely two jets. This is due to the Second Connectivity Theorem: any S component must

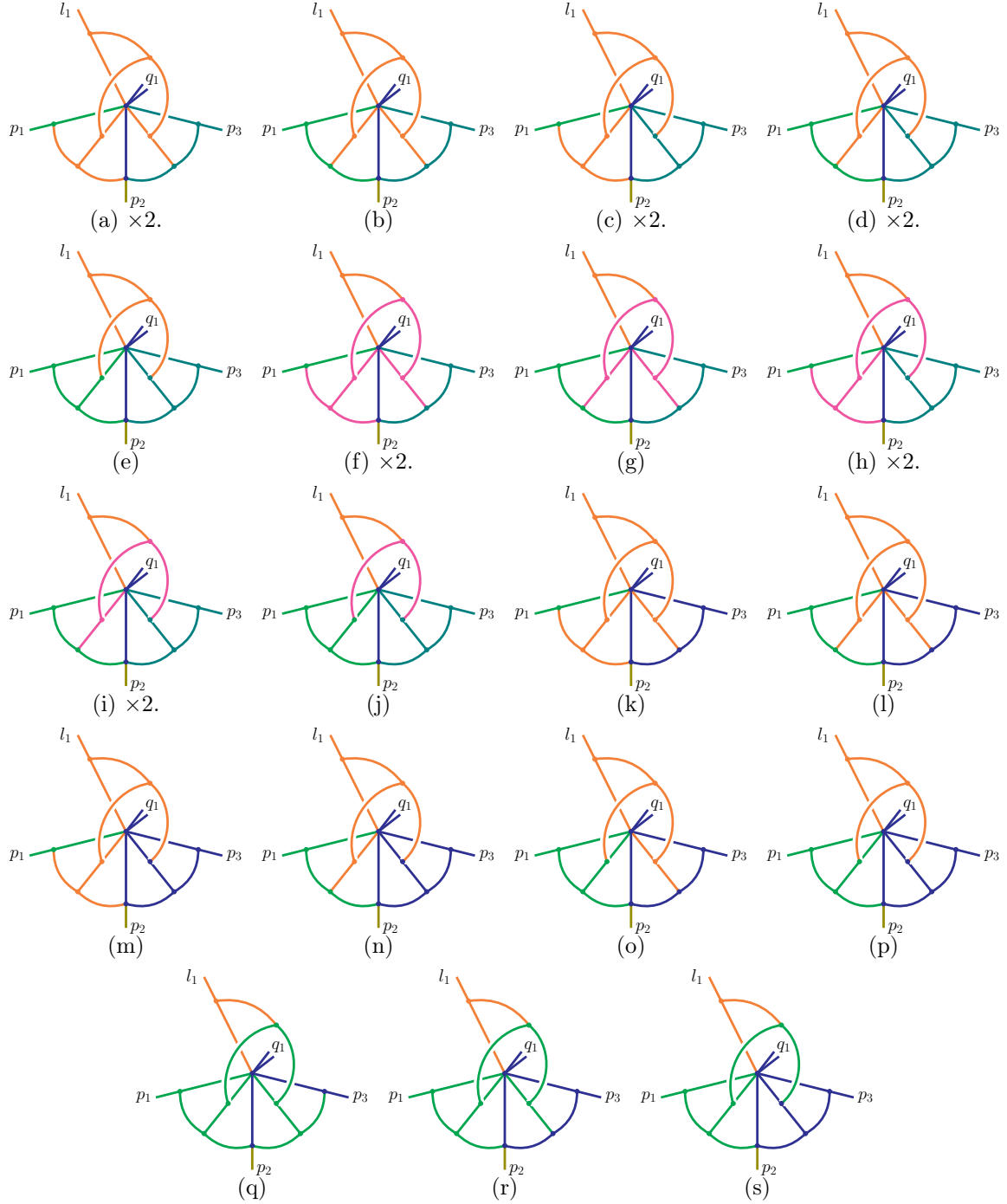


Figure 46. Some regions of figure 41 characterized by the SC_4 mode. Graphs (a)–(j): 10 representatives of the 16 regions with $\mathcal{J}_1, \mathcal{J}_3 \neq \emptyset$ and $\mathcal{J}_2 = \emptyset$, while the remaining 6 can be obtained by applying the reflection $1 \leftrightarrow 3$ to those marked “ $\times 2$ ”. Graphs (k)–(s): 9 regions with $\mathcal{J}_1 \neq \emptyset$ and $\mathcal{J}_2, \mathcal{J}_3 = \emptyset$.

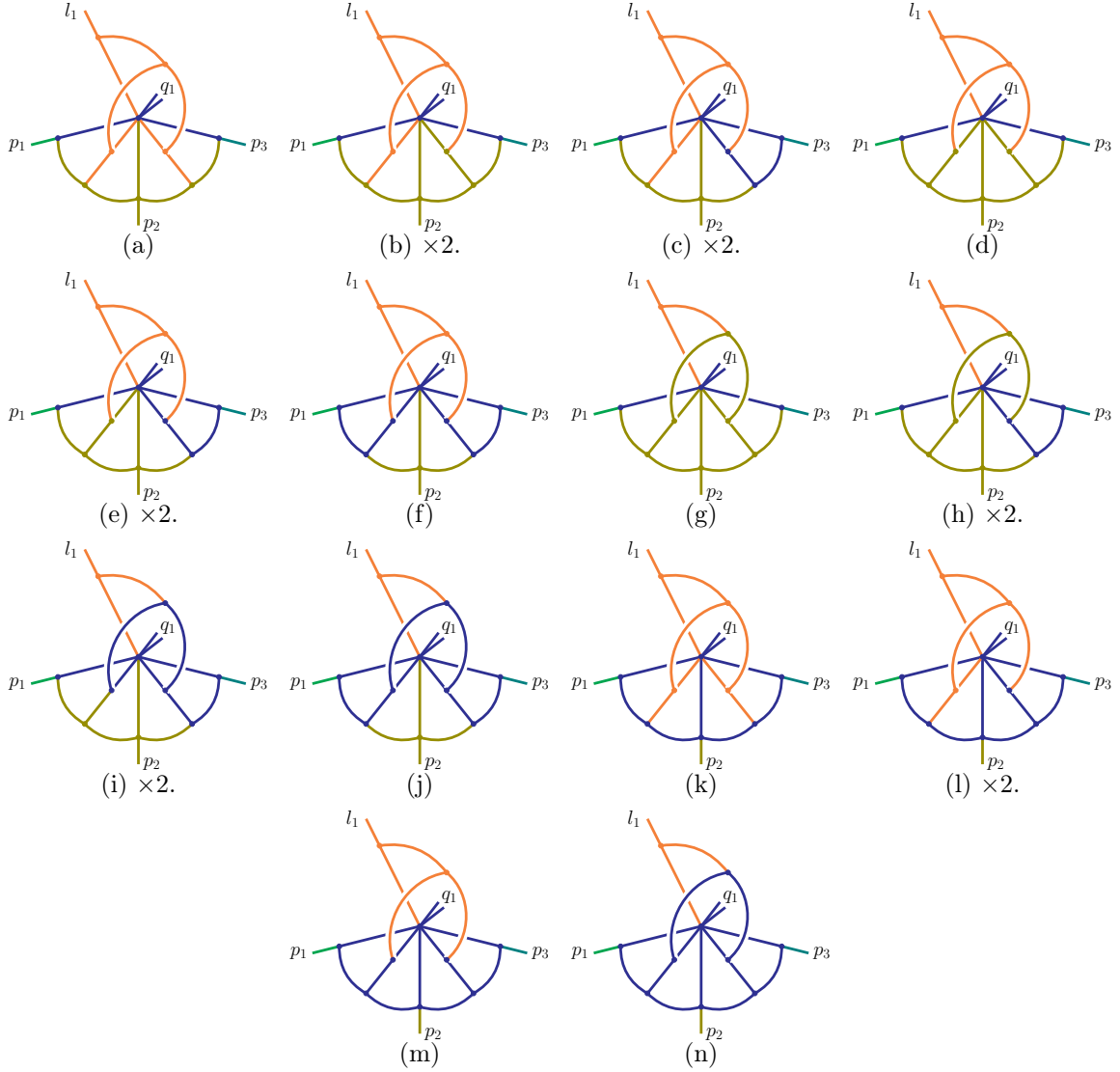


Figure 47. Some regions of figure 41 characterized by the SC_4 mode. Graphs (a)–(j): 10 representatives of the 15 regions with $\mathcal{J}_1, \mathcal{J}_3 = \emptyset$ and $\mathcal{J}_2 \neq \emptyset$, while the remaining 5 can be obtained by applying the reflection $1 \leftrightarrow 3$ to those marked “ $\times 2$ ”. Graphs (k)–(s): 4 representatives of the 5 regions with $\mathcal{J}_1, \mathcal{J}_2, \mathcal{J}_3 = \emptyset$, with the remaining one obtained from (l) by reflecting $1 \leftrightarrow 3$.

be relevant to two harder-mode subgraphs, which are jets in this situation. We can then consider all such possibilities and come up with 32 regions, depicted in figure 49.

Finally, we construct regions with only H and C_i modes and depict them in figure 50. There are 15 regions in total, with 14 featuring C_i modes and one hard region.

We have thus obtained all the regions directly from the knowledge of region structures.

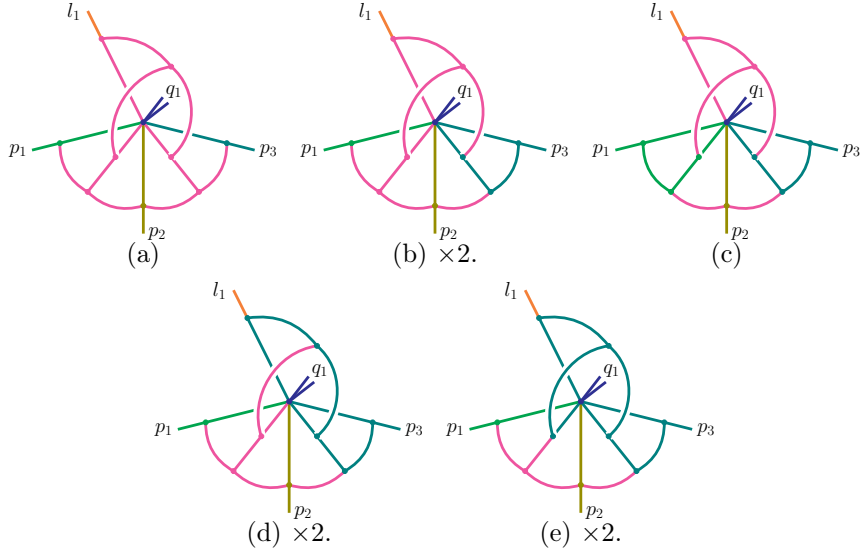


Figure 48. The 8 regions of figure 41 characterized by the $\textcolor{red}{S}$ mode and with all three jets $\mathcal{J}_1, \mathcal{J}_2, \mathcal{J}_3$ nonempty. Here we explicitly show 5 of them, with the remaining 3 obtainable from reflecting $1 \leftrightarrow 3$ for those with “ $\times 2$ ”.

The total number is:

$$16 + 8 + 22 + 22 + 22 + 16 + 9 + 9 + 15 + 5 + 8 + 32 + 15 = 199, \quad (7.6)$$

coinciding with the count in the output of `pySecDec`. One can further check their one-to-one correspondence via the relation (2.16).

7.3 Extension to massive cases: revisiting a recent work on $gg \rightarrow HH$

As emphasized earlier, the present work concentrates on massless Feynman integrals, although the methodology could be extended to massive cases. We now take a first step in this direction by examining the regions in a recent paper [25]. That study computed top-mass corrections to the $gg \rightarrow HH$ amplitude in the high-energy limit, i.e.,

$$g(p_1) + g(p_2) \rightarrow H(p_3) + H(p_4), \quad s, |t|, |u| \gg m_t^2 \gg m_H^2. \quad (7.7)$$

The asymptotic expansion takes the following form:

$$\frac{m_t^2}{s} \sim \lambda^2 \ll 1, \quad p_1^2 = p_2^2 = p_3^2 = p_4^2 = 0, \quad m_H = 0. \quad (7.8)$$

The limit $m_H = 0$ is permissible because the dependence of the $gg \rightarrow HH$ amplitude on the Higgs mass is analytic [41]. The external momenta lie along distinct lightlike directions.

Unlike the virtuality expansion in eq. (2.1), here each external momentum is exactly on a lightcone, and the small scale is provided by the top-quark mass m_t . This difference could profoundly alter the structure of the Symanzik polynomials in two ways:

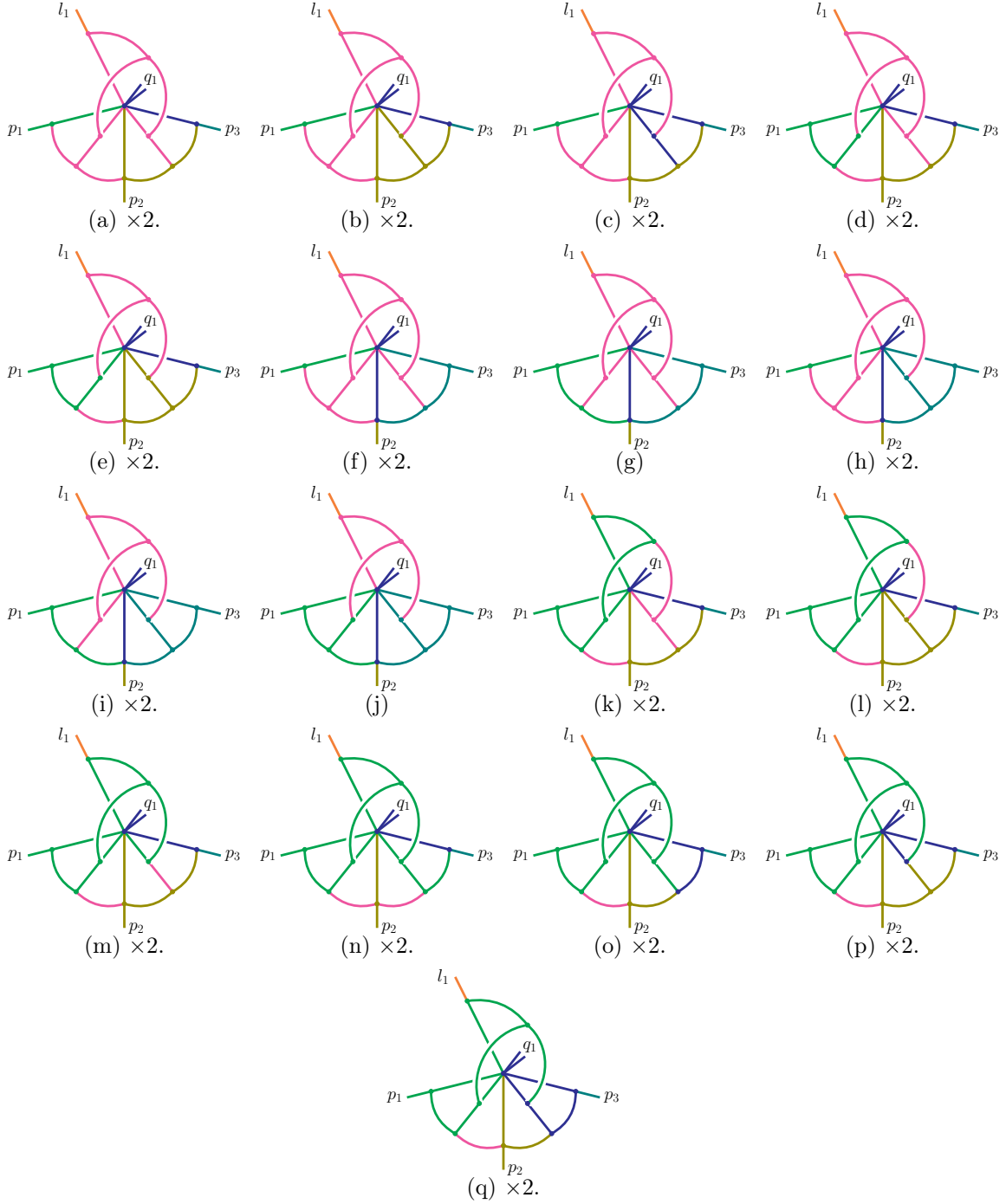


Figure 49. 32 regions of figure 41 characterized by the $\textcolor{blue}{S}$ mode with exactly two jets. Here we explicitly show 17 of them, with the remaining 15 obtainable from reflecting $1 \leftrightarrow 3$ for those with “ $\times 2$ ”.

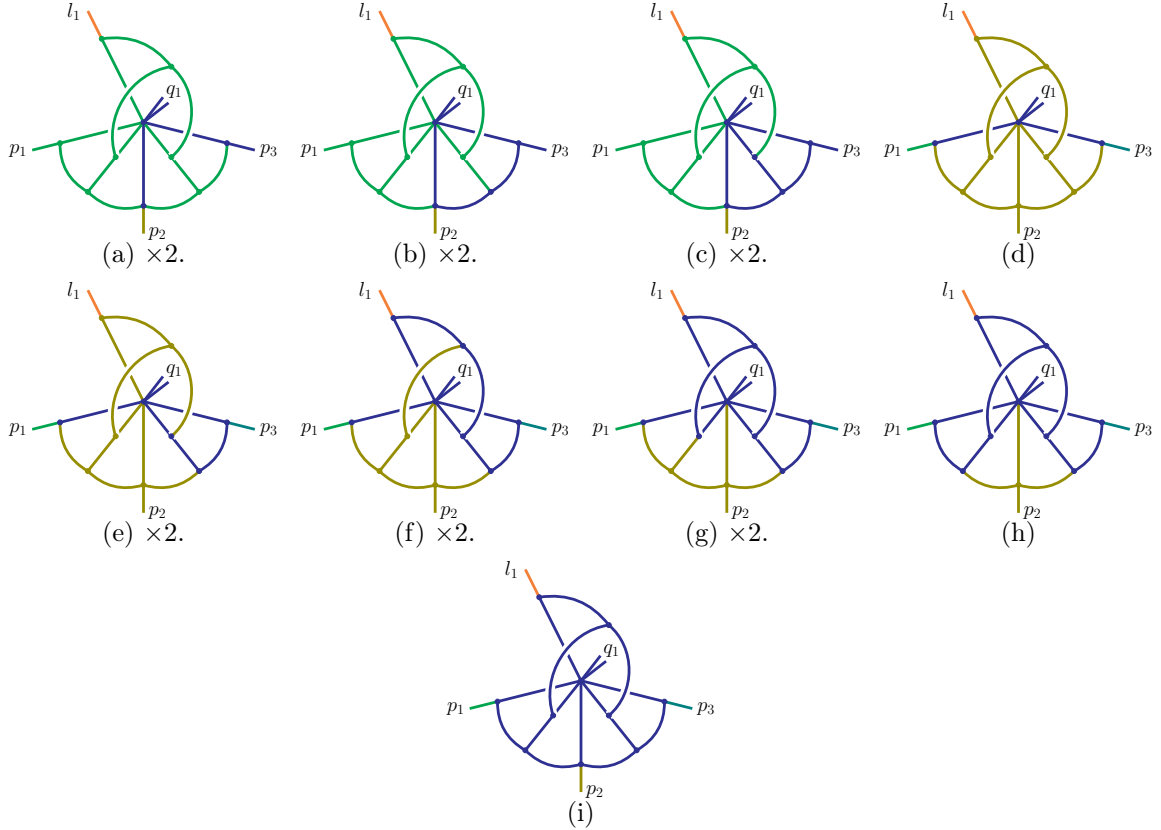


Figure 50. 15 regions of figure 41 characterized by the C_i and H modes only. Here we explicitly show 9 of them, with the remaining 6 obtainable from reflecting $1 \leftrightarrow 3$ for those with “ $\times 2$ ”. The last graph represents the hard region.

1. The presence of massive propagators introduces quadratic terms in the second Symanzik polynomial \mathcal{F} , in contrast to the linear form in eq. (2.14).
2. Because every external momentum is strictly lightlike, no \mathcal{F} term could correspond to a unitarity cut that isolates a single external momentum.

Consequently, a fully general all-order analysis would require substantial modification. Below, however, we propose that the fundamental pattern and the subgraph requirements remain applicable, with only a slight modification on the concept of infrared compatibility. We shall provide neither an all-order statement nor a rigorous proof of this proposition, which will be deferred to future research.

Proposition 7.1. *Each facet region in the expansion (7.8) corresponds to a configuration of the fundamental pattern shown in figure 5. Moreover, a configuration of the fundamental pattern is a region if and only if the following two conditions hold:*

- 1, the graph $\bigcup_{\mathcal{V}(X) \leq n} \Gamma_X$ is connected for any $n \in \mathbb{N}$.

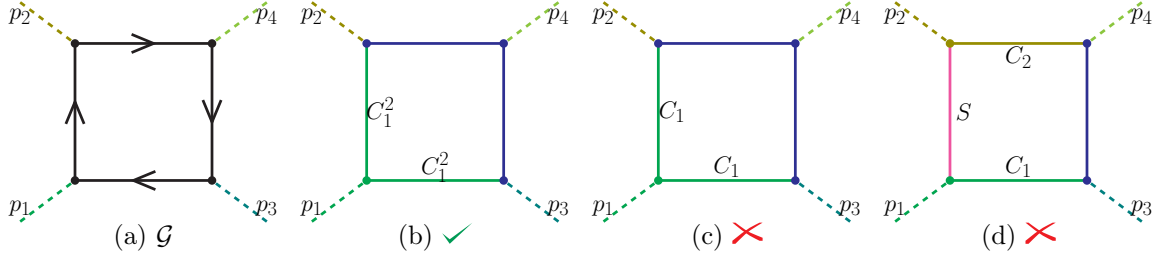


Figure 51. The one-loop graph (a) and one of its four collinear² regions (b), together with two non-region configurations (c) and (d).

2, all mode components are infrared compatible.

Here, a mode component γ is called *infrared compatible* if it satisfies at least one of the following:

- (1) the partial sum over external momenta flowing into γ has mode $\mathcal{X}(\gamma)$;
- (2) γ contains an edge e whose mass m_e scales as $m_e^2 \sim \lambda^{\mathcal{V}(\mathcal{X}(\gamma))}$.
- (3) γ is among the set of three or more mode components, which an already confirmed infrared-compatible mode component γ' is simultaneously relevant to.
- (4)

These conditions parallel the “message-delivery pattern” introduced for massless wide-angle scattering in section 5.2.2, where the “message” refers to the infrared scaling of γ . The first condition corresponds to obtaining the scaling directly from external kinematics, the second to obtaining it from its internal mass (which is m_t in our case), and the third to receiving it via a “messenger” γ' . The ellipsis “...” stands for further possible conditions not occurring in the graphs studied here, which are therefore omitted.

Now let us check the regions using proposition 7.1. At one-loop level, the external gluons and Higgs bosons attach to a top-quark loop (see figure 51a). Here massive (m_t) edges are solid, and massless edges are dashed. The expansion contains one hard region and four infrared regions, each involving a loop momentum of C_i^2 mode collinear to one of the external momenta. Figure 51b shows one example, where the loop momentum is in the C_1^2 mode—note that the mode is C_1^2 rather than C_1 because $m_t^2 \sim \lambda^{\mathcal{V}(C_1^2)}$. Figures 51c and 51d illustrate two non-region configurations (marked with “ \times ”), each containing mode components that are not infrared compatible. Specifically, the C_1 component in figure 51c fails to satisfy any of the conditions (1)–(3) above. In figure 51d, the S component is infrared compatible due to condition (2), whereas the C_1 and C_2 components are not.

At two-loop level, the graphs can be divided into planar and non-planar families. Some examples of regions and non-region configurations are displayed in figure 52. Again, massive (m_t) edges are solid, and massless edges are dashed. One can verify directly that each

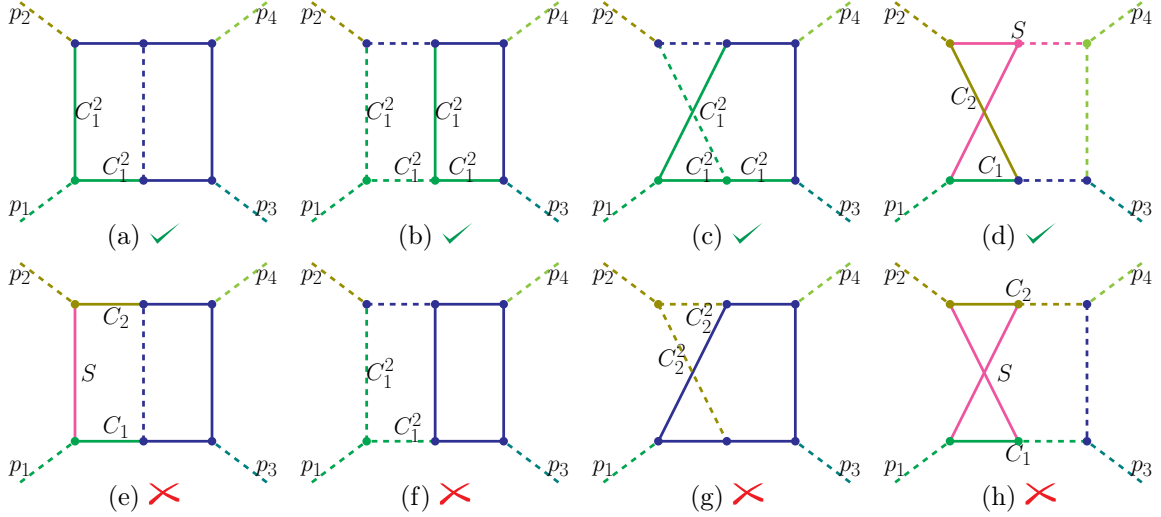


Figure 52. Some examples of regions and non-region configurations at two-loop level, where (a)–(d) are regions, while (e)–(h) are not due to the violation of the infrared-compatibility requirement.

region (figures 52a–52d) satisfies both subgraph requirements stated in proposition 7.1. In particular, we note that the S component in figure 52d acts as a messenger, rendering the C_1 , C_2 , and C_4 components infrared compatible via condition (3). By contrast, each non-region configuration violates the infrared-compatibility requirement because it contains at least one mode component that does not meet any of conditions (1)–(3).

8 Conclusions and outlook

In this work, we have provided a complete, momentum-space prescription for facet regions in generic massless wide-angle scattering, valid to all loop orders. To this end, we have unified a broad class of asymptotic expansions—including various limits of external momenta—with a single framework termed the *virtuality expansion*, defined in eq. (2.1). The diversity of external momentum types gives rise to rich and intricate structures of momentum modes in the corresponding regions.

A key conceptual advance of this paper is the algebraic characterization of momentum modes, developed in section 3.1. We have noticed that every momentum scale relevant to the virtuality expansion can be expressed in the form $S^m C_i^n$ with $m, n \in \mathbb{N}$. This observation allows us to endow the set of modes with a natural partial order based on “softness”, turning it into a *partially ordered set* (poset). By further introducing the join (\vee) and meet (\wedge) operations, we elevate this poset to a *non-distributive lattice*. The algebraic properties of this lattice (for example, the identity $\mathcal{V}(X_1) + \mathcal{V}(X_2) = \mathcal{V}(X_1 \wedge X_2) + \mathcal{V}(X_1 \vee X_2)$) play a crucial role in the subsequent region analysis.

From a graphical viewpoint, each region corresponds to a specific assignment of modes to the edges and vertices of the Feynman graph \mathcal{G} . This assignment naturally partitions

the graph into *mode components* (specific subgraphs that share a common momentum scale), which serve as the fundamental building blocks of a region. The problem of classifying regions then reduces to understanding how these components can be connected. Our starting point is the *fundamental pattern* introduced in section 4. This pattern rests on two well-motivated physical assumptions: that infrared regions correspond to solutions of the Landau equations, and that the hard scattering subgraph is connected. We have argued why both assumptions are natural for wide-angle kinematics.

The core of our analysis lies in identifying the necessary and sufficient conditions that a configuration of mode components must satisfy to yield a scaleful expanded integral and thus constitute a valid region. Remarkably, these conditions condense into only two concise requirements, summarized in section 5.4: (1) a connectivity condition on certain unions of mode subgraphs, and (2) an *infrared-compatibility* condition on each individual mode component. The latter, a novel concept developed here, formalizes how a component acquires its infrared scaling. Together, these requirements impose strong constraints on the allowed momentum modes and, as a corollary, exclude the appearance of *cascading modes* (unbounded number of soft hierarchies at the amplitude level) in the virtuality expansion. Applied to previously studied special cases, such as those in ref. [24], our framework reproduces known results with streamlined reasoning, replacing lengthy and technical proofs by surprisingly concise derivations.

The rigorous derivation of these subgraph requirements is presented in section 6, the most technical part of the paper. The proof proceeds in the following logical sequence: (1) the First Connectivity Theorem, (2) generic structure of leading terms, (3) the Second Connectivity Theorem, (4) the sufficiency of the infrared-compatibility condition, and finally (5) its necessity. Each step employs tailored graph-theoretical techniques that collectively provide a self-consistent foundation for the entire prescription.

We have validated our framework through extensive multiloop examples. In section 7, two representative cases, a three-loop four-leg graph and a six-loop five-leg graph, were analyzed in detail. In both examples, we derived the full set of momentum-space regions from first principles, translated them to the parametric representation, and found perfect agreement with the output of `pySecDec`. Moreover, as a first step toward extending the method to massive integrals, we examined a recent study of top-mass corrections in $gg \rightarrow HH$ [25]. With a minor adaptation of the infrared-compatibility condition to incorporate massive propagators, our analysis reproduces the regions identified in that work, confirming the robustness of our approach and highlighting its potential for extension to broader kinematic regimes.

The framework developed in this work already encompasses a broad class of asymptotic expansions in massless wide-angle scattering. The momentum-space prescription lends itself naturally to the development of efficient graph-finding algorithms to enumerate all relevant regions in arbitrary graphs, bypassing the need to construct high-dimensional polytopes in parameter space. For the special case of the on-shell expansion (see eq. (5.6)), such an algorithm has already been implemented in Maple [42] and is publicly available [43]. Extensions

to more general virtuality hierarchies are expected to be similar.

Nevertheless, the present analysis is restricted to massless wide-angle kinematics. We expect the methodology introduced here—combining graph theory, convex geometry, and the algebraic structures of momentum modes—to serve as a foundation for systematic treatments of other asymptotic expansions, despite anticipated subtleties. Massive propagators, for instance, introduce quadratic terms in the Symanzik polynomials that fundamentally alter the structure of the associated polytopes and the corresponding region analysis. While section 7.3 offers an initial exploration, a complete all-order prescription remains a distant goal. Possible threshold singularities [32, 44] could also affect the region structure by inducing the “potential region” [1]. Further challenges arise in kinematics involving spacelike-collinear external momenta, where Glauber exchanges may appear, requiring dedicated treatment and potentially invalidating the fundamental pattern due to factorization-violating effects [45–50].

A further limitation of this work is the exclusive focus on facet regions. Extending the all-order prescription to hidden regions (though rare in massless wide-angle scattering) would fully resolve the region structure in this regime. Ref. [11] conjectures that all hidden regions exhibit a Landshoff-type scattering pattern, a proposal verified for two-to-two kinematics up to three loops. Confirming this conjecture at higher orders and for processes with additional legs remains an open and technically demanding challenge.

Once some of these extensions are achieved, the prescription may find broad application across diverse computations. Beyond the standard loop integrals of the form (2.11), to which many applications have been made in recent years [51–58], the EbR technique have recently been applied to conformal correlators [59], cosmological correlators [60], $\mathcal{N} = 4$ super Yang-Mills theory [61–64], among others. A particularly promising direction is the treatment of phase-space integrals [65–69], which opens pathways to fully differential cross sections. Another interesting phenomenon resides in a recent work of soft-anomalous-dimension calculation [70, 71], where eikonal propagators give rise to ultraviolet modes (loop momenta scaling to infinity), in addition to the hard and infrared modes discussed in this work.

From a theoretical perspective, this work focuses on region identification, one of the fundamental aspects of EbR. A full understanding of this topic provides crucial insights into even harder questions: is EbR always correct, and why? Sophisticated mathematical deductions may be needed to answer these questions [9, 21, 72]. Another key challenge involves performing expansions for specific region sets, particularly when certain regions yield integrals with unregulated divergences, even under dimensional regularization. Such cases possibly arise when some regions degenerate [73], requiring additional regulators (e.g., the analytic regulator, see section 2.3 of ref. [17] for a pedagogical example) to carry out the integration. It remains to understand in general how this works out systematically, and how the complete set of regions depends on the regulators one chooses. Resolving these issues would also advance the reliability and further development of computational packages that employ EbR [74–78].

More broadly, the all-order prescription developed here may advance our understanding of infrared singularities in scattering amplitudes. A prominent example is the hard-collinear-soft

factorization formula for wide-angle scattering [79–84],

$$\mathcal{M} = \mathcal{H} \cdot \frac{\mathcal{J}_{\text{parton}}}{\mathcal{J}_{\text{eikonal}}} \cdot \mathcal{S}, \quad (8.1)$$

which asserts that collinear singularities reside in the jet factor ratio $\mathcal{J}_{\text{parton}}/\mathcal{J}_{\text{eikonal}}$, soft singularities in the soft function \mathcal{S} , and that the hard function \mathcal{H} is infrared finite. Although formally reminiscent of our region prescription, the two frameworks differ fundamentally: the factorization above applies locally (i.e., at the integrand level), whereas expansion by regions operates globally (i.e., at the integral level). Establishing a deeper connection between these structures could illuminate the interplay between ultraviolet and infrared singularities, potentially informing factorization-based local subtraction schemes, which have seen substantial recent development [84–93].

Finally, we highlight the broader potential of the algebraic structure of momentum modes uncovered in section 3.1. On the one hand, further exploration of this lattice—including its poset structure, explicit join and meet operations, virtuality additivity, pairwise reduction properties, and especially its non-distributivity—could reveal deeper mathematical insights with connections to ordered sets and geometric interpretations relevant to asymptotic expansions. On the other hand, this framework offers a promising new perspective on Soft-Collinear Effective Theory (SCET) and related effective field theories [17, 94–100], potentially systematizing operator bases, multipole expansions, and mode interactions in multiscale processes. We hope that these directions will enrich the analytical understanding of Feynman integrals and precision phenomenology in the years ahead.

Acknowledgments

I wish to express my gratitude to Samuel Abreu, Thomas Becher, Martin Beneke, John Collins, Einan Gardi, Sebastian Jaskiewicz, and George Sterman for their insightful discussions, which greatly enriched this work. I am also grateful to the Mainz Institute for Theoretical Physics (MITP) of the Cluster of Excellence PRISMA+ (Project ID 390831469), for its hospitality and its partial support during the completion of this work. This work is supported by the Swiss National Science Foundation under the project funding scheme, grant number 10001706.

A Some details in section 6

In this appendix, we elaborate some details that are skipped in section 6.

A.1 Comparing the kinematic factors in proving (6.5)

We shall demonstrate that $Q_{T_*^2}^2 \gtrsim Q_{T^2(\mathbf{r})}^2$ where $T^2(\mathbf{r})$ and T_*^2 refers to the spanning 2-trees in figures 16a and 16b, respectively. To see this, recall the difference of these spanning 2-trees: the subtree $\mathbf{t} = \gamma_* \cap t(\mathbf{r}; A)$, represented by the blob containing v_A in figure 16, lies in the same component with q_j in $T^2(\mathbf{r})$, while in different components with q_j in T_*^2 . If no external

momentum attaches to \mathbf{t} , the momentum flowing between the components of $T^2(\mathbf{r})$ and T_*^2 are identical. We thus have $Q_{T_*^2}^2 = Q_{T^2(\mathbf{r})}^2$.

If there are some external momenta attached to \mathbf{t} , we denote the total momentum entering \mathbf{t} as \mathbf{p}' , and the total momentum entering $T^2(\mathbf{r}; B)$ as \mathbf{p}_B . If $\mathcal{X}(\mathbf{p}_B)$ is hard (same as $\mathcal{X}(q_j)$), then for both $T^2(\mathbf{r})$ and T_*^2 , the total momenta flow between their components are off shell, and we have $Q_{T_*^2}^2 \sim Q_{T^2(\mathbf{r})}^2 \sim 1$. Otherwise, \mathbf{p}_B is in an infrared mode (collinear, soft, etc.), which must be identical to the mode of $Q_{T^2(\mathbf{r})}$. Similarly, $\mathbf{p}_B + \mathbf{p}'$ is in the same mode as $Q_{T_*^2}$. Namely,

$$\mathcal{X}(Q_{T^2(\mathbf{r})}) = \mathcal{X}(\mathbf{p}_B), \quad \mathcal{X}(Q_{T_*^2}) = \mathcal{X}(\mathbf{p}_B) \vee \mathcal{X}(\mathbf{p}'). \quad (\text{A.1})$$

It then follows that $\mathcal{X}(Q_{T_*^2})$ is harder than or equal to $\mathcal{X}(Q_{T^2(\mathbf{r})})$, and $Q_{T_*^2}^2 \gtrsim Q_{T^2(\mathbf{r})}^2$.

A.2 Solving for weights in figures 28b and 28c

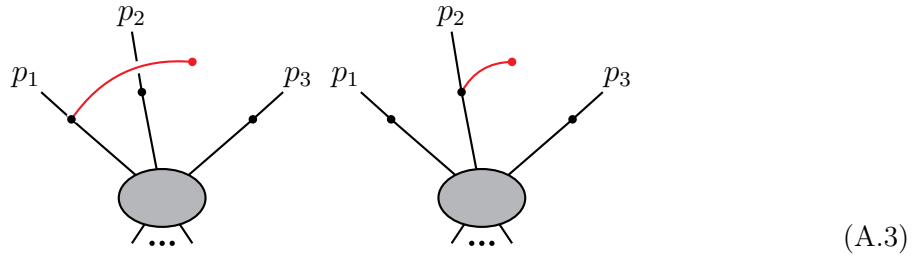
Here we show how to solve the weight w_γ for figures 28b and 28c, under the condition that the edge weights of γ_1 have been solved.

In figure 28b, the S^m component is relevant to γ_1 and γ_2 , while the $S^m C_3^{n_3}$ component, which we denote as γ' , is relevant to γ_1 , γ_2 , and γ_3 simultaneously. Each mode $\mathcal{X}(\gamma_i)$ is of the form $S^{m-m_i} C_i^{m_i}$. Since the edge weights of γ_1 have been solved (in Step 1) as $w_{\gamma_1} = -\mathcal{V}(\mathcal{X}(\gamma_1)) = 2m_1 - 4m$, its external momentum p_1 must be of the mode $\mathcal{X}(\gamma_1)$. We therefore have

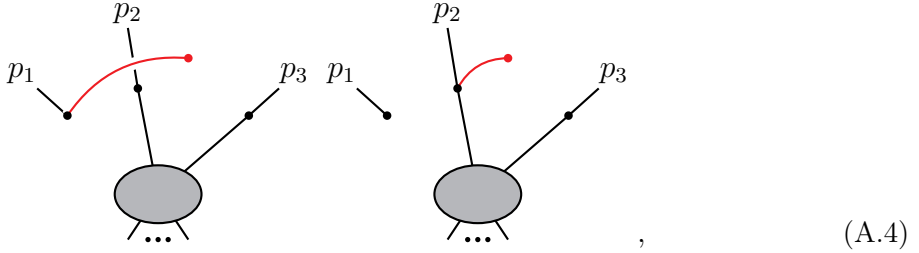
$$\mathcal{X}(\gamma_1) = S^{m-m_1} C_1^{m_1}, \quad \mathcal{X}(\gamma_2) = S^{m-m_2} C_2^{m_2}, \quad \mathcal{X}(\gamma_3) = S^{m-m_3} C_3^{m_3+n_3}; \quad (\text{A.2a})$$

$$\mathcal{X}(p_1) = S^{m-m_1} C_1^{m_1}, \quad \mathcal{X}(p_2) = S^{m-m_2} C_2^{m_2+n'_2}, \quad \mathcal{X}(p_3) = S^{m-m_3} C_3^{m_3+n_3+n'_3}. \quad (\text{A.2b})$$

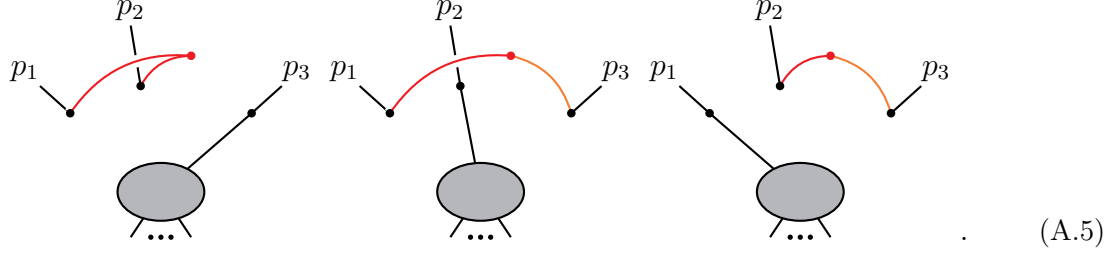
From section 6.2, the leading polynomial contains the following $\mathcal{U}^{(R)}$ terms



$\mathcal{F}_I^{(R)}$ terms



and $\mathcal{F}_{\text{II}}^{(R)}$ terms



Again, the gray blobs above represent certain set of tree subgraphs. The kinematic coefficient for the three $\mathcal{F}_{\text{II}}^{(R)}$ terms above are of the following scales:

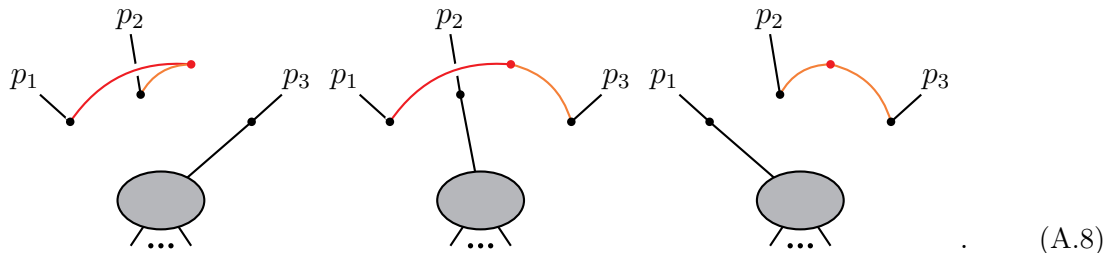
$$(p_1 + p_2)^2 \sim \lambda^{2m-m_1-m_2}, \quad (p_1 + p_3)^2 \sim \lambda^{2m-m_1-m_3}, \quad (p_2 + p_3)^2 \sim \lambda^{2m-m_2-m_3}. \quad (\text{A.6})$$

We then consider the characteristic equations of the $\mathcal{F}_{\text{II}}^{(R)}$ terms and compare them with those of the $\mathcal{U}^{(R)}$ terms. To be specific, the differences between the first $\mathcal{U}^{(R)}$ and $\mathcal{F}_{\text{II}}^{(R)}$ terms lie in the terms w_{γ_1} and w_{γ_2} (present in the $\mathcal{U}^{(R)}$ -term equation but absent from the $\mathcal{F}_{\text{II}}^{(R)}$ -term equation), a w_{γ} term (present in the $\mathcal{F}_{\text{II}}^{(R)}$ -term equation but absent from the $\mathcal{U}^{(R)}$ -term equation), and the kinematic contribution (which is 0 for the $\mathcal{U}^{(R)}$ term and $2m - m_1 - m_2$ for the $\mathcal{F}_{\text{II}}^{(R)}$ term). The sum over these contributions must be zero, which yields one equation. By comparing the $\mathcal{U}^{(R)}$ term and the other two $\mathcal{F}_{\text{II}}^{(R)}$ terms, we obtain another two equations:

$$\left. \begin{aligned} w_{\gamma_1} + w_{\gamma_2} - w_{\gamma} + (2m - m_1 - m_2) &= 0 \\ w_{\gamma_1} + w_{\gamma_3} - w_{\gamma'} + (2m - m_1 - m_3) &= 0 \\ w_{\gamma_2} + w_{\gamma_3} - w_{\gamma'} + (2m - m_2 - m_3) &= 0 \end{aligned} \right\} \Rightarrow w_{\gamma} = -2m. \quad (\text{A.7})$$

Meanwhile, w_{γ_3} and $w_{\gamma'}$ cannot be solved from these equations alone.

For figure 28c, the three $\mathcal{F}_{\text{II}}^{(R)}$ terms are



The three equations in (A.7) become

$$\left. \begin{aligned} w_{\gamma_1} + w_{\gamma_2} - w_{\gamma'} + (2m - m_1 - m_2) &= 0 \\ w_{\gamma_1} + w_{\gamma_3} - w_{\gamma''} + (2m - m_1 - m_3) &= 0 \\ w_{\gamma_2} + w_{\gamma_3} - w_{\gamma'} - w_{\gamma''} + (2m - m_2 - m_3) &= 0 \end{aligned} \right\} \Rightarrow w_{\gamma} = -2m. \quad (\text{A.9})$$

Meanwhile, w_{γ_2} , w_{γ_3} , $w_{\gamma'}$, and $w_{\gamma''}$ cannot be solved from these equations alone.

Summarizing from eqs. (6.64), (A.7), and (A.9), we conclude that the edge weight of the S^m component in a messenger $\Gamma^{[m]}$ can always be solved (provided it is relevant to some weight-solved mode component), whose value is the expected $-2m$. This justifies the corresponding statement in the weight-solving algorithm.

A.3 Derivation of eqs. (6.73) and (6.74)

For $S^m C_i^n = \mathcal{X}(\gamma_a) \vee \mathcal{X}(\gamma_b)$, we aim to solve $\mathcal{X}(\gamma_a)$ and $\mathcal{X}(\gamma_b)$ under the condition that $\mathcal{X}(\gamma_a), \mathcal{X}(\gamma_b)$ are both softer than $S^m C_i^n$. A first indication is that $\mathcal{X}(\gamma_a)$ and $\mathcal{X}(\gamma_b)$ are overlapping.

Next, any mode that is softer than $S^m C_i^n$ must take one of the following forms:

- (1) $S^{m'} C_i^{n'}$, with $m' \geq m$ and $m' + n' \geq m + n$,
- (2) $S^{m+n} C_j^{n'}$, with $j \neq i$ and $n' \in \mathbb{N}$.

Consider the case $\mathcal{X}(\gamma_a)$ and $\mathcal{X}(\gamma_b)$ are both of type (1), i.e.,

$$\mathcal{X}(\gamma_a) = S^{m'_a} C_i^{n'_a}, \quad \mathcal{X}(\gamma_b) = S^{m'_b} C_i^{n'_b}. \quad (\text{A.10})$$

Since $\mathcal{X}(\gamma_a)$ and $\mathcal{X}(\gamma_b)$ are overlapping, without loss of generality we can assume $m'_a > m'_b$ and $m'_a + n'_a < m'_b + n'_b$. From theorem 3.1, we have

$$\mathcal{X}(\gamma_a) \vee \mathcal{X}(\gamma_b) = S^{m'_b} C_i^{m'_a + n'_a - m'_b}. \quad (\text{A.11})$$

In order that this is equal to $S^m C_i^n$, we must have $m'_b = m$ and $m'_a + n'_a = m + n$. Since $\mathcal{X}(\gamma_a)$ and $\mathcal{X}(\gamma_b)$ are both softer than $S^m C_i^n$, we have

$$m'_a > m, \quad m'_a + n'_a = m + n; \quad m'_b = m, \quad n'_b > n. \quad (\text{A.12})$$

Then, we consider the case $\mathcal{X}(\gamma_a)$ is of type (1) while $\mathcal{X}(\gamma_b)$ is of type (2), namely,

$$\mathcal{X}(\gamma_a) = S^{m'_a} C_i^{n'_a}, \quad \mathcal{X}(\gamma_b) = S^{m+n} C_j^{n'_b}. \quad (\text{A.13})$$

It follows immediately that $m'_a = m$; otherwise ($m'_a > m$) $\mathcal{X}(\gamma_a) \vee \mathcal{X}(\gamma_b)$ would be equal to or softer than $S^{m'_a}$, which is softer than $S^m C_i^n$. This implies $n'_a > n$. In other words,

$$m'_a = m, \quad n'_a > n; \quad n'_b \in \mathbb{N}. \quad (\text{A.14})$$

Finally, eq. (6.73) is a combination of eqs. (A.12) and (A.14).

For $S^m C_i^n = \mathcal{X}(\gamma_a) \wedge \mathcal{X}(\gamma_b)$, we aim to solve $\mathcal{X}(\gamma_a)$ and $\mathcal{X}(\gamma_b)$ under the condition that $\mathcal{X}(\gamma_a), \mathcal{X}(\gamma_b)$ are both harder than $S^m C_i^n$. Again, $\mathcal{X}(\gamma_a)$ and $\mathcal{X}(\gamma_b)$ must be overlapping, and any mode harder than $S^m C_i^n$ must take the form of $S^{m'} C_i^{n'}$, with $m' \leq m$ and $m' + n' \leq m + n$. We then denote

$$\mathcal{X}(\gamma_a) = S^{m'_a} C_i^{n'_a}, \quad \mathcal{X}(\gamma_b) = S^{m'_b} C_i^{n'_b}, \quad (\text{A.15})$$

and assume $m'_a > m'_b$ without loss of generality. From theorem 3.1, we have $\mathcal{X}(\gamma_a) \wedge \mathcal{X}(\gamma_b) = S^{m'_a} C_i^{m'_b + n'_b - m'_a}$. In order for this to equal $S^m C_i^n$, we obtain $m'_a = m$ and $m'_b + n'_b = m + n$. This is precisely eq. (6.74), up to swapping a and b .

References

- [1] M. Beneke and V. A. Smirnov, *Asymptotic expansion of Feynman integrals near threshold*, *Nucl. Phys. B* **522** (1998) 321–344, [[hep-ph/9711391](#)].
- [2] G. B. Pivovarov and F. V. Tkachov, *Euclidean asymptotic expansions of green functions of quantum fields (ii) combinatorics of the as operation*, *International Journal of Modern Physics A* **08** (1993), no. 13 2241–2286, [<https://doi.org/10.1142/S0217751X93000898>].
- [3] V. A. Smirnov, *Asymptotic expansions in limits of large momenta and masses*, *Communications in mathematical physics* **134** (1990), no. 1 109–137.
- [4] V. A. Smirnov, *Asymptotic expansions in momenta and masses and calculation of Feynman diagrams*, *Mod. Phys. Lett. A* **10** (1995) 1485–1500, [[hep-th/9412063](#)].
- [5] V. A. Smirnov, *Applied asymptotic expansions in momenta and masses*, *Springer Tracts Mod. Phys.* **177** (2002) 1–262.
- [6] A. Pak and A. Smirnov, *Geometric approach to asymptotic expansion of feynman integrals*, *The European Physical Journal C* **71** (2011), no. 4 1–6.
- [7] B. Jantzen, A. V. Smirnov, and V. A. Smirnov, *Expansion by regions: revealing potential and glauber regions automatically*, *The European Physical Journal C* **72** (2012), no. 9 1–14.
- [8] B. Ananthanarayan, A. Pal, S. Ramanan, and R. Sarkar, *Unveiling regions in multi-scale feynman integrals using singularities and power geometry*, *The European Physical Journal C* **79** (2019), no. 1 1–20.
- [9] T. Y. Semenova, A. V. Smirnov, and V. A. Smirnov, *On the status of expansion by regions*, *The European Physical Journal C* **79** (2019), no. 2 1–12.
- [10] G. Heinrich, S. Jahn, S. Jones, M. Kerner, F. Langer, V. Magerya, A. Poldaru, J. Schlenk, and E. Villa, *Expansion by regions with pysecdec*, *Computer Physics Communications* **273** (2022) 108267.
- [11] E. Gardi, F. Herzog, S. Jones, and Y. Ma, *Dissecting polytopes: Landau singularities and asymptotic expansions in $2 \rightarrow 2$ scattering*, *JHEP* **08** (2024) 127, [[arXiv:2407.13738](#)].
- [12] Y. Ma, *Identifying regions for asymptotic expansions of amplitudes: Fundamentals and recent advances*, *Int. J. Mod. Phys. A* **40** (2025), no. 29 2530013, [[arXiv:2505.01368](#)].
- [13] T. Becher, P. Hager, S. Jaskiewicz, M. Neubert, and D. Schwienbacher, *Low-energy theory of jet processes and PDF factorization*, *JHEP* **01** (2026) 024, [[arXiv:2509.07082](#)].
- [14] G. F. Sterman, *An Introduction to quantum field theory*. Cambridge University Press, 1993.
- [15] J. C. Collins, D. E. Soper, and G. F. Sterman, *Factorization of Hard Processes in QCD*, *Adv. Ser. Direct. High Energy Phys.* **5** (1989) 1–91, [[hep-ph/0409313](#)].
- [16] J. Collins, *Foundations of perturbative QCD*, vol. 32. Cambridge University Press, 2011.
- [17] T. Becher, A. Broggio, and A. Ferroglia, *Introduction to Soft-Collinear Effective Theory*, *Lect. Notes Phys.* **896** (2015) pp.1–206, [[arXiv:1410.1892](#)].
- [18] G. P. Korchemsky, *Sudakov Form-factor in QCD*, *Phys. Lett. B* **220** (1989) 629–634.
- [19] V. A. Smirnov, *Applied asymptotic expansions in momenta and masses*, vol. 177. Springer, 2003.

- [20] V. Smirnov and E. R. Rakhmetov, *Strategy of regions in the asymptotic expansion of the two-loop vertex feynman diagrams*, *Teoreticheskaya i Matematicheskaya Fizika* **120** (1999), no. 1 64–71.
- [21] B. Jantzen, *Foundation and generalization of the expansion by regions*, *JHEP* **12** (2011) 076, [[arXiv:1111.2589](https://arxiv.org/abs/1111.2589)].
- [22] V. A. Smirnov, *Problems of the strategy of regions*, *Phys. Lett. B* **465** (1999) 226–234, [[hep-ph/9907471](https://arxiv.org/abs/hep-ph/9907471)].
- [23] J. H. Kuhn, A. A. Penin, and V. A. Smirnov, *Summing up subleading Sudakov logarithms*, *Eur. Phys. J. C* **17** (2000) 97–105, [[hep-ph/9912503](https://arxiv.org/abs/hep-ph/9912503)].
- [24] Y. Ma, *Identifying regions in wide-angle scattering via graph-theoretical approaches*, *JHEP* **09** (2024) 197, [[arXiv:2312.14012](https://arxiv.org/abs/2312.14012)].
- [25] S. Jaskiewicz, S. Jones, R. Szafron, and Y. Ulrich, *The structure of quark mass corrections in the $gg \rightarrow HH$ amplitude at high-energy*, *JHEP* **09** (2025) 015, [[arXiv:2501.00587](https://arxiv.org/abs/2501.00587)].
- [26] R. N. Lee and A. A. Pomeransky, *Critical points and number of master integrals*, *JHEP* **11** (2013) 165, [[arXiv:1308.6676](https://arxiv.org/abs/1308.6676)].
- [27] E. Gardi, F. Herzog, S. Jones, Y. Ma, and J. Schlenk, *The on-shell expansion: from Landau equations to the Newton polytope*, *JHEP* **07** (2023) 197, [[arXiv:2211.14845](https://arxiv.org/abs/2211.14845)].
- [28] G. Birkhoff, *Lattice theory*, vol. 25. American Mathematical Soc., 1940.
- [29] H. P. Sankappanavar and S. Burris, *A course in universal algebra*, *Graduate Texts Math* **78** (1981) 56.
- [30] B. A. Davey and H. A. Priestley, *Introduction to lattices and order*. Cambridge university press, 2002.
- [31] L. Landau, *On analytic properties of vertex parts in quantum field theory*, *Nuclear Physics* **13** (1959), no. 1 181–192.
- [32] R. J. Eden, P. V. Landshoff, D. I. Olive, and J. C. Polkinghorne, *The analytic S-matrix*. Cambridge University Press, 2002.
- [33] J. Collins, *A new and complete proof of the landau condition for pinch singularities of feynman graphs and other integrals*, *arXiv preprint arXiv:2007.04085* (2020).
- [34] S. Coleman and R. E. Norton, *Singularities in the physical region*, *Nuovo Cim.* **38** (1965) 438–442.
- [35] J. C. Collins and G. F. Sterman, *Soft Partons in QCD*, *Nucl. Phys.* **B185** (1981) 172–188.
- [36] P. V. Landshoff, *Model for elastic scattering at wide angle*, *Phys. Rev. D* **10** (1974) 1024–1030.
- [37] J. Botts and G. F. Sterman, *Hard Elastic Scattering in QCD: Leading Behavior*, *Nucl. Phys. B* **325** (1989) 62–100.
- [38] D. Fontes and R. Szafron, *An effective field theory for muon conversion and muon decay-in-orbit*, *JHEP* **05** (2025) 171, [[arXiv:2412.05702](https://arxiv.org/abs/2412.05702)].
- [39] E. Gardi, F. Herzog, S. Jones, and Y. Ma, *Regions in the Regge limit of two to two scattering* – in preparation.

[40] P. Bargiela, F. Caola, A. von Manteuffel, and L. Tancredi, *Three-loop helicity amplitudes for diphoton production in gluon fusion*, *JHEP* **02** (2022) 153, [[arXiv:2111.13595](https://arxiv.org/abs/2111.13595)].

[41] J. Davies, G. Mishima, M. Steinhauser, and D. Wellmann, *Double Higgs boson production at NLO in the high-energy limit: complete analytic results*, *JHEP* **01** (2019) 176, [[arXiv:1811.05489](https://arxiv.org/abs/1811.05489)].

[42] Maplesoft, a division of Waterloo Maple Inc., “Maple.”

[43] “On-shell expansion regions finder.” https://bitbucket.org/franz_herzog/ose.

[44] Z. Capatti, *Exposing the threshold structure of loop integrals*, *Phys. Rev. D* **107** (2023), no. 5 L051902, [[arXiv:2211.09653](https://arxiv.org/abs/2211.09653)].

[45] S. Catani, D. de Florian, and G. Rodrigo, *Space-like (versus time-like) collinear limits in QCD: Is factorization violated?*, *JHEP* **07** (2012) 026, [[arXiv:1112.4405](https://arxiv.org/abs/1112.4405)].

[46] J. R. Forshaw, M. H. Seymour, and A. Siodmok, *On the Breaking of Collinear Factorization in QCD*, *JHEP* **11** (2012) 066, [[arXiv:1206.6363](https://arxiv.org/abs/1206.6363)].

[47] M. D. Schwartz, K. Yan, and H. X. Zhu, *Collinear factorization violation and effective field theory*, *Phys. Rev. D* **96** (2017), no. 5 056005, [[arXiv:1703.08572](https://arxiv.org/abs/1703.08572)].

[48] L. Cieri, P. K. Dhani, and G. Rodrigo, *Catani’s generalization of collinear factorization breaking*, [arXiv:2402.14749](https://arxiv.org/abs/2402.14749).

[49] T. Becher, P. Hager, S. Jaskiewicz, M. Neubert, and D. Schwienbacher, *Factorization Restoration through Glauber Gluons*, *Phys. Rev. Lett.* **134** (2025), no. 6 061901, [[arXiv:2408.10308](https://arxiv.org/abs/2408.10308)].

[50] C. Duhr, A. Venkata, and C. Zhang, *Double Spacelike Collinear Limits from Multi-Regge Kinematics*, *Phys. Rev. Lett.* **135** (2025), no. 24 241601, [[arXiv:2507.05355](https://arxiv.org/abs/2507.05355)].

[51] J. Davies, G. Mishima, K. Schönwald, M. Steinhauser, and H. Zhang, *Higgs boson contribution to the leading two-loop Yukawa corrections to $gg \rightarrow HH$* , *JHEP* **08** (2022) 259, [[arXiv:2207.02587](https://arxiv.org/abs/2207.02587)].

[52] F. Herzog, Y. Ma, B. Mistlberger, and A. Suresh, *Single-soft emissions for amplitudes with two colored particles at three loops*, *JHEP* **12** (2023) 023, [[arXiv:2309.07884](https://arxiv.org/abs/2309.07884)].

[53] J. ter Hoeve, E. Laenen, C. Marinissen, L. Vernazza, and G. Wang, *Region analysis of QED massive fermion form factor*, *JHEP* **02** (2024) 024, [[arXiv:2311.16215](https://arxiv.org/abs/2311.16215)].

[54] M. Niggetiedt and J. Usovitsch, *The Higgs-gluon form factor at three loops in QCD with three mass scales*, *JHEP* **02** (2024) 087, [[arXiv:2312.05297](https://arxiv.org/abs/2312.05297)].

[55] X. Guan, F. Herzog, Y. Ma, B. Mistlberger, and A. Suresh, *Splitting amplitudes at N^3LO in QCD*, *JHEP* **01** (2025) 090, [[arXiv:2408.03019](https://arxiv.org/abs/2408.03019)].

[56] J.-Y. Hou, J. Wang, and D.-J. Zhang, *Region analysis of $H \rightarrow \gamma\gamma$ via a bottom quark loop*, *JHEP* **06** (2025) 164, [[arXiv:2501.11824](https://arxiv.org/abs/2501.11824)].

[57] M. Stahlhofen, *NNLO electron structure functions (PDFs) from SCET*, *JHEP* **11** (2025) 171, [[arXiv:2508.16964](https://arxiv.org/abs/2508.16964)].

[58] Z. Capatti, L. Huber, and M. Ruf, *Multi-partonic interactions, iterated discontinuities and the virtuality expansion in deep inelastic scattering*, [arXiv:2506.16489](https://arxiv.org/abs/2506.16489).

[59] Z. Li, *Conformal 3-point correlators in momentum space, method of subgraphs and the $1/N$ expansion*, *JHEP* **12** (2025) 066, [[arXiv:2509.07106](#)].

[60] M. Beneke, P. Hager, and A. F. Sanfilippo, *Cosmological correlators in massless ϕ^4 -theory and the method of regions*, *JHEP* **04** (2024) 006, [[arXiv:2312.06766](#)].

[61] A. V. Belitsky and V. A. Smirnov, *An off-shell Wilson loop*, *JHEP* **04** (2023) 071, [[arXiv:2110.13206](#)].

[62] A. V. Belitsky, L. V. Bork, A. F. Pikelner, and V. A. Smirnov, *Exact Off Shell Sudakov Form Factor in $N=4$ Supersymmetric Yang-Mills Theory*, *Phys. Rev. Lett.* **130** (2023), no. 9 091605, [[arXiv:2209.09263](#)].

[63] A. V. Belitsky, L. V. Bork, and V. A. Smirnov, *Off-shell form factor in $\mathcal{N}=4$ sYM at three loops*, *JHEP* **11** (2023) 111, [[arXiv:2306.16859](#)].

[64] L. V. Bork, R. N. Lee, and A. I. Onishchenko, *Method of regions for dual conformal integrals*, *JHEP* **12** (2025) 107, [[arXiv:2509.12056](#)].

[65] D. Bonocore, E. Laenen, L. Magnea, L. Vernazza, and C. D. White, *The method of regions and next-to-soft corrections in Drell-Yan production*, *Phys. Lett. B* **742** (2015) 375–382, [[arXiv:1410.6406](#)].

[66] N. Bahjat-Abbas, J. Sinnenhe Damsté, L. Vernazza, and C. D. White, *On next-to-leading power threshold corrections in Drell-Yan production at N^3LO* , *JHEP* **10** (2018) 144, [[arXiv:1807.09246](#)].

[67] M. A. Ebert, B. Mistlberger, and G. Vita, *Collinear expansion for color singlet cross sections*, *JHEP* **09** (2020) 181, [[arXiv:2006.03055](#)].

[68] V. A. Smirnov and F. Wunder, *Expansion by regions meets angular integrals*, *JHEP* **08** (2024) 138, [[arXiv:2405.13120](#)].

[69] J. Haag, *Dissecting Exclusive Multijet Cross Sections*, [arXiv:2509.06612](#).

[70] E. Gardi and Z. Zhu, *Computing the soft anomalous dimension with massless particles using the method of regions*, [arXiv:2509.18017](#).

[71] E. Gardi and Z. Zhu, *Infrared singularities of multileg amplitudes with a massive particle at three loops*, [arXiv:2510.27567](#).

[72] T. Y. Semenova, *Asymptotic Series for a Feynman Integral in the One-Dimensional Case*, *Russ. J. Math. Phys.* **27** (2020), no. 1 126–136.

[73] W. Chen, *Unregulated divergences of Feynman integrals*, *Phys. Lett. B* **862** (2025) 139299, [[arXiv:2406.12051](#)].

[74] X. Liu and Y.-Q. Ma, *AMFlow: A Mathematica package for Feynman integrals computation via auxiliary mass flow*, *Comput. Phys. Commun.* **283** (2023) 108565, [[arXiv:2201.11669](#)].

[75] M. Hidding, *DiffExp, a Mathematica package for computing Feynman integrals in terms of one-dimensional series expansions*, *Comput. Phys. Commun.* **269** (2021) 108125, [[arXiv:2006.05510](#)].

[76] T. Armadillo, R. Bonciani, S. Devoto, N. Rana, and A. Vicini, *Evaluation of Feynman integrals with arbitrary complex masses via series expansions*, *Comput. Phys. Commun.* **282** (2023) 108545, [[arXiv:2205.03345](#)].

[77] W. Chen, *Semi-automatic calculations of multi-loop Feynman amplitudes with AmpRed*, *Comput. Phys. Commun.* **312** (2025) 109607, [[arXiv:2408.06426](https://arxiv.org/abs/2408.06426)].

[78] H. Zhang, *Massive two-loop four-point Feynman integrals at high energies with AsyInt*, *JHEP* **09** (2024) 069, [[arXiv:2407.12107](https://arxiv.org/abs/2407.12107)].

[79] A. Sen, *Asymptotic Behavior of the Wide Angle On-Shell Quark Scattering Amplitudes in Nonabelian Gauge Theories*, *Phys. Rev.* **D28** (1983) 860.

[80] G. F. Sterman and M. E. Tejeda-Yeomans, *Multiloop amplitudes and resummation*, *Phys. Lett.* **B552** (2003) 48–56, [[hep-ph/0210130](https://arxiv.org/abs/hep-ph/0210130)].

[81] L. J. Dixon, L. Magnea, and G. F. Sterman, *Universal structure of subleading infrared poles in gauge theory amplitudes*, *JHEP* **08** (2008) 022, [[arXiv:0805.3515](https://arxiv.org/abs/0805.3515)].

[82] I. Feige and M. D. Schwartz, *Hard-Soft-Collinear Factorization to All Orders*, *Phys. Rev.* **D90** (2014), no. 10 105020, [[arXiv:1403.6472](https://arxiv.org/abs/1403.6472)].

[83] O. Erdoğan and G. Sterman, *Ultraviolet divergences and factorization for coordinate-space amplitudes*, *Phys. Rev.* **D91** (2015), no. 6 065033, [[arXiv:1411.4588](https://arxiv.org/abs/1411.4588)].

[84] Y. Ma, *A Forest Formula to Subtract Infrared Singularities in Amplitudes for Wide-angle Scattering*, *JHEP* **05** (2020) 012, [[arXiv:1910.11304](https://arxiv.org/abs/1910.11304)].

[85] C. Anastasiou and G. Sterman, *Removing infrared divergences from two-loop integrals*, *JHEP* **07** (2019) 056, [[arXiv:1812.03753](https://arxiv.org/abs/1812.03753)].

[86] C. Anastasiou, R. Haindl, G. Sterman, Z. Yang, and M. Zeng, *Locally finite two-loop amplitudes for off-shell multi-photon production in electron-positron annihilation*, *JHEP* **04** (2021) 222, [[arXiv:2008.12293](https://arxiv.org/abs/2008.12293)].

[87] G. Bertolotti, L. Magnea, G. Pelliccioli, A. Ratti, C. Signorile-Signorile, P. Torrielli, and S. Uccirati, *NNLO subtraction for any massless final state: a complete analytic expression*, *JHEP* **07** (2023) 140, [[arXiv:2212.11190](https://arxiv.org/abs/2212.11190)]. [Erratum: JHEP 05, 019 (2024)].

[88] C. Anastasiou and G. Sterman, *Locally finite two-loop QCD amplitudes from IR universality for electroweak production*, *JHEP* **05** (2023) 242, [[arXiv:2212.12162](https://arxiv.org/abs/2212.12162)].

[89] L. Magnea, C. Milloy, C. Signorile-Signorile, and P. Torrielli, *Strongly-ordered infrared counterterms from factorisation*, *JHEP* **06** (2024) 021, [[arXiv:2403.11975](https://arxiv.org/abs/2403.11975)].

[90] G. Gambuti, D. A. Kosower, P. P. Novichkov, and L. Tancredi, *Finite Feynman integrals*, *Phys. Rev. D* **110** (2024), no. 11 116026, [[arXiv:2311.16907](https://arxiv.org/abs/2311.16907)].

[91] L. de la Cruz, D. A. Kosower, and P. P. Novichkov, *Finite integrals from Feynman polytopes*, *Phys. Rev. D* **111** (2025), no. 10 105013, [[arXiv:2410.18014](https://arxiv.org/abs/2410.18014)].

[92] C. Anastasiou, J. Karlen, G. Sterman, and A. Venkata, *Locally finite two-loop amplitudes for electroweak production through gluon fusion*, *JHEP* **11** (2024) 043, [[arXiv:2403.13712](https://arxiv.org/abs/2403.13712)].

[93] C. Anastasiou, J. Karlen, R. Sahoo, G. Sterman, and M. Vicini, *General finite two-loop amplitude integrand for photoproduction in quark annihilation*, [arXiv:2509.07805](https://arxiv.org/abs/2509.07805).

[94] C. W. Bauer, S. Fleming, and M. E. Luke, *Summing Sudakov logarithms in $B \rightarrow X(s \gamma)$ in effective field theory*, *Phys. Rev.* **D63** (2000) 014006, [[hep-ph/0005275](https://arxiv.org/abs/hep-ph/0005275)].

- [95] C. W. Bauer, D. Pirjol, and I. W. Stewart, *Soft collinear factorization in effective field theory*, *Phys. Rev.* **D65** (2002) 054022, [[hep-ph/0109045](#)].
- [96] C. W. Bauer, D. Pirjol, and I. W. Stewart, *Power counting in the soft collinear effective theory*, *Phys. Rev.* **D66** (2002) 054005, [[hep-ph/0205289](#)].
- [97] M. Beneke, A. P. Chapovsky, M. Diehl, and T. Feldmann, *Soft collinear effective theory and heavy to light currents beyond leading power*, *Nucl. Phys. B* **643** (2002) 431–476, [[hep-ph/0206152](#)].
- [98] M. Beneke and T. Feldmann, *Multipole expanded soft collinear effective theory with nonAbelian gauge symmetry*, *Phys. Lett. B* **553** (2003) 267–276, [[hep-ph/0211358](#)].
- [99] I. Z. Rothstein and I. W. Stewart, *An Effective Field Theory for Forward Scattering and Factorization Violation*, *JHEP* **08** (2016) 025, [[arXiv:1601.04695](#)].
- [100] M. Beneke, P. Hager, and R. Szafron, *Soft-Collinear Gravity and Soft Theorems*. 2023. [arXiv:2210.09336](#).